QUANTIFICATION OF ACOUSTIC EMISSION FROM SOILS FOR PREDICTING LANDSLIDE FAILURE

Matthew Spriggs

A thesis submitted in partial fulfilment of the
requirements of Loughborough University
for the degree of Doctor of Philosophy

September 2004

QUANTIFICATION OF ACOUSTIC EMISSION FROM SOILS FOR PREDICTING LANDSLIDE FAILURE

Matthew Spriggs

Abstract

Acoustic emission (AE) is a natural phenomenon that occurs when a solid is subjected to stress. These emissions are produced by all materials during pre failure. In soil, AE results from the release of energy as particles undergo small strains. If these emissions can be detected, then it becomes possible to develop an early warning system to predict slope failure. International research has shown that AE can be used to detect ground deformations earlier than traditional techniques, and thus it has a role to play in reducing risk to humans, property and in mitigating such risks.

This thesis researches the design of a system to quantify the AE and calculate the distance to the deformation zone, and hence information on the mechanism of movement.

The quantification of AE is derived from measuring the AE event rate, the output of which takes the form of a displacement rate. This is accurate to an order of magnitude, in line with current standards for classifying slope movements The system also demonstrates great sensitivity to changes within the displacement rate by an order of magnitude, making the technique suitable to remediation monitoring.

Knowledge of the position of the shear surface is critical to the planning of cost effective stabilisation measures. This thesis details the development of a single sensor source location technique used to obtain the depth of a developing or existing shear surface within a slope. The active waveguide is used to reduce attenuation by taking advantage of the relatively low attenuation of metals such as steel. A method of source location based on the analysis of Lamb wave mode arrival times at a single sensor is summarised. An automatic approach to source location is demonstrated to locate a regular AE source to within one metre.

Overall consideration is also given to field trials and towards the production of monitoring protocols for data analysis, and the implementation of necessary emergency/remediation plans.

Key words: acoustic emission, source location, waveguide, slope instability, Lamb waves, AE event rate

Acknowledgements

The research described herein was conducted at Loughborough University Department of Civil and Building Engineering and was funded by Engineering and Physical Science Research Council (EPSRC).

There are many people to whom I owe a great deal of gratitude for their help in enabling me to undertake and complete this period of research. My thanks go to my supervisors Dr. N. Dixon (Department of Civil and Building Engineering) and Dr R. Hill (Department of Chemistry and Physics, The Nottingham Trent University). My particular thanks go to Neil Dixon for his tremendous help, enthusiasm and attention to detail towards producing this thesis, and for all his time and patience throughout this research.

The laboratory work of this investigation would not have been possible if it were not for the expertise provided by Mr. Mark Harrod and Mr. Alex Harrison. Thank you for your ideas and hard work.

Thanks are due to Charnwood Brick Company for providing us with the clay required for experiments, and to Mr. Peter McAvoy for generously printing out this thesis.

I would like to thank Harshal Galgale for his hard work in helping me with data analysis, and the following PhD students for their help and camaraderie; Karan Jalota, Lorenc Hoxhallari and Jonny Woodrow.

My heartfelt thanks go especially to my family. Thanks Mum and Dad for all you've done over the years in getting me my education, this is for you. Thanks Becks for sustaining me throughout it all, especially over the last few months. Your proof reading skills and constant patience have enabled me to reach this far. I'm indebted to you all. My thanks also go to the guys at LEEC for putting up with the endless prayer requests!

Finally my thanks go to God, my Creator and Saviour, for the unsurpassed privilege of being part of His family. *'I count everything as loss because of the surpassing worth of knowing Christ Jesus my Lord For his sake... I count them as rubbish, in order that I may gain Christ and be found in him, not having a righteousness of my own that comes from the law, but that which comes through faith in Christ.' Philippians 3*

Table of Contents

List of Figures

List of Tables

Chapter 1

Introduction

1.1 The need for landslide research

The following is an article printed in the Daily Telegraph newspaper in August 2004 after intense thunderstorms triggered a landslide near the Scottish village of Lochearnhead, trapping 50 people in their vehicles.

The Daily Telegraph, Friday 8th August 2004
By Roger Highfield, Science Editor

Britain can expect to suffer more landslides, say experts

LANDSLIDES of the kind that trapped 50 people and isolated the village of Lochearnhead in Scotland are likely to become more common, an expert warned yesterday

The type of landslip seen on Wednesday is common in the Tropics and, after earthquakes, is the most destructive process on Earth.

They have killed hundreds of thousands over the past century· in Peru in 1970, 18,000 people died in the Andes when the peak of the Mount Huascaran collapsed

Although still unusual in Britain, the cost of landslides already runs to several million pounds each year in repair work and closures and Alan Forster, a principal engineering geologist of the British Geological Survey, said they are already becoming more common

Although climate modelling suggests that summer rainfall will decline, extreme downpours are predicted to become more frequent, triggering more landslides, he said

Other factors include rising sea levels and human interference, from unwise excavations to uncontrolled water drainage down slopes

With Dr Stuart Marsh, [researchers at Edinburgh University and the Environment agency] hope to use a research aircraft to fly over [landslide hazard areas] Lasers and cameras will map the local landscape

The British Geological Survey will use the information to hone a computer model, part of a national assessment of geological hazards called GeoSure, to predict the risk of landslips from local geology, gradients and landscape

"If we know the places that are most at risk, we can use that information to plan for the future and avoid the danger areas, or put in protection systems if economically viable, or add the information to the early warning system to give people ample time for evacuation " [said Mr Foster]

Currently there exists a great need to further landslide research, not only within Great Britain but also across the world, where many countries experience landslides of far greater frequency, intensity and impact. The US government spent approximately $9 9 billion on damages and remediation of landslide induced damage between the years of 1970 to 2000. In Japan on average about 40% to 50% of all deaths by natural geological hazards were attributed to landslides (Transport Research Board 1987). Factors such as global warming and human intervention have caused the frequency and intensity of Landslides to increase resulting in the constant development of new and improved methods for identifying potential hazardous areas, analysing the risks, providing an early warning, and designing effective remediation strategies.

This project is concerned with the use of acoustic emission (AE) as a non-destructive technique to provide an early warning of slope failure. To achieve this central aim, two areas of research are considered. Firstly, the use of AE in measuring displacement rates at very small strains or low strain rates, and secondly, to locate deformation zones within a soil slope in order to provide an assessment of the failure mechanism.

AE is a natural phenomenon that occurs when a solid is subjected to stress This stress, from an external source, causes a sudden release of sound waves resulting in microseismic activity, which can be detected by transducers. It is an occurrence that happens in all materials; metals, glasses, fibres, concrete, ceramics, rock and soil. These sound emissions are produced at pre-failure stages of any material and result from the release of energy as particles undergo small strains. If these emissions can be detected, then it becomes possible to predict failure.

Traditional methods of monitoring slope movements have included surface surveying and sub-surface surveying techniques. However, many of these instruments can lack the sensitivity to monitor displacement at very low strain rates. Research undertaken over the past 30 years into the use of AE from soils, has clearly shown the potential use of AE in providing an early warning of slope

failure. More recently, this has been aided by advancements in computer processing power and available data acquisition software, both of which now enable large quantities of data to be analysed in real time.

1.1.1 Acoustic emission in soil

AE are sound waves produced by movement within a stressed material. Even materials that are designed to withstand very high stresses emit AE. Some materials can be considered to be very 'noisy' (emit high levels of AE) such as brittle heterogeneous materials, whilst ductile materials are considered to be relatively 'quiet' (emit lower levels of AE). The difference in their response is dependant on their individual structures. Within a slope the stress induced by destabilizing forces causes a re-arrangement of particles along developing shear surfaces. This inter-particle friction results in the release of AE, and is an indication of straining within a soil body. Typically clay is a 'quiet' soil as it undergoes a ductile failure, whereas gravel is considered to be a 'noisy' soil due to its greatly increased particle size and angularity, which result in the generation of higher energy events. In all cases, without the presence of an applied stress, there is no generation of AE.

This investigation in principally concerned with the application of AE to soil slopes. A landslide is a downward and outward movement of slope forming materials; rock (natural), soils, artificial fills or a combination. It occurs when the forces acting on the slope are greater than the resisting forces of the materials that form the slope. These forces con be summarised into those that contribute to an increase in shear stress acting on the slope (removal of lateral or underlying support, surcharge, localised changes in earth stresses), and those that contribute to reduced shear strength within the soil slope (weathering, soil structure, composition and texture).

Slope movements are recognised by the following principle mechanisms; falls, slides and flows. Most classifications are based on a combination of the above mechanisms and by the types of material involved in the movement. This

investigation is wholly concerned with slides. Sliding (translational and rotational) occurs when instability results from a moving mass that always stays in contact with the ground. The movement is progressive, and thus failure is not always instantaneous across the slope, but relies on the development of a slip plane, or shear surface, along which shearing takes place between the underlying stable materials and the moving mass It is from this shear surface that the generation of AE occurs at its most concentrated.

Within an unstable or potentially unstable slope, there are many types of measurements required, usually subjected to time and cost constraints Despite this, magnitude, rate and distribution of any movement are critical when studying landslides. Equally important are the measurements of the in-situ soil characteristics, especially the pore water pressure.

If the zone of sliding is apparent, then surface surveying (electromagnetic distance meter, Terrestrial photogrammetry, crack gauges) is often carried out. However, if it is not possible to visually see the extent of the slide, subsurface techniques (inclinometers, extensometers, strain meters, and more recently time domain reflectometry) are used to detect any movement AE is a subsurface technique for assessing soil deformation; its advantage is its sensitivity to small pre-failure deformations, the increasing rate of which could be used to assess the likelihood of catastrophic failure.

Of particular interest are slopes formed in strain softening materials, (plastic clays and shales) and those which incorporate discontinuities with strain softening behaviour (joint/bedding surfaces and fault zones), which can experience progressive failure and hence undergo deformation prior to collapse. In these types of material, shear deformations of the order of a few millimetres may be sufficient to reduce this shear strength to post peak values and lead to failure. The earlier decreasing stability can be detected, the earlier that a warning can be given to those likely to be affected by any failure, and remedial measures can be carried out to arrest the ground movements.

Over 40 years of research has been conducted into the use of AE to monitor soil movements. The main body of research into AE applications has been carried out in the U.S.A. (e g. Hardy 1989, Koerner *et al.* 1981), Japan (e g. Chichibu *et al* 1989, Shiotani & Outsu 1999) and UK (e g Rouse *et al.* 1991, Dixon *et al.* 2003). To date only the following qualitative method exists for the assessment of slope movements (Koerner *et al.* 1981). Slopes that:

- Generate little or no AE – Probably not deforming and are therefore stable.
- Generate moderate levels of AE – Deforming slightly but marginally stable, continued monitoring is necessary.
- Generate high levels of AE – Substantial deformations, considered unstable, immediate remedial measures required.
- Generate very high levels of AE – Undergoing large deformations and are probably in a state of failure

As with all qualitative scales, they are open to human error in interpretation and implementation. For AE to be used as an early warning device, only a quantitative approach would achieve the necessary accuracy and reliability needed to produce a rigorous early warning of slope instability.

The use of a waveguide to provide a path of low attenuation from the source of the AE (within a soil slope) to the sensor (usually situated above ground surface) has become standard practice in AE research. The presence of a waveguide, typically a metal pipe inserted within an unstable slope, greatly increases the monitoring range of the sensor. Dixon et al (1996) outlined two generic types of waveguide; passive and active (discussed in detail in sections 2.3.3 and 3.3). A passive waveguide does not introduce additional sources of AE, and thus all detected AE is assumed to originate from the surrounding soil slope. In comparison the active waveguide uses an annulus of high AE responsive backfill material around the waveguide. As the slope deforms the waveguide, AE is assumed to originate from the backfill only.

The active waveguide has the advantage that the generated AE suffers less attenuation before reaching the waveguide, because of the close proximity between the backfill and the waveguide. If the acoustic properties of the backfill are known, then a calibrated waveguide monitoring system can be used within an unstable soil slope without prior knowledge of the slope's geological characteristics.

1.2 Aims and objectives

The following are the aims and objectives for this investigation.

Aim

- To develop a quantitative approach for the prediction of slope instability using acoustic emission monitoring techniques.

Objectives

- To create a real time 'data acquisition and analysis' acoustic emission monitoring system.
- To develop a technique of source location using a single sensor, and validate by means of laboratory experiments.
- To establish a relationship between the generated acoustic emission, with soil type, mode of failure and rate of slope deformation using large-scale model slopes.
- To produce a quantitative approach for the prediction of slope instability.

1.3 Original contribution to knowledge

This investigation has been concerned with the utilisation of detected AE generated by an active waveguide system for the development of an early warning system of slope instability. Particular attention has been given to advancing the

current qualitative method of assessing slope stability, and the identification of the mechanism of movement within a deforming soil body. The following original contributions to knowledge have achieved this aim.

- Quantification of very slow displacement rates via monitoring of AE in terms of event rate.
- Development of a quantified relationship between event rate and displacement rate accurate to one order of magnitude.
- Successful application of source location techniques on backfill generated AE within the active waveguide arrangement over lengths of up to 20m.
- The design of an automatic source location system capable of monitoring many thousands of events in real time.

1.4 Outline of chapters

Chapter 2 is a review of existing research into the use of AE within soil studies. It provides an up-to-date picture of the current trends within landslide research globally, and demonstrates how the utilisation of AE could compliment and improve upon existing methods of slope instrumentation. Research into the fundamentals of soil generated AE and the associated effects of propagating AE through soil have been outlined, as well as the development of waveguide technology and the sensitivity of monitoring systems. Relevant laboratory and field studies into the generation, capture and analysis of AE within unstable soil bodies have been considered. Particular discussion has also been given to techniques of identifying the distance over which AE has travelled between its source and receptor.

Chapter 3 outlines the necessary hardware and software required to produce a real time AE monitoring system. Each component is outlined in detail, and its role within the monitoring system is considered. Detailed discussion is given to the selection and make up of the active waveguide, and an appropriate criterion for measuring AE is outlined.

Chapter 4 examines the need to quantify AE. It details a technique of deforming soil within a controlled environment to generate AE, and validates that approach against previously published research. Two types of tests are considered to produce a quantified relationship between generated AE and rate of displacement The first test involves the use of compression test apparatus to deform soil around a waveguide, while the second technique aims to apply the same principles as the first, but within a more realistic testing environment. A relationship between the recorded AE and displacement rate is generated.

Chapter 5 is concerned with the development of a single sensor source location technique. The issue of attenuation and how it affects different measurement parameters is highlighted The chapter outlines the theory of Lamb wave modes to determine the distance to source. Lamb wave mode theory is first tested on a controlled repeatable source of AE, and then on soil generated AE. Both a manual and an automatic approach to source location were employed, and the respective advantages and disadvantages are discussed

Chapter 6 seeks to bring together conclusions from chapters 4 and 5 to propose an early warning system for assessment in field trials. Further experiments demonstrate the sensitivity of a monitoring system to changes in displacement rates, and the automatic source location technique is validated on soil generated AE. The requirements of an early warning system are put forward and an outline methodology of monitoring AE within the field is produced.

Chapter 7 summarises the conclusions of this investigation and recommends some future work.

Chapter 2

Literature Review

2.1 Introduction

The following chapter is a historical summary of pertinent work done by an international field of researchers. Section 2 2 begins with a summary of the current areas that are receiving the most attention in general landslide research, namely mitigation and risk analysis A review of current instrumentation used with landslide monitoring is also discussed with respect to potential use as an early warning device. Section 2.3 lays down the fundamentals of acoustic emission (AE); characterising AE signals, attenuation, waveguide development and signal frequency. Section 2.4 details the development of understanding of AE and soils from laboratory investigations. Section 2 5 discusses the use of AE within the field to detect and predict the onset of failure, and finally section 2.6 considers research that specifically seeks to develop a system to detect the depth of landslide movement, referred to as source location.

2.2 The 'big picture' of landslide research

In an attempt to determine the current position on landslide research, proceedings from the International Conference 'Fast Slope Movements Prediction and Prevention for Risk Mitigation', held in Naples Italy 2003, were considered. The following is a brief over view of current trends in landslide research.

2 2.1 Mitigation and risk analysis

For many countries around the world landslides can be the most severe of all natural disasters, with large humanitarian and economic consequences. Italy is one

such country, where it is estimated that the cost of landslide remediation since 1944 totalled 500 million euros, with an average of 1000 million euros being spent each year in damages to individuals affected by landslides (Barla *et al.* 2003). In 1989 Italy's Minister of Civil Protection requested the National Research Council (CNR) and the Group for Hydrogeological Disasters Prevention (GNDCI), to compile an inventory of sites historically affected by landslides and floods in Italy, for the period 1918-1990. In 1998 a revised version of the map showed the location of more than 15,000 affected sites (9086 landslides and 6456 floods). This map became the most accurate and updated view of the distribution and frequency of catastrophic events in Italy.

In May 1998, devastating mud and debris flows occurred at the towns of Sarno and Quindici in the Campania region (Versace 2003). This gave rise to new national legislation on hydrological and geological protection. The legislation required flood, landslide and erosion hazards to be mapped in detail and this information to be compared with elements at risk in the landscape in order to identify locations of major risk to people, buildings and infrastructure.

Since 1900, 728 flood events and 816 landslide events that resulted in fatalities have been documented. The risk of landslide in Italy is a high profile threat to both humanity and infrastructure. Hence this conference/workshop was designed to pool together an international community with the intention of improving the criteria of risk assessment and mitigation.

The main thrust of current research was towards risk analysis and mitigation. Intensive rainfalls and earthquakes were highlighted as the two main causes of landslides. Risk analysis ranged greatly and many models were demonstrated. These models ranged from a visual perception of risk to a more involved 'Quantitative Risk Analysis' (QRA), which required large amounts of available data to produce a fully informed study of any associated risk (Mouroux *et al.* 2003). QRA was shown to be a very persuasive tool when debating with governments. Especially where the balance between accepting fatalism verses resisting fatalism was not straight forward given the economy of the country

involved. Indeed there can be no universal risk assessment model, unless it takes in account the socio-economic status of the country.

In mitigation, many different solutions were presented, and each differed from country to country. In Hong Kong for example, a slope catalogue has been produced, and made available to the public. Slopes were prioritised for any stabilisation work required and hazard maps were used to classify areas of low, medium and high risk for future building and land planning. Building has been allowed on slopes up to 35 degrees provided people are aware of the risk, and that the risk has been taken in to account during the design of the structure. Further to this, the Hong Kong government now has the ability to remove and re-house people living in dangerous areas (Morgenstern 2003).

Much of the research presented, involved the modelling of failure mechanisms and run out characteristics from case studies. These would result in design solutions to reduce the risk of future flows. Often these solutions would include rain fall monitoring gauges to ascertain possible trends and thresholds for future prediction. Hong Kong has established a rainfall network by creating regional systems that monitor rainfall in order to provide a national database to further research into the prediction of rainfall induced landslides.

2.2.2 Early warning systems

Monitoring systems and strategies for detecting slope instability at an early stage are required in order to provide sufficient time for implementation of an appropriate action plan. Depending upon the expected speed of slope movement, the size of area affected and the potential risk to human life and property, information from monitoring is required to plan remedial measures and, in extreme cases, to order evacuation of people, livestock and removal of property. For slopes formed in strain softening materials it is possible for the onset of movement to be rapid. In these cases, early detection of instability is of paramount importance.

An early warning monitoring system should meet the following criteria:

- Provide sufficient warning to enable action to be taken (i e. implementation of emergency plan).
- Minimise the number of false alarms as these undermine confidence
- Enable the mode of failure to be identified as this is required to assess the significance of the event
- Provide information on rates and magnitude of movement to help assess the significance of the event.

A brief summary of monitoring methods available for use as early warning systems is presented in Table 2.1. It can be seen that none of the techniques provide all the information required to fully assess the mode and hence likely consequences of slope failure. For this reason it is common for a range of techniques to be used as part of a monitoring strategy.

The use of acoustic emission (AE) clearly has a role to play within the current research of landslides, both for risk analysis and mitigation. The historical development of AE monitoring is discussed later within this chapter, but the emergence of recent technology for monitoring AE and an increase in computer processing power, has led to AE emerging as a valid option in landslide monitoring.

2.3 Acoustic emission fundamentals

2 3.1 Characterising acoustic emission

Figure 2.1 (Dixon *et al.* 1996) shows a simplified AE pulse waveform from a transient event. Acoustic emission is recorded by a piezoelectric sensor, which converts the mechanical micro-seismic waves into a variable electrical voltage, which can be processed digitally and analysed (section 3.2.1). Such a waveform is characterised by a number of parameters as shown. Ring Down Count (RDC) measures the number of times the AE pulse rises above a pre-determined

threshold, in this example the RDC has a value of nine. Event Counts, record one pulse at a time, i.e. when the pulse first crosses the threshold until it drops below the threshold for a pre-determined length of time. The example in Figure 2.1 shows one such event. The established threshold for these measurements is set to eliminate the influence of background noise on the AE pulse. Other parameters such as rise time, peak amplitude and the energy under the envelope can successfully be used to quantify AE.

2 3.2 Attenuation

Detecting AE generated by a developing shear surface within a slope is not an easy task. Even if the host soil is considered to be relatively noisy, soil is not a conducive medium for transferring low energy AE data. As AE propagates through soil, it suffers from attenuation. Attenuation is the loss of signal amplitude over distance as the emission propagates through a medium. Attenuation is high in soils because it is a particulate medium, and energy is lost as AE travels from one particle to another (i e. losses energy at particle boundaries).

An effective AE monitoring system is designed to reduce the impact of attenuation on the pathway from the source to the receptor. In brief, the attenuation suffered by an AE is dependant on two characteristics, the nature of the soil (e g. grading, density etc) and AE frequency (Koerner *et al.* 1981).

$$\alpha = \frac{20}{\chi} \log \frac{A_1}{A_2} \qquad [2.1]$$

Where

α = attenuation coefficient in dB/distance

χ = distance between pickup points

A_1 = amplitude of the first wave

A_2 = amplitude of second wave

Koerner *et al* (1981) evaluated the effect of attenuation on sands and clays using a simple test set up consisting of a box filled with soil, two AE pickup points, and an AE source. As the AE signal sequentially passed by the two pickups, their output was monitored on a dual channel oscilloscope. By a simple calculation using their amplitudes, an attenuation coefficient was calculated, using equation 2.1.

The results of this experiment are shown in Figure 2.2. The attenuation characteristics of dry sand and clayey silt are shown alongside typical attenuation ranges for rock and coal, and for iron and steel. Clearly the attenuation of AE within soil is significantly higher than that of rock or steel, and hence the advantage of using steel waveguides to aid the transmission of AE from within a soil body can be appreciated. This experiment also showed the influence of frequency on attenuation. Depending upon frequency, attenuation coefficient in dry sand varied from 0 09dB/cm at 500Hz to 10dB/cm at 16kHz. For a clayey silt, the attenuation coefficient varies from 1.9dB/cm in the dry state to 1.0dB/cm near saturation (both values were taken as AE frequency of about 1.0kHz).

Shiotani & Ohtsu (1999) investigated the characteristics of attenuation in Toyoura sand. Toyoura sand has a homogeneous distribution of grain size, and is thus recognised as standard sand for testing in Japan Twelve AE senses of 60kHz residence type were set in the sand as shown in Figure 2.3. An artificial AE was generated by hitting nails of stainless steel, and was detected by the sensors. The peak amplitude of AE signal was used to characterise the incoming AE at each sensor.

The results of AE attenuation at frequencies of 1, 5, 10, 30 and 50kHz are shown in Figure 2.4. The general trend demonstrates an increase in attenuation with an increase in frequency. For Toyoura sand the attenuation characteristics are 1.91 dB/cm at 1 kHz, 5.3 dB/cm at 5 kHz and 6.6 dB/cm at 10 kHz. Shiotani & Ohtsu (1990) concluded that AE was significantly attenuated when it had propagated further than 8cm, and suggested that a distance of 5cm at 50kHz was the utmost distance that an AE signal could be efficiency detected in Toyoura sand. Accordingly, the effective frequency range for AE monitoring of slope failure was

proposed at under 10 kHz. The authors went on to make the case for the need of waveguides in order to minimise the attenuation of AE.

2.3.3 Waveguide development

In general the waveguide has become a vital part of AE apparatus, especially in the monitoring of larger soil masses within the laboratory and the field. Its primary aim was to overcome the high attenuation characteristics of soil and other geological materials. Many investigations initially relied on a number of sensors being buried within the soil mass in an attempt to ensure that at least one sensor would happened to be located near the AE source. By locating a sensor on a waveguide that penetrates the geological material, the monitored area significantly increases. This section discusses the development of the waveguide for this role.

Within this literature review there are 2 generic types of waveguide, the passive and the active waveguide. In the passive waveguide model, as described by Lord *et al.* (1982), acoustic emission is generated and propagated only by and through the host soil body to the waveguide and is then transmitted to the sensor. Any detected AE can be used to provide a direct indication of the presence of strains within the host soil body and hence can provide an assessment of stability. However, the high attenuation of AE in soils means that a very small volume of soil can be monitored even using a wave guide. The low levels of AE signal generated by deforming soils, particularly fine grained soils, means that limited acoustic emission data is likely to be detected.

The method of installing the waveguide also has to be considered. For small slopes it may be possible to drive waveguides to the required depth (PWRI 1998). However, for larger slopes it will be necessary to install the steel tube in pre-drilled boreholes. This installation system leads to the major question of what type of material should be selected to backfill the annulus around the central steel element.

A passive waveguide must be designed to ensure that installation, including the backfill, does not create additional sources of AE during deformation of the host soil. Driven systems are likely to be passive as a result of the waveguide being in direct contact with the in situ material. But for systems located in boreholes, the annulus around the waveguide should be backfilled with low AE activity (i e quiet) material. However, these materials (e.g. Bentonite grout) have high acoustic emission attenuation properties and their use would severely restrict the amount of AE from the deforming host soil reaching the waveguide and hence being detected by the sensor.

The active waveguide design relies upon the waveguide system as a whole (i.e. the composite behavior of the steel tube and the backfill material) generating AE in response to being strained by the deformation of the host soil body. AE is then generated by a variety of mechanisms including; the straining of the steel tube directly (i.e. in bending), shearing at the interface between the backfill and steel tube and compression and shearing within the backfill material. It is considered that minimal amounts of AE generated within the deforming host soil will propagate to the steel tube as a result of the high attenuation. Transmission path lengths within the backfill to the steel tube are short, hence attenuation is limited and this results in relatively high-energy signals being transmitted through the steel waveguide to the sensor (Dixon *et al* 2003)

If the annulus around the waveguide is backfilled with 'noisy' material, it is possible to obtain effective acoustic emission data in response to deformation of 'quieter' fine-grained host soils. As the host material deforms, the column of high AE response backfill material will be deformed leading to the production of detectable acoustic emission.

Koerner *et al* (1975) was one of the first to investigate the use of a waveguide for AE monitoring. Long metal rods were used to transmit the emissions from the soil mass to the ground surface where monitoring would occur. Rather than permanently burying sensors in the ground, sensors could now be re-used and easily protected against relatively hostile environments. Koerner *et al.* (1975) studied the effect of the waveguide on the propagation of a generated signal.

Resonant frequencies (a resonant frequency is a natural frequency of vibration determined by the physical parameters of the vibrating object) were transmitted along the waveguide. Two metals rods were used (12.7mm and 3.175mm diameter) as waveguides, the results are shown in Figure 2 5, which demonstrates the relationship between the frequency of the first resonance and the waveguide length. This study was not concerned with the generation of AE, but the transmission of AE along a waveguide.

The authors drew the following conclusions about the transmission of AE:

- Longer waveguides lower the frequency of the first resonance of the detector system (lower frequencies exhibit less attenuation).
- Different diameter rods do not appear to influence the first resonant frequency of the system.
- Different surface conditions (threaded versus smooth) do not appear to affect the location of the first resonance.
- The method of connecting one rod to another does not appear to influence the resonances, so long as such connections are solid and firm in their metal-to-metal contact.

In short, this study was important in asserting that the use of the waveguide didn't in its self change the nature or the frequency of the propagating AE signal. This was shown over distances of 16ft (4.8m).

The influence of soil, surrounding the waveguide, on signal propagation was also considered. A silty sand soil was placed around the waveguide. Soil density and moisture content were varied to see their effect on the resonant frequencies of the waveguide. Koerner *et al.* (1975) concluded that 'it appears that the influence of the soil mass around the waveguide is negligible on the detectors' frequency response but does reduce it's sensitivity to a certain extent.'

Lord *et al.* (1982) continued the investigation to determine the extent of the soil covering loss on the acoustic emission waveguide system. A signal ranging

between 1 and 8 kHz was created by a pulse generator and sent down a 2m long steel bar (of 12mm diameter) waveguide. Both longitudinal and transverse waves were tested. Either Ottawa Sand or Kaolinite Clay at varying moisture contents from dry to saturated, were then placed uniformly surrounding the bar. Either side of this soil-covered section accelerometers were placed to output the various voltages of the in-going and out-going signal. It was assumed that any attenuation of the signal would be as a direct result of absorption into the surrounding soil, and thus referred to as soil covering loss (SCL).

The following conclusions were made:

- For longitudinal waves, the soil covering loss varied from 0 – 6 dB/m dependant on soil and moisture content. These values of attenuation were higher than that of steel alone, and lower than that of soil alone.
- Transverse waves had higher attenuations of 10 – 17dB/m. These values approached those of soil alone, signifying that the transverse waves are attenuated much more than longitudinal waves.
- It was generally found that increased soil water content increases the soil cover loss attenuation, but not by significant amounts.
- Increased soil density has the effect of increasing attenuation.
- The resonant frequencies of the rod were only altered some 0.05 – 0.1kHz due to the presence of soil.

Lord *et al.* (1982) explained a theoretical model, which demonstrated the effectiveness of using a waveguide, as opposed to simply placing a sensor on the soil surface. Three areas of signal loss contributing to the over attenuation of a waveguide monitoring system were identified as 1) Propagation loss in the soil as AE reaches the waveguide, 2) Coupling loss, that is as the signal propagates over the soil/waveguide boundary and 3) the effect of SCL as described above. This theoretical model showed that the use of a waveguide increased the volume of soil being sensed by approximately 30 times, and an increase in sensed soil depth by approximately 60 times.

Lord *et al.* (1982) concluded that the use of steel rods as waveguides were highly recommended for monitoring soil structures. This use of waveguide in which a rod is inserted directly into the ground to detect AE from the deforming host soil is known as a 'passive waveguide', because it was assumed that the waveguide played no role what so ever in the generation of AE, but merely acted as a path of low attenuation from the AE generated by the deforming soil slope to the sensor.

Styles *et al.* (1988) investigated the effect of 'acoustic coupling'. That is the changes that occur to the AE as it propagates across the boundary between the waveguide and the soil. To illustrate this effect, Styles *et al.* (1988) considered two boundary conditions. It was shown that 30% of acoustic energy travelling in a soil medium will cross a soil steel boundary, where as 85% will cross a soil water boundary. This was further studied by Shiontani *et al.* (1999) who considered the acoustic impedance of waveguide materials which in turn affected the amplitude of the reflected and the transmitted AE. Shiontani *et al* (1999) used a PVC pipe to reduce the transmission loss between the soil/waveguide interface. The PVC pipe was also filled with water in order to decrease the attenuation of the AE as it propagated along the waveguide. The author's experiments showed that this arrangement reduced the attenuation by almost a half compared to a traditional metal wave guide.

Hardly (1992) worked on mechanical waveguide's for use in rock tunnel roof stability monitoring. Rock exhibits lower attenuation levels than soil however the attenuation of rock is still relatively high due to the presence of discontinuities and thus the use of a waveguide is essential when observing large rock structures. Deformations in rock are usually clearly defined and of high amplitude, making AE a viable method of monitoring. Figure 2 6 shows a system proposed for use within rock tunnels, in which rock bolts were placed within the rock tunnel roof. Each rock bolt was connected to a horizontal waveguide. Hardy (1992) was particularly concerned with zones of attenuation within the monitoring system, such as waveguide materials, connections and acoustic coupling between the rock bolts and the rock. Hardy (1992) also investigated the effect of connections within a waveguide. Table 2.2 shows the results for the effect of different types of connection.

Wood *et al.* (1990) used waveguides to monitor structures to provide ongoing integrity evaluation and defect location. They designed 3 waveguides to attach to a pressure vessel operating at 580^{0}C, a storage tank at –40^{0}C and a fibre reinforced containment vessel operating at 96^{0}C. Waveguides were used in each case to protect and allow easy access to the sensors in such extreme working environments. In each case, the authors experimented with different materials for the waveguide and different fixings.

Wood *et al.* (1990) concluded that using a solid steel bar waveguide (with a flat end surface contact) only incurred a further 5 – 6 dB attenuation compared with directly fixing the sensor to the vessel surface. Investigations were carried out on the same vessel using sharp pointed waveguides (tapered end), which displayed a higher attenuation of 20 dB.

A fibre reinforced plastic (FRP) waveguide was constructed for monitoring vessels made of the same material. This enabled the waveguide to be readily bonded direct to the vessel's surface Compared to fixing a transducer directly to the surface, this waveguide produced an extra attenuation of 30 dB. The author stresses the need for using waveguides in such hostile environments when long term monitoring was required. In the case of the containment vessel operating at 96^{0}C, sensors placed directly on the vessel demonstrated a loss in sensitivity within a range of 30 to 50 dB over a period of 4weeks. Comments were also made on the necessity of a good connection between the waveguide and the source of emission, however useful information as to the length of waveguides used and the success of using such a system to monitor fatigue are absent.

The passive waveguide, as described by Lord *et al.* (1982), relies on acoustic emission propagating directly from the soil to the waveguide. As discussed by Lord *et al.* (1982), there are many potential sources of attenuation. Nakajima *et al.* (1991), when monitoring a sliding mass of loose cohesionless material, commented that generally it is impossible to detect directly acoustic emissions from the sliding mass. Nakajima *et al.* (1991) thus designed a composite waveguide in order to use the deformation of the waveguide itself as the source of

acoustic emission. The waveguide was mainly composed of a PVC outer pipe, and an inner pipe composed of the composite materials of resin and glass fibre which generated acoustic emissions in proportional to its deformation (Figure 2.7) The outer pipe is in contact with the inner pipe through nylon rings, whilst transducers were located at either end.

This composite waveguide achieved two things: firstly, the attenuation on the signal amplitude, caused by friction on the surface of the waveguide, was now greatly reduced by improving the contact conditions between the waveguide and the borehole. Secondly, the use of a resin and glass fibre composite material provided a very clear response to deformation. An example of the waveguide's response to deformation is shown in the results of a bending test (Figure 2 8). Nakajima *et al.* (1991a) installed 50m waveguides in the Numamae Landslide, Hokkaido, Japan. Here it was possible to monitor seasonal changes in the ground water level by detecting fluctuations in the seismic response, this additional data made it possible to identify possible factors that caused the landslide movement, this is further discussed in section 2.6.

Dixon *et al* (1996) developed the waveguide further, by introducing the concept of an active waveguide. The active waveguide is discussed in detail in section 2.4 and 3.3. As opposed to the passive waveguide, the active waveguide not only transfers AE from the deformation zone to the sensor, but it is also generates the AE from interaction between the metal waveguide and the surrounding placed backfill material. Dixon *et al.* (1996) successfully used active waveguides in field trials at two separate sites: actively eroding coastal cliffs formed in glacial stiff clay on the NE coast of England, and in Gault Clay at a brick pit near Arlesey, SE England. At both sites monitoring of slope movements was achieved using the active waveguide, and a direct relationship between the produced AE and the type of backfill used in the active waveguide was established. Dixon *et al.* (1996) concluded that while the active waveguide approach did not allow the stress state of the host material to be obtained directly, it did produce a system which was capable of detecting ground deformations at an early age, and assessing any changes in the relative stability of the slope.

2.3.4 Signal frequency

Signal frequency of an AE is dependant on the nature of the material and the nature of the deformation causing the emission. It should also be noted that the recorded frequencies are also a product of the test environment, and the derived waveform detected by the sensor is not the actual waveform propagating through the soil body. As such the frequency content of an AE is hugely variable from case to case. Much work has been done to determine the frequency content of AE from soil, in order that correct equipment might be selected to detect AE from soil.

Lord *et al* (1977) carried out a study in which soil samples were subjected to unconfined compression and also a triaxial compression shear test. A waveguide was placed within the samples Two types of soil were tested, clayey silt soil and a silty sand soil. An accelerometer with a responsive range from 0 – 15 kHz was placed on the waveguide, and was in turn connected to a recording device. The AE was recorded and subsequently played back through an Octave filter, set to determine the percentage of emissions within each octave frequency band (In most cases it is sufficient to measure sound levels in bands of frequencies, rather than at individual frequencies. The width of the band often chosen is the octave band - this is a band where the upper frequency is twice that of the lower. Each band is denoted by its centre frequency). The results of these tests are shown in Figure 2.9.

All of the unconfined samples had dominant frequencies within 1 kHz to 2 kHz range. However when the tests were done under confining pressure (69kPa), the frequency band shifted to 4 kHz to 8 kHz. This shift in frequency was thought to be due to the difference in failure mode experienced between the confined and the unconfined samples.

The same technique was used by Koerner *et al.* (1981) to produce AE from soil samples. Koerner *et al.* (1981) used a Fast Fourier Transform to analyse the frequency spectrum of the recorded AE. Clay, silt and sand all showed high levels

of AE energy below 10 kHz, but Silt and Sand also demonstrated activity near 100 kHz The frequency spectrum of these is seen in Figure 2.10.

Koerner *et al.* (1981) also cited work by Hakuno *et al* (1968) who found the frequency to be a function of the sand's density, with a maximum value in the region of 6 kHz .

Naemura *et al.* (1990)b carried out a study to examine the applicability of AE to judge the ground soil condition for the boring of small diameter holes. A rod equipped with an AE sensor was pushed into the soil sample at a specified speed and the AE waveforms were monitored and analysed for their frequency spectrum. For compact clay, mountain sand, and gravel, the dominant frequencies were 850 Hz, 800 Hz, 3.65 kHz and 850 Hz respectively. For loose samples the corresponding dominant frequencies were 100 Hz, 100 Hz, 3 30kHz and 3.35kHz. Whilst in both cases dominant frequencies of 6.0, 11 0, 15.0 and 19.0 kHz were found.

2.4 Laboratory investigations

The following is a review of historic laboratory research concerned with the work of understanding acoustic emission from soils.

Lord *et al.* (1974) investigated the acoustic emission response from a series of axially stressed dry soil samples in an attempt to explore the use of AE as a non-destructive field evaluation technique. Two soil samples were used; a granular soil (decomposed mica schist), and a finer soil, which was a clayey silt (river transported deposit). The sand and clayey silt were then blended into different gradings varying from 100% sand to 100% clayey silt. The samples were then tested in unconfined compression, and the AE emitted was collected by an accelerometer (flat frequency response from a few Hz to 6000 Hz) via a 1/4 inch (6.35mm) diameter steel rod waveguide. The results demonstrated that the cumulative AE counts were greater in the sandy soils than in the fine grained soils. This suggested that sliding friction was probably more significant than

rolling friction in producing AE. The AE generated also showed great sensitivity at low stress levels.

Lord *et al.* (1977) went on to test soil samples in confined triaxial conditions, detecting the AE using a flat response accelerometer with a range from a few Hz to 15kHz. The following generalised conclusions were reached:

- Under constant load, the strain and acoustic emission behaviour is identical.
- Stress/strain and stress/acoustic emission behaviour always resulted in similar shaped curve at all confining pressure levels.
- For a given soil type, greater water contents lower the gross acoustic emission counts.
- For completely dry soil samples, coarser sized particles appeared to give higher acoustic emission counts.

Tanimoto and Noda (1977) studied the acoustic behaviour from sandy soils during triaxial compression tests to establish a method of predicting the failure life (time to failure) of soils by emission counts. Two series of tests, stress controlled and strain controlled, were carried out on well graded unsaturated sands, under drained conditions. A 40 kHz piezoelectric transducer was accommodated within the base plate of the triaxial cell. In the strain controlled tests the emission count rate (counts per minute crossing a threshold of 1 volt) increased with strain during the first process from point '0' to point 'T' (see Figure 2.11), but became steady during the second process from 'T' to 'F' at the point of failure. In this steady state process the authors demonstrated that a linear relationship between the emission counts and the strain rate existed (see Figure 2.12). In stress controlled tests a two phase process also occurred (see Figure 2.13). The increase in emission count from point 'B' was related to a quick rate of strain likely to have been developed before failure.

In strain controlled tests, the strain rate was seen to be proportional to the emission count, and so the possibility of predicting a failure time was considered.

The relationship of emission counts per minute, during a steady state process with time to failure from the start of the test is shown in Figure 2 14. This Figure shows a linear relationship when plotted on a logarithmic scale, which is independent of strain rate, water content and dry density, but not of confined stress. In an attempt to remove the effects of confining pressure (cell pressure), the authors defined an emission rate 'R', (which is illustrated in the corner of Figure 2.15) calculated by equation 2.2:

$$R = \frac{\Delta N}{N} \qquad [2.2]$$

Where:

N Is the total emission count observed during the first process (that is from 'O' to 'T' in Figure 2.11

ΔN Is the emission count observed in a small period (30 seconds) directly after the end of the first process

Figure 2.15 shows the results of this improved correlation which indicated a good linear correlation between failure time and emission rate 'R' in strain controlled tests. Whilst this relationship was shown to be independent of soil type, confined stress, water content and dry densities, the Authors commented that the emission count would change with the sensitivity of the monitoring device and the location of the transducer.

Tanimoto *et al.* 1978 added to the previous paper by investigating the relationship between acoustic emission and work dissipated in friction. Tanimoto *et al* (1978) stated the assumption that AE is generated from inter-particle friction, and thus might be related to the energy dissipated by friction as a soil sample is sheared The accumulated emission count monitored during a specific period of time was proportional to the accumulated work done, during the same period, by external stresses (work dissipated in friction).

Tanimoto *et al.* (1981) considered the application of acoustic emission for in-situ testing of soils. Repetitive loading triaxial compression tests were performed on decomposed granite to demonstrate the Kaiser stress memory effect (in which AE levels are low until the material is stressed beyond that which it has experienced in the past) could also be applied to soils. Figure 2.16 demonstrates that intensive emissions could only be monitored when the soil sample was in a virgin state of loading. A few emissions were observed in the state of preloading. Similar findings were also produced by Kavanagh (1997).

This effect was further investigated in a pressure metre test in a fill of decomposed granite. Figure 2.17 shows the experiment set up with the transducer (DC 55 kHz) placed within a pressure cell. Figure 2.18 demonstrates the result of analysing the emission counts and three separate threshold levels, 0.25 V, 0.5 V and 1 0 V. AE monitoring is shown here to be an effective tool for in-situ testing, and when shown alongside the pressure metre test results, it is clear that the merit of using AE was that the emission counts underwent a very marked change at particular stress states (yield stress state etc), and thus gave a clearer indication of preconsolidated pressures than the results provided by the traditional pressure meter testing.

Koerner *et al.* (1981) conducted direct shear box (10.2cm x 10 2cm) tests on a well-graded angular beach sand, a river transported clayey silt, and kaolinite clay. A 4mm diameter steel waveguide was placed horizontally in the lower box. Each soil was sheared in intervals (stress controlled tests) under a normal load of 76kN/m^2. The waveguide was connected to a sensor (130 kHz) a pre-amplifier (20 dB) and an amplifier (30 dB). The sand was shown to be the most emittive, then the silt and lastly the clay, these results are shown in Figure 2.19. Further triaxial tests were undertaken to determine the effect of particle characteristics on AE generation in stressed soil samples. Triaxial tests were carried out for granular soils and the fine grained soils.

For granular soils, four types of sands were evaluated within these tests, in order to provide a good range of variation in particle shape and uniformity. The following conclusions were drawn.

- Particle shape: the more angular the soil, the more emittive the sample was under stress. It was also noted that a longer time period was needed for the soil to regain equilibrium (no significant AE produced) after loading.
- Coefficient of Uniformity: As the coefficient of uniformity (U) increased (the soil becomes well graded), the cumulative AE also increased. However, the author also stated that the more angular soils also happened to have the highest coefficient of uniformity. Thus the actual cause of greater emissions might be as a result of both uniformity and angularity.
- Effective size: no firm conclusions were made as the range in effective size of the sands, 0.20 to 0.45 mm, was quite limited.

For fine-grained soils,

- Confining Pressure: Clayey silt and Kaolinite clay were tested at confining pressures of 34 kN/m^2, 69 kN/m^2 and 138 kN/m^2. The tests were consolidated drained, sustained load (creep), triaxial shear tests. Figure 2 20 shows a close parallel in the behaviour of stress/strain and stress/AE curves. Slightly higher AE Count levels being registered for the clayey silt (due to the presence of silt size particles) than for the Kaolinite clay. Thus strain and AE are related parameters that can be used in conjunction with stress to characterise or monitor a given soil.
- Water Content· Clayey silt samples were compacted at different water contents and tested in unconfined compression. Figure 2.21 shows a marked decrease in strength and AE with increasing water content.
- Plasticity Index: Four fine grained soils were tested in consolidated drained triaxial creep at 34 kN/m^2 confining pressure. Figure 2.22 shows the clayey silt (which has the lowest plasticity index) is the most emitted soil, whilst bentonite clay, with a relatively high plasticity index, is the least emitted.

Koerner *et al.* (1981) also carried out some large scale testing on embankment stability. A steel box 1.8m x 1 2m x 0.92m high was constructed with a base made

up of independent movable squares (Figure 2.23). A soil (clayey silt) embankment was constructed within the steel box. As the base was lowered, AE monitoring was carried out until equilibrium was reached, i.e. when AE ceased This was done for varying water contents and it was shown that the maximum AE response was close to the optimum water content of that soil.

Koerner *et al.* (1981) finally investigated the use of AE in testing the bearing capacity of shallow foundations. Figure 2.24 shows the experimental setup and the results for a model footing placed on the surface of dry Ottawa sand. The load was incrementally applied with simultaneous surface deflections and any AE data being recorded. The load/deflection curve show showed a gradual curved response as the soil behaviour moves from elastic to plastic deformation. By contrast the load/AE curves showed a more abrupt transition between elastic and plastic behaviour. Koerner *et al.* (1981) concluded that the AE response curve more accurately described the process of bearing capacity failure than the results obtained using dial gauges.

This state-of-the-art paper produced by Koerner and his fellow authors is the most comprehensive investigation to date into the effect of the physical characteristics of soil on acoustic emission. This paper is further discussed in section 2.7, field trials.

Mitchel and Romeril (1984) recorded acoustic emission from undisturbed block samples of Champlain Sea Clays which were deformed within the laboratory as shown in Figure 2.25. Typically, the hinged wall was deformed no further than 6° from the vertical by both continuous and incremental loading imposed by the load cylinder. AE was measured in terms of its amplitude and its rate of counts. Mitchel and Romeril (1984) concluded that it was not possible to determine the amount of shear stress from looking only at the AE data, but that the AE amplitude and the rate of AE counts were both higher in cases of grained soils than in fine-grained soils. Over consolidated clays with a high liquidity index were found to be not very emittive.

Koerner *et al.* (1984a) was the first in a series of three papers to specifically investigate the potential use of acoustic emission to predict pre-consolidation pressure in the field. Five soils were tested all of which were cohesionless sands or silts. Pre-consolidation loads were applied to a predetermined amount, held until consolidation had virtually ceased, as evidenced by the dial gauge, and then released. Each sample was then immediately reloaded, with each load increment being held for 5minues until the original pre-consolidation load had been exceeded (5 minutes was found to be sufficiently long to so that both deformation and AE ceased to occur). A 175kHz resonant transducer was used to detect any AE as the soil sample was preloaded. A series of 80 tests were carried out on samples at 0%, 30%, 70% and 100% saturation levels. It was found that both AE and deformation responses could predict the original applied pre-consolidation pressure to within approximately 5%

This study showed the use of granular materials to be very acoustically responsive to changes within the stress state. This data was compared with further studies performed on fine grain soils (Koerner *et al* 1984b) in which the pre-consolidation pressure was on average predicted within 10% This measure of accuracy was calculated by averaging the percentage errors of each pre-consolidation test regardless of the soil type or degree of saturation. As such the authors commented that this was not statistically valid, but it provided a simple comparison between the acoustic sensitivities of granular and cohesive soils.

Garga and Chichibu (1990) studied the characteristics of AE parameters during stress path controlled triaxial tests on sands. AE signals were monitored between 0.5 kHz & 30 kHz by a preamplifier (30 dB) integrated low frequency type sensor mounted on the base pedestal of a triaxial cell. A further gain of 40 dB was provided through the main amplifier. The following parameters were recorded: event counts, ring down count, rise time, duration time, peak amplitude, AE energy (E).

Figure 2.26 shows the relationship between energy rate, ring down count (RDC) rate and the event count rate in a typical result. Early on in the test all three rates increased with strain, however the event count rate became nearly constant at

approximately 2 - 4% of the strain. This levelling out of the event rate did not coincide with the strain at which the maximum rate of dilatency of the sample was achieved (as shown by the volumetric strain). As the RDC rate continues to increase with strain, the size of an event must be increasing with strain whilst the number of events remains constant. The authors concluded that event rate could not be used to monitor the progress of failure, but energy rate and RDC rate together provided good indicators as to changes in the characteristics of AE signals, resulting from changes in the volumetric strain, and thus could be used as indicators of failure.

Naemura *et al.* (1990a) undertook large-scale laboratory testing to identify the location of the AE sources and to predict collapse of a retaining wall. A retaining wall 6m high and 8m wide was constructed and held by jacks capable of moving 0.1mm at a time. The wall also contained geotextiles for other monitoring purposes. Sensors were placed one on each end of a waveguide, with up to three waveguides (six sensors) placed within the soil wall. Accelerometers, with an inbuilt pre-amp (30 dB), were used with a frequency range of 0 – 10 kHz and a resonant point at 15 kHz The jacks slowly moved back from the wall at 30mm intervals, each time waiting for equilibrium to be achieved before moving another 30mm. Event count, ring down counts and AE energy were monitored, as well as measuring any cracks that appeared on the surface (Figure 2 27)

A complex active condition was set up in the sand backfill. So each time the wall moved the slope would collapse within its new boundaries and reach equilibrium This process was repeated each time the jacks were released by 30mm. And thus no major failure actually took place.

AE peaked at locations other than on the slip plane. This was thought to be due to sliding surfaces occurring in many places, and due to the presence of the geotextiles preventing a simple sliding surface developing. Event count, RDC and AE energy all peaked after the wall had moved 7.5mm, which was noted to be before the minimum required theoretical earth pressure conditions to cause a definite slide. It was concluded that it was possible to predict the location of a

slide failure, within the embankment, by comparing the source location data from each waveguide. This is demonstrated in Figure 2 28.

Naemura *et al.* (1990b) carried out a study to examine the applicability of AE to judge the ground soil condition for the boring of small diameter holes. Four soil samples were placed in a tank (700mm deep) in compact or loose conditions. A rod equipped with an AE sensor was pushed into the soil sample at a specified speed (see Figure 2.29) The compact condition meant that the maximum drying density was 85% or more, whilst a loose condition implied that the soil was placed into the box by freefall from a height of 1m.

Figure 2.30 shows that the AE amplitude for gravel varied between its 1.6 V – 2 V, and was higher than that of sand 0.4 V – 0.8 V. Based on ring down counts Figure 2.31 shows a clear relationship between total AE counts and the particle size which exceeds 50% of the sample soil. Further conclusions were inhibited due to different threshold levels being selected for different soil types. Analysis of the frequency spectrum is discussed in section 2.3.4 of the literature review.

2.5 Field investigations

The use of acoustic emission for monitoring soils started as far back as 1961. Beard (1961) reported the use of AE to predict the onset of failure in a soil mass. Beard's work was primarily concerned with rocks, and found that higher magnitudes of AE were emitted as instability increased. Beard concluded that soft materials such as sand, clay and mud (i.e. soil as opposed to rock) did not produce acoustic emissions that were clearly definable. Since then a large amount of work has been done in both the laboratory (see section 2.4) and in the field as detailed below.

McCauley (1977) investigated the application of AE monitoring to two sites in the USA AE was recorded by placing transducers 10 to 15 ft. (3-4m) below the surface, for 15 minutes the emissions were recorded as counts per minute. The sensitivity of the transducers was not reported, but the frequency response of the

monitoring system was described as ranging from 4 to 40,000 Hz. In general, McCauley concluded the following;

- Rock and earth slopes can and do emit detectable noises
- A given slope will emit more noise in an unstable condition
- AE rates alone are not sufficient for evaluating slope stability
- Changes in AE rates indicate changes in stability

At Kern Canyon, construction of a new road was cut into the natural slopes (gradient 1.2 in 1) of weathered granite rock. Failure occurred along a 40° plane within the rock and resulted in 8 in. (200mm) of displacement. Transducers were drilled into the rock in six locations and revealed significant activity which led to the decision to take remedial action.

At Thornton Bluffs, California, a segment of coastline (consisting of poorly consolidated marine sand, silt and clay), 150 metres high and with a slope angle of 30° to 45° was subject to continuous erosion at the base of the cliff resulting in a rotational failure. Six transducers were placed in hand augured bore holes, and these were monitored twice a week. Figure 2.32 shows the results of the monitoring, with SARN SI-3 referring to counts per minute whilst readings denoted NAIL POINT #6 and SI-3 AT 95' refer to displacement readings in inches. The sudden increase in AE recorded in December 1972 suggested an increase in activity within the slide about a month before evidence was available from other monitoring techniques. McCauley concluded that AE could be used to monitor stability, but was most effective when used in conjunction with other monitoring techniques.

Koerner *et al.* (1981) investigated using AE to monitor dam and embankment stability. Five case studies were undertaken.

Case Study 1: A stockpile was purposely brought to failure. A 4.6m high stockpile consisting of a well-graded silty sand soil fill was brought to failure by successive excavations from the toe of the slope, see Figure 2.33. Waveguides, 13mm

diameter, were placed within the slope to aid monitoring. After each cut the excavator left the site to minimise the background noise. After 5 cuts and 21 days the stockpile failed. AE generally increased after each cut, with a high initial rate of emission followed by an exponential decay. The fifth cut followed the same pattern, but after an extra 30 min. the AE rate increased rapidly up to failure and then returned to a normal curve (see Figure 2.34). Failure occurred as a large wedge shaped section of soil pulled away from the intact mass and slide down the remainder of the slope. Failure was accelerated due to rainfall which occurred after the forth cut. It was concluded that a loss of stability in slopes is not a linear process, but one in which instability progresses at an increasing rate as failure is approach, as demonstrated in Figure 2.34.

Case Study 2: A dam containing a storage lagoon was monitored. Steep sided embankments, varying in heights from 2.4m to 6.1m formed the side of a chemical waste lagoon. The embankments were built on a silty sand with a low SPT value. AE data was detected and recorded via twelve 13mm diameter waveguides, 1.2m in length, which were 'pushed' into the ground. Monitoring had shown that activity was present, but that count rates varied considerably. Figure 2 35 shows the response of a waveguide at the toe of the slope where a failure occurred in January 1976.

Case Study 3: Study of a dam containing a water reservoir. Whilst an old Dam was emptied for repairs, seepage induced failure occurred due to a high surrounding water table. Movement was very slow and thus there was time to put in place an AE monitoring system, which was able to monitor the failure for a month despite the fact that almost 30 - 60mm of settlement had already occurred at this stage. Low rates of AE reflected the nature of the clayey soil, probably because of the mobilisation of 'slicken-sides' on each side of the failure plain where the individual plate like clay particles aligned themselves with the failure plane. Such a condition was considered to be not as 'emittive' as in granular soil.

Case study 4: Monitoring of the horizontal movement of trench walls. In order to evaluate the use of AE in trench walls, three trench walls were constructed and brought to failure by use of an excavator. Three different monitoring techniques

were tested, they are illustrated in Figure 2.36. Firstly a hydrophone was placed freely at the bottom of a casing filled with water, secondly a 30 kHz transducer was taped on the outside of the casing above ground level, and thirdly a transducer with a flat response between 0.1 – 30 kHz was wedged against the inside of the casing wall. Each trench was brought to failure by a loader bearing on the top of the trench wall. The Authors made no comments on the merit of using each monitoring system, but all three successfully recorded increases in AE activity during failure. Conclusions were made on the frequency of the generated AE and sensors were recommended to be responsive between 1 kHz and 30 kHz.

Case Study 5: Vertical compression due to surcharge fill. Surcharge was placed upon a pile to monitor its consolidation. The pile itself was used as a waveguide plus an extra waveguide, which was installed within a case so that AE would only be picked up from the tip of the waveguide and thus within a specific stratum. The soil produced many emissions when in an active state, but declined once equilibrium was achieved. Site set up is shown in Figure 2.37.

Koerner *et al.* (1981) concluded with the following qualitative classification system for soils that,

a) Generate little or no AE – Probably not deforming but in equilibrium
b) Generate moderate levels of AE – deforming slightly but are marginally stable, continued monitoring is necessary.
c) Generate high levels of AE – Substantial deformations, considered unstable, immediate remedial measures required.
d) Generate very high levels of AE – Undergoing large deformation and probably in a state of failure.

However, terms such as 'little, moderate, high and very high' are all relative terms and thus impossible to define. A qualititive scale would be required in order to translate this scale to different geological/geographical sites.

AE monitoring of landslides at Kanisawa field, Mayagi Perfecture, Japan was carried out in 1982 and 1983. Yuda *et al.* (1984) successfully identified unstable

soil blocks, which were monitored before and after landslides occurred. The landslides were triggered by concentrated heavy rains, which weakened the alternate layers of tough, silt and sandstone. A piezoelectric accelerometer was placed on a carbon steel rod (1 – 2 m long) which was driven into the soil as a waveguide. They AE was monitored within the range of 1.6 Hz to 7 kHz and recorded as ring down counts, over a period of 20 minutes per location.

Yuda *et al.* (1984) describes two types of AE event, the first had a frequency greater than 1kHz thought to be generated from friction between small particles of sand and rock. The second type of event had a lower frequency of about 200 Hz, which was thought to result from the slip plane. The measured AE activity distribution across the landslide was in agreement with empirical measurements.

Forrester (1987) used piezometric levels and AE activity to demonstrate the effective stabilisation of a failed slope. The construction of Carnley Avenue, New South Wales Australia, had brought on instability by excavating the toe of the slope, and the onset of substantial rainfall. The geology of the slope consisted of a conglomerate cap over successive layers of coal, clay, coal and sandstone. A series of horizontal drains and a toe restraint structure were used to stabilise the slope.

The slope was monitored by immersing transducers in water, usually within a borehole. Over a period of five minutes the event count rate was recorded within a frequency range of 4 Hz to 17 kHz. Readings were taken before the horizontal drains were constructed and subsequently after their placement. Post stabilisation, all but one of the nine boreholes monitored demonstrated a reduction in the recorded event rate. AE was used to pinpoint areas of greater instability, and when used alongside piezometric readings gave a good indication as to the effectiveness of the remedial works.

Chichibu *et al.* (1989) investigated a slope failure (in mudstone). Excavations at the toe of the slope caused a sudden failure even though a previously installed monitoring stake had indicated minimal movement (less than 5 mm). Consequently, an embankment was immediately constructed at the exposed

surface in order to prevent further failure (see Figure 2 38). As A ground surface displacement meter and a borehole inclinometer were installed alongside an AE monitoring programme.

The counterweight embankment was monitored by an accelerometer (with a frequency range 1 – 30 kHz) mounted on a 5.5 m steel reinforcing bar waveguide, which was driven into the embankment. The horizontal and vertical movements were also measured by installing a stake close to the waveguide. Initial results showed an increase in AE activity and a displacement rate of 2.7 millimetres per day so an additional embankment was constructed to support the first (November 15). Four days later the AE count rates almost diminished to zero, implying that overall stability had been achieved (see Figure 2.39). Heavy rains on November 26 caused the onset of movement, and the AE rates increased rapidly. Within two weeks after the embankment started to move, AE activity diminished and horizontal movement of the stake became small.

The natural slope was also monitored (Figure 2 40) using a ground displacement meter, a borehole inclinometer and a 17 m long reinforcing rod waveguide which was installed into a borehole and back filled with mortar. Figure 2 41 shows the daily results. High AE activity was continually observed during February and March despite the measured displacements being small. The authors concluded that the AE was produced by micro cracks within the mortar backfill, which although it could be a precursor to slope failure, were undetected by the ground surface displacement meter.

From the first of March AE monitoring was started at a new position by lowering the transducer to a depth of 20 metres within the inclinometer borehole. High readings of the AE activity were immediately recorded, and were considered to be a precursor to slope failure. However, the authors also commentated that AE activity was decreasing (late March to early April) when displacements had become significant. This might be explained by the nature of the waveguide. Once significant displacement had occurred, i e. the grout surrounding the waveguide had cracked, then further movements would only result in opening the cracks, which would only generate low levels of AE.

Large-scale fieldwork was carried out by Rouse *et al.* (1991). Two landslip areas in South Wales were monitored for AE, Pantteg and Glynrhigos. Both were in a general state of instability. In both cases thick superficial deposits overlay rock strata, which acted both as an aquiclude and an aquifer.

Monitoring system in both landslides consisted of:
4 Accelerometers
1 Hydrophone
Signal passed through the line drivers to an analogue recorder
Digital oscilloscope (on-line monitoring)

Steel waveguides were placed in boreholes filled with water The presence of the water was to improve the transmission of the AE into the waveguide.

It became apparent that many events were generated by noise within the system, this had a significant effect on the data as the signal to noise ratio was close to one. Most of the AE was within a bandwidth of 1 – 7 kHz with various peaks in between. Marked changes were observed after rainfall periods, which resulted in an increase in AE. The reason for this could be two fold. Firstly due to a decrease in stability brought on by the rain, or secondly due to a decrease in attenuation caused by the presence of water. The time delay between maximum rainfall and the maximum AE may represent the time it takes for the soil to reach saturation levels.

Precursory activity could be detected before a failure, and even during periods of slow movement, significant AE was present. The field trials demonstrated that four distinct types of pedogenic AE existed with frequencies generally within 1 – 7 kHz, with particular peaks at 1.2, 2 0, 4 2, 4.9, 5.5 and 6.5 kHz. These frequencies were expected to change with soil types.

Dixon *et al.* (1996) completed two field trials in response to the need for developing a waveguide that produced measurable AE at small prefailure strains,

and also to develop a portable system to use on site. The AE monitoring instrumentation used in both sites is detailed below.

30 kHz Sensor
Pre-amplifier 40 dB
Band pass filters 15 - 45 kHz
Amplifier 50 – 108 dB
Signal rectifier

Case study 1· Cowden test site, on the NE coast of England, consisted of 20m high cliffs made up of stiff cohesive (high sand content) glacial till. Two inclinometers plus twelve 50mm diameter steel tube waveguides were placed in 150mm diameter boreholes and back filled with one of three materials; Bentonite grout, medium sand or fine gravel. Their layout in relation to the later developed rear scarp of a failure is shown in Figure 2.42. The lengths of the waveguides were sufficient to penetrate any potential shear zone. Control waveguides were placed back from the slope to monitor background noise. AE recording lasted three minutes at a time but due to a slip/stick mode of failure cumulative changes in the main parameters were used for analysis, this missed any local variations in the data, i.e. between periods of monitoring.

Initial pre-failure readings were taken from the inclinometers, however the quality of AE data recorded at that time made it impracticable to determine whether the AE had also detected the pre-failure movements. Over the next 6 months data was compared between the displacements recorded from the inclinometers and the cumulative area under the AE signal for waveguides 1, 2 and 3 (Figure 2.43). This comparison showed a strong correlation, as rates of displacement increased, so did the rate of change of cumulative area with time

Tests at Cowden proved that a direct relationship existed between the produced AE and the type of waveguide. Those with grout backfill (passive) produced the least AE, then the fine gravel (active), with the medium sand (active) producing the most AE. Thus AE was detected from deformations in the backfill instead of

those from the host soil. Pre-failure couldn't be monitored as the site was in a state of pre-failure before instrumentation was fully operational.

Case study 2: Arlesey test site. A brick pit formed in Cretaceous Gault Clay (heavily over consolidated deposit) provided a 4.5m slope instrumented with 6 waveguides and 2 inclinometers. Failure of the slope was brought about in a controlled manner by excavating from the toe Figure 2.44 shows the location and the instrumentation relative to the slope cuts. A total of 5 cuts were made before monitoring was discontinued. The inclinometers showed that small movements only began 24 hours after the 4th cut was made. High levels of AE were recorded after cuts 4 and 5, however continuous monitoring would have given a more complete picture.

Active waveguides were used because of high attenuation within the soil, due to its cohesiveness, and expected slow strain rates during pre-failure. Data was analysed by calculating the standard deviation of the AE counts recorded (Figure 2.45). By measuring the standard deviation of the data, additional periods of activity were identified in response to the cuts. The results indicated that if a continuous monitoring system was used, then prediction/monitoring of pre-failure deformations would be viable

In 1989 the Public Works Research Institute (PWRI) and the Ministry of Construction in Japan, launched a joint research project entitled 'Study on AE monitoring system for slope failure.' Two types of AE systems were used. 1) Simplified type, which recorded hits and amplitude distribution, and 2) A system, which recorded individual waveforms in addition to the no. of hits. This was used in conjunction with passive waveguides, whose materials and length was selected in accordance with the geographical features, size and configuration of the given slope. Two slopes were monitored, Kisarazu from June 1997 to August 1997, and Kagoshima in October 1997. (PWRI, no. 73, 1998)

The monitoring systems included 60 kHz sensors for small areas, 20 kHz sensors for larger areas. All sensors were insulated and buried in the ground to minimise noise caused by climatic factors. Waveguides were hammered

into the ground. Two separate parameters were recorded; No. of hits per unit time and Ib-value. The Ib-value is a parameter that takes into account the number of peak amplitudes that occur within a given time, and the amplitude distribution of those peak amplitude events. This statistical representation of the AE data was found to be very sensitive to slope conditions, and can provide an indicator of slope failure. Source location was to be carried out by using multiple waveguides.

The PWRI documented further field trials on the Shirasa Slope collapse (PWRI, no. 73, 1998). The geology of the area was made up of non-molten sedimentary rock placed there by a pyroclastic flow some 20,000 years ago. Excavating at the toe of the slope triggered an artificial collapse. Six, 60 kHz resonant type sensors, 4 with waveguides and 2 directly buried, were aligned in the slope along with 3 inclinometers and 2 extensometers. It took 5 cuts over a period of 6 hours to bring about failure

At 30 minutes prior to failure the count rate increased exponentially, while the event rate decreased. It was thought that the large amounts of AE being released must have superimposed themselves on other waveforms and thus individual hits were hard to distinguish. It is interesting to note that by plotting the reciprocal of the count rate it was possible to predict the time of failure.

In 2000, the joint research by the PWRI and The Ministry of Construction, confirmed that 15 kHz and 60 kHz sensors had been buried within the slides at Kisarazu and Kagoshima. The report could not determine which was the more effective sensor, but concluded that it was able to detect when the slope became more unstable as it approached failure. On site endurance testing was done on the sensor against lightning damage, electrical ground current and its water receptivity. It was also stated that a back up power supply was also necessary, and real time, remote observing was to be done utilizing the telephone circuit (PWRI, no 81, 2000).

2.6 Methods of source location

The ability to know the depth from which AE has propagated is crucial in considering the factors that have affected the waveform between its source and receptor. Within a landslide it not only provides the depth of any movement, and hence likely mechanism of failure and possible consequences of failure, but is also necessary in order to apply the correct amplification and correction factors to any incoming signal in order to standardise that signal for any further analysis. A great deal of work has been done in recent years on this area, with the most notable contribution by Maji *et al.* (1997), on performing source location with a single AE sensor arrangement, and by Alleyne *et al.* (1997) with their contribution on detecting defects within pipes using Lamb wave propagation.

Within any monitoring system, the form of the original wave is profoundly changed during propagation through a medium, the signal emerging from the sensor has little resemblance to the original pulse. This must be taken into account when analysing waveforms. The transformation of the AE waveform is important both to the researcher interested in source function analysis and to the practical NDT inspector interested in testing structures (Pollock 1989) date unknown).

"The researcher interested in determining the original source waveform uses broadband sensors and performs a detailed analysis of the early part of the received signal. There are many difficulties associated with this, primarily the nature of the geometry of the signal. The NDT inspector is interested in the broader statistical features of the AE activity and does not need to know the precise details of each source event. Thus narrowband sensors and electronic equipment that measures only a few features of the received waveform are used. Source location is performed instead by using a number of sensors and considering the arrival times of the same event at different sensors By calculating the relative arrival times of the AE wave at several sensors, it is possible to locate the source either to within a particular zone or to a particular point. The attainable accuracy of such a system is governed by wave propagation processes and depends upon such factors as geometry, plated thickness, and any contained fluids

within the structure or waveguide These factors often render the wave velocity uncertain and hence lead to errors in source location." Pollock 1989.

Hardy *et al.* (1989) experimented with the concept of a dual transducer waveguide in rocks. Such an arrangement uses the waveguide to propagate AE events from a rock fracture source to a transducer on either end of the waveguide. (see Figure 2.46). The time of arrival at each transducer would depend on the location of the source and the propagation velocity of the waveguide material. The difference in arrival time at the two transducers, the velocity characteristics of the waveguide, and a suitable one-dimensional source location method made it possible for Hardy *et al* (1989) to locate the source of a fracture/movement. Figure 2.47 shows the experimental set up and typical results. With a suitable array of waveguides, it would be possible to map the location of an active failure surface.

Nakajima *et al.* (1991) devised a composite monitoring waveguide, already discussed in section 2.3.3, from which AE would propagate to both ends of the waveguide, and would be detected by a sensor at each end. Nakajima *et al.* (1991) performed a bending test on the waveguide material (resin and glass fibre thread). One dimensional source location analysis was done on the AE produced as a result of these bending tests. The results are seen in Figure 2.8. The histogram of acoustic events and the diagram of bending moment have a similar distribution. Nakajima *et al.* (1991) implied that the histogram of acoustic events can be transformed into the deformation of the waveguide, and hence determine the point of load acting upon the waveguide.

Nakajima *et al.* (1991) successfully installed a 50m long waveguide in the Numamae Landslide, Hokkaido, Japan. Strain gauges were pasted onto the waveguide at half metre intervals. Figure 2.48 demonstrates the relationship between these strain measurements and the one dimensional source location on the incoming AE. Acoustic emission is concentrated at the depth of 35 metres in each histogram. In Figure 2.48 it was not possible to determine the depth of sliding on day 16 or day 23 from the strain gauges alone, where as it was very clear from day 12 based on the one dimensional source location. Nakajima *et al*

(1991) concluded that the use of acoustic emission for detecting the depth of movement within a landslide, was more sensitive than the pipe strain gauges.

Common source location monitoring strategies encompass a network of AE sensors positioned at different points on or around a structure to enable the source to be pinpointed. Labuz *et al.* (1996) used an acoustic emission system with four sensors to locate the source of AE to within 3 millimetres for rock and concrete slabs. By knowing the relative arrival times of the P-wave (longitudinal wave), which is the component of the signal that arrives first, the P-wave velocity of the material and the coordinates of each receiver, the event source can be estimated with a minimum of four sensors. In this study, rock specimens were brought to failure under uniaxial compression and four-point bend loading. The AE signals were captured using piezoelectric transducers attached to the specimen surface and preamplified (40 dB gain) before recording. The sensors had a flat frequency response from 0.1 – 1 MHz.

The results of the test on a charcoal granite specimen under uniaxial compression are shown in Figure 2.49. With the use of a high-speed data acquisition system, localised zones of deformation were identified (in real-time) prior to visual observation.

In a solid, AE typically travels as bulk waves (longitudinal and shear) which propagate in 3-dimensions and will thus radiate energy three dimensionally. Therefore, if excited from a point source, their amplitude decreases inversely as a function of distance squared. In contrast, Lamb waves are guided along a plate and thus no lateral spreading can occur and the propagation is essentially one-dimensional. Lamb waves propagate in one dimension, minimising attenuation and making them ideal for performing source location over large distances.

Maji *et al.* (1997) carried out work on the propagation of plate waves. Where two parallel surfaces exist, as is the case in a plate, then Lamb waves become the predominate mode of propagation. Maji *et al.* (1997) investigated the use of AE on steel beams and plates to monitor cracking, defective connections and overall fatigue. Rather than using P-waves, Maji *et al* (1997) explored the use of Plate

wave modes (Lamb waves) and in particular the arrival of different frequency components.

Two extreme conditions exist for plate wave propagation. At very low frequencies where the wavelength is much larger than the thickness of the plate, then plane longitudinal and shear waves propagate. If the wavelength is much smaller than the plate thickness, then bulk waves are set up in the interior of the plate while Raleigh waves are excited on the surface. It is between these extremes that numerous Lamb wave modes propagate (i.e. where the wave length is similar to plate thickness). For a typical AE frequency of 200 kHz, the wavelength is about 2.75 cm (corresponding to a bulk longitudinal wave speed of 5,500m/s) which is very similar to the thickness of a steel structural member. This leads to the formation of dispersive plate wave modes that travel long distances with little attenuation, and hence are more easily detected at greater distances. A typical tube thickness ranges from 1 – 6mm.

Lamb waves travel in an infinite number of modes, these modes belong to one of two groups; Symmetrical and Asymmetrical. In Figure 2.50 the modes L_{11} and L_{12} are symmetrical about the centre line of the propagating plate (these are longitudinal modes) whilst L_{21} and L_{22} are asymmetrical (flexural modes). The velocity at which these modes propagate is a function of the plate thickness '*t*' (mm) and the frequency of the emission '*f*' (MHz). As the waves propagate, the different frequencies disburse and propagate at different velocities.

Maji *et al.* (1997) exploited the use of Lamb waves for source location purposes. The technique involved determining the separation of two frequency components within the same AE event at a single transducer. Knowing the propagation velocities of these two Lamb wave modes, the source to transducer distance was determined.

A Physical Acoustics' 'R15' transducer was used because of it's high signal to noise ratio. This sensor exhibited resonant frequencies at 100, 160 and 240 kHz. As the AE event was monitored with increasing distance from its source, Maji *et al.* (1997) observed a progressively larger separation of the 100, 160 and 240 kHz modes. By determining the difference in arrival times of two frequencies, the distance to source could be found. Equation 2.3 below was used to determine this distance.

$$\Delta s = \frac{\delta t}{\left(1/C_1 - 1/C_2\right)} \qquad [2.3]$$

Where:

Δs = Distance to Source

δt = Difference in arrival times of frequencies

C_1 C_2 = Velocities of the two frequencies

In order to establish these resonant frequencies, a Fast Fourier Transform (FFT) was performed on the incoming AE. An FFT provides a frequency spectrum of the signal. Another technique using Lamb waves, is to consider the arrival of the first two modes at a sensor within the same frequency range. This technique was used in part by Alleyne *et al* (1995) to detect corrosion in chemical plant pipe work, and by Kousteni (2002) on soil samples.

Alleyne and Cawley (1997) used a ring of transducers around a pipe to excite stress waves which would propagate along the pipe in the form of cylindrical lamb waves. The same transducers would then monitor the response of the pipe for changes in the received signal, which would indicate the presence of an impedance change (caused by possible defects) within the pipe.

Figure 2 51 shows a group of velocity dispersion curves over the frequency range of 0 to 100kHz for 152mm nominal bore, steel pipe with a wall thickness of approximately 7mm. The group velocities of each Lamb wave mode displayed in Figure 2.51 is a function of the plate thickness of the pipe as well as the frequency. This is the same as that described above by Maji *et al.* (1997) concerning plates (a pipe is assumed to act like a cylindrical plate). Note the difference in labelling of the modes by Maji *et al.* (1997) and that used by Alleyne and Cawley as described below. Each Lamb wave mode is denoted by the following labels $L_{(n\,m)}$, $T_{(n,m)}$ and $F_{(n,m)}$, where L, T and F relate to longitudinal, torsional and flexural type notes respectively. In a cylindrical system there may be an integer (n) number of wavelengths around the circumference, n = 1,2,3,4... n = 0, the system is axially symmetric and when n > 0 the propagating waves have components in both the circumferential and axial directions. The integer (m) denotes the number, or rank order, of the mode.

Alleyne and Cawley (1997) successfully excited and propagated $L_{(0,m)}$ modes over distances of 50m, detecting welds, flanges, pipe bends, and hence showing great promise for detecting defects.

Kousteni (2002) investigated the use of an active waveguide for landslide monitoring and in particular the ability of the waveguide to detect the depth of a shear plane within a landslide. Kousteni used Lamb wave modes to perform single sensor source location on AE events. The instrumentation composed of two 1.63 m sections of 6mm wall thickness and 60 mm diameter steel tubes, which were connected by a steel threaded collar. The entire waveguide was held above the ground on wooden supports. AE was generated by breaking a 0.3 mm pencil led of 3mm length at a constant angle (enabling a consistent reproducible event, ASTM 2001). A 30 kHz resonant transducer was coupled to the waveguide, to detect the first two Lamb wave modes to arrive, S_0 and a_0 travelling at 5500 m/sec and 3050 m/sec respectively (see Figure 2 52). Analysis was performed on the early part of the AE arriving from pencil lead breaks at 0.36, 0.54, 0.72, 0.90 and 1.08 m from the sensor. Figure 2 53 shows a linear relationship between

propagating distance and arrival times, which shows a clear indication of a constant velocity difference between the fastest mode (S_0) which triggers the clock, and the flexural mode (a_0) which arrives with a high amplitude.

Similar experiments were carried out with the transducer moved further away from the edge of the waveguide in order to investigate the effect of any possible reflections from the end of the waveguide on the arrival of modes S_0 and a_0. These results are shown in Figure 2 54. The slope of the line in both Figure 2.53 and 2.54 are very similar, indicating that there was no interference of reflections. Kousteni successfully performed source location analysis on other Lamb wave modes, however these tests were only performed over distances of less than 1.6 m.

The use of lamb waves as a technique for propagating AE has been shown to be both a viable and practical means of source location. Further work however is needed to investigate its potential use on AE emitted from soil. Note that for the purpose of clarity; the remainder of this thesis will use the Lamb wave notation set out by Alleyne and Cawley (1997) as shown in Figure 2.51.

2.7 Chapter summary

This chapter has outlined pertinent studies relating to the development of techniques for the application of AE in landslide monitoring Chapter 1 highlighted the need to move from qualitative research to quantitative research Event count rate, ring down count (RDC) rate and energy have been shown to be effective indicators of changes within the stress state of a soil body, and as potential pointers of slope failure. Garga and Chichibu (1990) concluded that parameters such as energy rate and RDC rate could provide good indications as to changes in the characteristics of AE signals, which result from progression to failure of a soil body. A particular contribution was provided by Tanimoto and Noda (1977), by measuring the count rate of sand under triaxial compression. By producing a modified parameter 'R' based on the count rate, a linear relationship

between time to failure and emission rate R was found to exist irrespective of strain rate.

A key aspect in the advancement AE as a monitoring technique has been the ongoing development of the waveguide. Various types of waveguides have also been discussed; two generic models have been suggested, 'active' and 'passive'. The active waveguide has been shown to have the advantage of being able to be used within 'quiet' soil slopes, as the generating medium is replaced with a 'noisy' backfill. Passive waveguides lack the ability to be driven to significant depths, and if placed within boreholes, great care is needed to backfill around the waveguide in such a way as to recreate surrounding soil conditions.

Variations on these were also considered A grout backfilled waveguide was put forward by Chichibu *et al.* (1989), however the long monitoring ability of such a waveguide was limited beyond failure of the grout after which ongoing deformation could go undetected. A water filled waveguide was suggested by Nakajima *et al.* (1991) to reduce the attenuation suffered by propagating AE. Installation of this would be highly complicated especially at great depths, and the waveguide is vulnerable to leaks. Field trials by Kavanagh (1997) demonstrated use of the active waveguide backfilled with granular material to be relatively straightforward to install, and sensitive to pre-failure deformations

The most notable contribution in terms of field monitoring was provided by Koerner *et al.* (1981) and Dixon *et al.* (1996). Dam embankments, stockpiles of soil, trench walls and sea cliffs were all monitored, and all demonstrated that AE instrumentation was robust enough to be used outside of the laboratory. AE monitoring was validated by the presence of other sub-surface instrumentation, particularly at pre-failure deformations, where traditional techniques were unable to detect or locate movement.

The use of a single sensor source location technique has been shown to be very effective when measuring Lamb waves propagating along a pipe wall. The technique has been applied to structural steel monitoring (Maji *et al.* 1997), chemical pipe monitoring (Alleyne and Cawley 1995) and to the active waveguide

(Kousteni 2002). However, Kousteni (2002) was only able to perform source location over waveguide lengths of less than 1.6m.

This investigation builds on the research described within this chapter. Particular areas in need of further development include. the use of single sensor source location over longer lengths of a waveguide, and the use of AE parameters such as count rate and energy to provide a quantified indication of slope stability. Consideration towards the development of slope monitoring protocols is also needed to produce a standard for the use of AE monitoring instrumentation.

Technique	Provide an early warning	Identify mode of failure	Quantify rate and magnitude of movements	Produce false alarms
Acoustic emission	YES	Possibly	Possibly	Unknown
Surface extensometer	YES	Possibly	YES	Unlikely
Inclinometer (read by site operative)	In some cases only	YES	YES	Unlikely
Inclinometer (continuously read)	YES	YES	YES	Unlikely
Rainfall thresholds	YES but only on a regional scale	NO	NO	YES
Surface surveying (automated/by site operative)	Possibly	Possibly	YES	Unlikely
Tiltmeter (e g electro levels)	YES if movements are rotational	Possibly	Partially	Possibly
Time Domain Reflectrometry	YES if calibrated	Partially	NO	Unlikely

Table 2.1 Comparison of slope monitoring techniques.

Method of Connection	Percentage Amplitude Loss at Connection
Welding	22.2%
Brazing	27.8%
Silver Soldering	38.2%
Clamping	71.3%
Clamping with solder pillow	67 3%

Table 2 2 Amplitude loss at waveguide joints as a function of connection method (Hardy 1992).

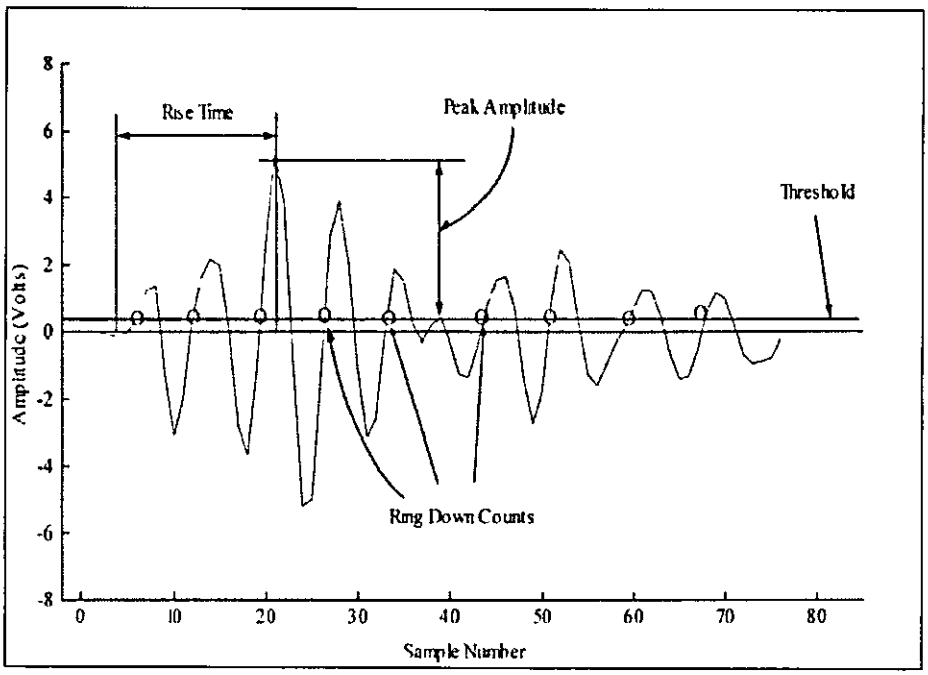

Figure 2.1 A Typical AE event waveform and envelope with main parameters defined (Dixon *et al.* 1996)

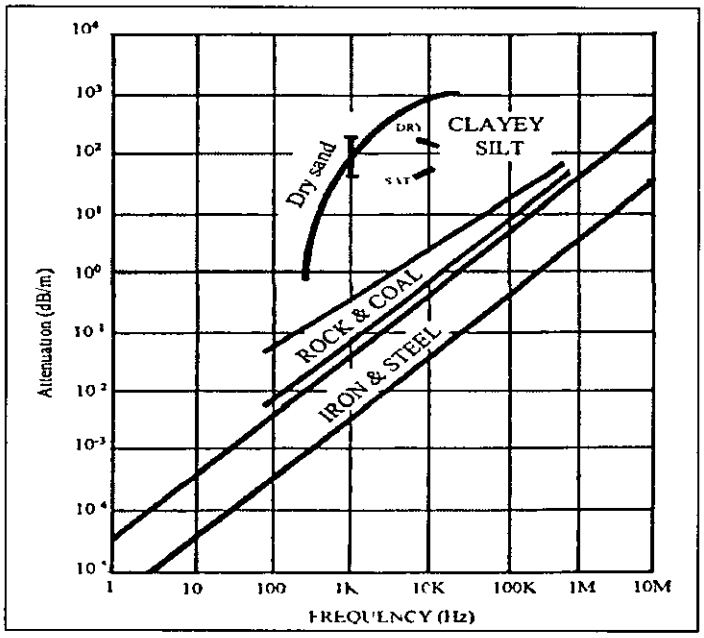

Figure 2.2 Attenuation response of different soil types contrasted to rock/coal and iron/steel (Koerner *et al* 1981)

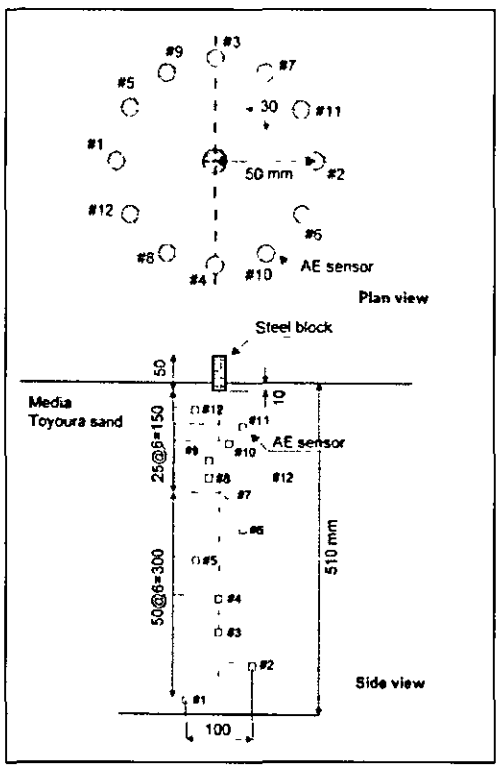

Figure 2.3 Experimental set up of AE attenuation in sand (Shiotani & Ohtsu 1999)

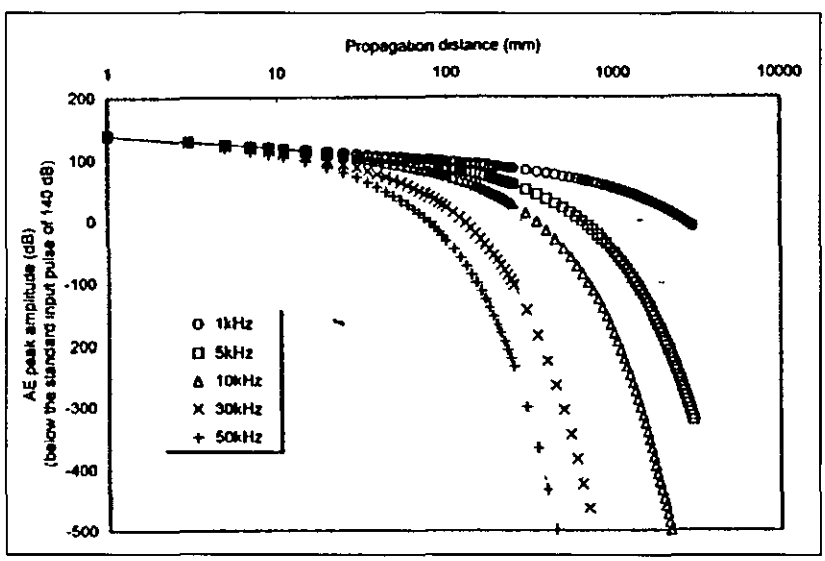

Figure 2.4 Relationship between the attenuation of sand and frequency (Shiotani & Ohtsu 1999)

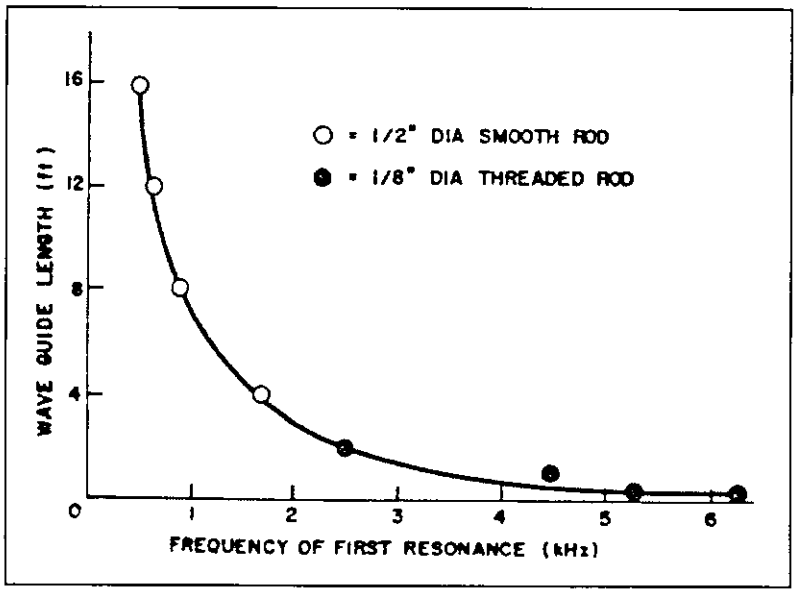

Figure 2.5 The influence of various lengths and diameter of steel rod wave guides on acoustic emission response (Koerner *et al.* 1975)

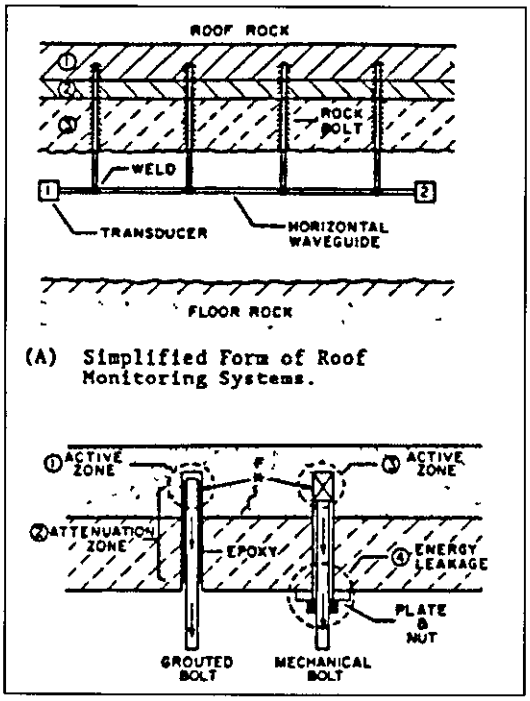

Figure 2.6 Roof monitoring System (Hardy 1992)

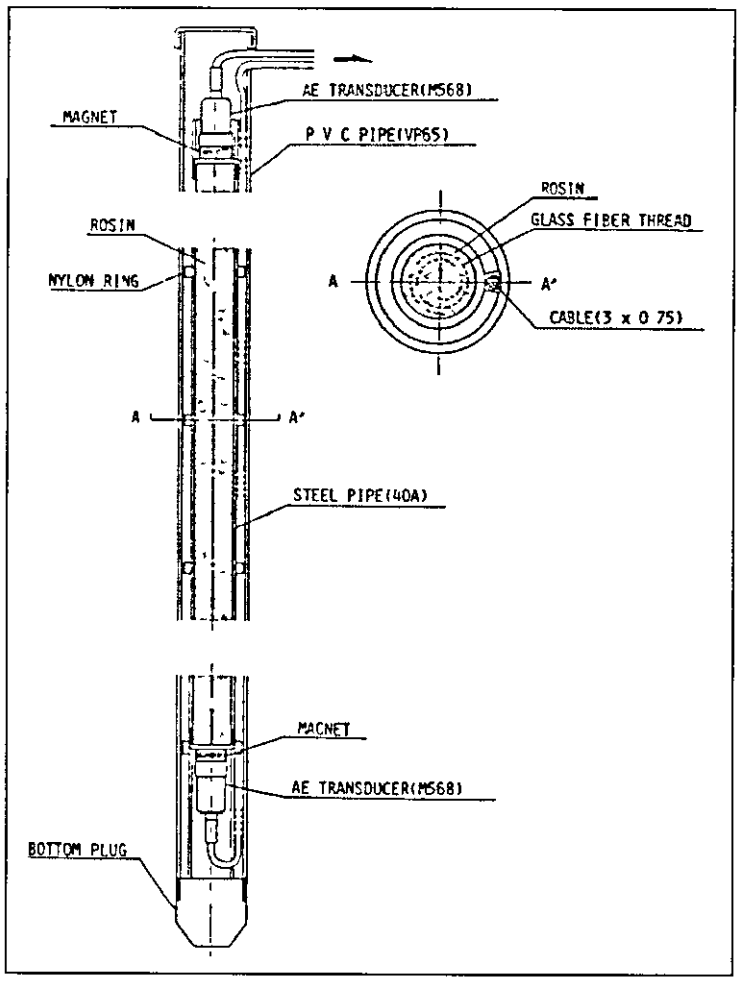

Figure 2.7 Structure of the acoustic emission monitoring rod (Nakajima *et al* 1991)

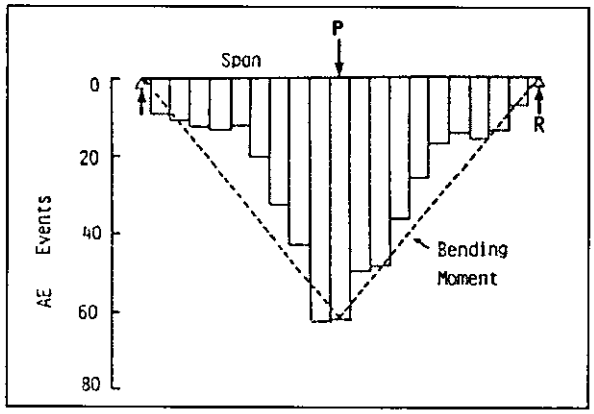

Figure 2.8 Location histogram of acoustic events on span and diagram of bending moment (Nakajima *et al.* 1991)

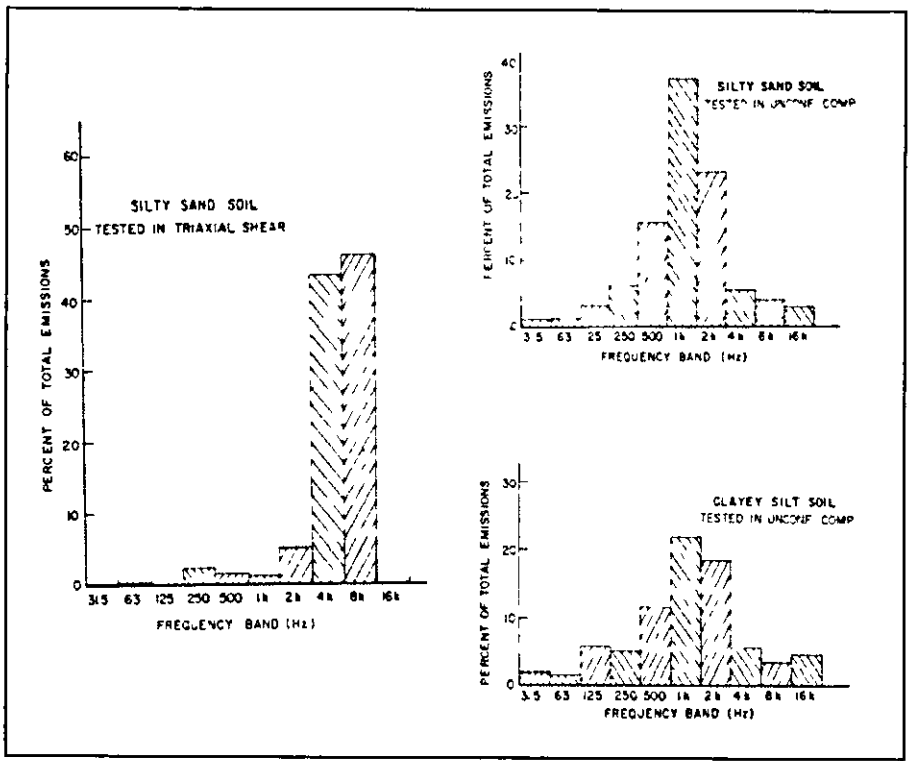

Figure 2.9 Frequency distribution of acoustic emissions response from unconfined compression test (Lord *at al.* 1977)

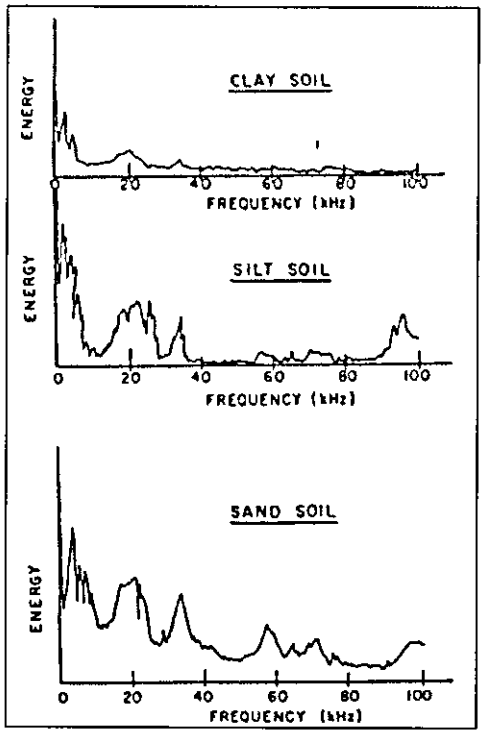

Figure 2.10 Frequency spectra of sand, silt and clay near failure (Koerner *et al.* 1981)

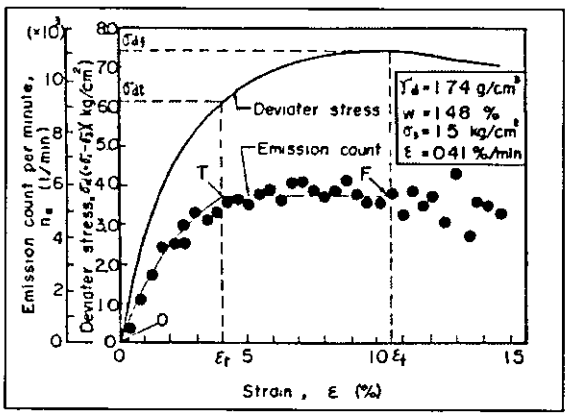

Figure 2.11 Emission count per minute, deviator stress and axial strain relationship in strain control tests (Tanimoto & Noda 1977)

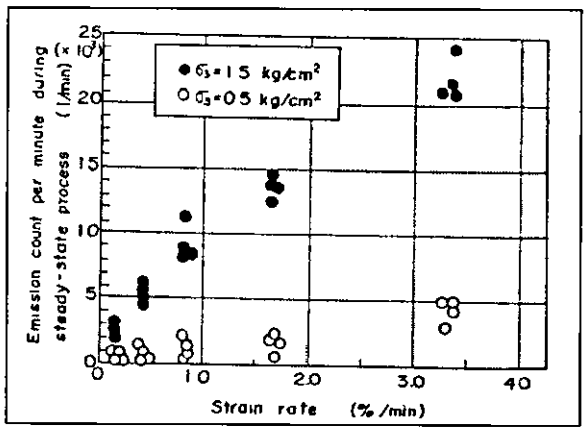

Figure 2.12 Relationship between strain rate and emission count per minute monitored during steady-state process of strain tests (Tanimoto & Noda 1977))

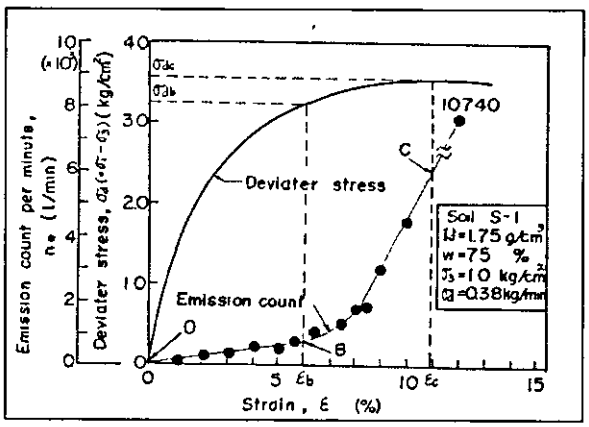

Figure 2.13 Emission count per minute, deviator stress and axial strain relationship in stress control test (Tanimoto & Noda 1977)

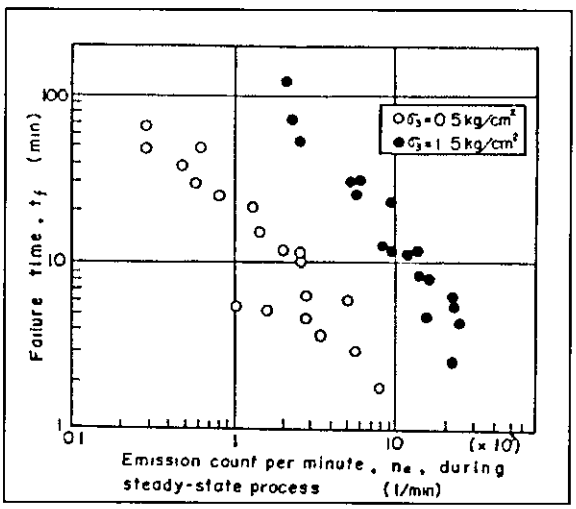

Figure 2.14 Prediction of failure time by emission count per minute monitored during steady-state process of strain controlled tests (Tanimoto & Noda 1977)

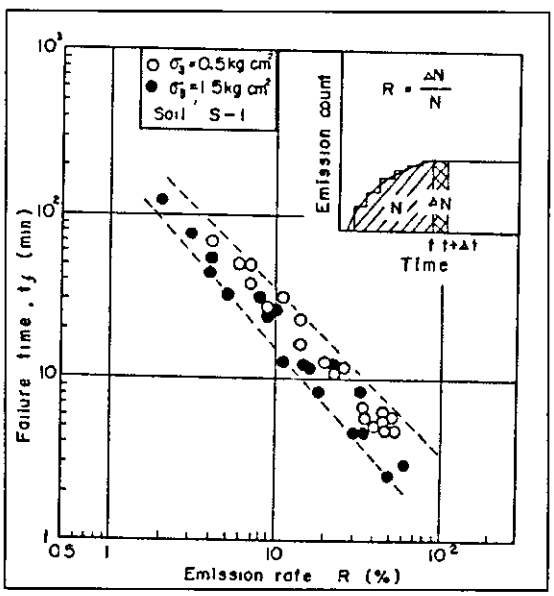

Figure 2.15 Prediction of failure time by emission rate in strain control tests (Tanimoto & Noda 1977)

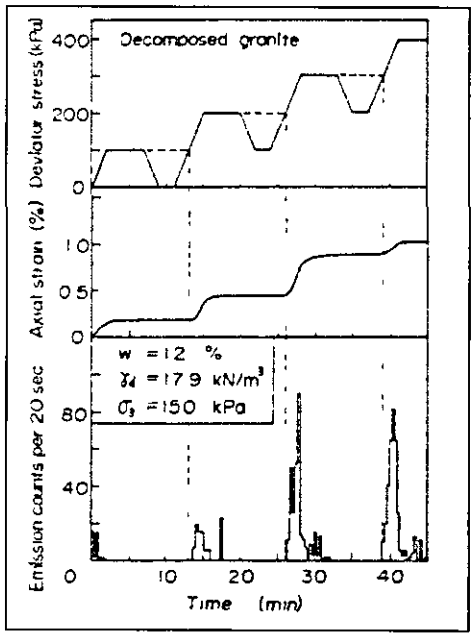

Figure 2.16 Acoustic emission characteristics in repetitive loading triaxial test (Tanimoto *et al* 1981)

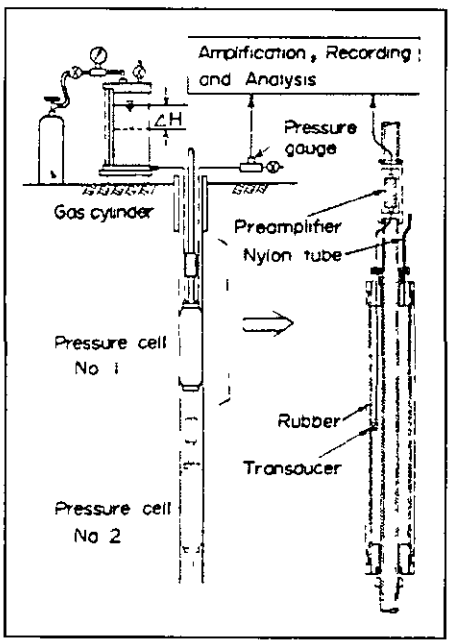

Figure 2.17 Acoustic emission monitoring in pressure meter test (Tanimoto *et al.* 1981)

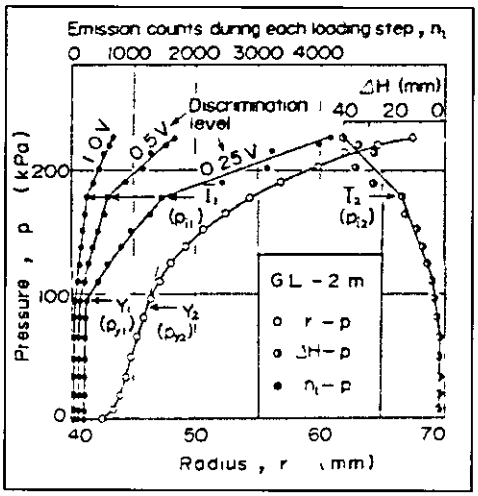

Figure 2.18 Results of preliminary pressure meter test (Tanimoto *et al.* 1981)

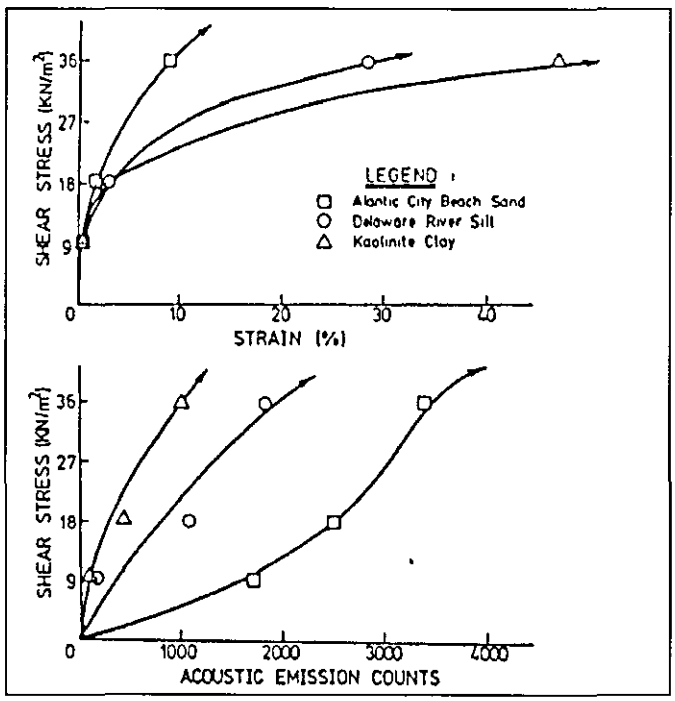

Figure 2.19 Stress versus strain and stress versus AE behaviour of a sand, silt and clay tested under identical conditions (Koerner *et al.* 1981)

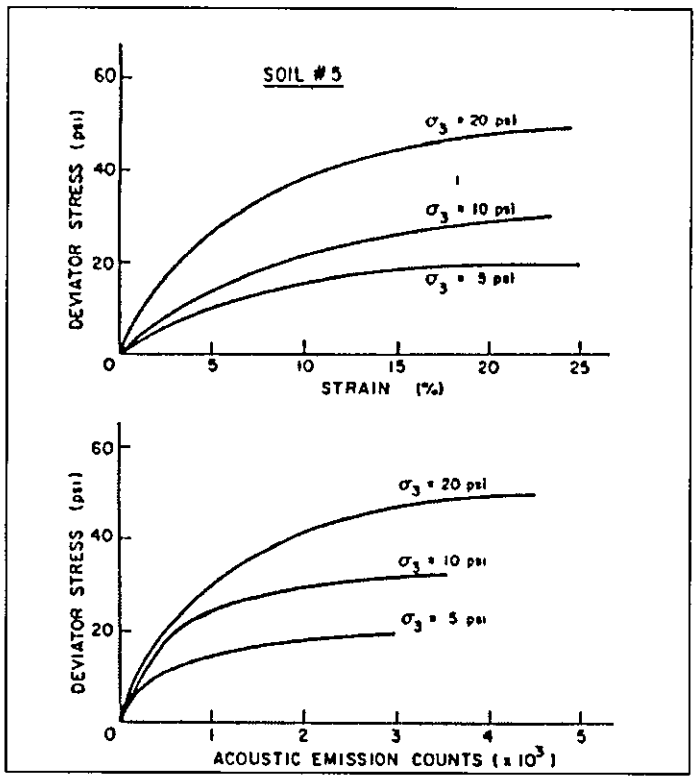

Figure 2.20 Stress versus strain and stress versus AE of a clayey silt at varying cell pressures tested in sustained load triaxial shear (Koerner *et al.* 1981)

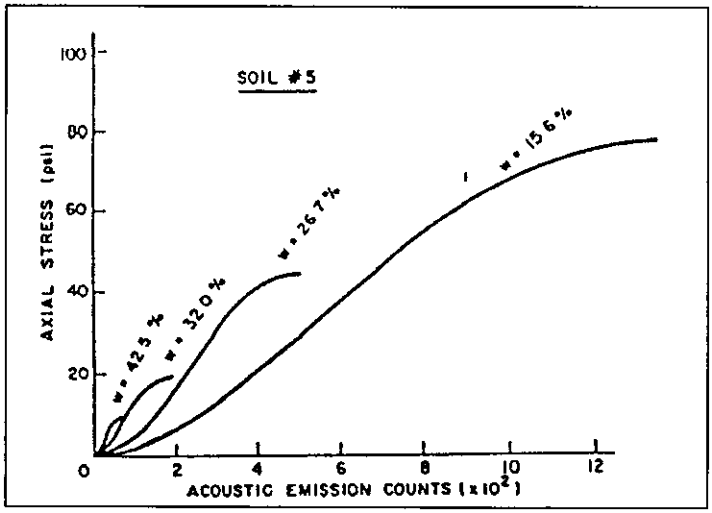

Figure 2 21 Stress versus AE of a clayey silt at varying water contents tested in unconfined compression (Koerner *et al* 1981)

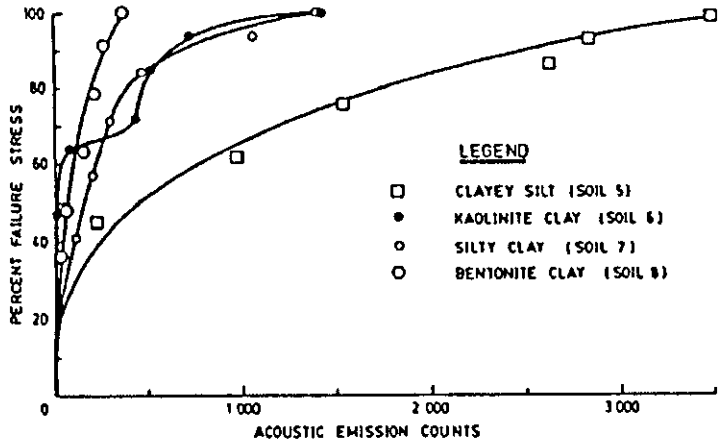

Figure 2.22 Stress versus AE of four fine grained soils with varying plasticity indices tested in sustained load triaxial shear at 34 kN/m^3 confining pressure (Koerner *et al.* 1981)

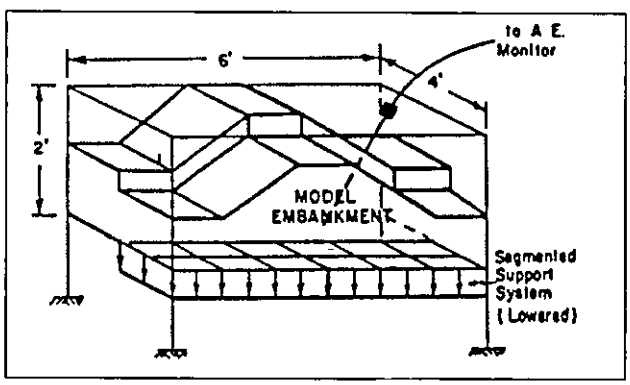

Figure 2.23 Schematic diagram of a large scale embankment stability model (shown In cracked position) (Koerner *et al.* 1981)

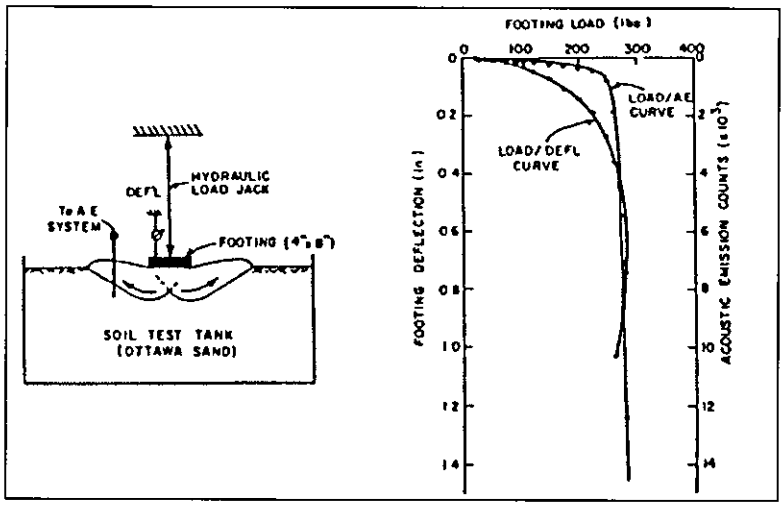

Figure 2.24 Schematic diagram of bearing capacity failure of a shallow foundation and resulting load versus deflection and load versus AE response (Koerner *et al.* 1981)

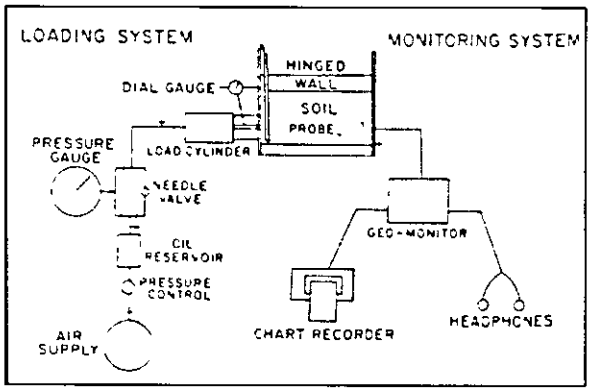

Figure 2.25 Schematic diagram of experimental set up (Mitchell & Romeril 1983)

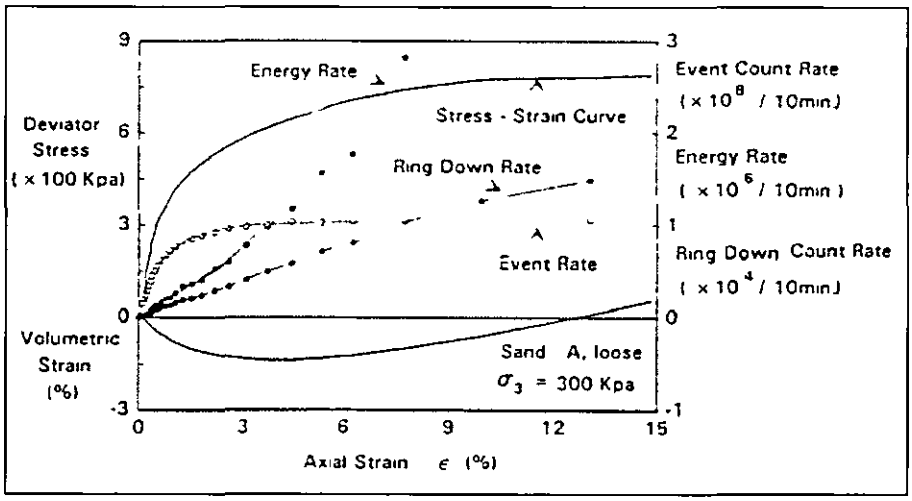

Figure 2.26 Relationship between energy rate, ring down count rate, event count rate, deviator stress, volumetric strain and axial strain in a typical result (Garga & Chichibu 1990)

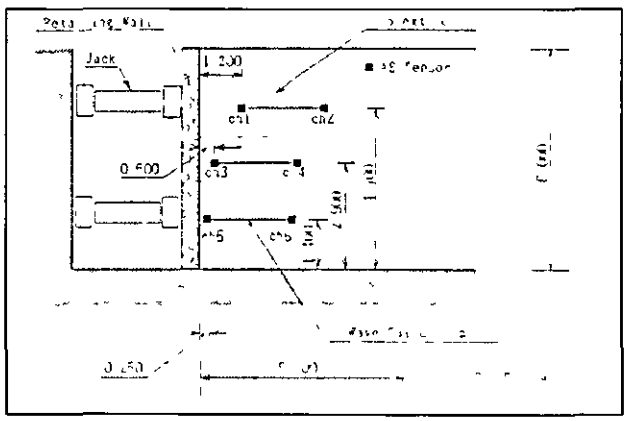

Figure 2.27 Schematic view of experiment (Naemura *et al.* 1990a)

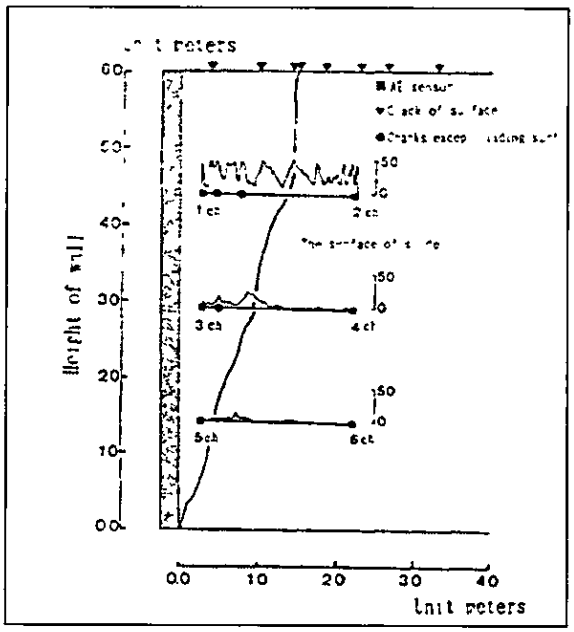

Figure 2.28 Comparison between location of the surface of slide and AE source location at waveguide (Naemura *et al.* 1990a)

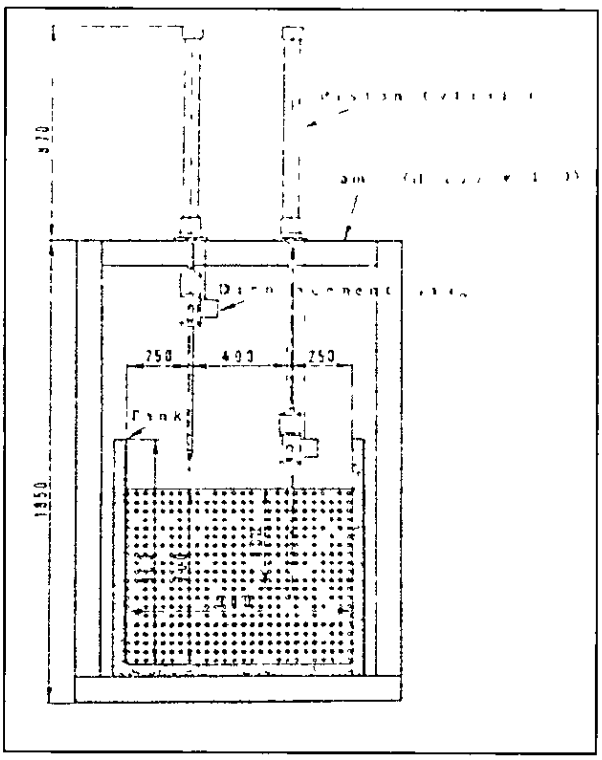

Figure 2.29 Schematic view of experiment (Naemura *et al* 1990b)

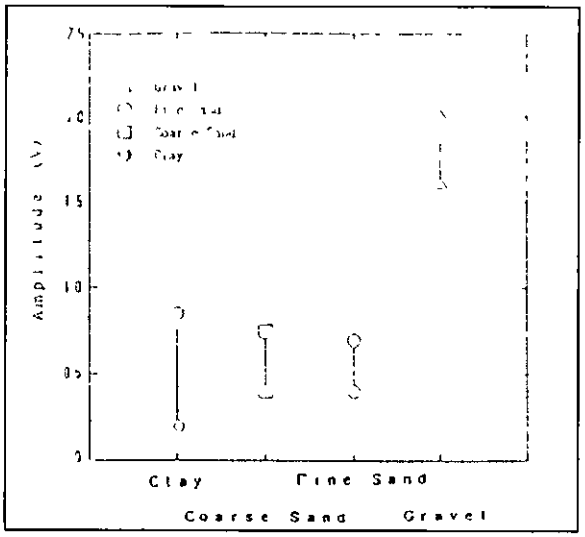

Figure 2.30 The AE amplitude according to soil samples (Naemura *et al.* 1990b)

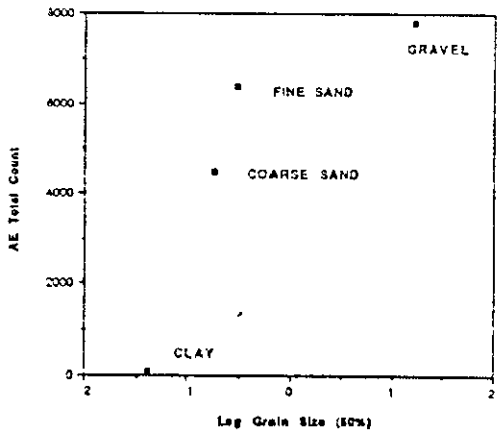

Figure 2.31 The total count according to the grain size (Naemura *et al.* 1990b)

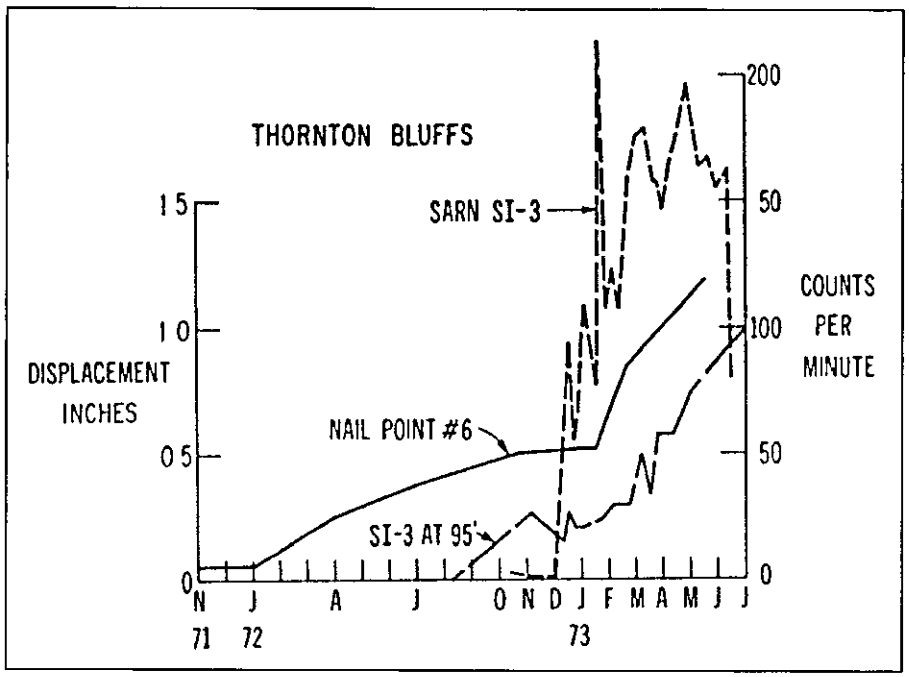

Figure 2.32 Noise rates and displacements at Thorton Buffs field site (McCauley 1975)

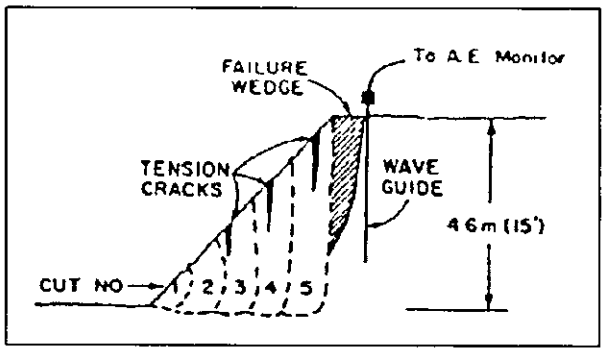

Figure 2.33 Schematic view of stockpile brought to failure (Koerner *et al.* 1981)

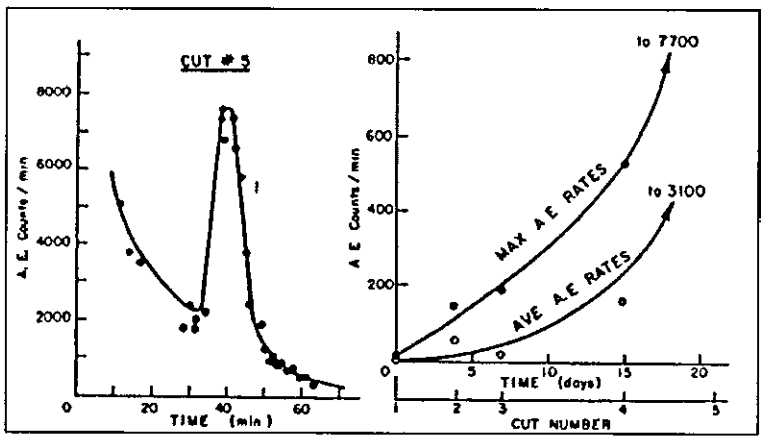

Figure 2.34 Acoustic emission rate versus response time for cut 5 of embankment, and summary of AE rate response from all five cuts (Koerner *et al.* 1981)

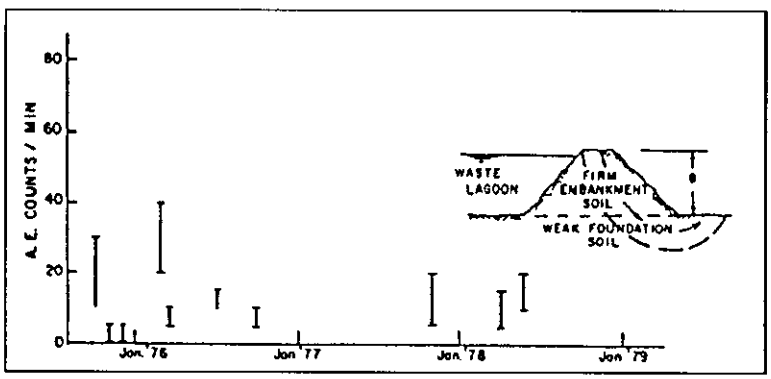

Figure 2.35 Acoustic emission rate versus time response from earth dam containing waste liquid storage lagoon (Koerner *et al.* 1981)

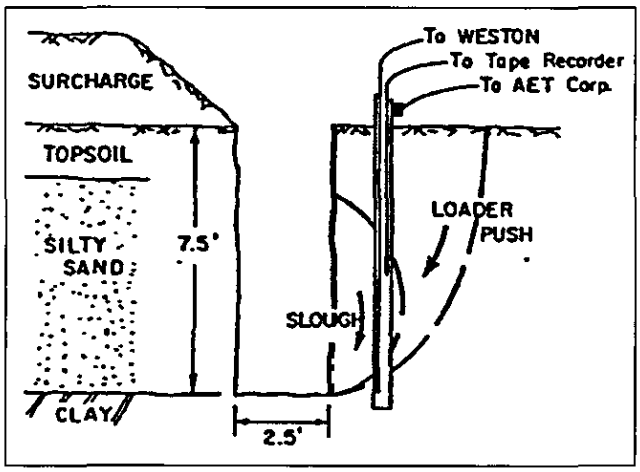

Figure 2.36 Schematic representation of horizontal movement of trench walls (Koerner *et al* 1981)

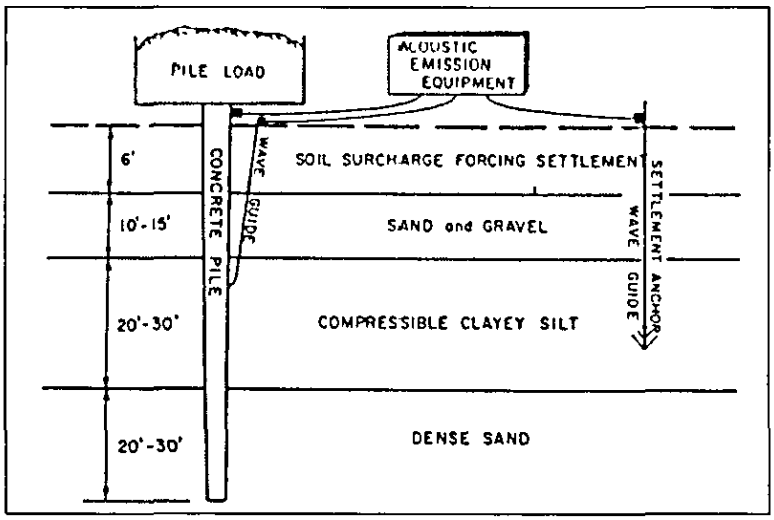

Figure 2.37 Elevation view of soil surcharge mobilising vertical consolidation of clayey silt soil and associated waveguide and AE instrumentation (Koerner *et al* 1981)

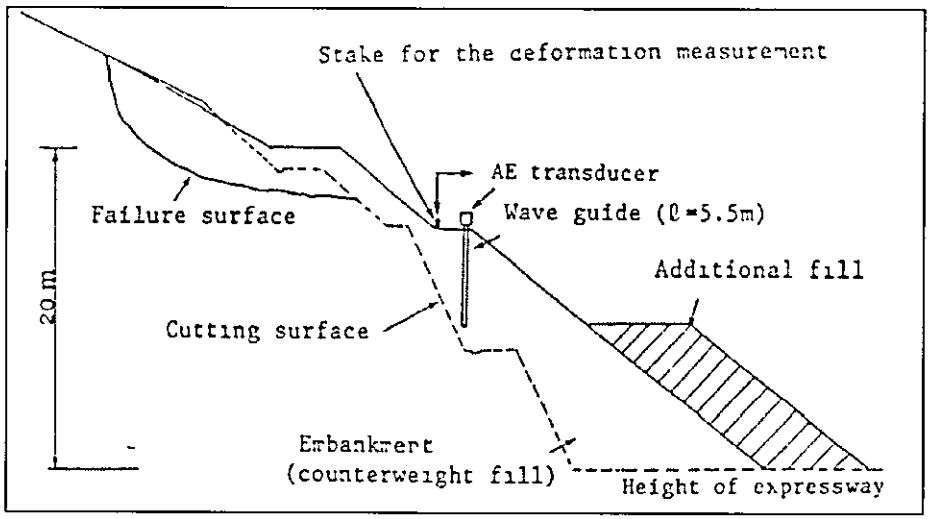

Figure 2.38 A sketch of the embankment and cutting slope (Chichibu *et al.* 1989)

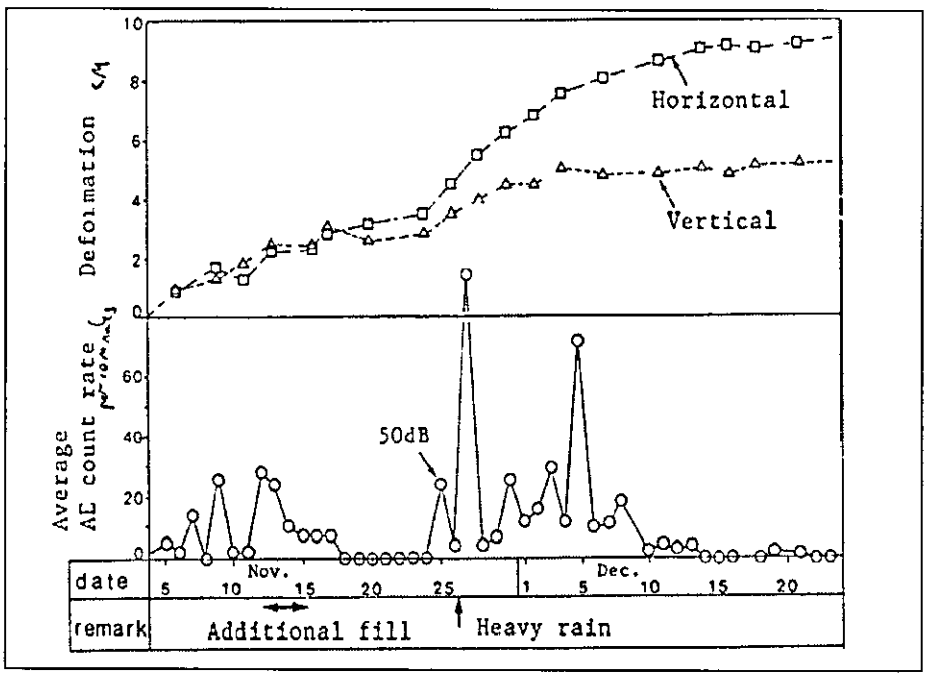

Figure 2.39 Results of monitoring for the embankment. AE counts are for 10min periods and deformation is measured in cm (Chichibu *et al* 1989)

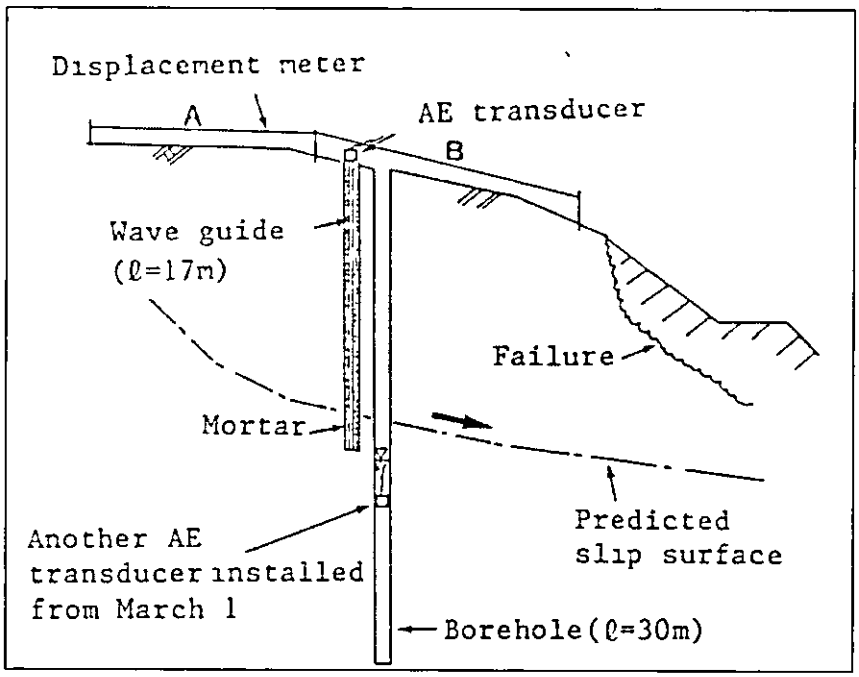

Figure 2.40 A sketch of the natural slope (Chichibu *et al* 1989)

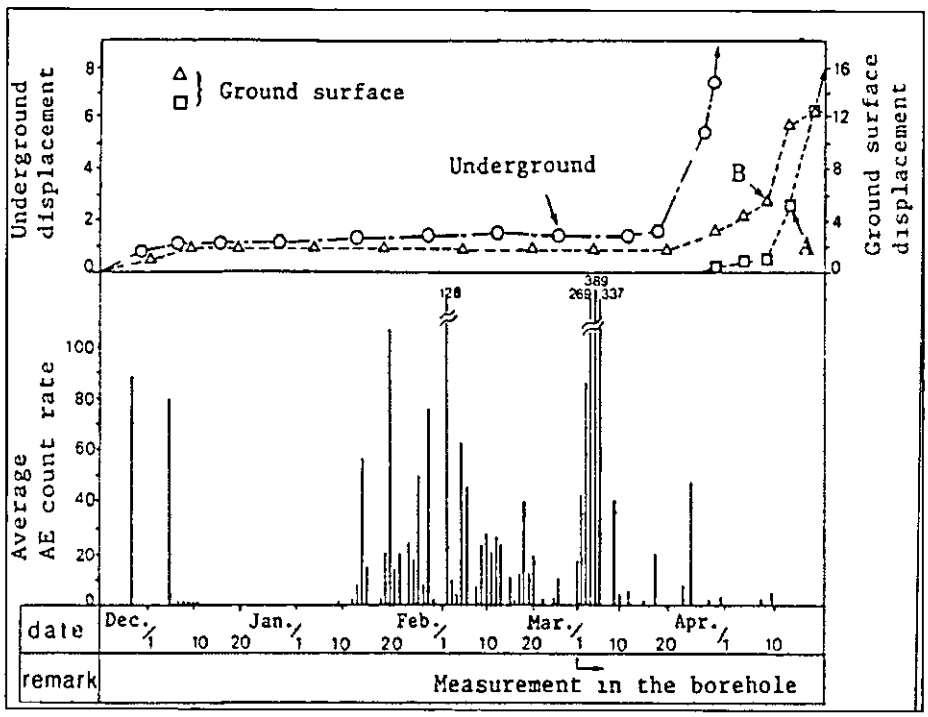

Figure 2.41 Results of monitoring for the natural slope. AE counts are per 10min periods. Underground displacement is measured in mm while ground surface is in cm (Chichibu *et al.* 1989)

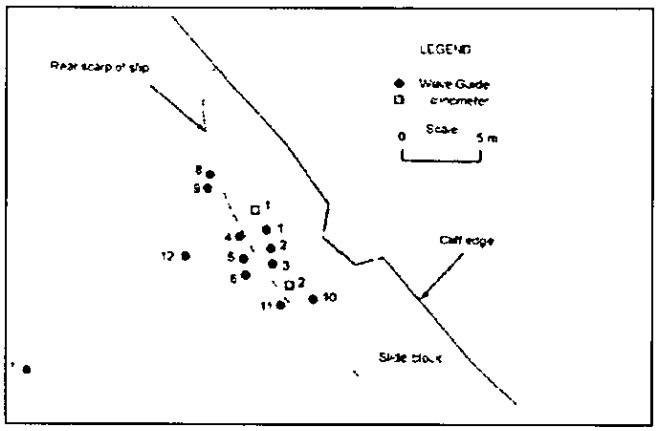

Figure 2.42 Layout of waveguides at Cowden test site (Dixon *et al.* 1996)

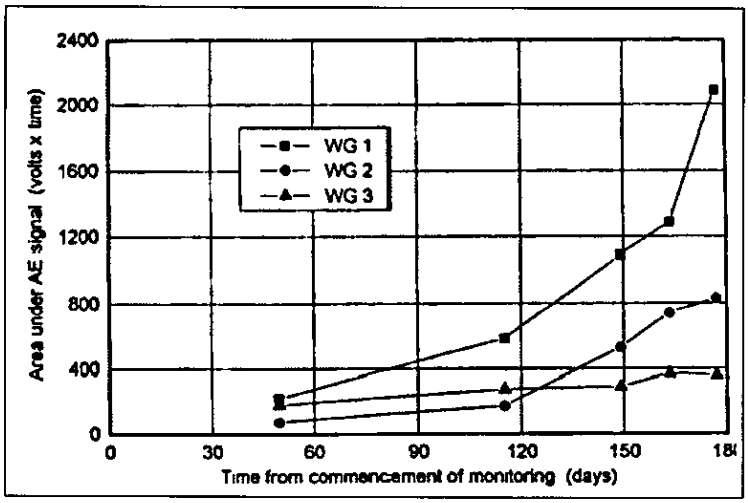

Figure 2.43 Cumulative area under AE signals for waveguides 1, 2 and 3 (Dixon *et al.* 1996)

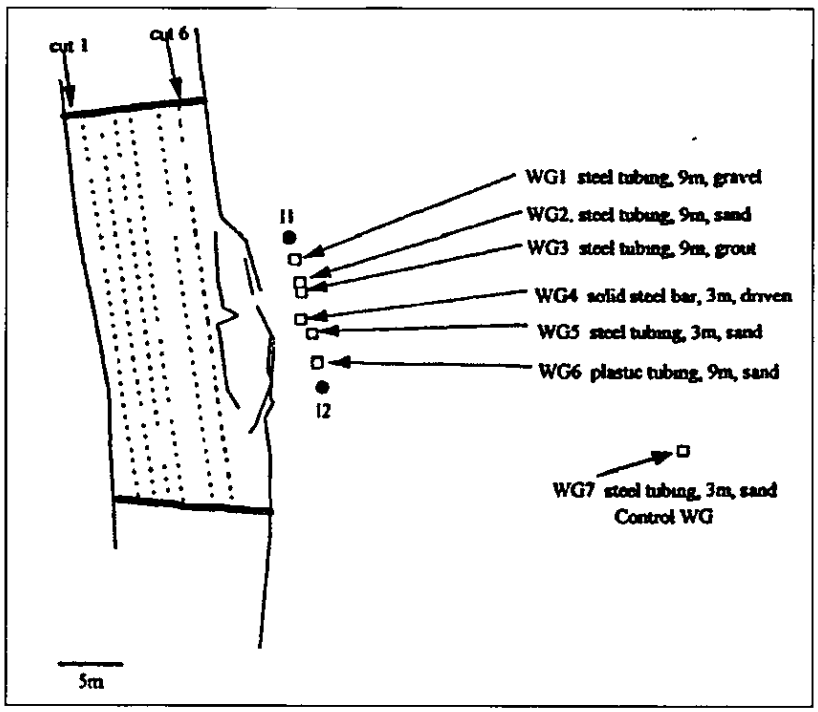

Figure 2.44 Instrument locations at the Arlesey test site (Dixon *et al* 1996)

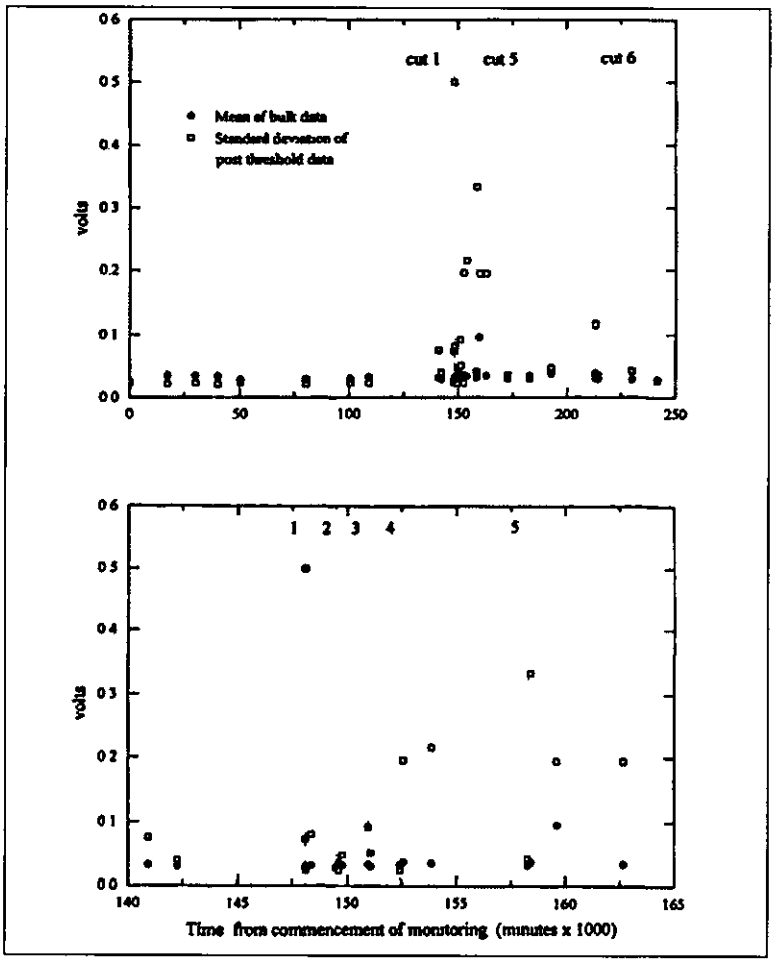

Figure 2 45 Comparison of results from waveguide 2 obtained using mean voltage of bulk data and standard deviation of data above the voltage threshold (Dixon *et al.* 1996)

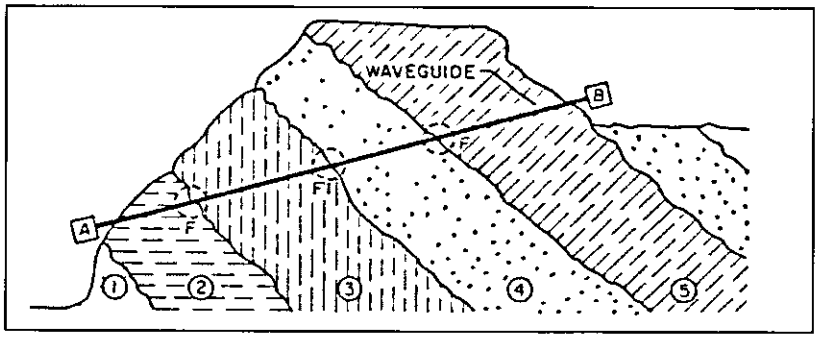

Figure 2.46 Dual Transducer waveguide configuration applied to rock mass monitoring (Hardy jnr. *Et al.* 1989)

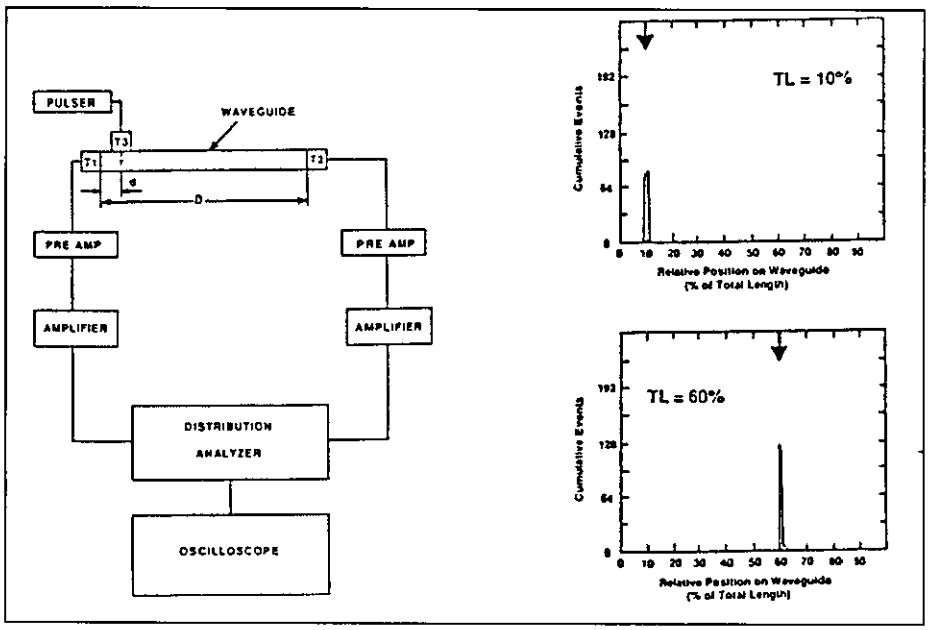

Figure 2.47 Test arrangement to evaluate source location accuracy and the results for tests on straight, dual transducer waveguide (arrows show true source locations). (Hardy jnr *Et al.* 1989)

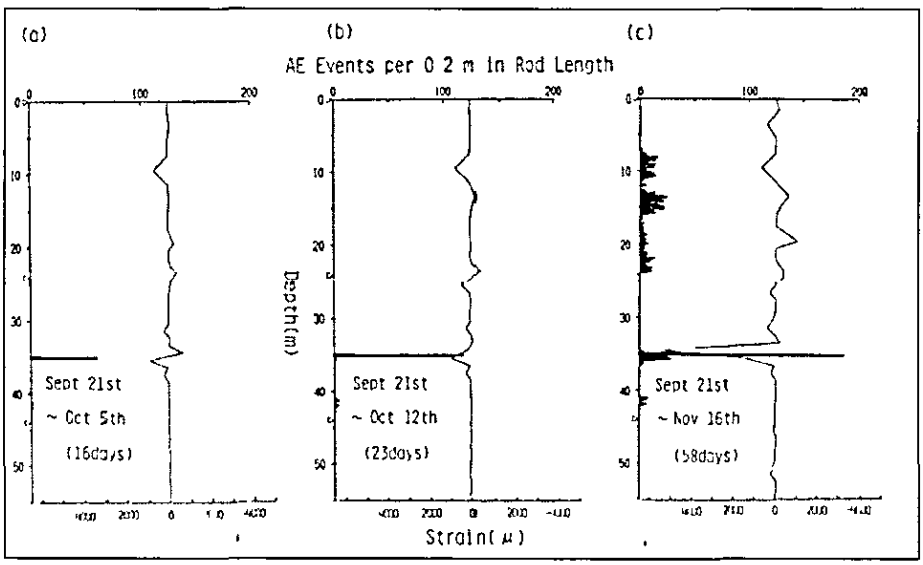

Figure 2.48 Histogram of acoustic events on depth of monitoring rod (Nakajima *et al.* 1991)

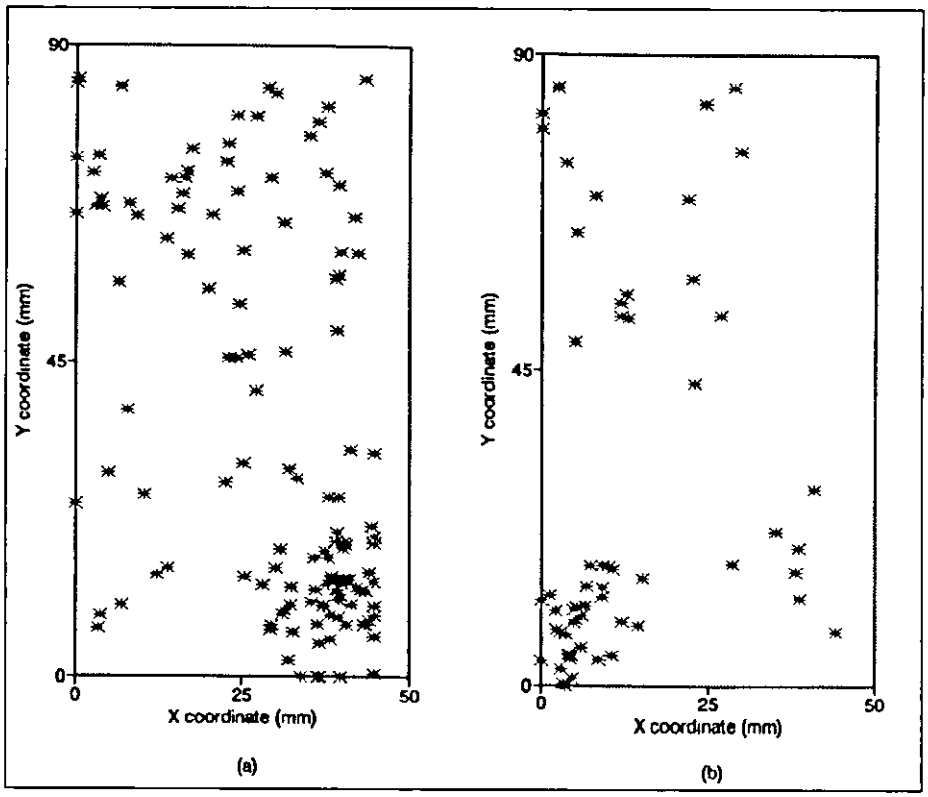

Figure 2 49 AE locations in charcoal granite under uniaxial compression: (a) up to 90% of peak load; (b) from 90% peak to limit load (Labuz *et al.* 1996)

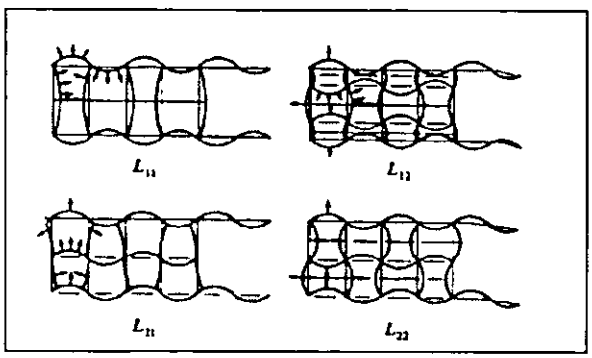

Figure 2.50 Lamb wave modes and displacements (Maji *et al.* 1997)

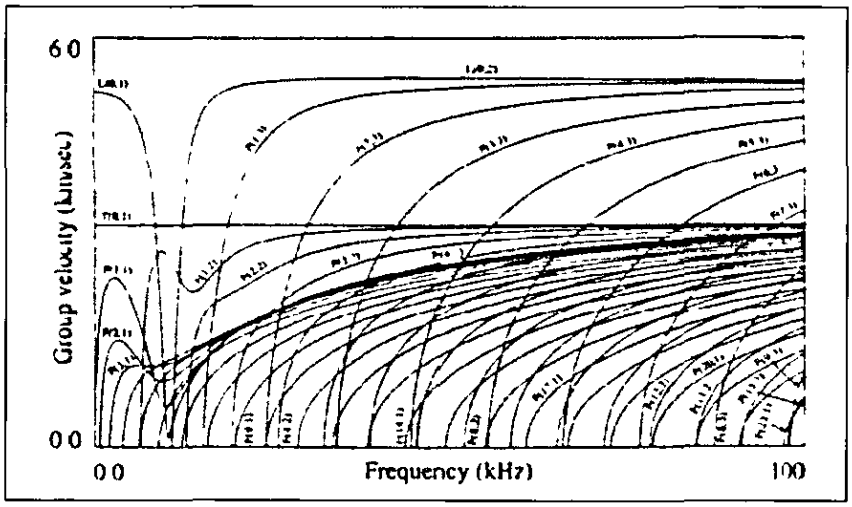

Figure 2.51 Group velocity dispersion curves for 152 mm diameter steel pipe (Alleyne & Cawley 1997)

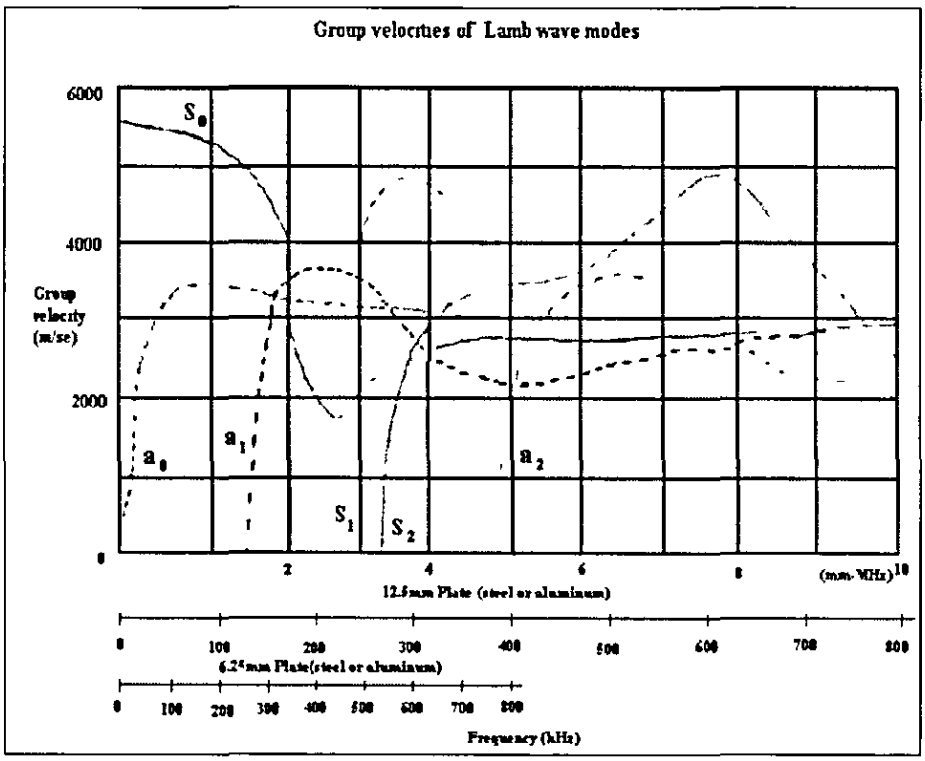

Figure 2.52 Frequency dependence of the different Lamb wave modes after Dunegan Engineering Consultants Inc (Kousteni 2002)

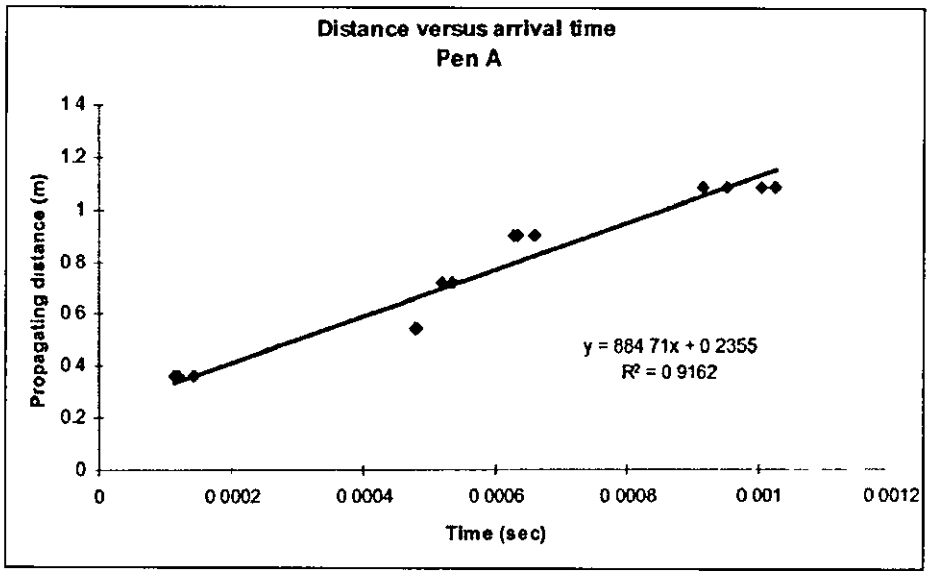

Figure 2.53 Propagating 'Pencil Lead Breaks' distance with respect to time difference between triggered point and first peak of the shear wave. Transducer location A. (Kousteni 2002)

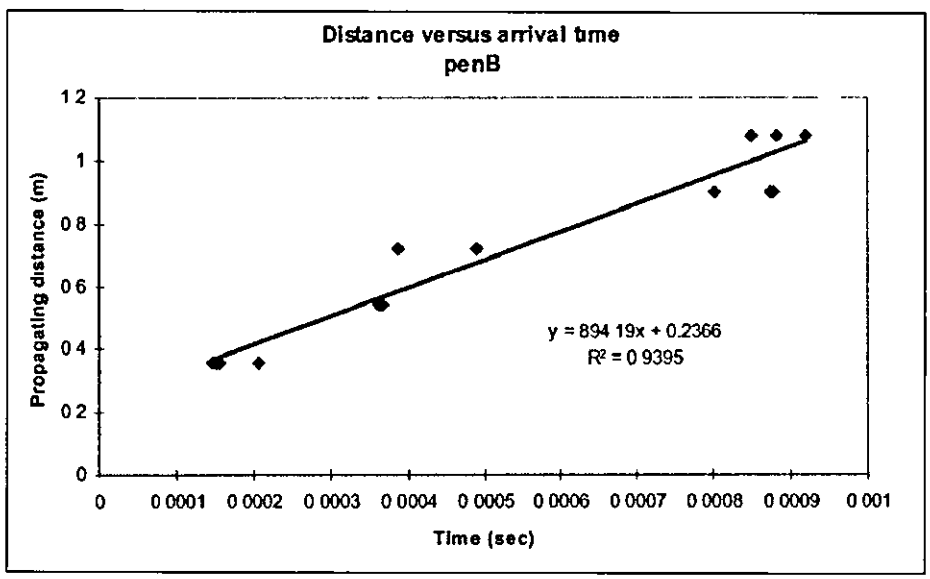

Figure 2.54 Propagating 'Pencil Lead Breaks' distance with respect to time difference between triggered point and first peak of the shear wave. Transducer location b. (Kousteni 2002)

Chapter 3

Acoustic Emission Instrumentation

3.1 Introduction

This chapter discusses the various components involved within the capture of AE data. Section 3 2 goes through each individual element and discusses its role within the whole experimental set up. Justification is given for the choice of each part, and where possible links to industrial standards have been identified and adhered to. Specific software programmes relating to data capture and analysis, have not been reviewed here, but are covered within their relevant chapters, 4 and 5. Section 3.3 covers the various aspects of the waveguide in further detail, namely the choice of backfill required within the active waveguide set up. Section 3.4 describes the way in which AE has been quantified for further analysis.

3.2 Electrical hardware and software

Figure 3.1 shows a typical schematic representation of an AE instrumentation system. The components used within this investigation have been detailed below.

3.2.1 Sensor

A piezoelectric sensor contains an external plate upon which a crystal is attached. This crystal, attached by a thin wire to a connector on the sensor housing, is made up of non-symmetrical unit cells. When mechanical pressure or tension is applied to the non-symmetrical crystal, via the external plate, an electric field is developed. This electric field is directly proportional to the mechanical pressure or tension applied. As the mechanical force changes from tension to compression, the sign of the resulting electrical voltage changes. Therefore, the transducer will

convert mechanical micro-seismic waves into a variable electrical voltage, which can be processed digitally and analysed.

The sensor used within this project was a Physical Acoustics Corporation R61-AST. Figure 3.2 shows the calibration certificate of the sensor. This sensor displays particular sensitivity, or resonance, around 50 kHz, but has the ability to monitor higher frequencies between 50 kHz and 100 kHz This resonant sensor was chosen, as were those used by Kavanagh (1997) and Koustein (2002), to create a balance between the effects of attenuation at higher frequencies and the intrusion of background noise at lower frequencies.

A high-quality acoustic coupling between the external plate of the sensor and the waveguide is essential for an effective system. For each experiment, the sensor was wiped to maintain a smooth and clean surface. To ensure good acoustic transmission, silicon gel was applied thinly to act as a coupling layer between sensor and waveguide. This filled any gaps caused by surface roughness and eliminated possible air pockets. The sensor was attached to the waveguide using a compression mount (magnetic hold down device) to provide repeatable connection conditions, and to guarantee that the sensor always remained stationary throughout testing.

This procedure was conducted for each test in order to adhere to the guidelines proposed by the ASTM (2202) – Standard guide for mounting piezoelectric emission sensors.

- Calibration test

Acoustic emission data can be affected by several different characteristics of the instrumentation Within the typical AE instrumentation set up, shown in Figure 3.1, the transducer is the component most prone to changes in sensitivity. This can be due to the physical conditions of its mounting on the waveguide or more generally because of damage or aging. In view of this a calibration test has been

recommended by ASTM – Standard guide for determining the reproducibly of acoustic emission sensor response, 2001. This test is detailed below.

A repeatable acoustic wave can be generated by carefully breaking a pencil lead against the waveguide When the lead breaks, there is a sudden or transient release of the stress on the surface of the waveguide where the lead is touching. This stress generates an acoustic wave. In order to ensure that the breaking happens in a controlled manner, a Nielson shoe (ASTM 2001) is attached to the end of an automatic pencil (Figure3.3). The lead (0.3mm diameter and 2-3mm in length) was thus always broken at the same angle.

Within the context of this research, this process has been referred to as the 'pencil lead break test'. Pencil lead break tests were used in the development and testing of each experimental set up. The pencil lead break test was also used in the development of analysis programs within DASYLab, before testing was carried out on pedogenic AE (emission that results from the interaction of soil particles, a highly complex and variable source of emission).

3.2.2 Preamplifier

A pre-amplifier was used to boost the AE received direct from the sensor, to enable the signal to travel down lengths of cable without being subsequently affected by background or electrical noise. The pre-amplifier, a Physical Acoustics Corporation 1220A, provides an amplification gain of either 40 or 60dB. At this stage the AE signal remains unfiltered.

3.2.3 Post amplifier and power source

This provided the final amplification necessary for analysis. A Physical Acoustics Corporation 1221A, 0-41dB gain, with a built in high pass filter of 10kHz and a low pass filter of 100kHz was chosen The filters were selected to filter out unwanted noise (this is discussed in section 4.3.1). Further filters to refine the

incoming signal were selected within the data acquisition program DASYLab. Combined with the preamplifier, this system provided a total variable gain from 40 to 101dB. This amplifier also provided the 28V power supply need to run the sensor and preamplifier.

3.2.4 Analogue to digital conversion board

The A-to-D board was used to convert the analogue voltage input to a digital value. The main criterion for choosing an A/D board was the maximum sampling rate. A CIO-DAS16/M1 board from Adept Scientific was selected. This A/D board had a sampling rate of 1MHz, and was intended to run at or near its capacity. However, Microsoft Windows has a maximum sampling rate limit at 0.5 MHz. A minimum sampling frequency was also required , this is discussed in section 3.2.7. The function of the board was only to convert the incoming signal to digital format, all triggers, thresholds and filters were controlled and applied within DASYLab.

3.2.5 DASYLab

The following criteria was set down for the selection of a suitable software package;

- Real time full signal processing capability
- Easy to use interface
- Pre, post and standard triggering functions
- The ability to set threshold values
- Create digital/graphical output
- Flexibility of design for new functions

DASYLab was selected because it fulfilled the above criteria. DASYLab has an easy to use Microsoft Windows interface that consists of selecting modules from

drop down menus. It is capable of performing more than one function on up to 8 data input channels simultaneously. Each program was constructed on a DASYLab worksheet, where data could either be analysed in real time or stored to file for post processing. The versatility of DASYLab meant that it was possible to manipulate the incoming digital signal for all forms of real time analysis. These included: trigger functions; mathematical functions, statistical functions; and signal analysis such as soft filtering, Fast Fourier Transforms (FFT) and graphical outputs.

3.2.6 Soft Filters

A feature of DASYLab is the ability to set soft filters at any stage within a DASYLab worksheet The ease of selecting the type, order and value of high pass and low pass filters enabled all analysis to be exactly suited to the nature of the incoming AE. A Fast Fourier Transform (FFT) provided the analysis tool to determine the frequency make up of the recorded AE, and thus facilitated the selection and placing of filters. Their specific characteristics for each experiment are discussed in chapter 4 and 5.

3.2.7 The computer

The computer used to perform laboratory testing was a Contender 2 Plus, Pentium III 800MHz Processor, 30GB Hard disk, 256MB RAM. This was chosen in order to run the A/D board effectively with DASYLab. However, it became apparent that the processing power of the computer required to run a DASYLab worksheet in real time was not always sufficient. The complexity of real time analysis sometimes took significant processing power. When the computer was unable to deal with the amount of data it would halt the experiment. Thus, where possible, experiments were simply recorded as raw input data at high sampling rates and then post processed. Where this was not possible, the sampling rate was lowered to reduce the amount of data being analysed. Provided the sampling rate was always twice the Nyquist frequency, this wouldn't cause any problems.

The Nyquist frequency of a sampled signal is equal to half the sampling rate of that signal. In order for the incoming signal to be represented as a continuous spectral range and still be compatible with the sampling theorem, the Nyquist frequency represents the highest frequency that the incoming signal can be unambiguously represented. For example, if the fastest sampling rate possible is 0.1MHz, then the Nyquist frequency is 0 05MHz – that is only frequencies below 0.05MHz can be sampled. Any frequency range monitored above that becomes unreliable and doubtful in its meaning.

3.3 Active waveguide

As discussed in section 2.3.3 the role of the waveguide is fundamental in determining whether or not the monitoring of landslides via acoustic emission is feasible. Current technology certainly makes the analysis of AE relatively straight forward, but greatly relies on the proviso that the incoming AE is both of sufficient amplitude, and has it's origin in the slip zone of the landslide. Both passive and active waveguides utilise the effectiveness of a low attenuation 'conductor' to penetrate possible slip zones. However, the active waveguide has the advantage of generating the AE, so that AE propagates from a regulated, noisy backfill material of known characteristics, through which it is less likely to suffer attenuation before reaching the waveguide.

3.3.1 Waveguide

Steel waveguides were used for all experiments. Steel was chosen primarily because of its attenuation characteristics, which is < 0.1dB/m compared to that of soil, which can have attenuation rates that are > 4000dB/m. A steel waveguide has been shown to be effective in both laboratory and field applications (Kavanagh (1997) and Koustein (2002),). Further detailed discussion on attenuation can be found in section 5.2.

The majority of investigations into the quantification of AE and the identification of the depth of a shear surface were carried out on 3 m length drill rods. Each 3m length (50mm diameter and 3mm wall thickness) was coupled via threaded connections to enable testing over distances of up to 21m. Studies of threaded connections between lengths of tubing have shown that low levels of signal loss do occur, but are acceptable (Hardy 1992, Koustemi 2002). The steel tube was elevated above ground level on wooden supports, to reduce any intrusion of ground vibrations.

Experiments were also undertaken on 6m lengths of steel tubing with varying wall thickness; 4.55mm, 5.08mm, 6.35mm, 7.14mm, and 8.75mm. As discussed in section 2.6, wall thickness is a key parameter when analysing incoming waveforms to determine the associated Lamb wave modes for any given event. Thus these pipes were used to explore the effect of wall thickness on calculating the distance to the generated AE from within a developing shear zone in a landslide.

3.3 2 Backfill material

The second component to the active waveguide was the backfill material, which required careful selection in order to maximise on the effectiveness of the active waveguide. Crushed river gravel with a nominal size of 5mm was chosen for all experiments.

Kousteni (2002) showed that gravel emitted higher levels of AE than sand. Kousteni compared the acoustic output from samples of sand and gravel being deformed under load. Figure 3.4 shows the number of AE events recorded from the deformation of the gravel and sand The propagating distance refers to the distance travelled by the AE from the source of the deformation to the sensor. Figure 3.5 shows the mean amplitude of the recorded AE. The results showed that whilst sand produced a greater number of events, the gravel produced events of greater amplitude. The sporadic nature of the AE response from gravel was due to the mechanism of deformation. As sand was loaded, it was able to move and re-

arrange in to a more dense structure until a larger force would cause further deformation For gravel though, due to its increased size and angularity, large forces were required to re-arrange the interlocked particles, and thus the mechanism was more sudden and severe.

This can be a disadvantage of using angular material. AE result from the movement of soil particles against other soil particles and against the waveguide, interlocking of soil particles however restricts this movement. Too much interlocking would result in high-energy bursts of AE, but fewer events would take place. Crushed river gravel was thus selected as a compromise. A particle size distribution chart is shown in Figure 3 6

3.4 Measurement criteria

In section 2.3.1 an idealised waveform was characterised by the following terms; rise time, peak amplitude, envelope, threshold, ring down counts and Event. Each of these terms is a way of characterising an AE waveform in a quantifiable manner. By considering these different approaches to viewing incoming data, previous research aimed to isolate one or more particular characteristics that might define the types of movement around a waveguide.

Kavanagh (1997) extracted similar parameters from a rectified wave envelope. Kavanagh's investigation also considered the statistical measurements of arithmetic mean and standard deviation (and to a lesser extent, the root mean square) to provide insights into the mechanisms of AE generation. Two modes of generated AE were discovered. The first, consisting of relatively large magnitude emission generated over a short duration of time, was considered to arise as a result of a sudden disturbance within the soil mass. The second, consisting of a relatively small magnitude emission generated over a more sustained period, was considered to arise in response to a more gradual, longer term, deterioration in slope stability (i.e. the re-organisation of backfill particles).

Kavanagh was unable to monitor rise time and event duration, but by comparing the mean magnitude within an AE waveform with its standard deviation, the following was concluded: That an increase in acoustic activity is due to the generation of a greater number of similar sized events rather than the generation of events of increased magnitude.

The approach taken within this investigation was based on the fact that events were shown to be a clear indication of activity within the backfill material, for both long and short duration events. Thus AE was monitored and quantified using event counts. RDC was also used, but experiments showed event counts to be more reliable and repeatable (see section 5.2). Another parameter was also used to aid in monitoring attenuation along a waveguide, Energy. Energy was indirectly monitored by calculating the area under a rectified waveform. Although the output of this wasn't strictly speaking an energy parameter, the area under the wave envelope was a fair representation of the energy within an AE waveform.

The aim was to produce a monitoring system that was responsive to small strain movements, but remained simple in its approach to quantifying AE generated by an inhomogeneous, highly variable, natural medium; that being the soil body.

3.5 Chapter summary

This chapter has outlined the instrumentation needed to detect and analyse generated AE from a deforming active waveguide. Section 3.2 justified the choice of the instrumentation and its role within transporting AE data from the zone of deformation to the computer with least interference from background and electrical noise, and minimal attenuation. Section 3.3 determined the choice and design of the active waveguide, gravel backfill was chosen because it generated large amplitude events, and steel pipes were chosen because of their low attenuation characteristics for Lamb wave propagation. Section 3.4 explained the approach to quantifying AE based on previous work, by measuring event counts, ring down counts, and the area under the waveform as reliable indicators of backfill deformation.

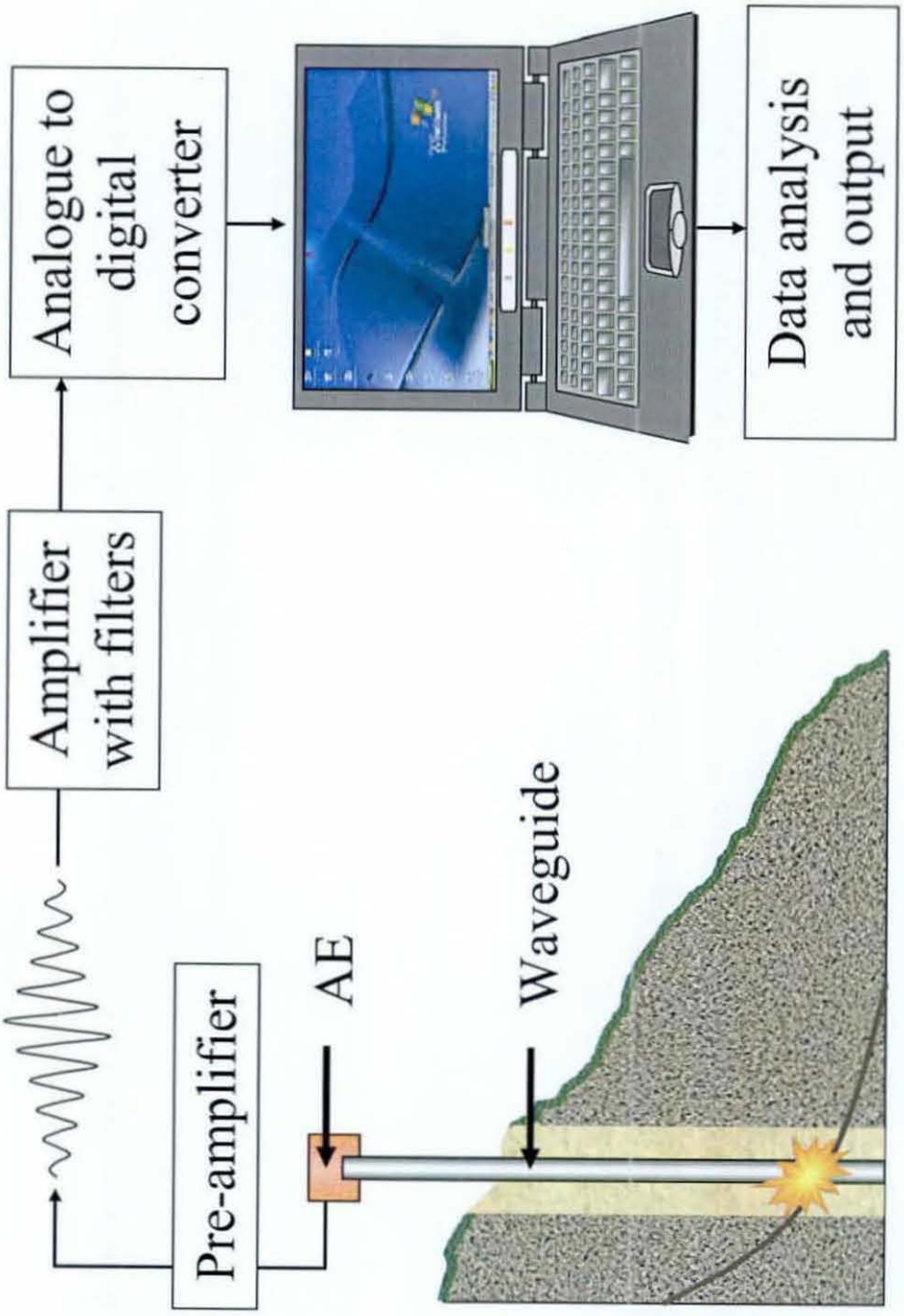

Figure 3.1 Schematic representation of a typical AE monitoring system

PHYSICAL ACOUSTICS CORPORATION
A MISTRAS Holdings Company

AE SENSOR CALIBRATION CERTIFICATE

Sensor Name:	R6	Test Date:	1/11/01	Max. Value (dB):	-55.28
Sensor S/N:	AD60	Tested By:	C.P.	Peak Freq.(kHz):	171.87
Comment:					

PAC Certifies that this sensor meets all performance, environmental and physical standards established for applicable PAC specifications.
Calibration methodology based on ASTM standard E976 "Guide for Determining the Reproducibility of Acoustic Emission Sensor Response."

Figure 3.2 AE sensor calibration certificate

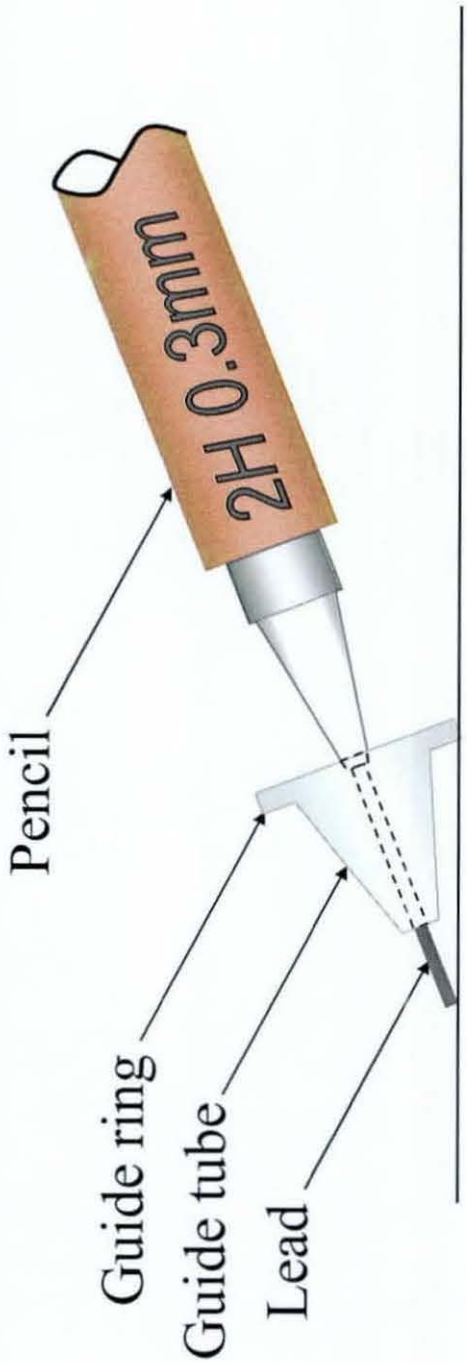

Figure 3.3 Schematic view of a Nielson shoe

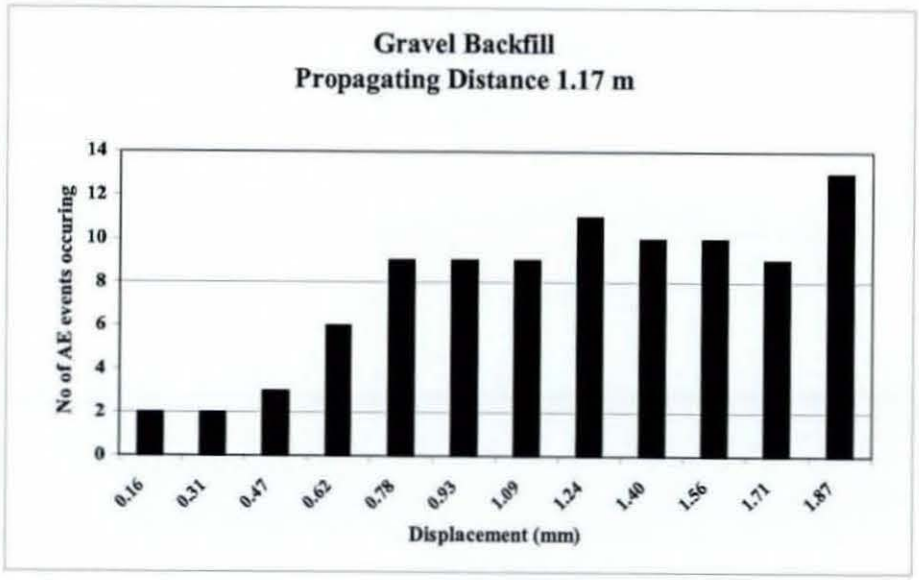

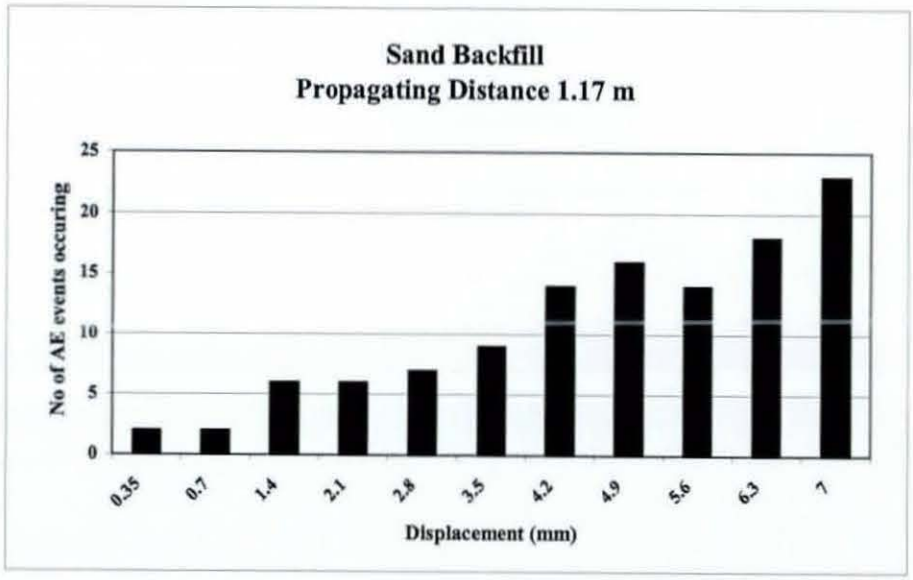

Figure 3.4 Number of AE events with respect to displacement for sand and gravel (Kousteni 2002)

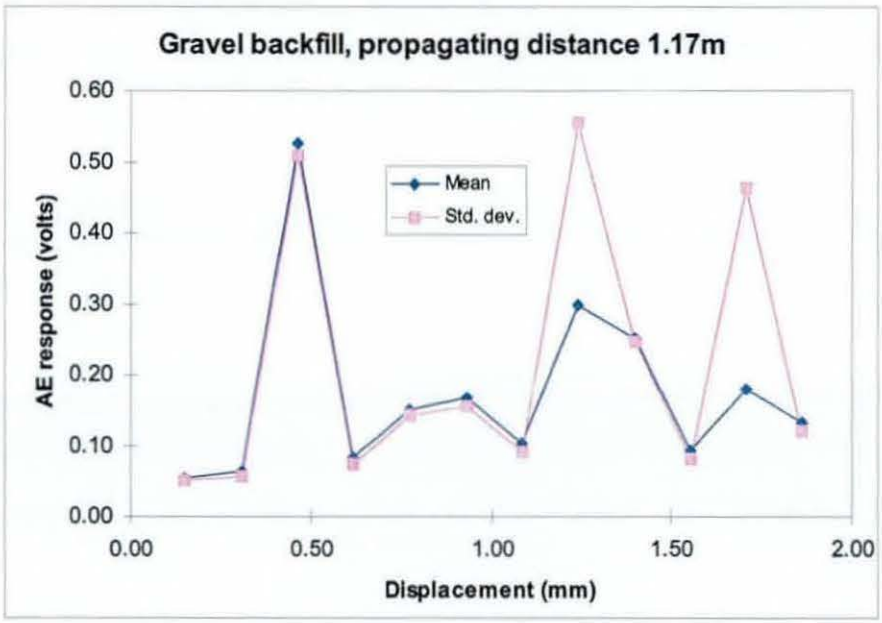

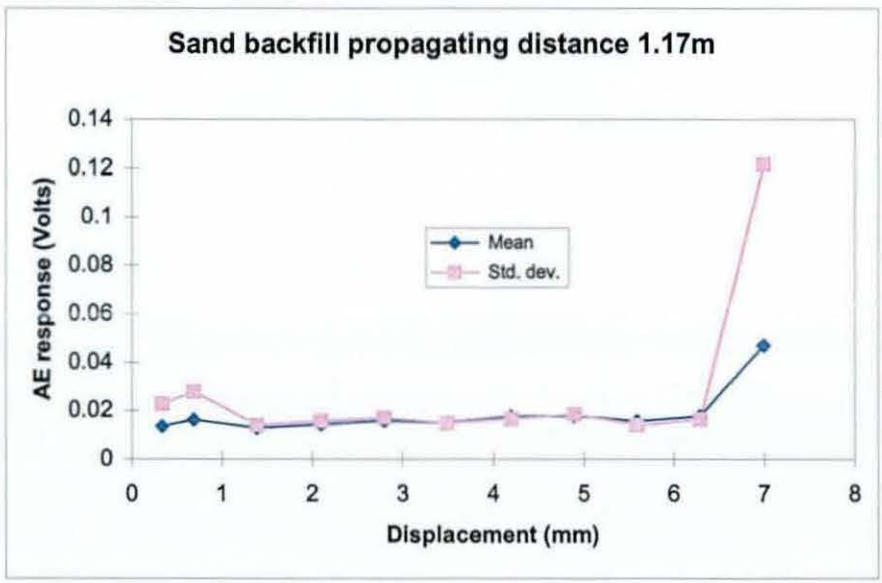

Figure 3.5 AE response (amplitude) of gravel and sand with respect to displacement (Kousteni 2002)

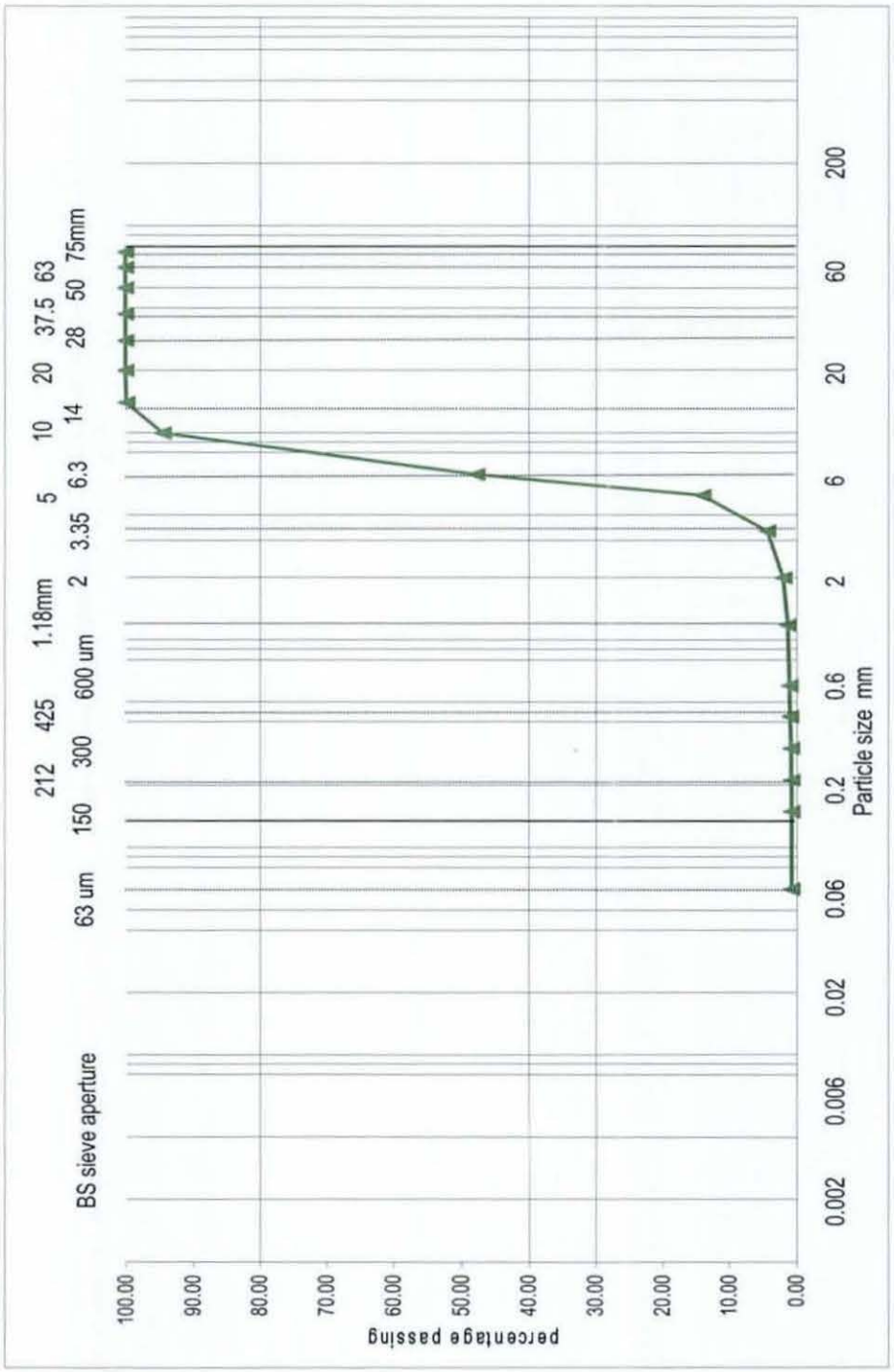

Figure 3.6 Particle size distribution curve for crushed river gravel

Chapter 4

Quantifying Acoustic Emission

4.1 Introduction

This chapter is primarily concerned with the question of whether or not acoustic emission (AE), generated from the interaction of back fill around a waveguide within a deep seated rotational landslide, can be quantified. This is the first step towards investigating the use of AE to predict the failure of a landslide. Section 4.2 highlights this need and discusses the role of the active waveguide in this process, it also summarises the current methods used to categorise landslide deformation rates. Section 4 3 outlines the software and hardware required to analyse AE and details initial experiments used to demonstrate confidence in the monitoring system (described in chapter 3) Two different laboratory tests are considered in Section 4.3, where AE is generated by two different testing mechanisms. The effect of the testing environment and the mechanism of deformation is analysed in section 4.4, and the ability of AE to be reliably quantified for the purpose of classifying slope movement is determined.

4.2 Why quantify acoustic emission?

4.2.1 Current measures of slope deformation

Table 4.1 shows the current language for characterising slope displacement. These displacements are typically monitored by instruments such as inclinometers, extensometers and other surface surveying equipment.

Landslides that move at rates equivalent to 'moderate', 'slow', 'very slow' and 'extremely slow' (as defined by the Transport Research Board 1978) are separated by orders of magnitude. An early warning detection system based on AE must be

able to detect the onset of failure at potentially very low deformation rates, and have the potential to differentiate between 'moderate', 'slow', 'very slow' and 'extremely slow' rates of movement (orders of magnitude).

To date, the application of AE to landslide monitoring has only progressed as far as a qualitative guide. Koerner *et al.* (1981) produced the most comprehensive qualitative chart (section 2.5), and used terms such as 'little, moderate, high and very high' to describe the level of AE generation. These terms were linked to a description of the extent of slope movement (see section 2.5), and ranged from 'generating little or no AE' which referred to a slope that was probably not deforming, to 'generating very high levels of AE' which pertained to slopes undergoing large deformation and thus in a state of failure. All in-between deformation rates could only be characterised as either 'moderate' or 'high' in their level of AE activity. Such a system of characterising AE was unable to differentiate the various levels of movement as laid down by current standards (i e. the Transport Research Board 1978).

It is evident that in order to successfully monitor and predict the onset of failure, a quantitative output, in terms of a rate of displacement, is essential. This output must also be able to classify the rates of displacement into their relevant boundaries (i.e. 'moderate', 'slow', 'very slow', 'extremely slow' etc). Quantifying AE has been looked into for many years, but few studies have successfully linked the AE to the rate of displacement. Tanimoto and Noda (1977) successfully related the emission count rate (counts per minute crossing a threshold) with an initial increase in strain. The emission rate was then found to become steady as failure was approached. These tests were performed in strain controlled triaxial cells, and demonstrated the potential to predict failure using AE (section 2.4).

Tanimoto and Noda (1977) thus showed that the characteristics of a soil-generated AE had the potential to provide the relevant data for a successful early warning system. However, this relies on knowledge about the origin of the AE and the path travelled from source to sensor. Both the material responsible for the generation of AE, and the distance travelled by an emission before it is detected can

drastically modify the characteristics of a signal, meaning that the observed and analysed emission may bear little resemblance to its original form. The active waveguide has gone some way to controlling the nature of the emission at its source, and is discussed below. Chapter 5 discusses research done into determining the distance the AE has travelled before it has been detected, whilst this chapter concentrates first on determining a definite link between the physical characteristics of an AE signal and the rate of displacement within a landslide.

4.2.2 Active waveguide as an early warning tool

Soil in its natural state is extremely inhomogeneous, therefore AE generated from straining such a material is likely to be extremely variable. Previous attempts to quantify AE generated within a slope, which used the passive waveguide concept, were not just limited by the attenuation of the host soil slope, but also by the variability of that soil within the same slope. In addition difficulties were experienced when trying to correlate data from different slopes. As noted in section 4.2.1, the very nature of AE waveforms is crucial to the understanding and development of an early warning system. Variation in that signal from within the same slope would significantly reduce any confidence in the data to predict the onset of failure. Thus it became imperative that AE variability was removed as far as possible in order that a universal system might be developed for use in any site regardless of local conditions.

The active waveguide has to date been the most significant development in tackling this issue (section 3 3). The problem has been simplified by replacing the unknown variable soil with an annulus of soil with a known acoustic behaviour. This active waveguide thus operates such that the generated AE does not result from within the unknown host soil slope, but within the waveguide backfill as that is deformed by the host soil around it. This backfill material can then be selected to exhibit appropriate properties for AE generation, which could be investigated in advance within the laboratory. The use of a granular soil as a waveguide backfill has been shown to be effective as it is relatively 'noisy' compared with clay or silt Kousteni (2002). Kousteni also demonstrated the need to select an appropriate

sized granular backfill to strike a balance between high amplitude events (emitted from gravel) and a high occurrence of AE events (emitted from sand), see section 3.3.2.

Crushed river gravel with a nominal size of 5mm was chosen for all further experiments. A particle size distribution curve for this soil is shown in Figure 4.1, and was produced by means of the dry sieve method in accordance with BS 1377: Part 2 (1990). After each experiment, a fresh batch of gravel was used as the particles became rounded during loading. Such a material was also readily cheap and available.

For the purpose of clarity, the terminology used in chapter 4, 5 and 6 is defined below. All references to the broad term 'waveguide' are in relation to the use of an 'active waveguide' rather than a 'passive waveguide'. Thus the term waveguide will no longer refer to a system, but solely to the instrumentation responsible for assisting AE transfer from its source to the sensor, i.e. in this case a metal drill rod. The collective term 'active waveguide' thus consists of two components: the metal waveguide itself and the backfill material.

4.3 Instrumentation

All experiments detailed within this chapter were performed using the monitoring system as described in chapter 3. This system was chosen to be highly sensitive to the detection of AE generated by the development of shear strains within a granular material. The monitoring system was comprised of both hardware and software components; both of these elements are explained further and validated below.

4.3.1 DASYLab - the software

DASYLab provided a flexible and user-friendly real time signal processing capability. By a series of drop-down menus, a worksheet was created to filter

incoming digital AE (both in the sense of filtering out unwanted frequency bands, and in filtering out unwanted background AE), and to perform the required analysis

Figure 4 2 shows the DASYLab worksheet used for all experiments detailed within this chapter, unless otherwise mentioned. The following is a list of details as to the specifics of each module (its function and detail) within the worksheet. Apart from the A/D module and the high/low pass filter modules, all other modules have been grouped in relation to their output aim, namely ring down count (RDC), energy and event count.

- Analogue to digital converter module

The analogue to digital converter (A/D) module was the only module to appear on the worksheet that represents a specific item of hardware. All other modules described below were software modules and thus manipulated a digitised signal. In order for these modules to perform their analysis function, the incoming analogue signal was converted to a digital signal using a CIO-DAS16/M1 board from Adept Scientific (section 3.2.4). Thus the A/D module on the DASYLab worksheet merely existed to represent the appropriate hardware, and signify the beginning of the analysis process.

The sampling rate of the A/D board used for the experiments within this chapter was 0.0556 MHz. This sampling rate was kept as low as possible in order to reduce the amount of data being processed, but was also chosen to fit the criteria of the Nyquist frequency (section 3.2.7).

- High pass filter

The function of the filter was to cut off, or damped certain frequency components from the time signal. This module provided several digital filters of different

types (low pass and high pass) characteristics (Bessel, Butterworth and Chebyshev). It was also possible to set the filter order and the cut off frequency of the filter. The filter order was defined by the number of polls of the filter - increasing the number of polls increases the steepness of the cut off frequency.

The cut off frequency for the high pass filter was 25 kHz while higher frequencies could pass the filter unchanged. A high order Chebyshev filter was selected because of its steep response to the cut off frequency.

- Low Pass filter

The low pass filter worked in the opposite way to the high pass filter. The cut off frequency for the low pass filter was 28 kHz while lower frequencies could pass the filter unchanged.

These filter pass frequencies were based primarily on considering the frequency spectrum of the incoming signal. The AE sensor was originally selected to have a resonant frequency of about 50 kHz, which was considered to be an effective monitoring frequency (see section 3 2.1), with the ability to monitor at other frequencies above this value as well. The sensor calibration certificate can be seen in Figure 4.3, and shows high sensitivity at 47kHz and above 67 kHz. However, when data from the compression of gravel was analysed for its frequency content, the signal proved to be most active within the range of 25 – 29 kHz (Figure 4.4). Although the sensor shows low sensitivity within this range, it was considered that this sensor was still feasible based on the incoming data being of sufficient amplitude. But it is considered for any future investigations that a resonant sensor with peak sensitivities similar to those frequencies exhibited by soil generated AE would be highly preferable.

– Ring down count

The RDC was measured every time the AE waveform rose above a pre-determined threshold. This threshold was set and monitored using a statistics module called a 'counter'. In each experiment a survey of the level of background noise, including noise produced by associated experimental instrumentation, was performed. The threshold was then selected such that only AE that rose above the background noise in amplitude would be monitored. A threshold level of 0 3 volts was set for all experiments unless otherwise stated. It was assumed that any resulting AE greater in amplitude than the background noise was AE resulting from soil/waveguide interaction as the soil sample was subjected to stress.

Having a threshold set as close to the level of background noise as possible was important in order that the RDC would be an accurate representation of AE generated by soil/waveguide interaction. Even the smallest increase in AE activity above the background noise was considered to be significant and appropriate for analysis.

This module was then read by a display module, which displayed the output in the form of a digital meter.

– Energy

Energy was a relative parameter within these experiments. The energy of the generated AE was measured by the area under the waveform. The resulting output was measured in volt seconds. A pre/post trigger (labelled data trig) module monitored the incoming signal as an amplitude range against time. This module had the ability to trigger at a predetermined amplitude threshold, and to capture events preceding that threshold trigger and after that same trigger for a set duration of time. This trigger then acted as a switch thus allowing only data which fulfilled the trigger conditions to pass on for further analysis. For example, when an incoming AE signal was greater than the threshold, a command was sent to

open a relay switch and allow a specific time window of data to pass before the relay switch was closed. The relay switch would close when the amplitude of the signal fell below a threshold.

The threshold was selected to be 0.3V in all experiments, unless stated otherwise, in order that the system wouldn't trigger on background noise. To ensure that the whole of an event was captured, a pre-and post trigger condition was set to 0 001 seconds. This would enable 0.001 seconds of data, before and after the opening and closing of the relay switch, to pass through the relay and be included in the analysis of the AE event as a whole. This value was determined by viewing previous AE data. Often there was a time difference between the start of an event and the crossing of the threshold by that same event. This also applied to the tail end of the event signal.

This does mean that when the relay switch was opened, the recorded energy would also include any energy within the background noise present at the time of the AE event being recorded. This would have a greater effect on events of low amplitude. In an extreme condition, an event that might only just cross the threshold with a maximum amplitude of 0 31 volts, would be influenced far greater by the levels of background noise than an event registering a maximum amplitude of 10 V. Thus in order for the true energy of an event to be known, the energy of the background noise must also be known and subsequently be subtracted.

The data which met the pre/post trigger criteria was then rectified to ensure that the waveform was represented only within the positive domain This was achieved with a simple equation symbolised by the following:

$$\sqrt{(Input0)^2} \qquad [4\ 1]$$

Each component of the incoming signal was squared (SQR), and then squared rooted (SQRT). This ensured that the wave form retained its original characteristic shape, but rather than oscillating above and below 0 volts, the wave

form was now displayed as oscillating above 0 volts. This enabled a mathematics module to be inserted in order to perform the integral of the wave form, and thus provide the area under the wave form which has been identified as a reliable indication of energy. This output was again displayed using a digital meter.

– Event count

An event consists of many threshold crossings (measured as RDC) and is characterised as beginning when the threshold is first crossed and ending when a waveform falls below the threshold. Events were counted using a Combi trigger, which enabled simple stop/start conditions to be set. The output of this trigger was either a 5 volt 'high' value or a 0 volt 'low' value, which would then control a relay switch to open or close allowing the data to progress to further analysis. A threshold of 0.3 volts was again set to avoid events which originated from background noise. The Combi trigger would issue an open command (high value output) when the threshold was first crossed and then would then issue a close command (low value output) after a specified duration of time. A minimum duration of 0.02 seconds was set to ensure that the same event was not counted more than once. The minimum duration and value was selected by viewing previously collected data and taking into account the average event duration and the average time between events.

It was not necessary for the output of the Combi Trigger to be sent to a relay switch module. Instead, the output was sent direct to a 'counter' module which counted each time a 0 volt signal (trigger closed) changed to a 5 volt signal (trigger open). Each positive step increase in the output voltage of the Combi trigger denoted a new event. A digital meter recorded the output. All digital meters were then saved to memory in real time for post analysis.

It should be noted that such is the nature of the variability of AE and the sensitivity of a monitoring system that no two systems are alike. Thus the results from this system could not be directly analysed alongside data from an alternative system (i.e. monitoring systems comprised of alternative software or hardware).

However, trends and correlations within the data can be easily displayed and compared to other monitoring systems.

4 3.2 Validation of monitoring system

A series of simple experiments were first performed on Leighton Buzzard sand (uniformly graded coarse sand, sub angular, average particle size 1.18mm – see Figure 4 5). Their purpose was to authenticate the effectiveness of the instrumentation (both hardware and software) described in chapter 3 as a valid system for quantifying AE. This was achieved by reconstructing earlier experiments by Koerner into the acoustic properties of soils (Koerner *et al.* 1981). Koerner established that either strain or cumulative AE could be used to characterise soil behaviour. Figure 4.6 shows the close parallels between the curves produced from stress/strain and those from stress/AE for clay, silt and sand. This experiment was discussed earlier in section 2.4 This, and further work, became the basis of Koerner's qualitative system for analysing AE generation in soils.

Experiments were carried out on a 'Wykeham & Farrance' direct shear box (large shear box apparatus), in accordance with BS 1377 Part 7. Each sample (300x300x166mm) was compacted to achieve a density of around 1.67 Mg/m^3, subjected to a normal force of 111.1kN/m^2, and sheared at a rate of 1.2mm/min. The experiment set-up is shown in Figure 4.7. A 55 kHz resonant frequency piezoelectric transducer was secured onto the top loading plate using a magnetic clamp with a layer of silicon jelly between the sensor and the loading plate. The generated AE was amplified by 81dB, filtered between 10 – 100 kHz, and sampled at a rate of 0.2MHz. The data was displayed in ring down counts measured across a threshold of 1.5V. The placement of the sensor varied from Koerner's experiments in which a waveguide was used to collect AE direct from the shear zone. Instead the sensor was placed on top of the loading plate, which was assumed to be in direct contact with the sand sample.

Figure 4.8 shows the results from experiments numbered 16, 17 and 18. The Leighton Buzzard sand underwent typical failure for a confined cohesionless soil, by exhibiting classical peak and critical state stress conditions. All experiments (16 – 18) showed a good repeatability, with peak stress being obtained at approximately 0 03% strain. Figure 4.9 shows the acoustic response as recorded by the sensor mounted on the loading plate. It was not possible to place a waveguide within the shear box, however considering the fact that the sand was compacted within the box and thus in good contact with the loading plate, which itself had low attenuation characteristics and the relatively short distances between the shear plane and the sensor, it was assumed that adequate levels of AE would still be sufficient for detecting movement within the shear box apparatus.

All three experiments showed a strong correlation between the generated AE and strain, and a good repeatability (close correlation in relation to each other) prior to peak stress being reached and subsequent failure. After failure had occurred it can be seen that there is a visible change in the slope of the AE verses strain (Figure 4.9). The strain at which peak stress was achieved in each experiment has been displayed on Figure 4.9. At peak stress the slope of each experiment lessens, showing a reduction in the levels of generated AE against strain, with the most notable changes in slope around a strain < 0.04%. Before peak stress and the development of the shear plane is reached, there is a greater amount of soil interaction as interlocking particles are forced apart (dilation) to produce a shear plane. AE is a direct result from soil grain interaction, and thus once a shear plane has developed, less AE was generated (marked by the reduction of the slope, and a reduction in shear stress) and thus less soil interaction takes place. The AE clearly showed a change in mechanism within the sand, and in this case was thus able to highlight the stress at failure.

This supported Koerner's argument that recorded AE could be substituted for either monitoring in situ stress or deformation within a slope. This maintained the view that AE could provide vital information as to the stress state of a slope. A comparison of the 'shear stress/acoustic emission count' graphs of Figure 4.6 and Figure 4 9 showed a large discrepancy in the levels of generated AE counts. Koerner's experiments (Figure 4.6) showed counts in the order of thousands,

where as Figure 4.9 showed counts in the order of 100 thousands. This difference has been accounted for by the following: Koerner's total amplification gain was only 50 dB, and the use of a waveguide within the shear box would have enabled a higher threshold to have been set in order to assess only the clearest of signals (however, the value of this threshold is unknown). The placement of the sensor on top of the loading plate would have meant that the AE collected would not have just originated from the slip surface but from any movement of sand grains against other soil grains, but also against the sides of the box. This would also result in a higher number of AE events being recorded.

4.4 Controlled strain tests

4.4.1 Compression test set up

Figure 4.10 shows in diagrammatic form the instrumentation set up. The purpose of these experiments was to investigate a quantitative relationship between the rate of deformation and the generated AE when an active waveguide was stressed under controlled conditions. This experimental procedure was proposed by Kousteni (2002).

A metal pipe waveguide 3m in length (55mm diameter and 3mm wall thickness) was surrounded by an annulus of river gravel (Figure 4.1). This gravel was confined around the waveguide by a geomembrane sleeve and compacted to a density of 1506kg/m^3. The geomembrane, a lightweight flexible membrane 3mm thick, was chosen because of its sufficient rigidity to hold the gravel in place without controlling the deformation mode of the backfill material This enabled the gravel surrounding the waveguide to be confined under similar conditions as it would be placed within the field, where the granular backfill would be surrounded by the in situ soil. At each end of the sleeve, wooden caps were screwed in place to prevent loss of gravel from the sleeve. This arrangement simulated the set up of an active waveguide.

The geomembrane sleeve was 1 m in length This enabled three experiments to be performed for each experimental set up. These three loading positions are shown in Figure 4.10. It became apparent after initial experiments that after each gravel sample was loaded, individual gravel particles had become crushed and thus the particle size distribution curve of that gravel had changed, as had the angularity. Thus after each set of experiments the gravel was emptied and replaced with new gravel. Each sample was placed by dropping gravel vertically into the geomembrane sleeve in layers, with each layer being compacted using a tamping rod.

Figure 4.11 shows photo of the compression apparatus. This shows how the load was applied to the gravel within the geomembrane. A load ring was placed between the top loading arm and the geomembrane for load monitoring purposes, whilst wooden contact shoes were placed around the geomembrane to distribute the load (i.e. to minimise unrepresentative point loading).

A compression test apparatus was used to deform the gravel under strain controlled conditions (i e as used in triaxial test). Strain rates were selected to resemble the following landslide rates of movement, as classified by the Transport Research Board (1978): rapid, moderate, slow and very slow. Table 4.2 shows all available rates for the compression apparatus. The four chosen rates are highlighted in red with their associated classification labelled.

The AE sensor was secured using a magnetic hold down device, onto the metal waveguide with a layer of silicon gel to aid acoustic transfer between the waveguide and sensor. The use of a hold down device ensured a good contact between the sensor and the waveguide, and also helped to maintain similar testing conditions over all experiments (section 3.2.1). The sensor was always placed 1 8 metres from the loading position. The total length of waveguide was 3m. It was unnecessary for these tests to have longer lengths of waveguide as the primary concern was to quantify AE rather than test the ability of AE to travel long distances (see chapter 5). Thus a practical distance of 1.8 m between sensor and source was selected.

4.4.2 Compression test procedure

The control of background noise was a serious concern in these experiments. As described in section 4.3.1, the threshold for monitoring and analysing generated AE was determined by the level of background noise. It was important that the background noise levels were as low as possible, thus enabling the threshold to be lowered and thus increasing the amount and quality of AE detected. Before each test was run, the background noise level was tested (which included monitoring noise from the operation of the compression apparatus) to ensure the chosen threshold of 0.3 volts was appropriate.

The testing was performed in two separate locations, firstly within a sound proofed room which removed any outside extraneous noise (except noise within the room which was associated with the running of the experiment itself), and secondly within an enclosed standard room within the laboratory. The sound proofed room was the preferred option for eradicating background noise (other than that emitted from the equipment itself). However this did not resemble a realistic environment into which such a system would finally be placed. Thus the majority of tests were performed within a standard room, which was closed to the public.

Between three and six tests were performed at each selected rate of strain, with each sample of gravel being displaced no further than 12mm (6% strain).

4 4 3 Large scale test set up

Figure 4 12 illustrates the different waveguide deformation mechanisms involved in the compression tests and in a landslide. Within the compression tests, the granular backfill material was compressed above and below the waveguide within a compression zone. In a deep seated rotational landslide that compression zone is spread along the waveguide on opposite sides above and below the developing shear plane. This compression zone generates AE as the particles rearranged under stress. This however is not the only mechanism at work in a deep seated

landslide failure. In the development of a shear plane, interlocked soil particles are forced to dilate. This dilation produces thin planes of progressive failure which ultimately align to form the shear plane. In section 4.3.2 this was shown to be a major mechanism involved in the generation of AE. This mechanism is not the dominant process at work in the compression tests. Thus further tests were needed to prove whether or not the data provided from the compression testing technique would be valid for shearing mechanisms experienced within the field.

Large scale tests were set up to recreate a more realistic waveguide deformation environment. Figure 4.13 shows a diagrammatic representation of the apparatus used, whilst Figure 4.14 shows a photographic representation of the actual set up. Essentially strain controlled tests were performed upon an active waveguide encased within Mercia Mudstone clay A horizontal column of clay (1.48 x 0.64 x 0.49m) was constructed within three wooden boxes, which were housed within a reinforced steel box of dimensions 1.4 x 1.7 x 1 4 metres. The reinforced steel box provided a rigid support to hold the clay within the three wooden boxes, which were braced against the reinforced steel box to provide a reaction force to the mechanical screw jack. The reinforced steel box was designed to withstand a pressure of 250 kPa (E. J. Yonan 1993). Once set up, the middle of the three wooden boxes was displaced using a mechanical screw jack. This caused the clay to deform the granular backfill around the waveguide in a similar manner to that of a shear surface deforming in a slope.

Figure 4.15 shows a plan view of the clay encased within the three wooden boxes. Each box was further reinforced with angle iron to ensure that they were rigid and that the deformation measured was a true displacement of the soil within the box and not the deformation of the box under load.

The same waveguide and granular backfill used in the compression tests were used in the large scale testing. Figure 4.17 shows a cross section of the arrangement of the clay, backfill and waveguide, and the layers with which it was built up. First layer one was laid and compacted, followed by the building up of layers two and three. The granular backfill (layer three) and the waveguide were then placed before the final layer of clay was placed and compacted. Once the

waveguide arrangement and surrounding clay was placed, the top section of the wooden box was screwed in place. This prevented the escape of any moisture from the clay.

Three tests were performed. Each test was constructed with new gravel and remoulded clay. Two tests were performed at the equivalent of a moderate displacement rate, and one was performed at the equivalent of a slow displacement rate (see section 4 2 1) Due to limitations of available rates on the mechanical screw jack, the slow displacement rate was achieved by means of a stop-start experiment; the screw jack was run at a moderate rate for 10 minutes, and then stopped for a further 90 minutes before starting again. The actual rates chosen were: a 'moderate' rate of approximately 0.2 mm/min, and a 'slow' rate of approximately 0.02mm/min. It was important to validate the experiments performed on the compression apparatus, and to see whether similar trends took place on both experimental apparatus across an order of magnitude difference in the deformation rates.

The clay, Mercia Mudstone, was sourced from a local brick pit. The clay had a moisture content of 15%, and had 5 – 6% cement fines already mixed into the clay by the brick works. The cement fines were mixed into the bricks to help with the firing process; their effect on the clay may have increased the liquid limit but would have little effect on the characteristics of the clay. The following is a summary of the clay's characteristics, a full report in accordance with BS 1377: Part 2: 1990 regarding classification and plasticity can be seen in Table A4.3, Appendix A.

Classification	Clay with 7% course silt/fine sand present
Liquid limit	29.9%
Plastic limit	18.9%
Plasticity index	11.1%

The clay was compacted at 15% moisture content. At this moisture content the clay was still in a 'mouldable' state for placing within the box, but with a moisture content lower than the plastic limit to encourage a shear failure rather then a

plastic failure as the mechanism of deformation. The dry density of the clay was measured by sand replacement technique (BS 1377 Part 9 1990). An average density of 1765kg/m^3 was achieved. Confidence can be placed within the construction of each experiment, Figure 4.29 shows that the clay was successfully compacted with little or no air voids, and moisture contents taken soon after each experiment are all very similar, exp197, exp198 and exp199 had moisture contents of 15%, 16% and 15.5% respectively.

4.4 4 Large scale test procedure

Experiments were performed within a large open laboratory and were thus more susceptible to an intrusion of background noise. Therefore tests were performed outside of normal working hours. Again before each test was run, the background noise level was measured (which included associated noise from the mechanical screw jack apparatus) to ensure the chosen threshold of 0.3 volts was appropriate.

The aim behind reducing the intrusion of background noise was to investigate the possibility of producing an early warning system based on AE. Ultimately, such a system would be based within the field, where there would be limited control over background noise. Similar checks on background noise would still be necessary prior to monitoring in the field, but the effects of a raised threshold would minimise the amount of AE that could be monitored.

A load cell was placed between the screw jack and the middle wooden box, and either side of the middle wooden box linear variable differential transformer (LVDT) displacement gauges and manual dial gauges were placed to monitor displacement (Figure 4.16). The load cell and the LVDT displacement gauges were all connected to a data logger, which was synchronised with the computer used for monitoring the AE generated The AE sensor was positioned on the waveguide and held in place by a magnetic clamp. A layer of silicon gel was used to improve the contact between the AE sensor and the waveguide surface. The sensor was placed at 1.8m from the centre of the middle wooden box, between the two shear surfaces that would developed along the edge of that wooden box as a

result of loading. This position was chosen to try and maintain similar testing conditions as used in the compression tests, where the sensor was 1.8m from the compression zone.

4.5 Analysis of Results

4.5.1 Compression test

The results of the compression tests are shown in Tables A4.4 and A4.5 in Appendix A. Table A4.4 displays the results from experiments 151 to 159, which were performed within the sound proofed room. Table A4.5 displays results from experiments 160 to 176, which were all performed in a normal working environment. All experiments were labelled with the letters 'exp' followed by the experiment's number, for example experiment number 151 was denoted as 'exp151'.

Figure 4.18 is the load versus displacement graph for all compression test based experiments. Out of 26 experiments, only one (exp171) demonstrated behaviour which was different to the norm, but in most cases an increase in load with displacement was observed. A linear trend line was placed over each experiment data set to obtain a gradient of the line Table A4.6 in Appendix A shows the gradient and the R-squared values for those trend lines, which average 0.9832 and thus show the linear equation to be reliable trend line. The mean of the gradients was 0.194 with a standard deviation of 0.078, which demonstrated a close 'packing' of data for the load deformation graph These results showed not only good repeatability, but also demonstrated confidence that the constant reconstruction of samples and testing were performed to the same high standard every time.

The acoustic output of all compression based experiments in Figure 4 19 shows the rate of events (counts per hour) on a logarithmic scale against the displacement. Although there is no comparison for the data tested in the normal laboratory environment at the very slow rates, a grouping of rates can be seen

regardless of testing environment Thus it can be said with confidence that little or no extraneous background noise contributed to the recorded AE when tested in the normal laboratory environment. Noise emitted from the testing apparatus itself was successfully removed by the application of a threshold to the AE monitoring system Thus the AE recorded from the compression tests originated from interaction within the backfill and between the granular backfill and the waveguide under load.

Figure 4.20 shows data from all experiments carried out in the sound proofed room and in the normal laboratory environment (exp151 – exp176). This data has been displayed in the form of event rate versus time, with both scales being logarithmic. The choice of monitoring events rather than RDC is explained fully in chapter 5 2. The grouping of results became clearer as the different orders of magnitude of deformation rates were further separated out into clear bands. A modified version of this graph is shown in Figure 4 21, where the initial data has been removed until a steady settled pattern has emerged.

In each case the actual data removed from the early part of the graph represented less than 1mm of displacement. Within in an early warning system that first millimetre of movement is very important in order to establish the rate of movement of the slope and the predicted failure time as early as possible. Figure 4.18 shows that there was an immediate increase in load with deformation and thus no slack within the experimental set up, which might have explained the variation in data within the first millimetre of movement. Whilst there was no obvious slack (an increase in displacement without an increase in load), it is possible that there might have been slack between the geomembrane sleeve and the gravel backfill. The first millimetre of movement may have been between the deforming geomembrane and the gravel. Such displacement would have resulted in an increase in load, but would not result in the generation of AE in quite the same way as later on in the experiment.

Based upon the resulting patterns in Figure 4.21, measured AE from a deforming waveguide in a slope could be compared against this laboratory data, and provide information on the order of magnitude of movement rates. However, for the

compression test experiments there seems to be a 'settling down' period, in which the system is unable to reliably distinguish the rate of displacement within the first 1mm of displacement. In a field monitoring situation the geomembrane would not be present, and thus its effect would no longer be an issue, but the placing of the backfill within a borehole around the waveguide would become a fundamental concern. The backfill would need to be sufficiently compacted throughout it's depth to ensure that any initial displacement of the surrounding soil would immediately translate to a true deformation of the backfill, and subsequent generation of reliable AE.

4.5.2 Large scale test

The results were collated from the data logger, responsible for data from the load cell and the electronic displacement measurement devices (linear variable transformer device, LVTD), and from the computer used to record AE data. Both the computer and the data logger had synchronised clocks to facilitate the bringing together of data. This data is summarised in Appendix A, Table A4.7. Due to the nature of the mechanical screw jack, it was impossible to exactly preset the rate of deformation, and thus the rate was calculated afterwards Figures 4.22 and 4.23 are displacement time graphs, and show how the strain rate was calculated by comparing data from the manually read dial gauges and the electronic displacement measurement devices. Figure 4.22 illustrates data collected from exp197 and exp198, whilst Figure 4 23 illustrates data from exp199 which was run on a 'stop start' principle in order to achieve a lower strain rate. In each case the average gradient of the line was calculated and the following strain rates were deduced:

exp197	0.22mm/min	(moderate strain rate)
exp198	0 24mm/min	(moderate strain rate)
exp199	0.022mm/min	(slow strain rate)

The practice of the 'stop start' experiment could be brought into question as to it's validity as a method of simulating a 'slow' landslide. It would be true to say that

the mechanism at work was no different to that of a moderate rate landslide that had just been separated by time intervals, and thus when plotted on a time graph would naturally shift along the time scale by an order of magnitude. On the other hand, it is often unknown if a landslide measured at a slow rate, over a period of hours or days, actually deformed at a constant rate or in a 'slip-stick' fashion Figure 4.24 shows the load against displacement for the large scale tests. The work done by exp197 (constant rate of displacement) and exp199 (stop start rate of displacement) are very similar in their trend and their quantity, suggesting that the same mechanism of movement was in place for both experiments Unfortunately no load data was available for exp 198 due to hardware error.

The acoustic emission data can be seen in Figure 4 25, which shows the event rate plotted against displacement. In Figure 4.26, which presents the event rate against time on a logarithmic scale, the data has been superimposed onto the results received from the compression tests. The data can be seen again to group not just in relation to the other large scale box tests at moderate (exp197 & exp198) and slow strain rates (exp199), but also in relation to the compression test data. This further supports the ability of the system to differentiate between orders of magnitude of deformation However, the comparison does demonstrate a reduction in the levels of AE measured by the large scale testing. For example, after 10mm of displacement at a moderate strain rate, exp197 achieved a final event rate close to 16,000 events per hour, compared with exp166 which reached 48,000 events per hour at the end of the experiment.

This difference was accounted for in the nature of the deformation of the granular backfill. Figure 4 27 Further illustrates the different mechanisms of movement involved in the compression tests and the large scale tests. Initially it gives the impression that the area of gravel being deformed was greater in the large scale test, and that both compression and shear mechanisms were occurring. This would result in an increase in generated AE, however as previously noted, the opposite occurred which would suggest that there was actually less deformation of the gravel and thus less generated AE.

Figure 4.28 shows the deformation of the clay in relation to that of the middle wooden box after exp 197 was complete. It is not known how much of the displacement measured by the movement of the wooden box was taken up by actual deformation of the gravel or by compaction of the clay around the gravel backfill. This means displacement measured by the dial gauges and the LVDT gauges was not a true measurement of the deformation of the gravel. In the compression test the majority of the displacement was taken up by the gravel, in the large scale tests that same displacement has not been translated through to the gravel due to local compaction of the clay, and thus a reduction in generated AE results.

The compaction of the clay was achieved by placing the clay and dropping a free falling weight on the clay as it was constructed in layers. This achieved good compaction against the base and sides of the box, but voids existed beneath the top of each wooden box. These can be seen in Figure 4.29, where depressions (footprints) are still visible on the clay surface after testing. Thus it is assumed that although the wooden box deforms linearly the clay has space to remould around the gravel and fill the voids between the surface of the clay and the top of each wooden box. Thus the displacement provided by the mechanical jack was not translated direct to the gravel, but was taken up in the movement of the clay, and thus resulted in a reduction of generated AE.

A shear vane test was carried out to gain an estimate of the in situ shear strength of the clay. An average shear strength of 82 kPa was measured. This is classed as a stiff soil but in the field, over consolidated clays or hard soils can have an undrained shear strength greater than 150kPa (J. Atkinson *et al.* 1998). The large scale tests can thus be thought of as conservative in their modelling of the deformation of a waveguide. In the field, it is considered that the surrounding soil, of greater stiffness (such as over consolidated clay), would not be able to deform around the waveguides due to the lack of voids. Thus any displacement brought on by slope instability would be translated directly to the waveguide and the result in a true displacement of the backfill.

The deformation of the gravel backfill could not be quantified, and so the extent to which it was deformed remains unknown. Attenuation of AE within the backfill could have been partly responsible for a reduction in recorded AE. Assuming that only small deformations took place within the gravel, it is likely that these movements took place on the edge of the gravel backfill (away from the waveguide). Generated AE may have significantly attenuated before reaching the waveguide such that the AE amplitude fell below the monitoring threshold and went undetected. However, despite the effects of either attenuation or the movement of the clay around the gravel backfill, it was demonstrated in Figure 4.25 that exp197, exp198 and exp199 could still be differentiated into their respective orders of magnitude of displacement.

4.6 Chapter summary

This chapter has sought to investigate the quantification of AE generated in controlled laboratory experiments. Due discussion has been given to the need of a quantified scale for evaluating the recorded AE from a landslide as opposed to a qualitative scale which is open to misinterpretation. Two different methods of generating AE were described and implemented Compression tests were used for their ease and simplicity in construction and testing. This enabled many tests to be done at four different orders of magnitude of displacement. This provided a clear correlation between the rate of events recorded and the time over which the events were recorded. Clear groupings of data demonstrated the ability of the AE monitoring system to differentiate between orders of magnitude of displacement, and thus provided a reliable quantitative guide for assessing and characterising AE into the current standard for categorising landslide movement (see Table 4.1). Further large scale tests were carried out to demonstrate similar trends in a more realistic deformation environment, where the mechanisms involved more closely matched that of shear plane formation in a slope failure.

Description	Displacement rate (m/s)	Displacement rate equivalent
Extremely Rapid		
	3m/s	3m/s
Very Rapid		
	0.005m/s	0.3m/min
Rapid		
	0.0000174m/s	1.5m/day
Moderate		
	0.00000056m/s	1.5m/month
Slow		
	0.000000056m/s	1.5m/year
Very Slow		
	0.0000000018m/s	0.06m/year
Extremely Slow		

Table 4.1 Rates of landslide movement (Transport Research Board 1978)

		Approximate Rate of Feed (mm/min)				
	Driver	30	60	36	54	45
	Driven	60	30	54	36	45
Gear Change Position	A	0.3675	1.47	0.49	Rapid 1.1025	0.735
	B	0.0735	0.294	Moderate 0.098	0.2205	0.147
	C	0.0147	0.0588	0.0196	0.0441	0.0294
	D	0.00294	Slow 0.01176	0.00392	0.00882	0.00588
	E	0.000588	0.002352	0.000784	0.001764	Very Slow 0.001176

Table 4.2 Approximate rate of displacement from compression cell apparatus.

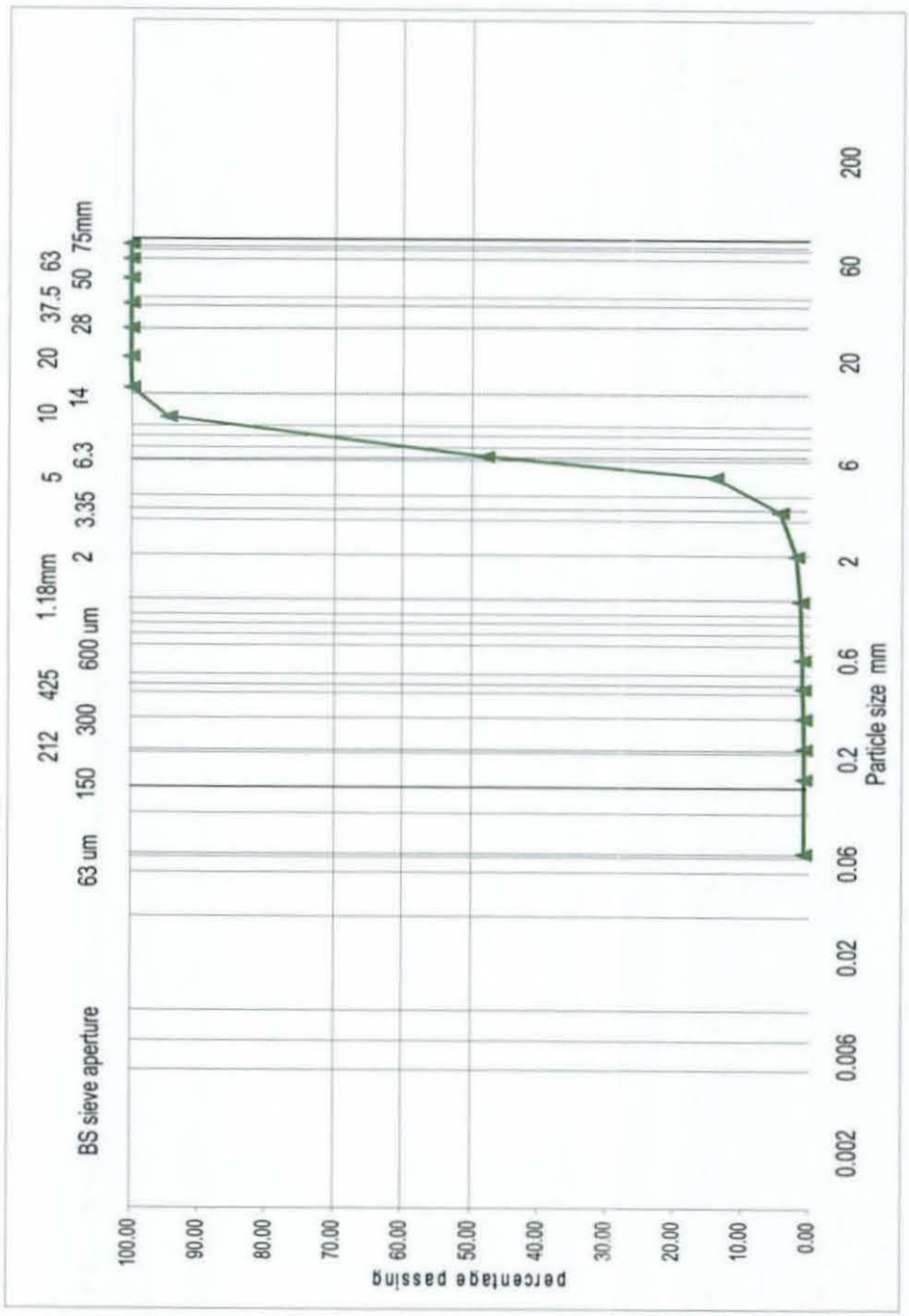

Figure 4.1 Particle size distribution curve for crushed river gravel

AE data is feed into the system via an 'analogue to digital converter board'. This is resembled by the module 'A/D'. The red lines show the path of data transfers from a module output to a module input. Each data transfer line carries the data in real time to the relevant module for analyses. Each module is explained in section 4.3.1.

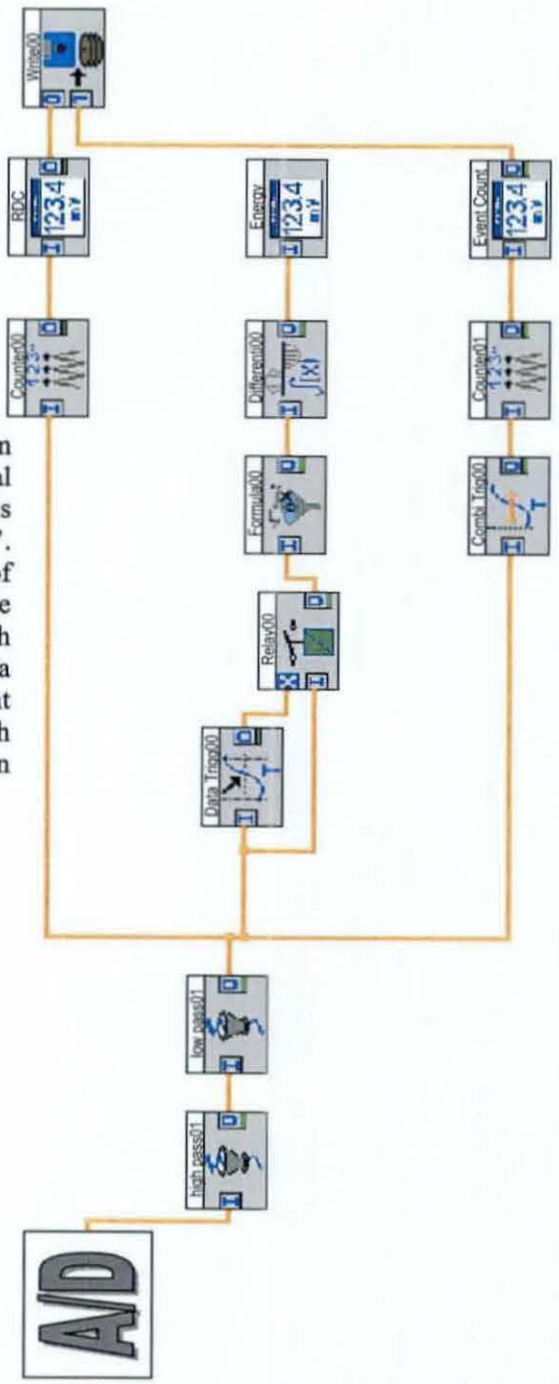

Figure 4.2 DASYLab worksheet

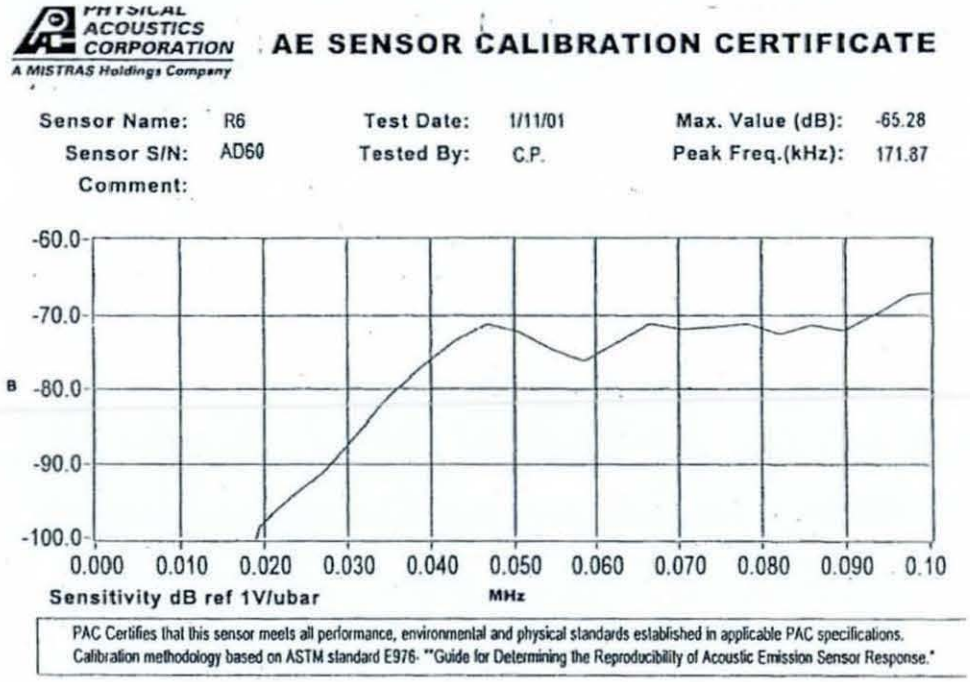

Figure 4.3 AE sensor calibration chart

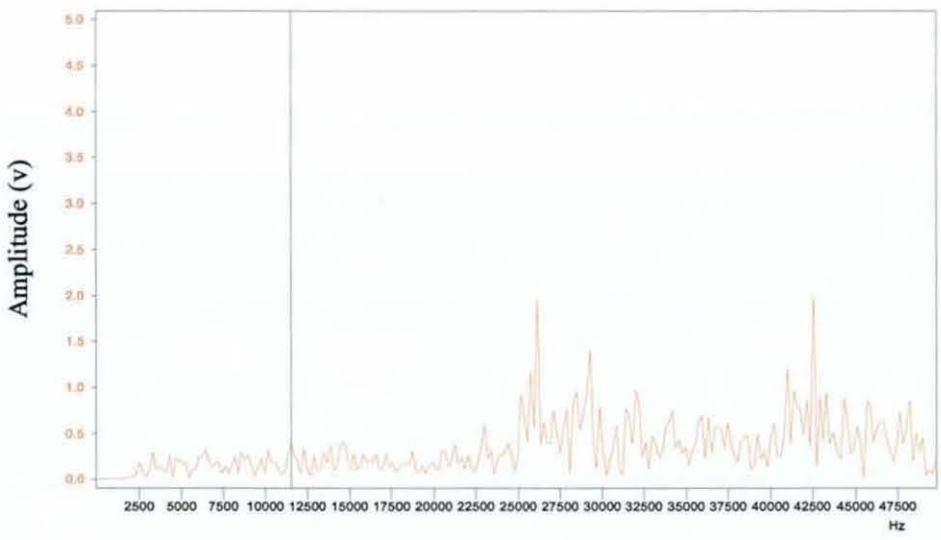

Figure 4.4 Fast Fourier Transform (FFT) of river gravel generated AE

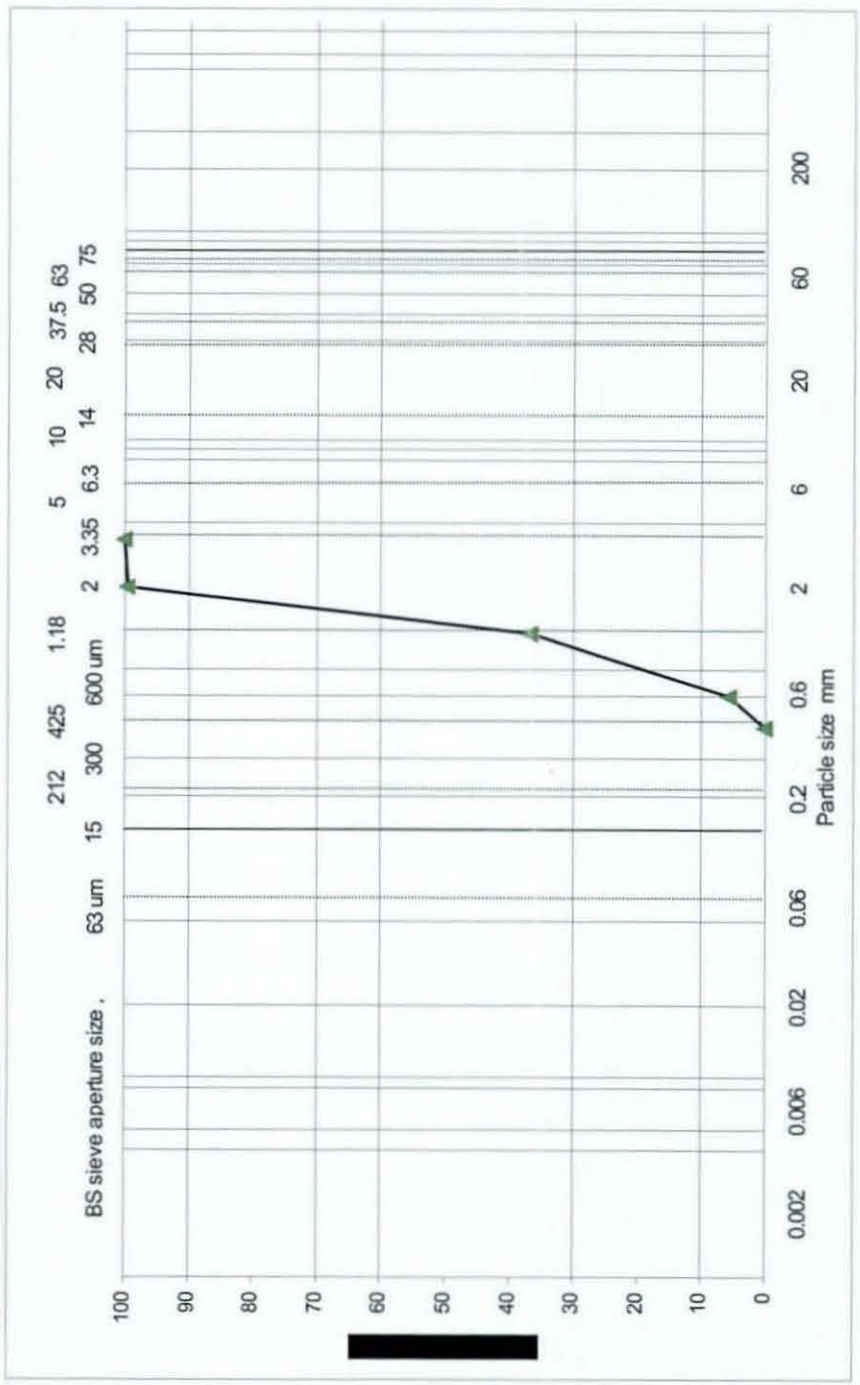

Figure 4.5 Particle size distribution of Leighton buzzard

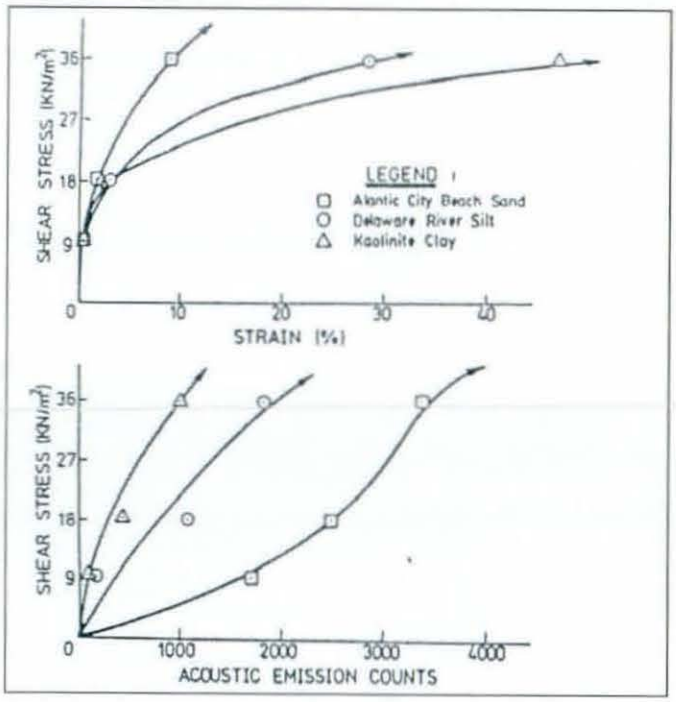

Figure 4.6 Stress versus strain and stress versus AE behaviour of a sand, silt and clay tested under identical conditions (Koerner *et al.* 1981)

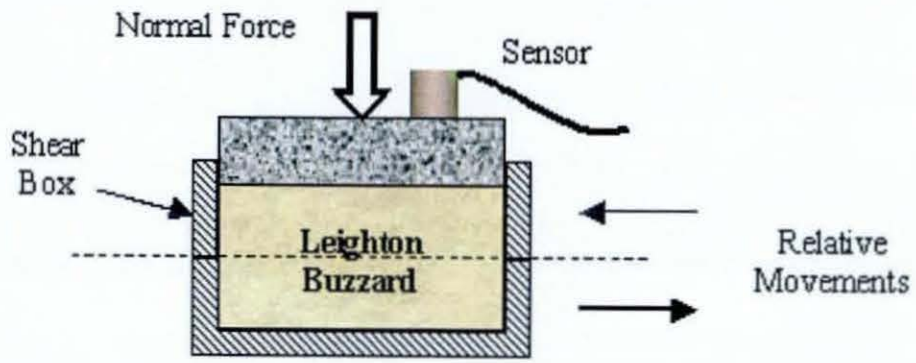

Figure 4.7 Experimental set-up of direct large shear box

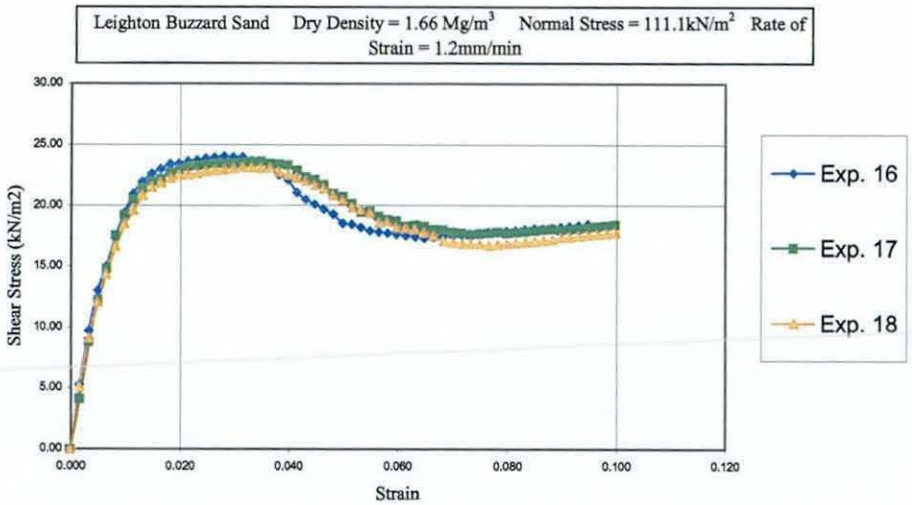

Figure 4.8 Stress Strain graph showing results from exp16, 17 and 18

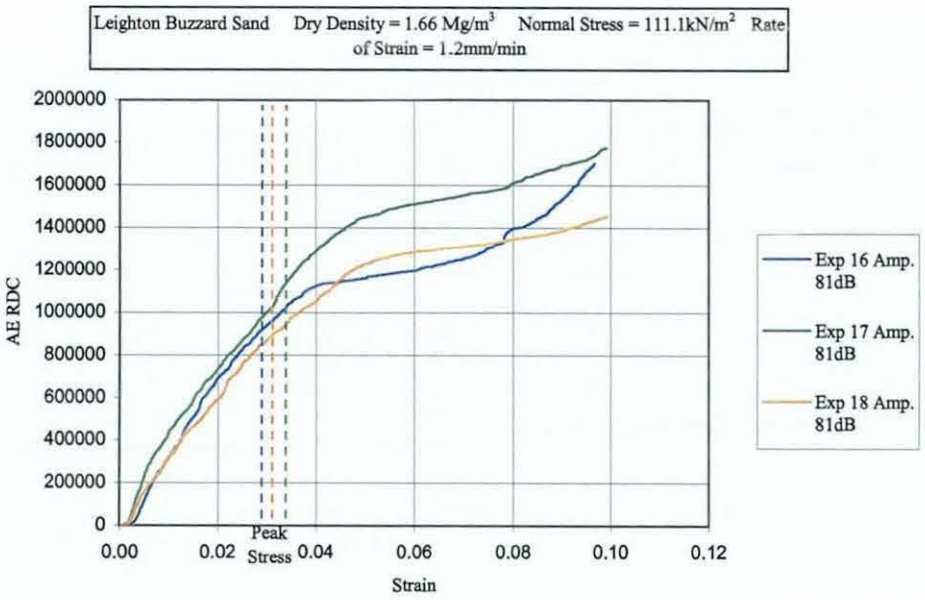

Figure 4.9 Acoustic emission output from exp 16, 17 and 18, showing RDC v strain

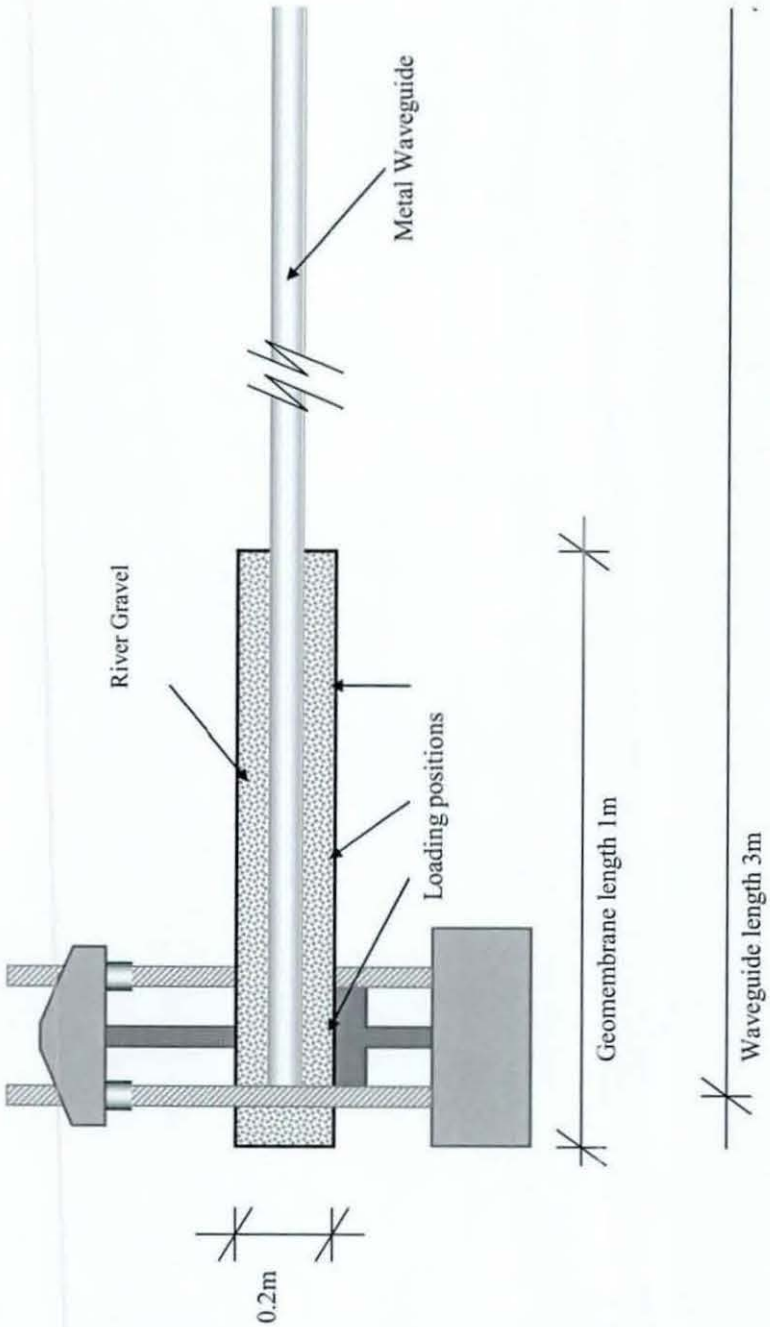

Figure 4.10 Compression test set up showing the three loading positions

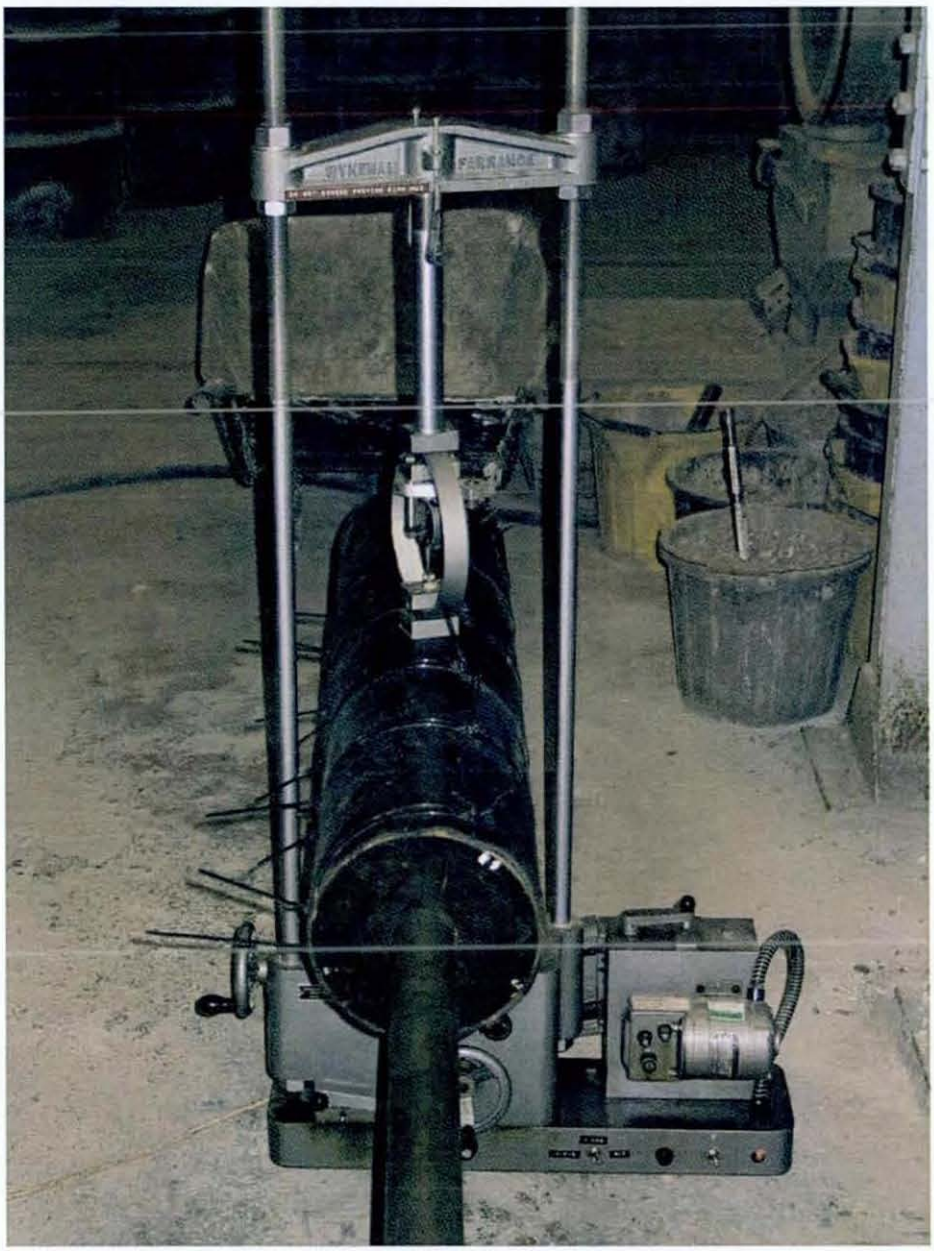

Figure 4.11 Photo showing the loading of the compression test set up

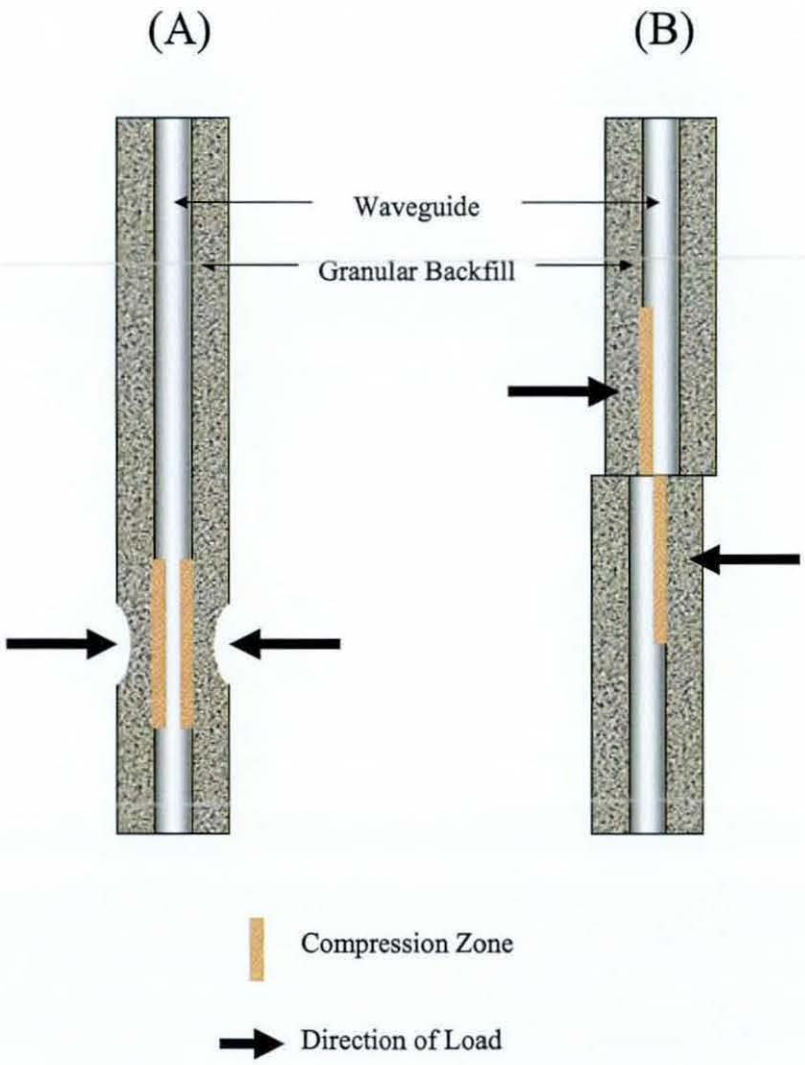

Figure 4.12 Illustration of difference deformation mechanisms on compression test set-up (A) and in the field (B)

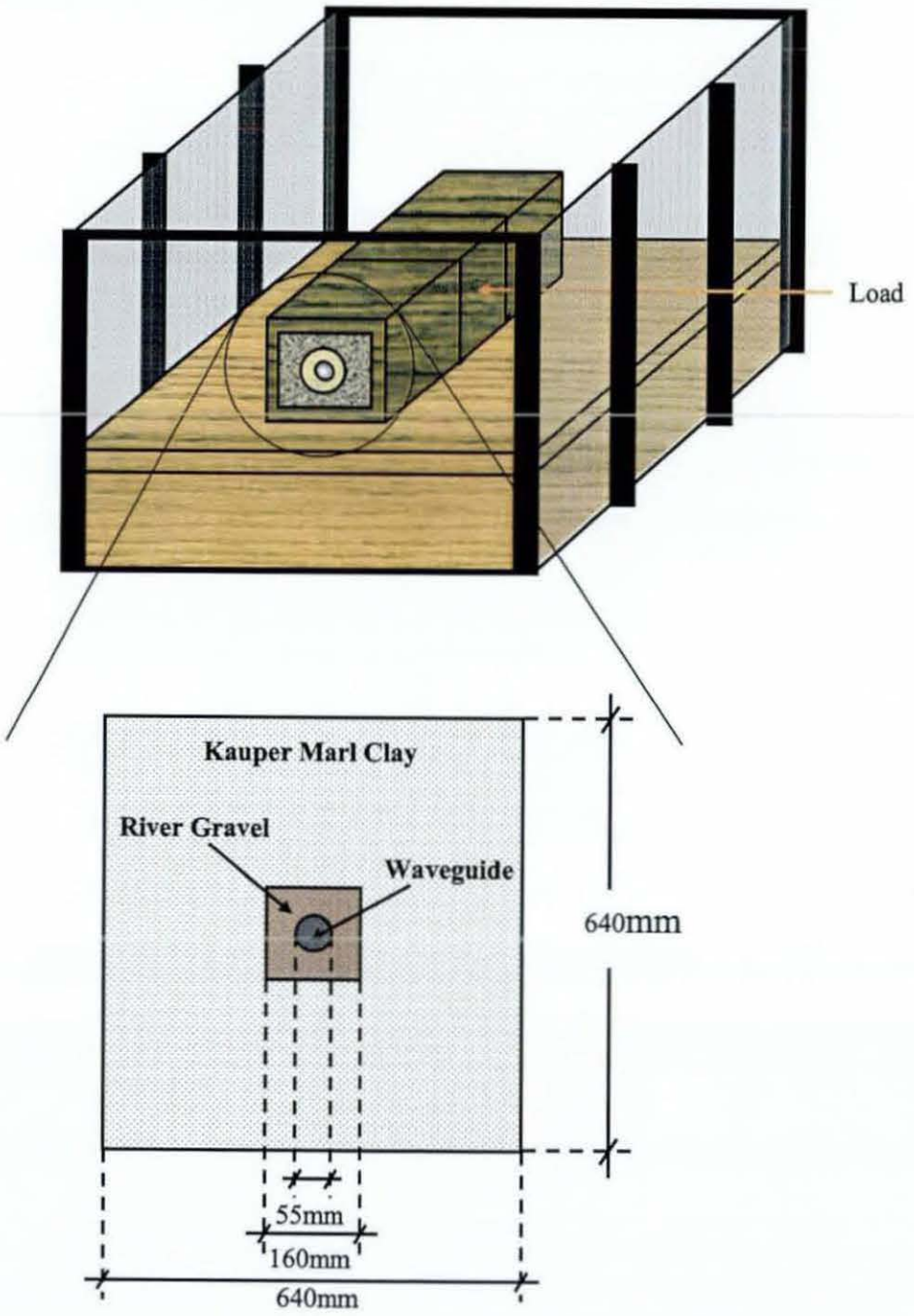

Figure 4.13 Diagrammatic representation of large scale test rig

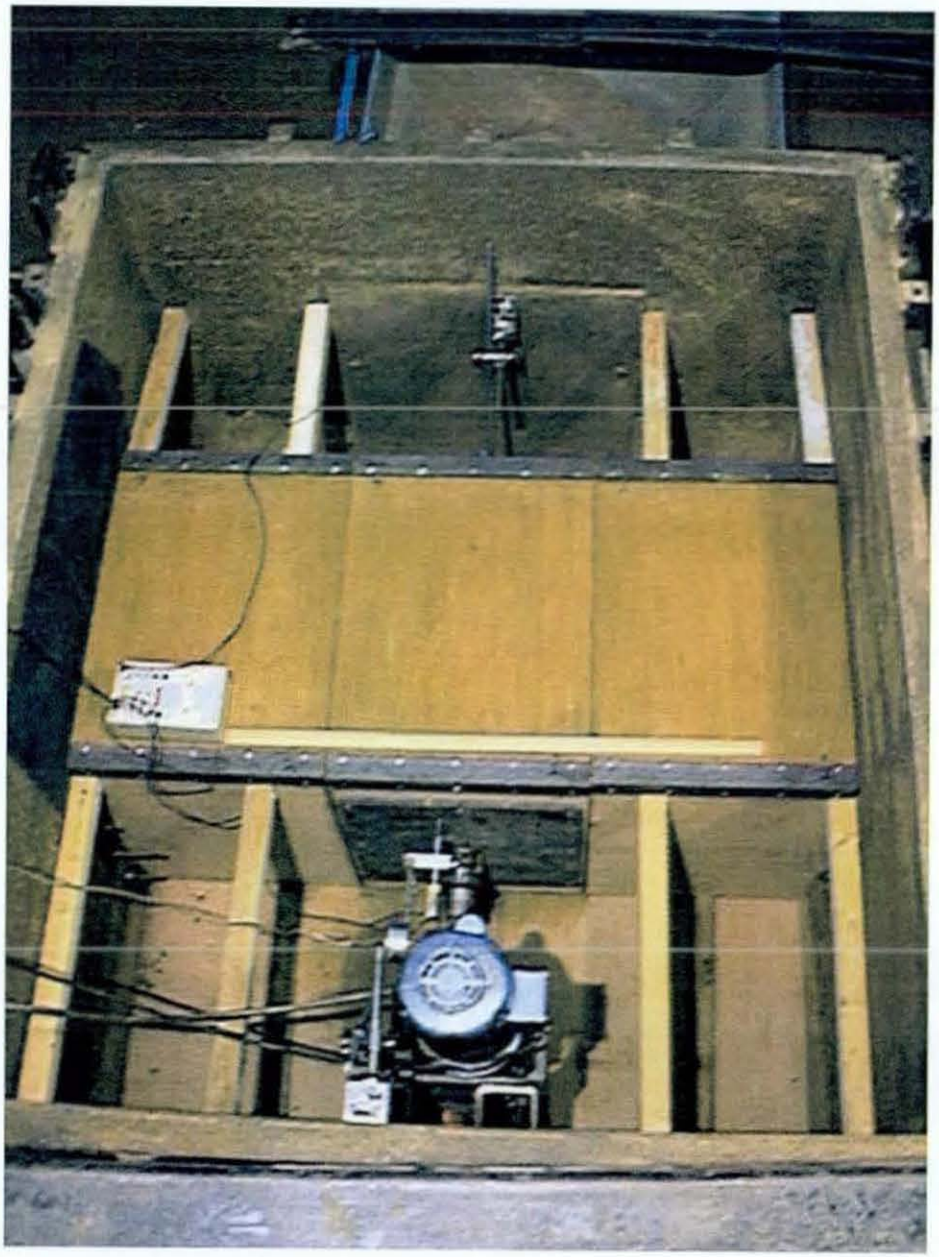

Figure 4.14 Photographic representation of large scale test rig

Figure 4.15 Plan view of clay and gravel within the 3 wooden boxes

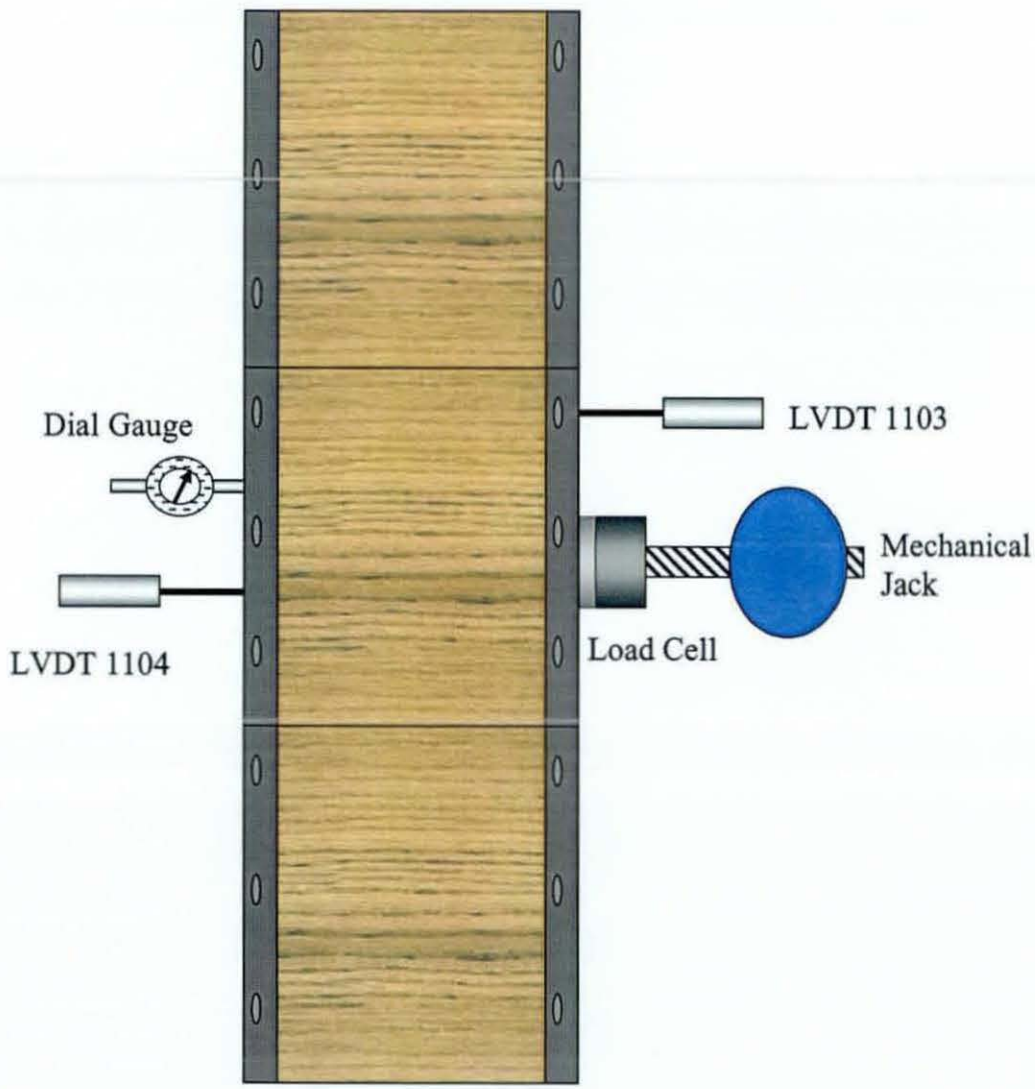

Figure 4.16 Plan view of instrumentation lay out for large scale testing

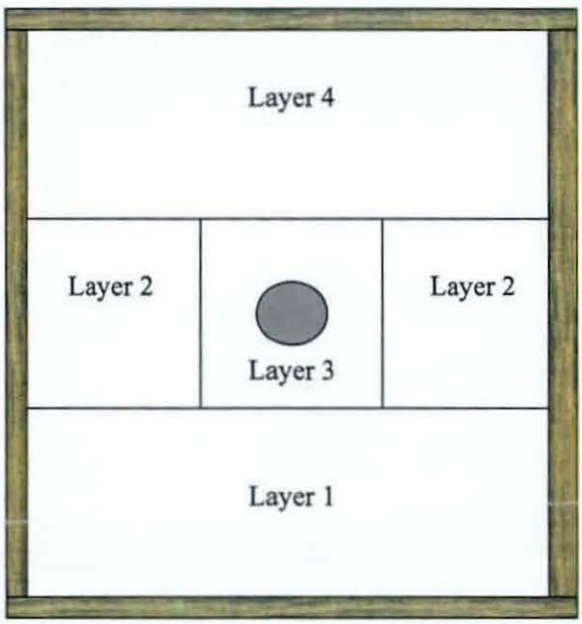

Figure 4.17 Cross section of large scale test rig showing layers of construction. Layers 1, 2 and 4 consist of clay whilst layer 3 consists of river gravel

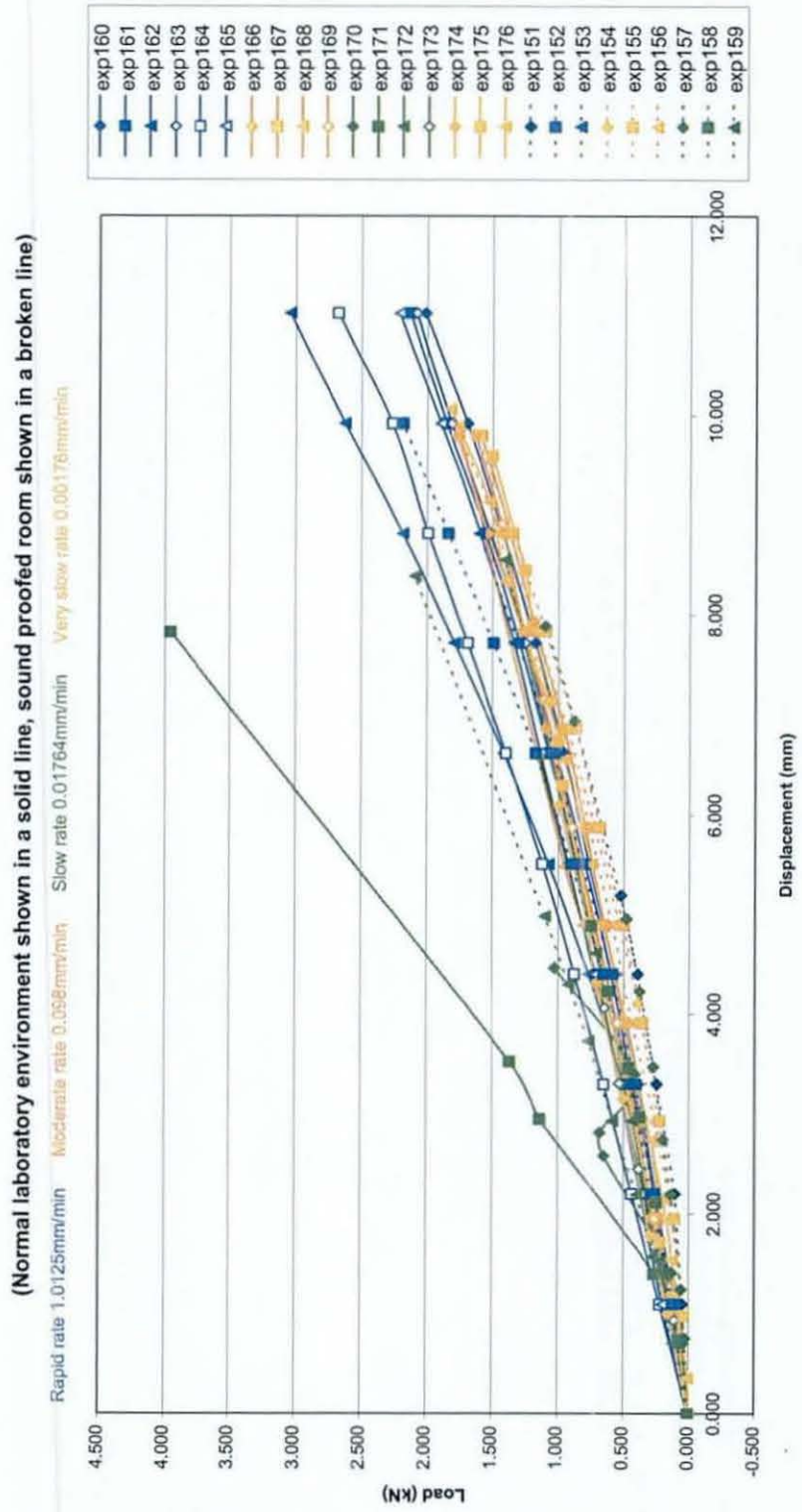

Figure 4.18 Load verses displacement for all compression based experiments

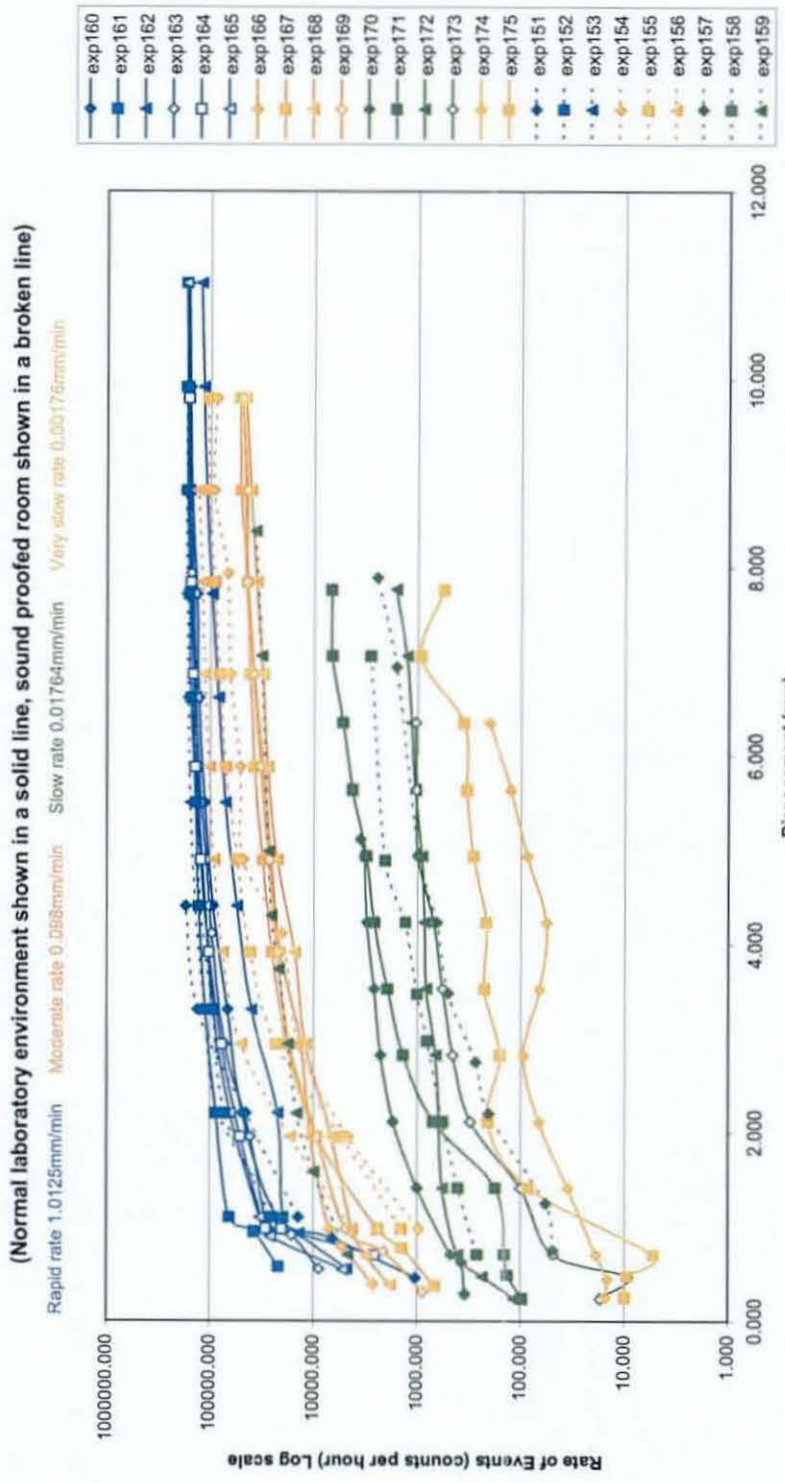

Figure 4.19 Rate of AE (events per hour) verses displacement for all compression based experiments

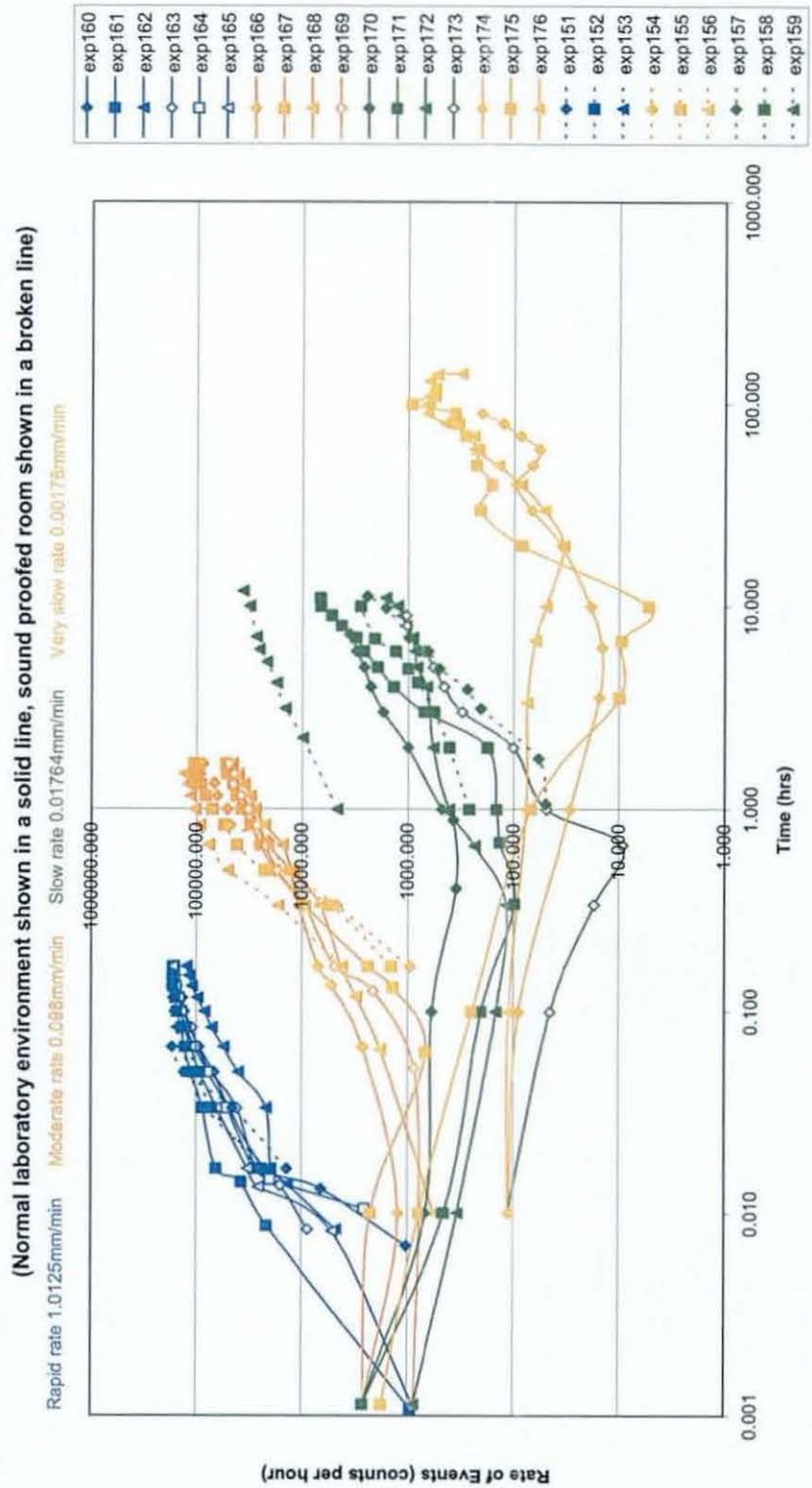

Figure 4.20 Rate of AE (events per hour) verses time, both on a logarithmic scale

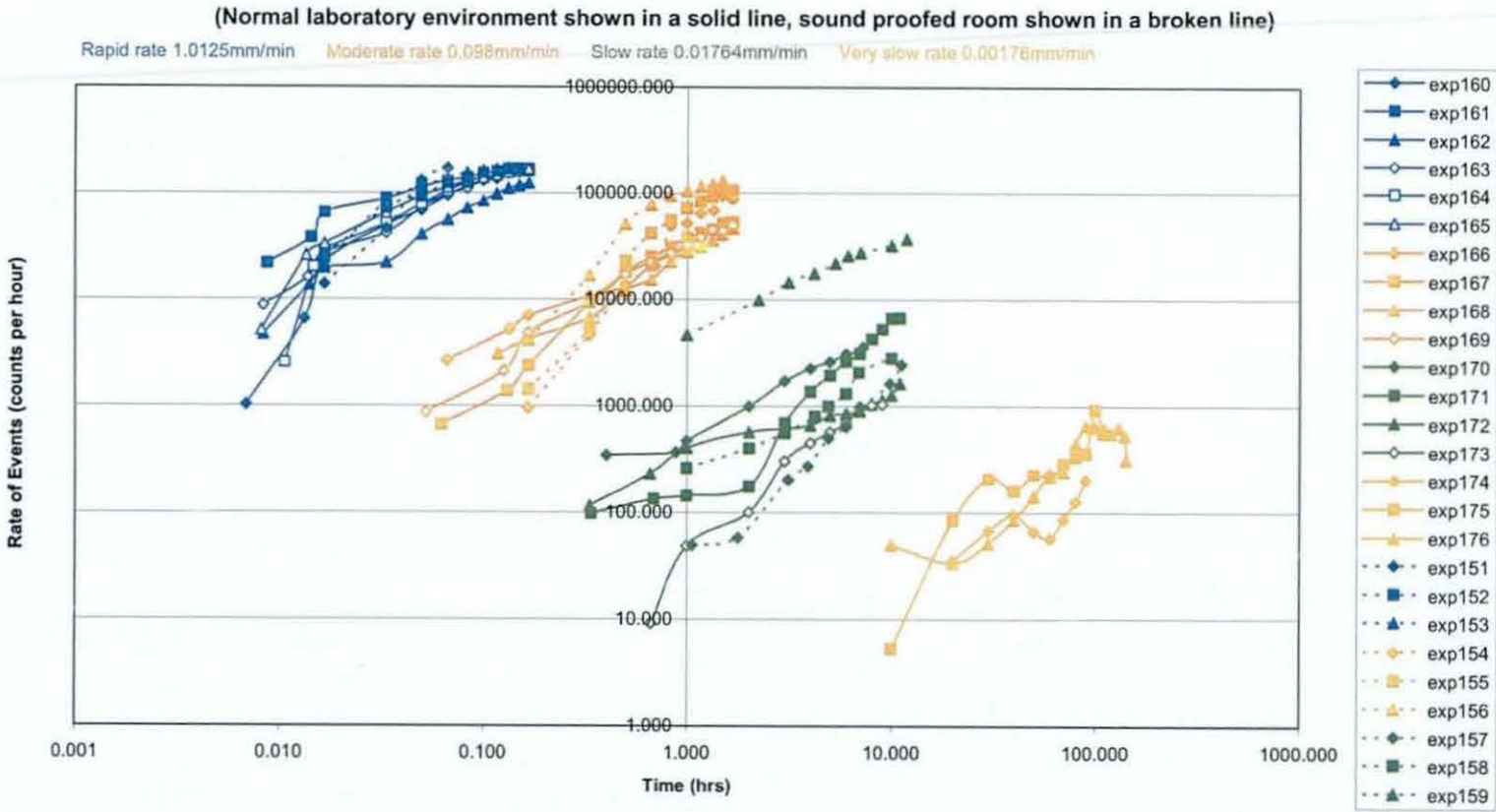

Figure 4.21 Rate of AE (events per hour) verses time Modified

(a)

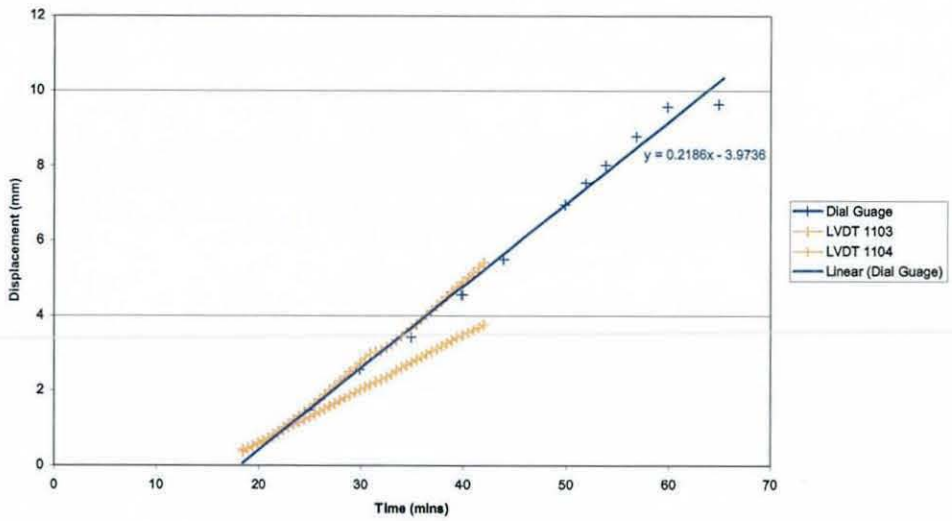

(b)

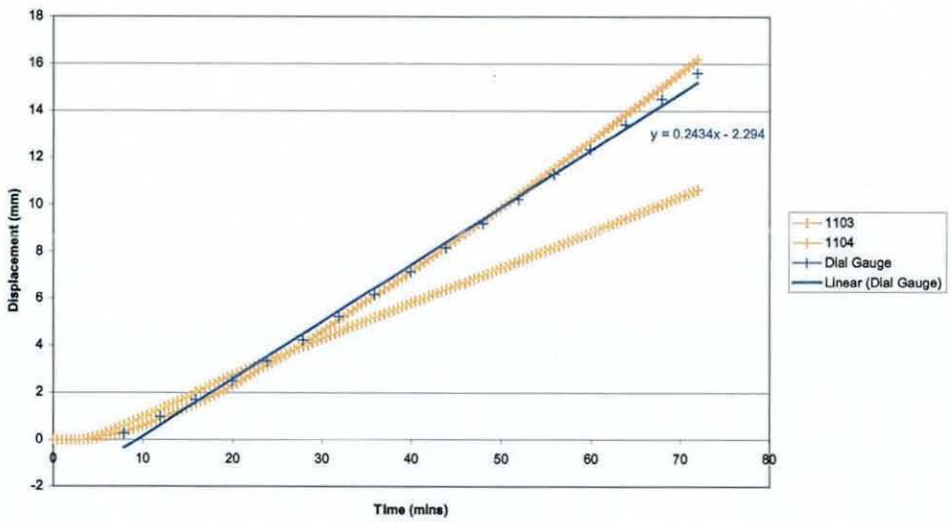

Figure 4.22 Displacement verses time graphs for exp197 (a) and exp198 (b) used to calculate the rate of displacement

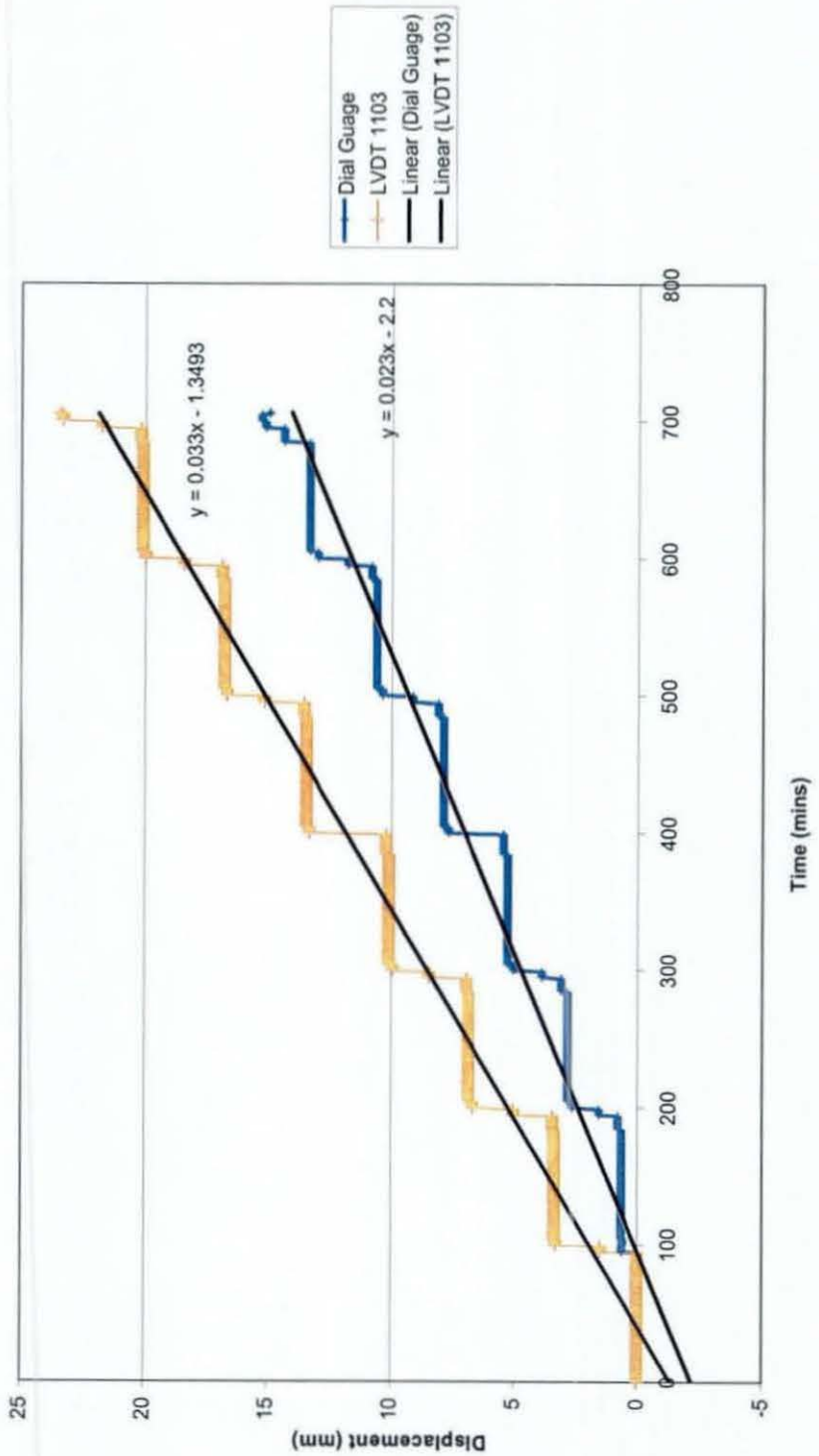

Figure 4.23 Displacement verses time graphs for exp199 used to calculate the rate of displacement

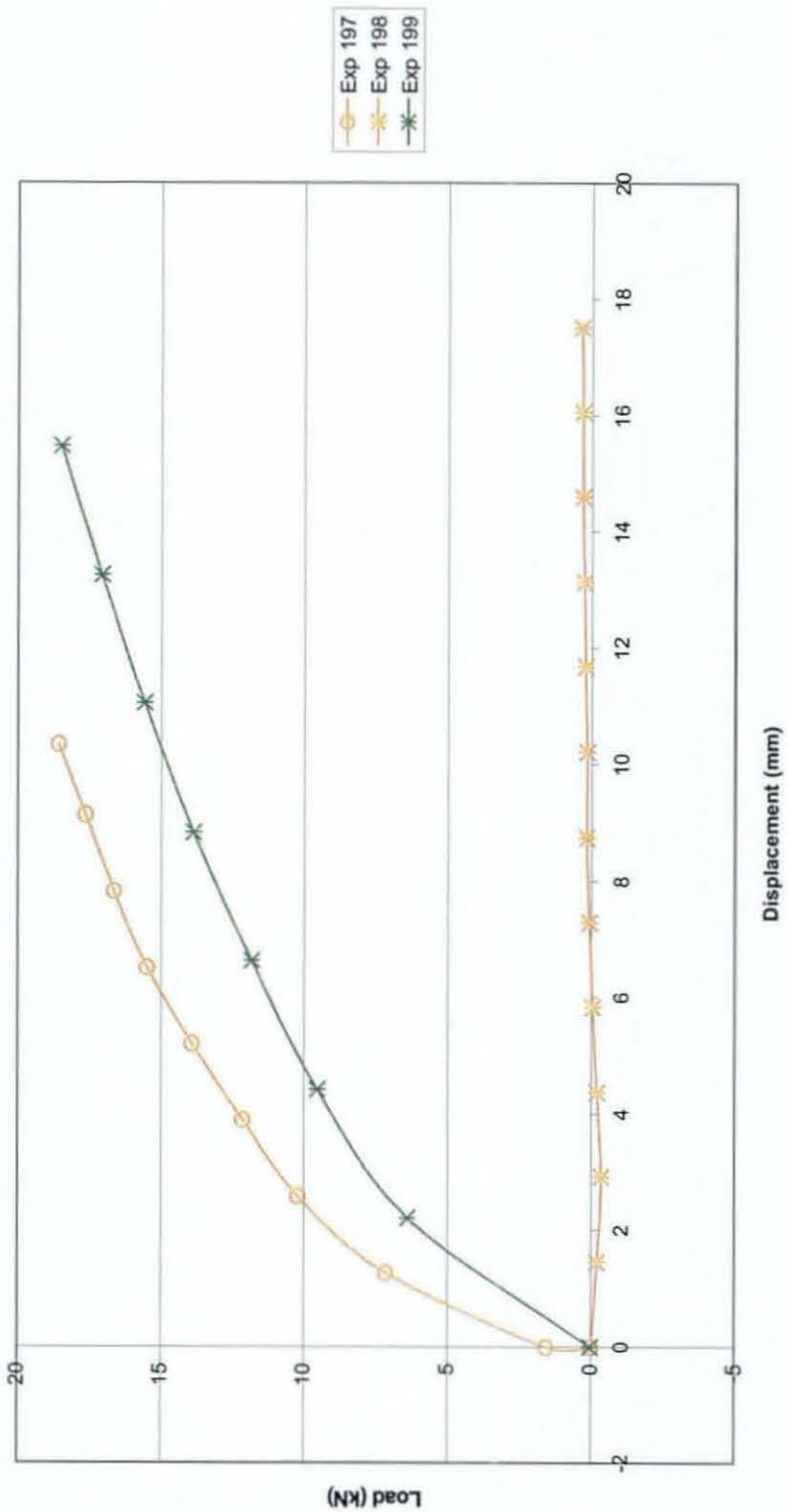

Figure 4.24 Load verses displacement for large scale tests

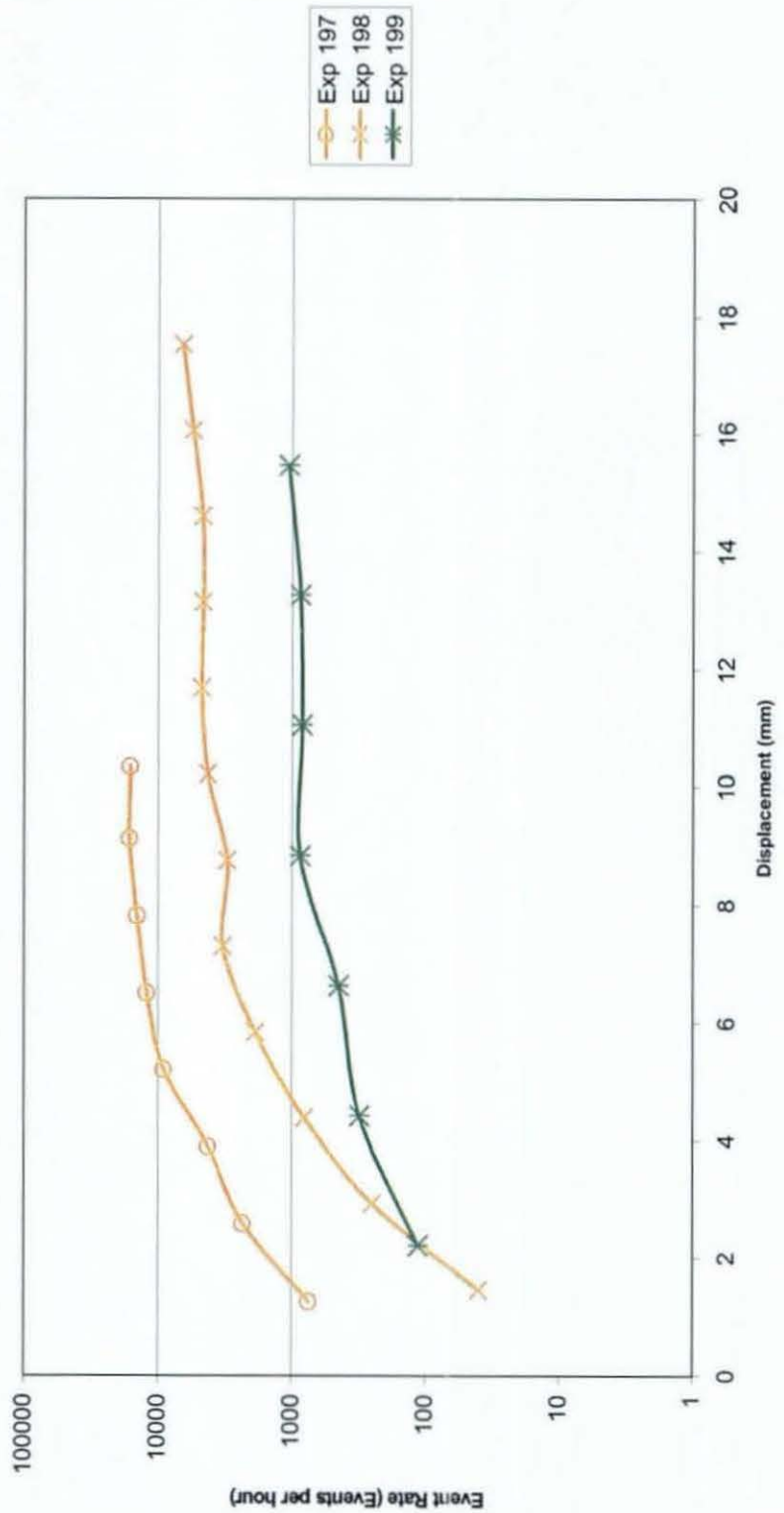

Figure 4.25 Event rate verses displacement for large scale tests

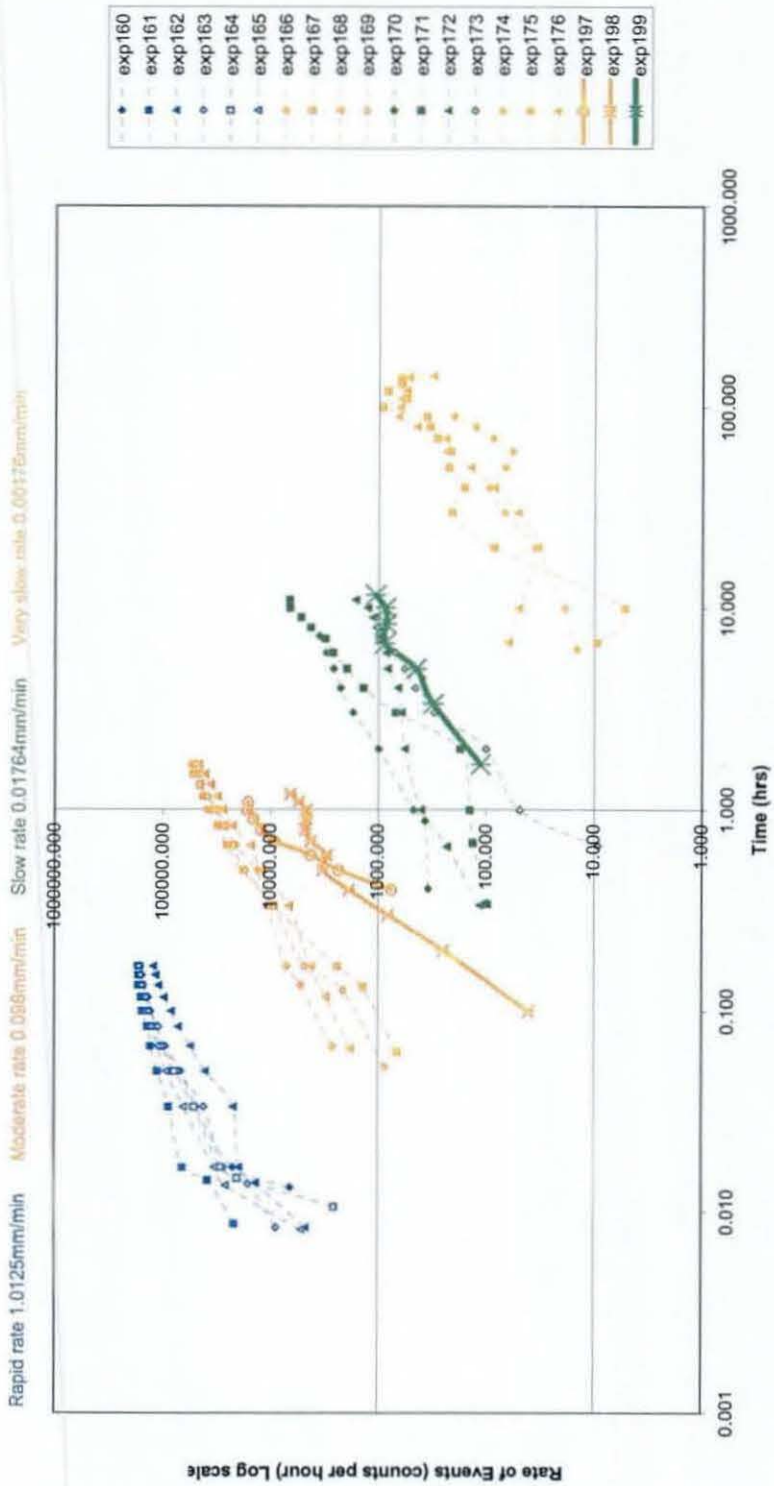

Figure 4.26 Rate of AE events verses time, showing compression test data and large scale test data

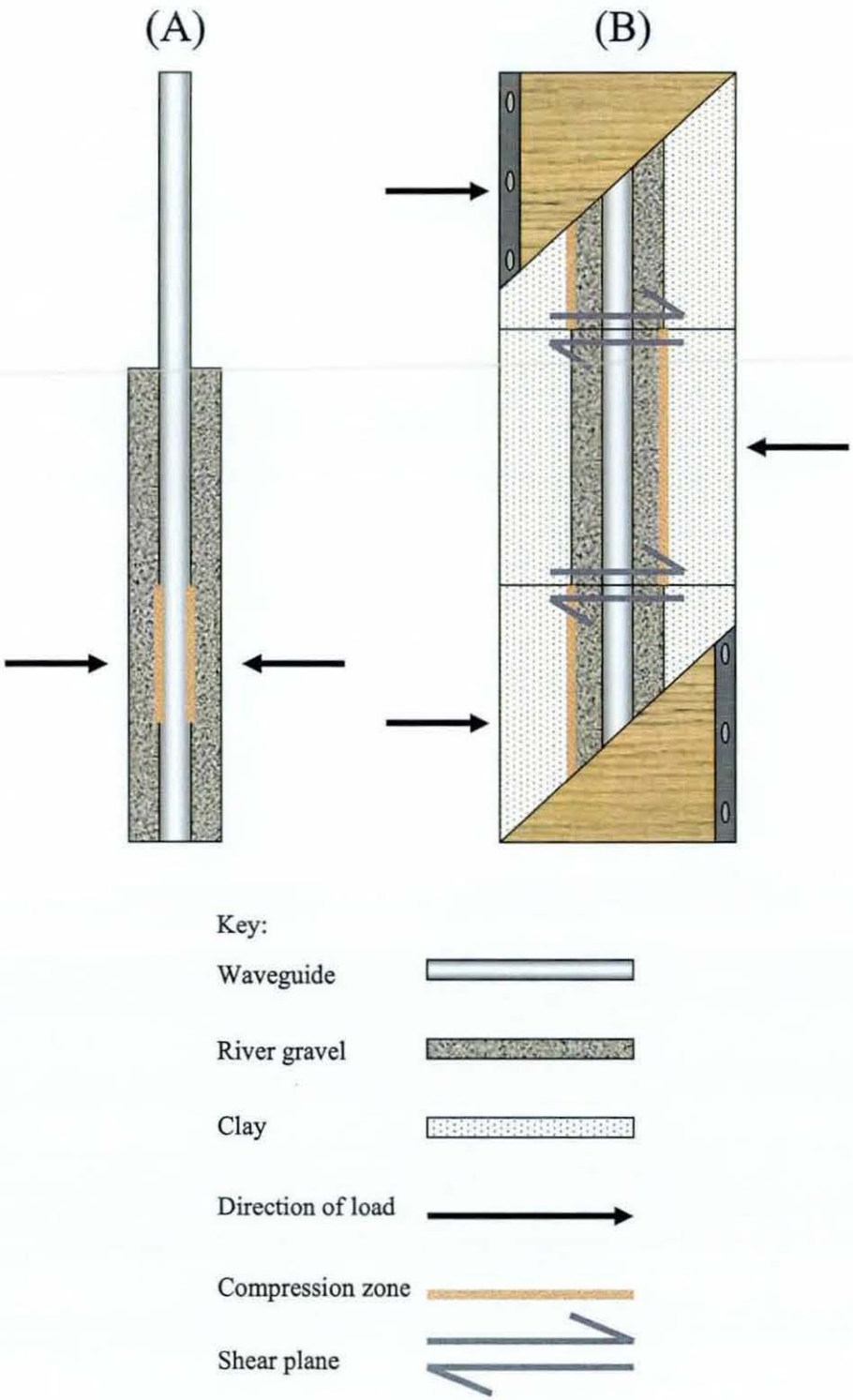

Figure 4.27 Mechanisms of deformation in compression tests (A) and in large scale tests (B)

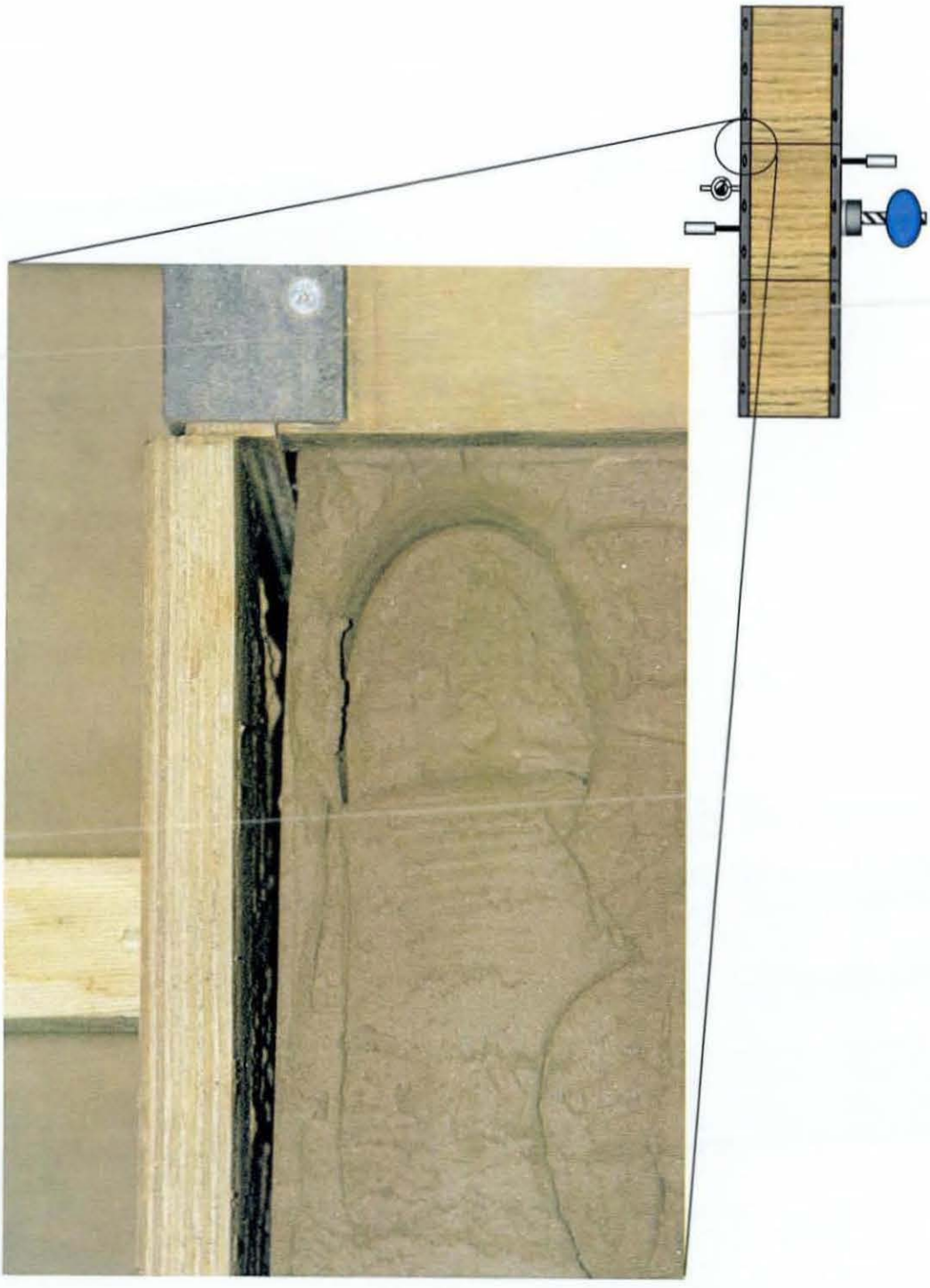

Figure 4.28 Photo showing the displacement of the middle box relative to the displacement of the clay

Figure 4.29 Plan view of the large scale test showing good compaction of clay

Chapter 5

Locating the Zone of Deformation

5.1 Introduction

Chapter 5 seeks to investigate the use of single sensor source location for an active waveguide. Knowledge of the location of a zone of deformation acting on an active waveguide is vital not just for slope mitigation purposes, but also to enable the correct setting of monitoring parameters required to reliably quantify the rate of displacement (see chapter 4). Section 5.1 introduces the need to identify the propagation distance of acoustic emission (AE) and justifies the use of monitoring the event parameter for quantifying AE. Section 5 2 outlines the experimental approach taken to develop a source location technique based on Lamb wave theory. Section 5 3 tests the theory first on a controlled source of AE, pencil lead breaks, and then in section 5.4, AE generated from the deformation of the backfill around the waveguide is tested to evaluate the use of Lamb wave theory as a reliable source location tool. Finally section 5.5 discusses the attenuation suffered by AE as it propagates over long distances and through connections within the waveguide.

5.2 The problem of attenuation

As noted within section 2.3.2, soil has a high coefficient of attenuation and thus dampens acoustic signals over a very short distance. In order for AE to be detected and recorded effectively, a path of low attenuation between the source and the receptor must be provided. Section 3 3 discussed the various considerations given to the design of the waveguide system to reduce the effect of attenuation on AE, but the influence of attenuation can never be fully removed. Although a steel waveguide has low attenuation, AE that has travelled 30m along

a waveguide from within a soil slope would have been attenuated further than AE resulting from deformation nearer the surface.

Chapter 4 developed an initial system that was able to quantify AE to within an order of magnitude of movement. This system relied on the counting of events over a given time period. Only events that exceeded a certain threshold were counted so that the influence of background noise would be removed as far as possible. Event counting was chosen rather than monitoring ring down counts because the effect of attenuation on an event was much less critical. As AE attenuates, the amplitude of the waveform is reduced. In any one event the number of threshold crossings (RDC) may be reduced considerably whilst it is still possible to record the presence of that same one event.

This is demonstrated in Figure 5.1 where a simplified AE event is illustrated three times, but the resulting reduction in amplitude due to an increase in attenuation relative to (a) is shown in (b) and to a greater extent in (c). Waveforms (a), (b) and (c) show the same event. But when comparing waveforms (a) and (b) there is a reduction in threshold crossings, (a) has a RDC of 14, while (b) has a RDC of only 6. However, when comparing the same waveforms by counting events, both waveforms register an event count of 1. The effect of attenuation is the same in both cases, but it is exaggerated when analysing AE with RDC. If the attenuation suffered results in the whole event dropping below the monitored threshold, as in the case of (c) in Figure 5.1, then no data is recorded. It is vital that AE data generated within the active waveguide backfill is not missed or ignored. In order for the recorded AE and the resulting rate of deformation to be an accurate portrayal of the deformation within the ground, then all generated AE must be accounted for. Thus it becomes essential that the correct amplification is applied to the recorded events.

The example given in Figure 5 1 might be defined as follows: (a) being an event that has travelled from a depth of 2m below ground surface, (b) an event originating from a depth of 10m and (c) an event originating from a depth of 25m. The further AE travels along the waveguide to the surface, the greater the attenuation. This can be overcome by increasing the amplification of the

monitoring system. However, if the amplification is too high, then events that originate near the surface, such as (a), could overlap each other, and a recorded event might end up actually being the amalgamation of two or more events Alternatively, if the amplification was set too low, events like (c) originating from a greater length along the waveguide would go unnoticed.

There are two reasons why it is necessary to know the exact origin of AE events resulting from deformations within the active waveguide:

1. So that the correct level of amplification can be applied to the monitoring system, so that deformation generated AE data is not lost below the threshold. This has implications for the quantification of AE discussed in chapter 4, which relies on the correct number of events being recorded in order to classify the rate of displacement.
2. So that mitigation/remediation strategies can be most effectively designed and implemented for the slope being monitored. This requires knowledge of the mechanism of failure and hence of the depth of shear surface development/continued movement

The distance travelled by any one event can not be assessed on the basis of its amplitude. A further complication might also be introduced to explain the difference in waveforms shown in Figure 5.1. Waveform (a) could be a small event near the surface, or it could be an event of high energy from further down within the landslide. Likewise, (c) could be a large event that has travelled a long distance along the waveguide or it could be a very low energy event near the surface of the landslide.

It therefore becomes necessary to know the exact origin of each event. This chapter explores one technique of doing that. The term 'source location' has been adopted to describe a technique which is able to determine the distance travelled by AE along a waveguide between source and receptor.

5.3 Technique of experimentation

Section 2.6 discussed a source location technique that analysed the 'front end' of an incoming event to separate Lamb wave modes, which travel at different speeds within the same one AE event The most notable advantages to using this technique are· a) when two parallel surfaces exist, as in the case of a plate or a pipe, and the wavelength of a sound wave is similar to the thickness of the plate, Lamb waves become the predominate mode of travel and propagate in one dimension which greatly minimises the attenuation, and b) source location is not dependant on the amplitude of the incoming AE – provided the amplitude is sufficient to distinguish the AE from background noise.

This chapter discusses two ways of generating AE for the purpose of source location, namely 'pencil lead break' and 'backfill generated'. AE generated from a pencil lead break was detailed in section 3.2.1. An automatic pencil with a 'Nielson shoe' adapter enabled repeatable AE events to be generated using this system. This followed a standard procedure as laid down within ASTM 2001. When a pencil lead is broken directly onto the waveguide, a sudden or transient release of stress generates an acoustic wave, which produces both a repeatable and highly distinguishable event. Backfill generated AE was provided by the compression test described in section 4 4.1. Each technique of generating AE is discussed in full in their respective sections 5.4 and 5 5.

5.3.1 Lamb waves

Section 2.6 outlined two methods of achieving source location on AE propagating via Lamb waves. The methods differ in the approach taken to analysing the Lamb waves. Maji *et al.* (1997) separated out two frequency components within the same AE event, and considered the velocities of the fastest Lamb wave mode operating within each frequency band. This technique was developed for crack monitoring within structural steel bridges, where the AE signal demonstrated two frequency 'peaks' within a signal. Alternatively, Alleyne and Cawley (1997)

looked at one dominant frequency within an AE event, and considered the velocities of the first two Lamb wave modes to arrive. In this case, only one dominant frequency existed because that AE signal was generated by a transducer to propagate along chemical pipes where a reflection in the generated AE would highlight areas of corrosion.

Both techniques have proved successful as the source of AE (structural cracking and induced AE) was high in amplitude and clearly identifiable. Kousteni (2002) successfully applied the latter approach to backfill generated AE. However, Kousteni (2002) concluded that testing was carried out on distances no greater than 1.6m, and that it was unknown whether the same technique could be applied on distances of 10's of meters. Further studies would be required to see the effect of attenuation and possible distortion on the AE while propagating over distances greater than 1.6m and through multiple connections.

In previous studies of soil generated AE by Kousteni (2002), the approach taken by Alleyne and Cawley (1997) was used Figure 5.2 shows a typical frequency spectrum of AE generated from the compression of river gravel around a steel waveguide. It can be seen that only one dominant frequency existed between 20 and 30 kHz. Kousteni stated that the presence of only one dominant or resonant frequency was typical for AE generated by the compression of river gravel around a waveguide. It was decided that the approach taken by Alleyne and Cawley (1997), and by Kousteni (2002) would also be taken in this investigation given that the same conditions (crushed river gravel surrounding a steel pipe waveguide) existed. The dominant frequency was obtained before each experiment by performing a Fast Fourier transform which provided a frequency spectrum of the backfill generated AE

Figure 5.3 shows a graph produced by Alleyne and Cawley (1997) for the propagation of Lamb waves in pipes. This Figure has been modified to show the relationship between the velocity of Lamb wave modes and a product of the frequency and the pipe wall thickness. When the upper and lower limits of the measured frequency have been selected, it is then possible to read from the graph which Lamb wave modes are detectable and at what velocity. Once the velocities

(C_1 & C_2) of the modes are known, the one remaining variable is the time difference (δt) between the arrival of the first and second Lamb wave mode. δt is measured by observing the front end of an incoming event. Equation 5.1 (Maji *et al.* 1997) was used to calculate the distance to source.

$$\Delta s = \frac{\delta t}{\left(1/C_1 - 1/C_2\right)} \qquad [5.1]$$

Where:

Δs = Distance to Source

δt = Difference in arrival times of frequencies

C_1 C_2 = Velocities of the two measured Lamb wave modes

The number of AE events generated within a compression test was demonstrated in chapter 4. At a 'slow' strain rate of 0.01764mm/min, approximately 3000 events were recorded after a displacement of 2mm. Theoretically that means source location calculations could be performed on 3000 separate events. Therefore, over a short deformation, a large number of results would very quickly indicate the calculated location of the generated AE. Even if there were many spurious results due to AE originating from other sources or depths along the waveguide, or incorrect calculations, the large number of events being generated would mean that quite rapidly it would become increasingly clear as to the true location below ground level of the deformation zone.

Such a technique would take into account the varied nature of backfill generated AE. AE from within an active waveguide would vary in its nature due to:

- The inhomogeneity of the backfill material (e.g. density).
- The mechanism from which the AE originates (i.e. interaction between backfill particles or interaction between the backfill and the waveguide).

- The propagation of AE through the backfill before reaching the waveguide.
- The effect of attenuation over long lengths as the AE propagates along the waveguide.
- The effect of connections within a long waveguide.

It would be unlikely that every event would provide the same calculation for source location, but provided enough events are recorded, it is expected that over time the true location of deformation would become increasingly apparent.

5.3.2 Determining distance to acoustic emission source

In order to reliably identify the relevant Lamb wave modes, it is important that the exact start of an AE event is known. This required the setting of a voltage threshold, based on knowing the level of background noise, so that background noise would not mistakenly be identified as the start of an AE event. In this investigation the start of an event was certified as a rise in amplitude above the threshold level. The arrival time of the Lamb wave modes was noted and the difference in arrival time of the first two modes 'δt' calculated. Figure 5.4 shows the same AE event twice. On top is the filtered incoming waveform (shown in red), whilst beneath (shown in purple), the same filtered AE event has had the amplitude squared to accentuate the peaks and troughs, and thus it is displayed only in the positive domain. This event was produced by the pencil lead break method on a steel pipe with a wall thickness of 3mm at a distance of 13m from the sensor.

The arrival of each lamb wave mode is demonstrated by a rise and fall in amplitude within an event. A subsequent rise and fall is thus the arrival of the next fastest Lamb wave mode As other Lamb wave modes arrive they overlap each other and the boundaries between subsequent modes become unclear. Source location calculations therefore are made on the arrival of the earlier modes as they are the clearest. As distance of AE propagation increases the Lamb wave modes

are spaced further apart. The arrival time of each Lamb wave mode is measured at the point of highest amplitude (see Figure 5.4), rather than at the beginning of the mode. This aids precision, as often the beginning and ends of each mode overlap, making it difficult to visibly identify the arrival of the start of the mode.

The identification of a Lamb wave mode arrival time was attempted both manually and automatically. The manual approach involved visually looking at the filtered waveform. The sampling rate of the experiments within this chapter (unless mentioned otherwise) was 0.2 MHz, and thus the recorded waveform was sampled every 0.000005 seconds. Readings could be taken from the waveform with an accuracy of 0 00001 seconds. The manual approach can thus be considered to be a very accurate process of analysis (length of an AE event approximately 0.01sec.). This process was performed on an amplitude/time graph within the DASYLab software; however it was a very time consuming task, and was potentially influenced by the subjectivity of the person interpreting the waveform. The automatic approach was developed to enable many thousands of events to be analysed very quickly such that the approach outlined in section 5.3.1 would be possible This would also remove any operator bias.

Viewing the data manually and automatically took place after the experiment. The acoustic data from each experiment was recorded as a DASYLab file for post analysis. Figure 5.5 shows the DASYLab worksheet used to manually measure the difference in arrival times of the first two Lamb wave modes. Each DASYLab module is described below, for further information on each module see section 4.3.1. Note, the individual settings for each module (i e filter frequencies) are detailed in their relevant sections in 5.4 and 5.5.

- Read module

This module read data from disk files of different formats. Each experiment was saved as a DDF. file, which was the original DASYLab format. This format retained the original date and time, and replayed the experiment as a real-time output

- High pass filter

The function of the filter was to cut off, or dampen, certain frequency components from the time signal. The high pass filter digitally dampened frequencies below a preset threshold, whilst allowing frequencies above the cut off frequency to pass unchanged.

- Low pass filter

The low pass filter provided digital signal filtering, by dampening frequencies above a preset threshold, while lower frequencies passed the filter unchanged. A high order (10) Chebyshev 0.5 filter was selected because of its steep response to the cut off frequency.

- Recorder

This module displayed the filtered AE data as amplitude (volts) against time. The recorder chart continuously scrolled from the right to the left, and could be used to display the current AE data together with its history for visual interpretation. Each AE waveform was magnified to enable digital cursors to be placed on the peak amplitude of each Lamb wave mode to obtain their arrival times and thus calculate δt.

Figure 5 6 shows the DASYLab worksheet used to prepare the data for automatic source location. Microsoft Excel performed the final analysis to calculate the difference in arrival time of the Lamb wave modes. The following is a breakdown of each module from Figure 5.6. (the Read module, high pass filter and low pass filter remained the same as described above).

– Pre/Post trigger and relay switch

The Pre/Post trigger (labelled Data Trigg), also discussed in section 4.3.1, was used to generate a trigger signal at the output depending on the input signal conditions, this output signal subsequently triggered a relay switch. This module had the ability to trigger at a predetermined amplitude threshold, and to capture events before and after that threshold trigger for a set duration of time. An amplitude threshold was determined based on the levels of background noise, which were measured at the start of each experiment. The trigger would open the relay switch to allow data through if the amplitude threshold had been exceeded, and subsequently closed a relay switch when the signal amplitude dropped below the threshold. The Pre-trigger was set to allow 0.001 seconds of data before the opening of the relay switch, whilst the Post trigger allowed 0 005 seconds of data to be processed after the closing of the relay switch.

The critical trigger was the Pre-trigger. In order to know when the first Lamb wave mode appeared, it was required to see a quiet time (where no AE data exceeds the threshold) preceding that first mode. It would ensure that the first mode measured was not part of the tail end of the preceding event. The time of 0 001 seconds was proven to be long enough to show evidence of a quiet time, whilst the Post trigger of 0.005 seconds prevented the next trigger from restarting on the tail end of the same event.

– Minima/Maxima

This module counted either the 'minima' or the 'maxima' in the data stream. An incoming signal oscillates about zero volts, and it is made up of minimum and maximum amplitudes. This module isolated the maximum amplitudes in each oscillation, and recorded no values in between each maximum. The output of the module was only a plot of those maximums, and resembled a wave envelope. Figure 5.8 is an illustration of the effect of this module, the top waveform, shown

in red, is the front of an AE event that has been allowed through the relay switch, whilst the same event displayed below in blue, is the output of the Minima/Maxima module.

- Write module

This module stored data to a disk or a file in a number of different formats. The data was saved as an ASCII file format, to enable the data to be viewed within Microsoft Excel.

In order to complete the automatic source location procedure, the data was finally analysed by a macro written in Microsoft Excel The macro would essentially look for a maximum and a minimum within the data. At each maximum (representing the peak of a Lamb wave mode) the time would be recorded. This macro is shown in a flowchart format in Figure 5.7, and in full in Appendix B. It identifies a maximum or a minimum as a change in the sign of a slope within the AE waveform. The first maximum was defined as a change in the sign of the slope of the waveform from positive to negative after a preset threshold (designed to be just above background noise) was exceeded. A further condition was added to prevent the tail end of an AE event triggering as the start of a new event. This was achieved by setting a time delay, triggered after the identification of a new wave, in which the macro would remain inactive.

The advantage of an automatic technique is that many thousands of AE events can be analysed in a very short space of time. Although the analysis did not occur in real-time, it is considered that with further time and expertise, a similar programme could be written within DASYLab to enable real-time source location. This investigation was only concerned with whether an automatic source location procedure could be developed to produce reliable results.

5.4 Pencil lead break source location

The use of a pencil lead break as a source of AE enabled many repeatable AE events to be generated. By generating these events at a known distance from the AE sensor, it was possible to investigate whether Lamb wave theory could be used to calibrate a waveguide in order to locate the zone of deformation. In this section, both techniques of analysing the recorded AE (manual and automatic) were tested, culminating in a 'blind test' in which Lamb wave theory was used to analyse AE generated along a waveguide at unknown distances.

5.4.1 Experimental set up

Experiments were carried out on a steel waveguide which was constructed in 3m lengths. Each 3m length (50mm in diameter and 3mm wall thickness) was coupled via threaded connections to enable testing up to distances of 25m The AE sensor (see section 3.2.1) was attached to the waveguide using a compression mount (magnetic hold down device) and a layer of silicon gel was applied between the sensor and the waveguide to act as a coupling layer. Data from the sensor was then sampled at a rate of 0 2 MHz by the analogue to digital conversion board.

Figure 5.9 shows a frequency spectrum for a pencil lead break generated AE on a steel waveguide at 3m from the sensor. It showed an active frequency response from 5 kHz to 60 kHz, with stronger frequencies existing between 20 kHz and 30 kHz. The placement of the high and low pass filters was further refined by observing the clarity of the AE waveform when altering the cut off frequencies up or down by 1 or 2 kHz. The filters were subsequently selected to remove frequencies below 22 kHz and frequencies above 29 kHz.

As testing was carried out over long lengths of the waveguide, the effect of attenuation (due to the propagation length and the effect of connections) had to be considered when selecting the appropriate amplification. The priority of the investigation at this stage was to produce AE of sufficient amplitude in order to

identify the arrival of the first few Lamb wave modes. The amplification was set in order to obtain AE with peak amplitudes in the region of 5 to 10 volts, and is shown in Table 5.1.

5.4.2 Calibrating a waveguide

An initial experiment (exp105) to test Lamb wave theory was carried out up to a distance of 23m from the sensor. Ten pencil lead breaks were performed at each 1m interval. They were recorded via the DASYLab worksheet shown in Figure 5.5. Each waveform was then manually analysed to identify the arrival times of the Lamb wave modes. The clearest modes to identify were those which arrived first, second, fourth and sixth. Figures 5.10 to 5.15 show an AE generated at 1m, 4m, 8m, 12m, 16m, and 20m respectively. Each Figure shows the same AE event twice, on top is the filtered incoming waveform (shown in red), whilst beneath (shown in purple), the same filtered AE event has been squared to accentuate the peaks and troughs, and is displayed only in the positive domain. On each Figure the first, second, fourth and sixth modes have been labelled in green.

It can be seen that the modes grow wider (i.e. arrival times increase at different rates) as the distance from source to sensor is increased. The second mode to arrive was masked by the first mode, and could not be distinguished as a mode in itself until a propagation distance of 8m was achieved The measured δt (difference in arrival times) between modes 2, 4 and 6 in relation to the arrival of the first mode, have been displayed in Figure 5.16, and trend lines have been added. δt can be seen to increase linearly with distance, and as expected the δt was greater when the arrival times of modes 4 and 6 were considered in relation to the arrival time of the first mode.

R^2 values of 0 8818, 0.9372 and 0.987 indicate acceptable correlation between the data and the linear trend line for modes 1 and 2, modes 1 and 4 and modes 1 and 6 respectively. However, each trend line does not pass through the origin of the graph. In Figure 5.16 at zero δt, the average distance from source is given as -2.8m. So although the distance between source and sensor was a known

measurement, it appears that the AE travelled a further 2.8m, independent of which modes δt is calculated from. One theory is that the sensor might have picked up reflections from the generated AE. The location of the sensor on the waveguide was approximately 1.5m from the end of the pipe, which might have caused reflections. Therefore, a reflected AE could have travelled a further 3m before being detected by the sensor.

Kousteni (2002) investigated the effect of reflections generated at the end of the waveguide. (1.63m in length, 6mm wall thickness and 60mm diameter steel tube). It was concluded that by placing the sensor (30kHz) at a distance > 0.4m from the end of the waveguide, any reflections would be delayed sufficiently so as not to interfere with the original arrival of the AE signal. Thus in the case of exp105 the position of the sensor at 1.5m from the end of the waveguide would have ensured that any reflections would not have been included in the recorded waveform. An alternative possibility is that the AE event did not register on the sensor until it had been reflected from the end of the waveguide However there is no evidence in literature that such an anomaly exists.

A more likely explanation comes from considering the mechanisms involved in the generation of AE from a pencil lead break. Two components might be responsible for the fact that at 0m from source, the Lamb wave modes do not have a predicted δt of 0 and thus might not all start instantaneously. Firstly the time it takes to snap a pencil lead break and secondly the subsequent mechanism involved in the generation of the different modes.

Although a pencil lead break is considered to be a transient AE event generator, the time taken from the moment of initiating a lead break, by the application of pressure to the lead, to the final snap could take many hundredths of a second. Within that time interval a number of 'micro' snaps occur within the lead which generates noise. The process of snapping a lead not only excites Lamb wave modes over a period of time, but also excites different types of Lamb wave modes.

Section 2 6 discussed the various types of Lamb wave modes, symmetrical (longitudinal and torsional) and asymmetrical (flexural) Both types of wave are

excited by the complex mechanism of snapping a pencil lead on a waveguide. If, for example, a bar could be struck with a hammer perfectly on it's end then only symmetrical waves would be generated along the bar, but if the hammer strikes a corner of the bar's end first then asymmetrical waves would also be generated. The snapping of a pencil lead break on a pipe surface is similar, and results in a number of mechanisms generating both symmetrical (longitudinal and torsional) and asymmetrical (flexural) modes The resulting Lamb wave event consists of modes which start from different times and have different mechanisms, and then propagate at an individual velocity dependant on its frequency and the pipe wall thickness of the waveguide. This explains why the different modes measured in Figure 5.16 do not pass through the origin.

Velocities of the Lamb wave modes are dependant on the medium in which they travel, and hence fluctuations can occur as the modes propagate in different sections of the waveguide (each waveguide section was 3m in length). Figure 5.17 shows the difference in arrival times of modes 1 and 6 from exp 105. Also plotted on the graph are vertical broken lines which indicate the boundaries of each waveguide section. It can be seen that the results group in threes within their section of the waveguide. Thus the fluctuation of the data points about the trend line is in part due to variations in the physical properties (e.g. density, elasticity and material properties) of the waveguide from section to section

Figure 5.16 therefore demonstrates that Lamb wave theory can be used to determine the distance of propagation of an AE signal. In this case, distances as small as 1 meter could be reliable calculated (depending on the modes monitored). Similar waveguides could also be calibrated in the same way as in exp105, and the calibration graph (such as Figure 5.16) could then be used to calculate the distance to the zone of AE generation (i.e. deformation of backfill) given δt.

5.4.3 Identification of Lamb wave modes

Figure 5.18 is a portion of the graph shown in Figure 5.3. It shows the frequencies that were filtered in exp105 (22 kHz & 29 kHz). Also labelled on the graph are the

velocities at which each Lamb wave mode appears within the frequency boundaries. The first mode to appear is L(0,2), followed by T(0,1), F(1,2) and L(0,1), with velocities 3575m/s, 3250m/s, 2860m/s and 2619m/s respectively. The notation of each mode is explained in section 2.6. These are the first four Lamb wave modes to arrive within the stated frequency band for a steel waveguide with a wall thickness of 3mm.

In section 5.4.2 the first, second, forth and sixth Lamb wave modes were identified. Using the above velocities it was possible to calculate a theoretical relationship between difference in arrival times (δt) and distance from source to sensor (Δs) using equation 5.1 Figure 5.19 shows the theoretical relationship of δt and Δs for modes 1 and 2 and modes 1 and 4 against the actual measured δt from exp 105 (Figure 5.17). These theoretical lines, calculated using the group velocities chart (Figure 5.18), are a very close match to the measured data. However, because the theoretical lines based on equation 5.1 pass through the origin, data below 10 meters appears to be underestimated by equation 5.1.

Equation 5.1 was derived by Maji *et al* (1997) for detecting defects within structural steel bridges (see section 2 6). The monitoring wasn't based on the difference in arrival time of two lamb wave modes from within the same frequency bound AE event. Instead, Maji *et al* (1997) considered the separation of different Lamb wave modes by frequency domain filtering. The identification of two dominant frequencies within an AE event enabled the time difference to be based on the arrival of the first Lamb wave mode from each dominant frequency. This theory was based on the assumption that at zero distance, the difference in arrival time between the two Lamb wave modes was like wise zero. Thus when data calculated using equation 5.1 is plotted on a graph (as in Figure 5.19) the data passes exactly through the origin.

As discussed within section 5.2.3, data obtained by measuring the difference in arrival times of 2 Lamb wave modes within the same frequency bound event, assumed that at individual modes did not start instantaneously at zero distance. This difference in assumptions is highlight in Figure 5.19, and explains why

distances less than 10m appear to be underestimated by the theoretical line of equation 5.1. However for distances greater than 10m, equation 5.1 provides an acceptable correlation to explain the actual measured data. The use of equation 5.1 helps to demonstrate the application of Lamb wave theory and allows the actual measured Lamb wave modes to be checked against group velocity chart in Figure 5.18. This provides confidence that the system is not hap-hazard in its approach, but is actually monitoring what it is intended to monitor.

Equation 5.1 enables Δs values to be calculated using the measured δt and the known mode velocities A histogram of calculated distance between source and sensor could be built up over time. This approach to source location enables many thousands of events to be displayed in a way that clearly shows the distance to source, and hence in slopes, the location of the deformation zone.

To illustrate this, an experiment (exp107) was performed where multiple events were generated from only two known distances along the waveguide, namely 9m and 17m from the sensor. At each location 50 pencil lead breaks were carried out, recorded by the sensor and saved to file for post analysis. This data was analysed using the DASYLab worksheet in Figure 5.5, with the same frequency band (22 kHz – 29 kHz) employed. Manual source location was carried out and the measured δt was converted to a Δs measurement using the group velocities chart (Figure 5.18). The results were displayed in a histogram with 0.5 m intervals (Figure 5.20), and in a statistical format below.

	$\Delta s = 9m$	**$\Delta s = 17m$**
Mean	10 852	15.787
Standard Deviation	0.904	1.365
Min	8.220	12.510
Max	12.510	19.310
Range	4.290	6.800

From Figure 5.20 alone, the histogram shows that the most frequently occurring Δs was 11.5m and 16.5m for pencil lead breaks performed at 9m and 17m

respectively. These errors mainly resulted from the process of manual source location. Both results have low standard deviations, and thus the spread of the data is acceptable, with the majority of the results being within 1.3m of the mean. This also shows the pencil lead break to be a reliable technique for generating transient repeatable AE events.

The error shown by the histogram highlights the precision at which the manual source location can operate. Section 5.3 detailed the need for source location analysis to provide a) the correct level of amplification so that deformation generated AE data is not lost below the threshold, enabling the AE to be quantified (chapter 4), and b) so that slope mitigation/remediation strategies can be most effectively designed and implemented.

In exp107 the error at 17m was 0.5m, but for the pencil lead breaks at 9m, the results from the histogram were 2.5m out. However, the mean distance was only 1.85m in error, which reflects the spread of the data shown on the histogram. This error might be due to the overlapping nature of the first two modes at low propagation distances. This could also be due in part to the assumptions underlying the use of equation 5.1 to calculate Δs. As discussed above, the actual measure dt is greater than the dt achieved by back calculating equation 5.1 (at distances below 10 meters). Thus, using the actual measured dt in equation 5.1 would result in an over estimation of Δs, as has occurred in exp 107.

It is possible that a correction could be applied to data below 10m to take into account the errors discussed. Figure 5.16 illustrated that distances below 10m were overestimated, but could be represented by a linear trend line, and thus a separate calibration rule could be applied.

Table 5.1 shows the amplification used to ensure that all events from a pencil lead break had a peak amplitude in the region of 5 to 10 volts. The amplitude was increased every 3m primarily due to attenuation suffered at the connection of each 3m length of waveguide. Accurate source location is therefore also required to

enable the correct level of amplification to be applied to the AE as discussed in section 5.2.

Both exp105 and exp107 demonstrated the effective use of the group velocity chart to provide an output measurement in terms of Δs, which when displayed within a histogram proved to be a very clear visual tool for displaying the build up of AE source location data. With each event analysed the histogram clarity and confidence in the predicted distance to the source of AE is gained. This is a vital step towards the development of a system that would need to perform source location both automatically and in real time.

5.4.4 Blind test

The manual approach to source location was based on the accurate measurement of the difference in arrival times of the Lamb wave modes. However, it was a method that was open to personal interpretation (i.e. bias), especially when the actual distance to source was known. A test was required to demonstrate that the technique worked when approaching the data without knowing the actual distance to source and thus having no idea of the expected difference in arrival times. A blind test was conducted on the same equipment as described in section 5 4 1, however the locations of each pencil lead break were not revealed until after the analysis was complete. At each location ten pencil lead breaks were performed in succession, and the amplification was set according to Table 5.1. Figure 5.21 shows the results on a graph of actual distance against calculated distance to source. The diagonal black line indicates a perfect relationship between the actual distance and the calculated distance to source.

The scatter of results at each distance is shown on Figure 5.21, with the average of all ten pencil lead breaks being indicated in pink. For distances above 10m the average calculated distance was accurate to within 1m The R^2 value of the average calculated distances in relation to the perfect relation line was 0.9608, thus showing a good correlation coefficient for the data. Unfortunately the pencil

lead breaks performed at a distance of 5m were subsequently calculated to have an average distance of 12.6m. In all source location experiments discussed so far, distances below 10m have resulted in a high degree of error in which the dt (and accordingly the Δs) have been over estimated. The reasons for this were outlined in the previous section. It must therefore be concluded that the manual source location approach, when using equation 5.1 to calculate Δs, is limited to distances of greater than 10m for the waveguide investigated.

5.4.5 Automatic source location

The automatic approach to source location described in section 5.3 2 was tested first on pencil lead breaks. In exp108 (as in exp107), fifteen pencil lead breaks were carried out on the waveguide 17m from the sensor. These were analysed by the DASYLab worksheet shown in Figure 5.6, the output was then entered into a Microsoft Excel spreadsheet for further analysis by the macro displayed in Appendix B. Figure 5.22 shows the results of the analysis in a frequency diagram (histogram), which shows a spread of results from 3.5m to 18m. Seven events were measured either at 16.5m or 18m which showed an error of 1m.

However, the six events measured at 3.5m were of an error too great and of too high a frequency of occurrence to award the automatic technique any degree of reliability. When those waveforms were viewed using the manual approach to source location, it became apparent that the Excel macro was detecting slight discrepancies within the waveform and reading them as Lamb wave modes. This is illustrated in Figure 5.23 where the arrival of the first two Lamb wave modes is labelled, but an abnormal drop in the signal amplitude before the peak of the Lamb wave mode caused the δt to be measured from the discrepancy to the arrival of the first Lamb wave mode. The recorded δt (in Figure 5 23 δt = 0.00008sec.) would result in a Δs of 3 – 3.5m, as highlighted on the histogram (Figure 5.22), (N B. DASYLab can accurately read the timing of a waveform to within 0.00001 seconds, in this experiment, that would be equivalent to a Δs of 0 44m). When discrepancies such as these occurred, a manual correction was made in

order that the correct arrival times were used to calculate δt. The results are shown in Figure 5.24, which displays the calculated distance to source with similar errors as those achieved with the manual source location approach (section 5.4 3).

The errors caused by the fluctuations within the AE waveform pose a problem to the automatic source location, whereas using the manual approach enabled such discrepancies to be seen and corrected instantly. A condition was placed within a revised version of the Excel macro; if the difference in amplitude of the maximum and the proceeding minimum was less than a stated value, then the maximum would be rejected as an indicator of a Lamb wave mode (N.B. maximums and minimums were defined by a change in the sign of the slope of the waveform). For example, in Figure 5.23, the difference in amplitude between the discrepancy and the peak of the first Lamb wave mode was 0.17 volts. A condition could be set to reject a maximum when the following minimum was less than 0.17 volts lower in amplitude. However, this also resulted in the rejection of actual maximums representing the arrival of Lamb wave modes. In Figure 5.23 the difference in the maximum representing the actual arrival of the first Lamb wave mode and the subsequent minimum was only 0.51 volts. This amplitude difference could be lower, especially at lower distances where the first two modes overlap.

The condition was further refined to take into account the time difference between a minimum and a maximum. When a discrepancy occurred within the AE waveform, then it occurred within the space of one wavelength, as in Figure 5.23. Within two wavelengths the waveform resumed it characteristic pattern. For the frequencies monitored, 22 – 29 kHz, the maximum time for a wavelength was 0.00005sec. Rather than placing a condition of acceptance on the maximum by observing the difference in amplitude to the next minimum, a time constraint of twice the wavelength of the signal was put in place. If a maximum and following minimum were less than two wavelengths (0.0001sec.) apart then that maximum would be rejected. When exp108 was automatically analysed using the above stated condition, the results were identical to Figure 5 24.

The automatic source location approach was shown to be reliable to within 1m for pencil lead break generated AE and the use of a frequency diagram clearly demonstrated the distance to the AE source.

5.5 Backfill generated acoustic emission

The active waveguide operation in the field generates AE as the unstable slope deforms the backfill around the waveguide. Section 4.4 2 discussed the selection of crushed river gravel as an appropriate backfill material, from this point forward it will just be referred to as 'backfill material'. Both the manual and the automatic approaches developed in section 5.4 were based on a controlled source of AE (pencil lead breaks), and have been applied to backfill generated AE to predict the distance from sensor to the source.

5.5.1 Experimental set up

Figure 5 25 shows the experimental setup used to generate AE from the deformation of the backfill. The "compression test" (as used in section 4.4.1 for the quantification of AE data) was used to provide a controlled rate of displacement on the backfill surrounding the waveguide. The backfill was placed around the waveguide within a geomembrane sleeve, and deformed in exactly the same way as in section 4 4.1, except that the waveguide was extended to 21 metres in length. A moderate rate of displacement was selected, 0.2205mm/min. and this ensured that over a monitoring period of five minutes a sufficient number of AE events would be recorded for analysis. The backfill was displaced approximately 4mm before monitoring commenced, this was in keeping with the data produced in chapter four (see Figure 4.19), which showed a steady increase in the rate of AE events generated in the first 4mm of displacement, after which the rate of AE event became relatively constant. This was an experimental consideration, it should be noted that the rate of displacement does not influence the source location calculations.

The AE sensor was placed at distances of 3.7m, 6.7m, 9.7m, 12.7m, 15.7m and 18 7m from the AE source, and secured in place via the magnetic clamp and acoustic gel. At each of these locations, backfill generated AE was recorded for five minutes using the DASYLab worksheet shown in Figure 5.6. Both the manual and automatic approaches to source location were performed on data recorded from that worksheet. The experiment was named 'exp137'.

The selection of filters was based on a frequency spectrum analysis provided by a fast Fourier transform facility within DASYLab. Many different events were monitored for their frequency content; Figure 5.26 is a typical example which characterises many of the AE events analysed. Figure 5.26 demonstrated that backfill generated AE showed a greater sensitivity within the region of 25 – 27 kHz. This range of frequencies for a steel waveguide with a wall thickness of 3 mm can be seen on the group velocity chart in Figure 5.27. From this Figure it is possible to obtain the arrival of the first two Lamb wave modes, T(0,1) and F(1,2), and their velocities of 3250 m/s and 2750 m/s respectively, within the selected frequency range. Although errors existed when using the two fastest Lamb wave modes for pencil lead break generated AE (section 5.4.2), the two fastest Lamb waves for soil generated AE remain the clearest to identify given the nature of the group velocities chart (Figure5.3) for the selected frequency band. Table 5.2 lists the amplification required at each test location along the waveguide.

5.5.2 Manual approach to source location

The manual source location approach was conducted on data from exp137. From each monitoring location along the waveguide, approximately 2000 events were recorded, however only events with a peak amplitude greater than 2 volts were considered for source location analysis. The greater the amplitude of the event, the clearer the arrival of each individual Lamb wave mode. Between 15 and 25 AE events from each location had a peak amplitude greater than two volts. Each event was visually analysed to determine the arrival of the first two Lamb wave

modes, and the difference in arrival times was noted, and then converted to a predicted distance to source using equation 5.1 and the velocities from Figure 5.27.

These results are shown in Figure 5.28. The actual distance is shown on the x-axis, and the range of results predicted from each location is shown on the y-axis. Within the data from each location, an average predicted distance has also been highlighted, as has the prediction which most frequently occurred (based on histogram data with intervals of 0.2m) With respect to the perfect relationship line, all the data underestimated the distance to source, except data from 3.7m.

The predicted distances varied considerably within each test location, sometimes as much as 7m. However this was expected. As discussed in section 5.4.4, a histogram approach was favoured because of its ability to identify the most frequently occurring predictions regardless of the range of predictions. Thus a more realistic display of the data was to observe the average prediction or the most frequent prediction. When a linear trend line was placed through the averages to intercept the origin, an R^2 value of 0.7939 was achieved showing a good correlation of the data to the trend line. However when the most frequent prediction was considered, an R^2 value of 0.9476 showed a much improved correlation with the linear trend line The use of this parameter showed not only a stronger linear relationship between the predicted distance and the actual distance source, but was less influenced by the overall range of results which could carry large errors.

Despite a linear relationship being displayed in exp137, the results of the predicted distance to source underestimated by half the actual distance to source. By using equation 5.1 it was possible to back calculate which velocities would be required to produce this linear relationship shown in Figure 5.28. In Figure 5.27, the group velocity curves, it is unmistakable that within the frequency boundaries of 25 – 27 kHz, the first Lamb wave mode to arrive must be T(0,1) at 3250m/s. Using data from exp137, an average difference in arrival times between the first two Lamb wave modes at a known distance of 18.7 metres from the source, was 0.00052 seconds Based on equation 5.1, this would require the velocity of the

second Lamb wave mode to be approximately 2980m/s. However in Figure 5 27 there are no Lamb wave modes with that velocity. This would suggest that the δt calculated in exp 137 was not based on the first two Lamb wave modes to arrive, but on subsequent modes within the same event or potentially on overlapping AE events.

Both of these possible errors result from an inability to correctly identify the start of an AE event. In order to confidently identify the first mode to arrive, a certain amount of 'quiet time' (AE amplitude below predetermined threshold) must exist before an event can be correctly identified as a new event. If the tail end of a previous event was caught or overlapped the start of the next event, then the first Lamb wave modes would either be masked or modified by the superimposed preceding event.

In an attempt to prevent this, a trigger was placed within the DASYLab worksheet (Figure 5.6). That trigger was designed to 'pre trigger' - so that the immediate preceding data could be viewed to see if it was 'quiet' or not, and to 'post trigger' - to prevent that trigger from re-activating on the tail end of the same event. It is possible that at the moderate rate of displacement, AE events were generated very close to each other which could have resulted in overlapped events. If this was the case then the start of each AE event was missed, and the Lamb wave modes that were analysed, were not the first 2 modes.

However, Figure 5.28 showed that despite this a linear relationship could be detected which was characteristic of Lamb wave theory. In this specific case, source location calculations could be performed with a high degree of reliability. The errors involved in using the trend line based on the most frequently occurring prediction were on average 0 45m with a maximum error of 1.1m (from test location 3.7m). Thus, in exp137 it was possible to locate the source of backfill generated AE, however a waveguide with different parameters would require individual calibration prior to placement within the field.

5.5.3 Automatic approach to source location

The same experimental data (exp137) was used for the automatic approach to source location. Data saved via the DASYLab worksheet (Figure 5.6) was copied to a Microsoft Excel worksheet for further analyses using the macro shown in Appendix B. The modifications detailed in section 5 4.5 were also added. Only waveforms with a peak amplitude of greater than 2 volts were considered for analysis. The results are shown in Figure 5.29 in the same format as the results from the manual approach to source location for backfill generated AE.

As in the manual approach, the predicted data underestimated the perfect relationship line. The full range of predicted results are shown for each test location along the waveguide. The same AE events were analysed as in the manual approach (Figure 5.28), but the range of results produced by each location was far greater. As discussed in section 5.5.2 the most effective representation of the data was to consider the most frequently predicted distance which occurred within the analysis. These are shown in orange on the graph. The trend line produced by the aforementioned data was approximately one third of the values given by the perfect relationship line. An average error of 0 61m, and an R^2 value of 0.7924 described the correlation of the most frequently predicted results to the trend line. Although this was not as reliable as the trend line produced by the manual approach (R^2 value = 0.9476), never the less, a linear relationship was shown to exist between the actual distance and the predicted distance.

As the same data (exp137) was used to test both the manual and the automatic approach to source location, it was likely that the AE data was again compromised by the unclear identification of the start of an AE event and thus the arrival times of the first two Lamb wave modes. However, the trend line representing the most frequently predicted distance to source was different for the manual and the automatic source location approach Although both were underestimated, the manual was underestimated by a half, whilst the automatic by a third. It is evident that the actual wave modes measured varied between the two approaches If the first one or two Lamb wave modes were missed or masked by overlapping

waveforms, then any of the following modes, which are very closely packed together on the group velocity chart (Figure 5.3), could have triggered the automatic system. The difference in trend lines also highlights the potential for operator bias when using the manual approach, and hence the need for an impartial automatic approach to be refined

Nonetheless, a linear relationship was produced between the calculated and the actual distance to source. It can thus be concluded that the relationship displayed in Figures 5.28 and 5.29 demonstrate that the automatic source location approach was successfully used on the specific waveguide arrangement used within exp137.

5.6 Waveguide design

The design of the waveguide has not been a primary factor of this research, but rather the use of a steel pipe in 3m lengths with screw connections was selected based on previous research (section 3.3.1). However some consideration needs to be given to the attenuation suffered by long distance AE propagation and by the presence of connections within the waveguide. A simple study was conducted along a waveguide 25 m in length. AE was generated from the deformation of river gravel backfill, as shown in Figure 5.25. A slow rate of displacement, 0 0294mm/min, was selected to reduce the possibility of AE events overlapping each other. Backfill generated AE was recorded for 10 minutes at distances from the source of 5 m, 10 m, 15 m, 20 m and 25 m. Filters were set at 25 – 27 kHz, and a threshold for background noise was set at 0.3 volts.

The AE was analysed within DASYLab using the worksheet shown in Figure 5.30 (for an explanation of each module see section 4.3.1), which provided an output in terms of energy. Energy (volt seconds), obtained by measuring the area under a rectified waveform envelope, would be a sensitive indicator of the attenuation suffered (section 5.2). The energy was recorded only once at the end of each experiment, thus a linear relationship for each test location has been assumed as displayed within Figure 5.31. The total energy was also plotted against the distance of propagated by the AE in Figure 5.32.

From Figure 5 32 it can be seen that the total energy of backfill generated AE (recorded after 10 minutes) was, in the most part, reduced by one order of magnitude for every 5 metres of propagation, until at 25 m where zero energy was recorded. The amplification for each test location was kept constant at 98 dB, which when compared to Table 5.2 is a very high amplification for AE recorded at low propagation distances. An amplification of 98dB at 5m resulted in the AE events having amplitudes greater than +/- 10 volts. DASYLab only records and analyses data within the limits of +/- 10 volts, any data outside of that is ignored Thus the energy recorded for 5m was lower than expected. In comparison, the amplification was insufficient for AE propagating from a distance greater than 25m.

For a steel waveguide (in 3 meter lengths) with a pipe wall thickness of 3mm, the attenuation suffered was a decrease in order of magnitude of the energy (measured by the area under the waveform envelope) for every 5m. It is expected that the attenuation resulted principally from the presence of joints within the waveguide, although testing was not performed in such a way as to enable the ratio between the attenuation at a joint compared to the attenuation lost within the pipe itself For a waveguide longer than 25 m, either a greater amplification would be required or longer lengths of waveguide sections could be utilised to reduce the number of connections. Further work would be required to examine this point and the consequences of this for a field monitoring system are discussed in chapter 6.

5.7 Chapter summary

Chapter 5 has shown the use of Lamb wave theory to be a very effective tool. The combination of low attenuation and the identification of Lamb wave modes within a single AE event have made single sensor source location possible for the active waveguide (section 5.3). In section 5 4 pencil lead breaks were used as controllable and repeatable source of AE. Linear relationship was shown to exist between the measured difference in arrival times between two Lamb wave modes and the actual distance of propagation Those modes were identified on a group

velocity chart (Figure 5 3), and with the use of equation 5.1, confidence was given that the modes measured were indeed the selected modes. An automatic approach was also tested, and source location on pencil lead breaks was shown to be accurate to within +/- 1 meter over distances of 23m.

Backfill generated AE (section 5.5) was examined using both the manual and automatic techniques for locating the source of an AE. Waveguide lengths of up to 19m were tested, and source location was performed to the same degree of accuracy as using pencil lead breaks. Although the actual modes measured were unknown a linear relationship between the actual distance and the calculated distance to source was produced. That relationship was specific to the waveguide tested, and changes to the waveguides properties would require further calibration.

In all cases of source location, there was a wide spread of calculated distances, but the use of a histogram to identify which distances are predicted the most frequently, proved to be a very reliable indicator as to the true location of the zone of AE generation. As the number of AE events analysed increase, so the error would subsequently decrease.

Studies into the waveguide design suggested that the attenuation suffered was mainly a result of joints. In this case, the attenuation resulted in a decrease in energy by an order of magnitude for every 5m for the specific waveguide in question (section 5.6). Further work was suggested to quantify the amount of attenuation suffered due to the joint specifically, to enable effective waveguide design.

Distance from AE source to sensor (m)	Number of connections	Amplification (dB)
1 – 2	0	55
3 - 5	1	72
6 - 8	2	78
9 - 11	3	83
12 - 14	4	89
15 - 17	5	92
18 - 20	6	95
21 - 23	7	98
24 - 25	8	101

Table 5.1 Amplification settings for pencil lead break generated AE along a steel waveguide

Distance from AE source to sensor (m)	Number of connections	Amplification (dB)
1 – 2	0	65
3 - 5	1	72
6 - 8	2	81
9 - 11	3	86
12 - 14	4	89
15 - 17	5	92
18 - 20	6	95
21 - 23	7	98
24 - 25	8	101

Table 5.2 Amplification settings for backfill generated AE along a steel waveguide.

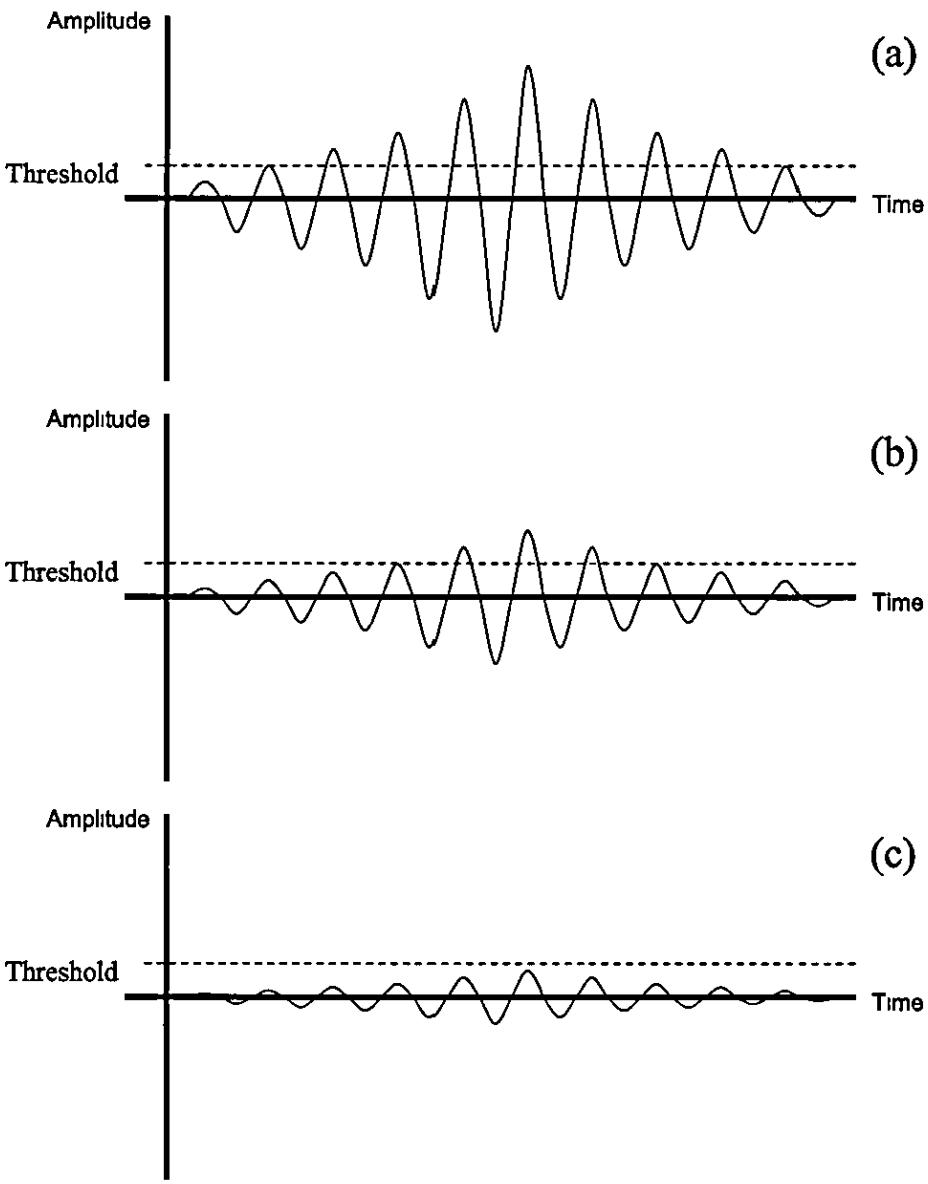

Figure 5.1 Illustration of the effect of attenuation on a simplified waveform.

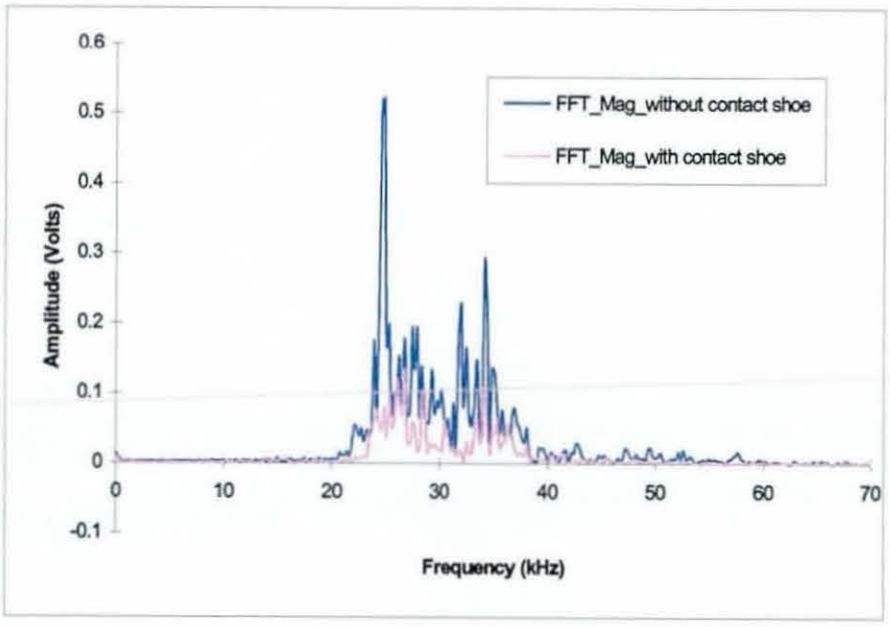

Figure 5.2 Frequency spectrum of river gravel (tested with and without a contact shoe – a device designed to enlarge the contact area between the sensor and waveguide) (Kousteni 2002)

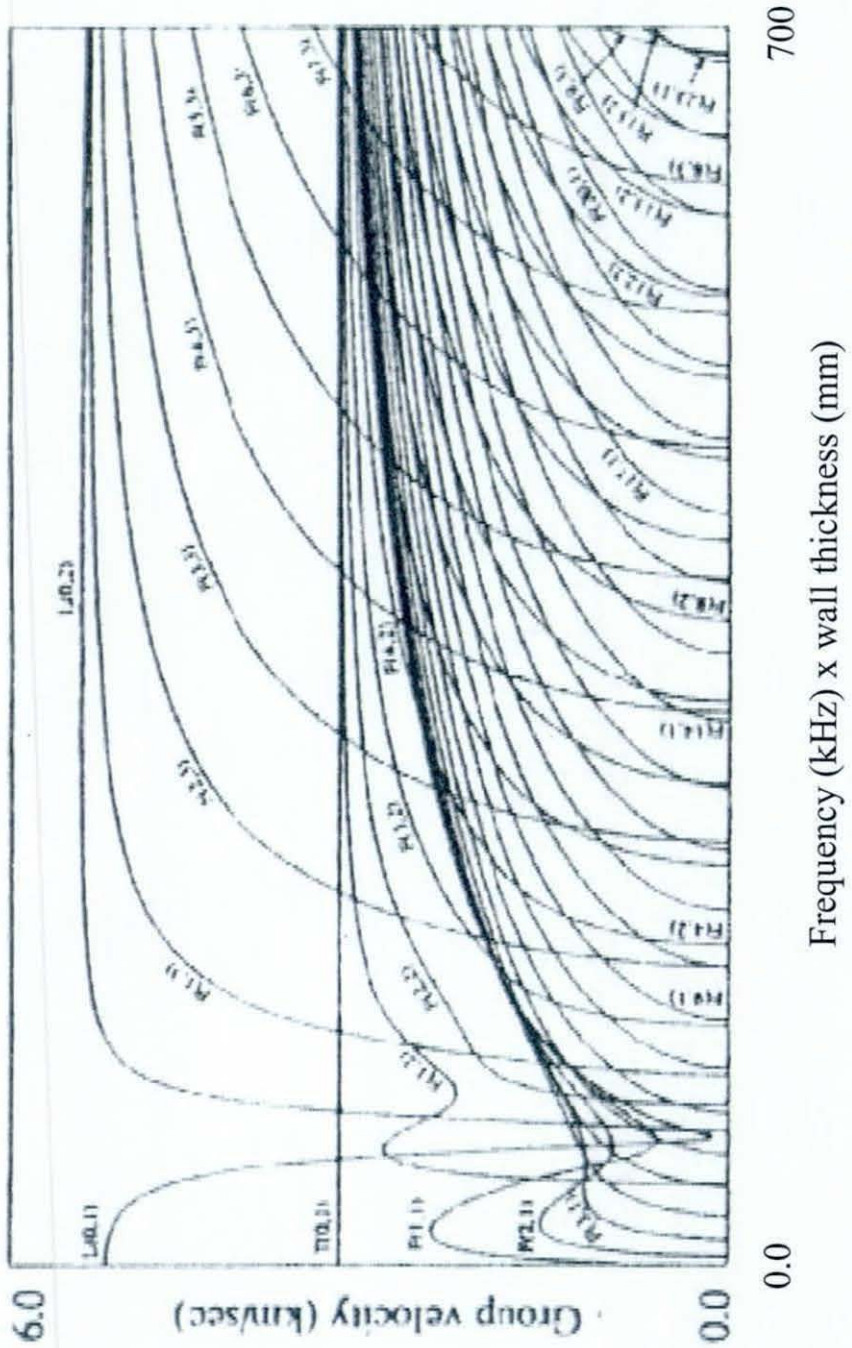

Figure 5.3 Group velocity curves for a steel pipe (after Alleyne and Crawley 1997)

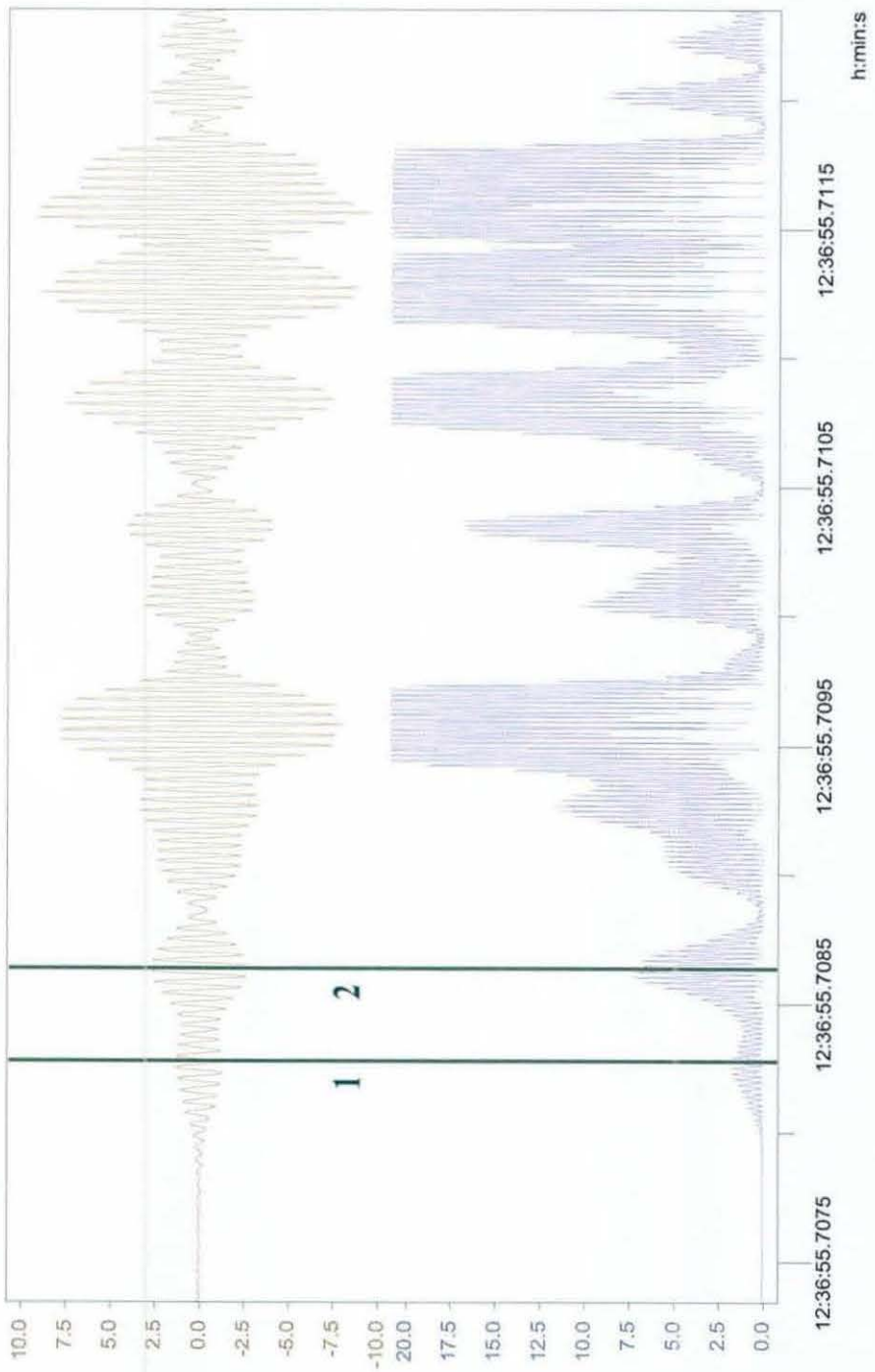

Figure 5.4 Example waveform showing the first two Lamb wave modes
(units; x-axis = Time (h:min:s) Y-axis = Volts)

Figure 5.5 DASYLab worksheet for manual source location calculations

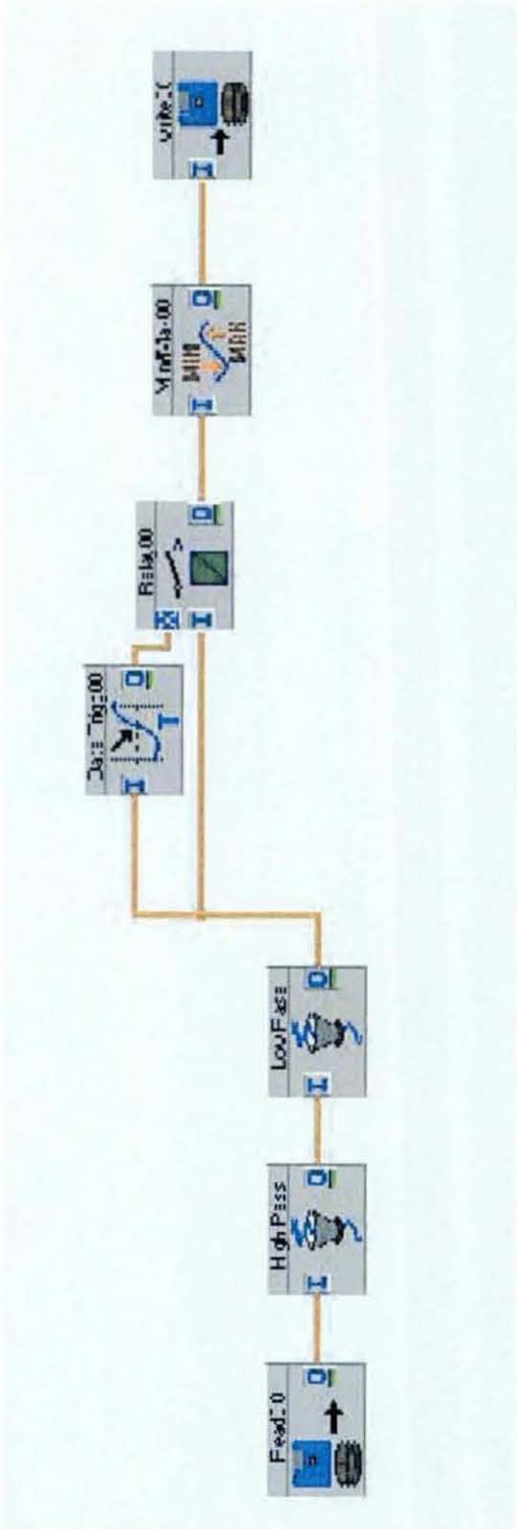

Figure 5.6 DASYLab worksheet for automatic source location calculations

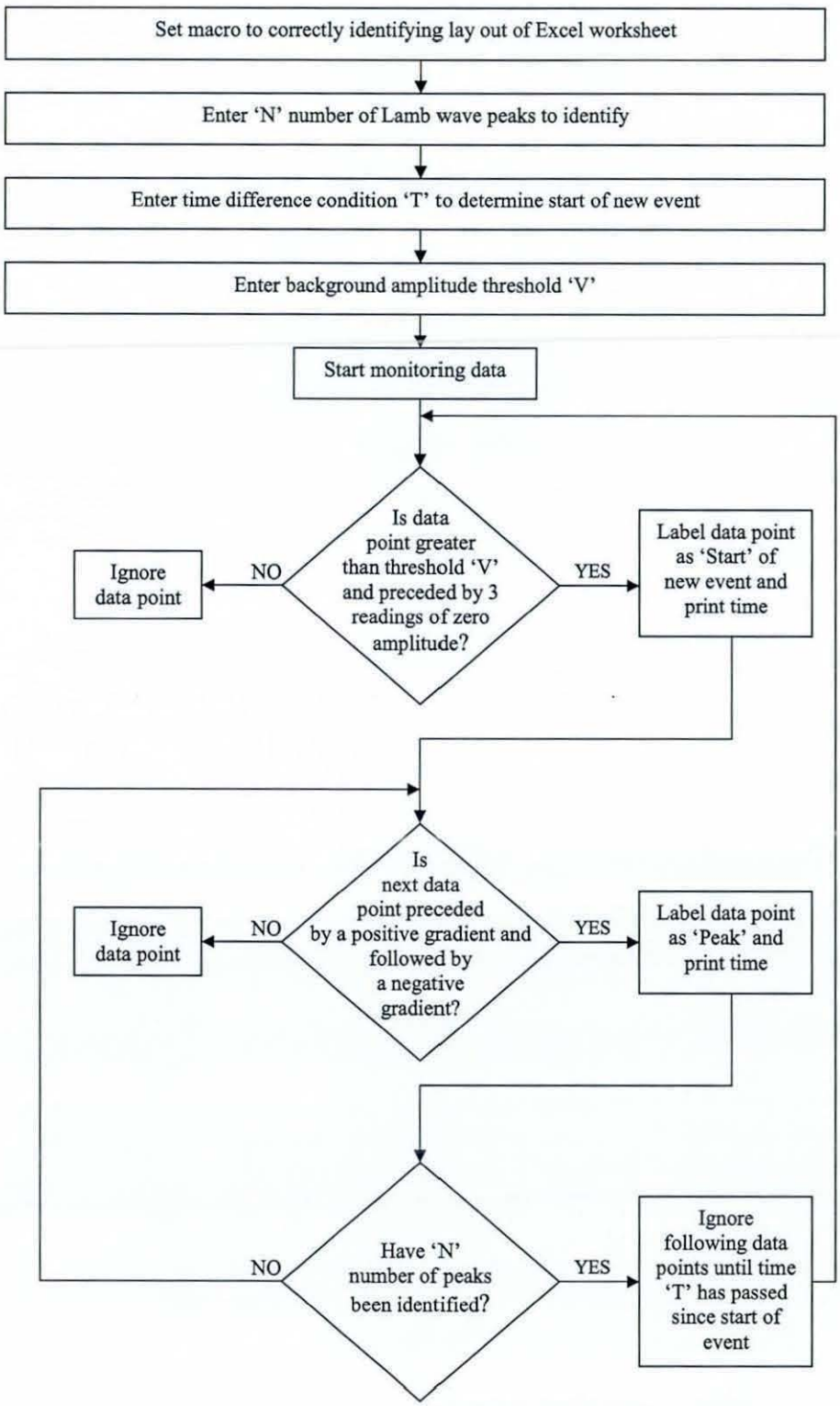

Figure 5.7 Flowchart of Microsoft Excel Macro for automatic source location

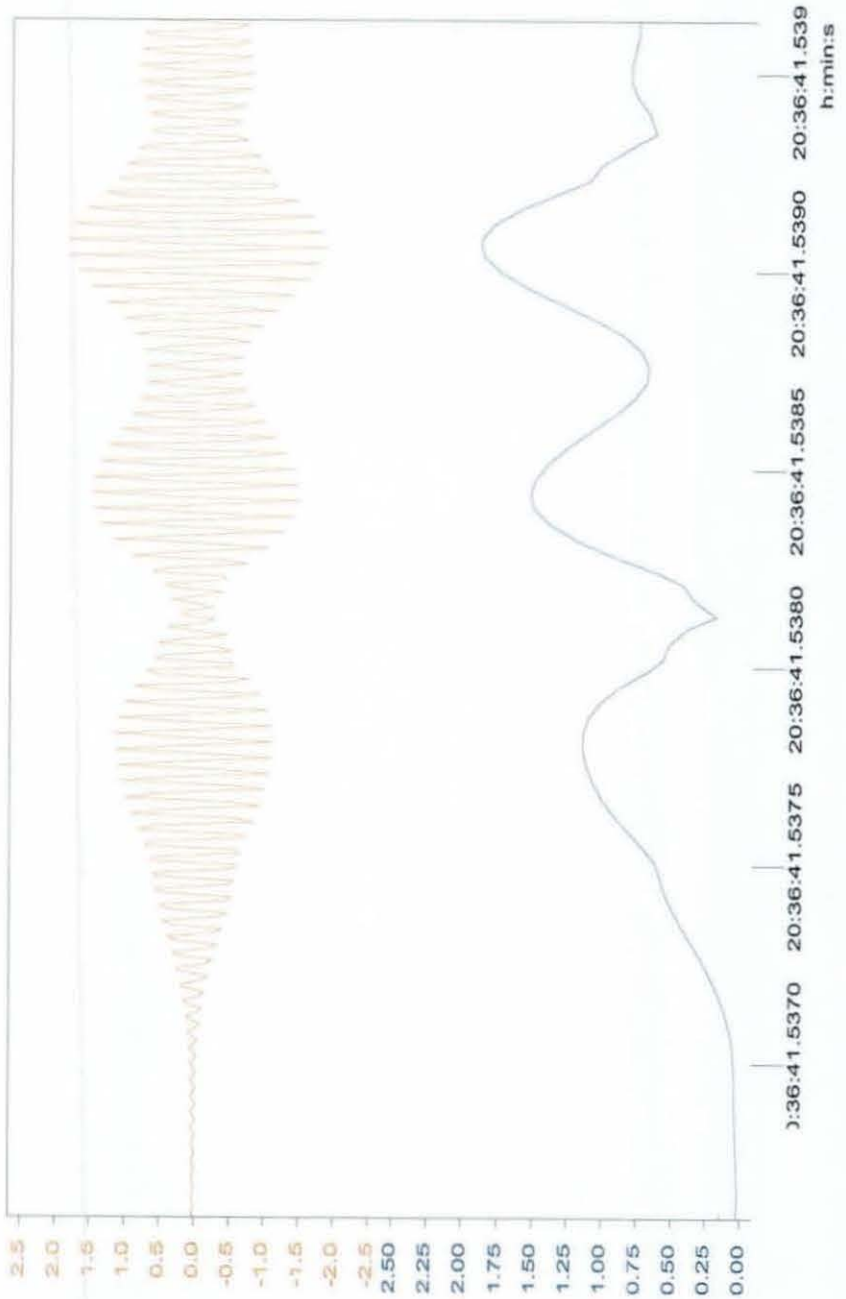

Figure 5.8 Example of AE event after relay switch displayed in red, the same AE event after processing using the Minima/Maxima module (units: x-axis = Time (h:min:s) Y-axis = Volts)

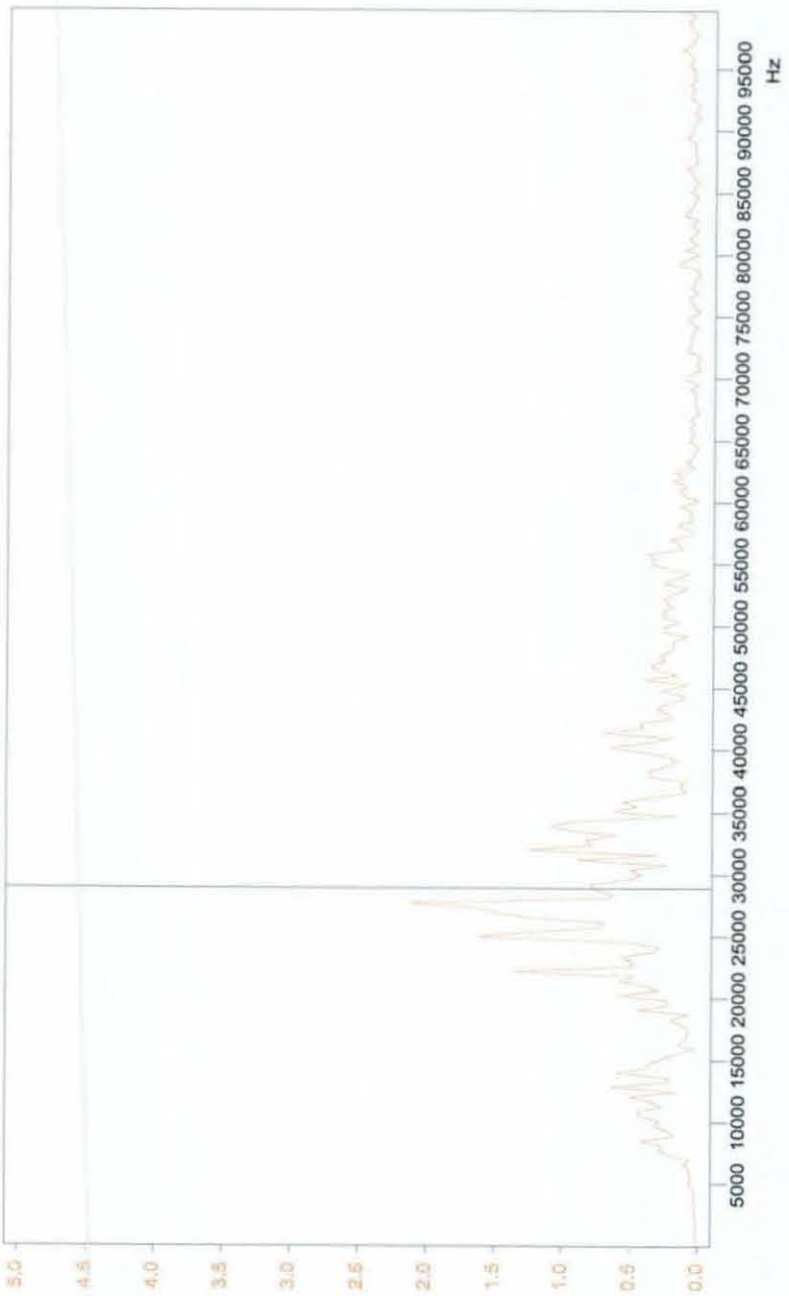

Figure 5.9 Frequency spectrum of a pencil lead break generated AE on steel waveguide at 3m from sensor (units; x-axis = Frequency (Hz) Y-axis = Volts)

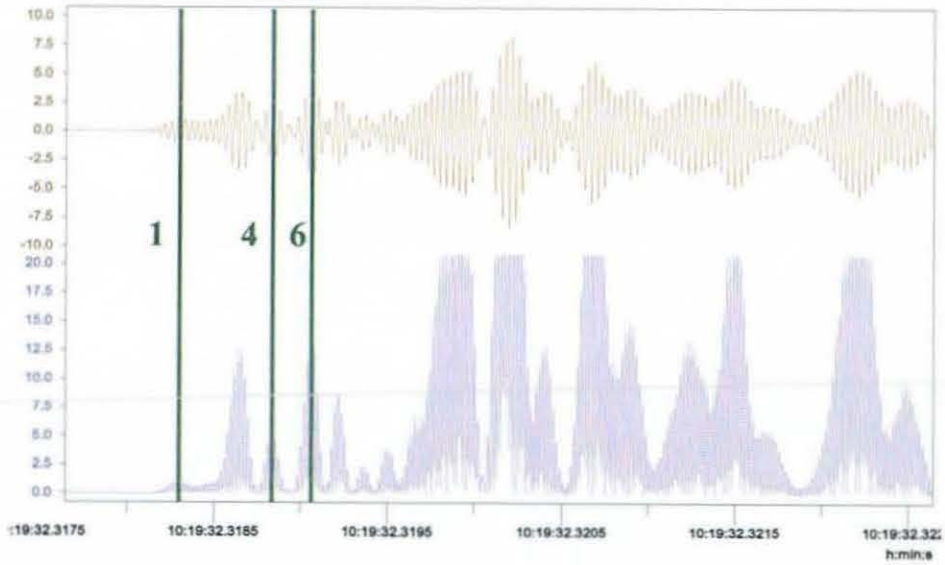

Figure 5.10 Amplitude verses time for pencil lead break generated AE at 1m
(units; x-axis = Time (h:min:s) Y-axis = Volts

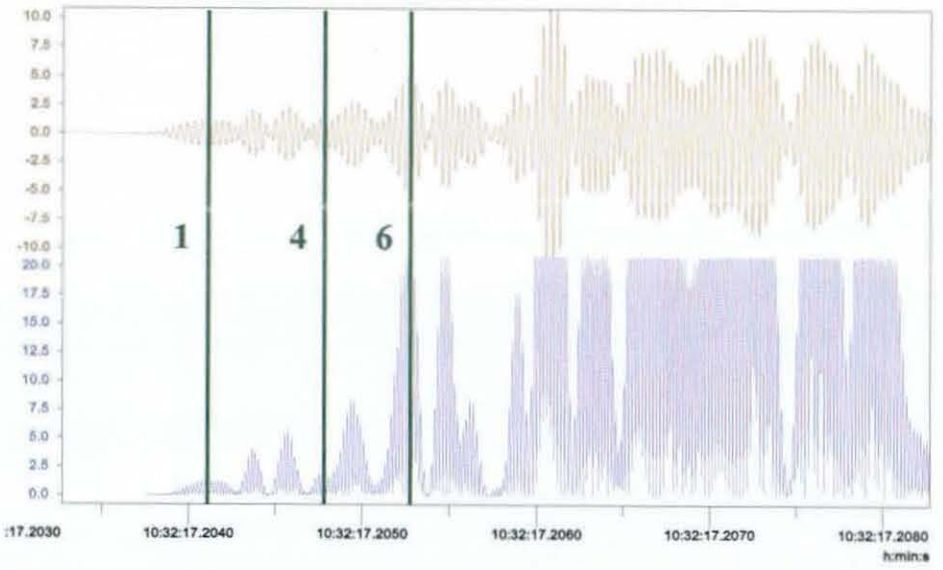

Figure 5.11 Amplitude verses time for pencil lead break generated AE at 4m
(units; x-axis = Time (h:min:s) Y-axis = Volts

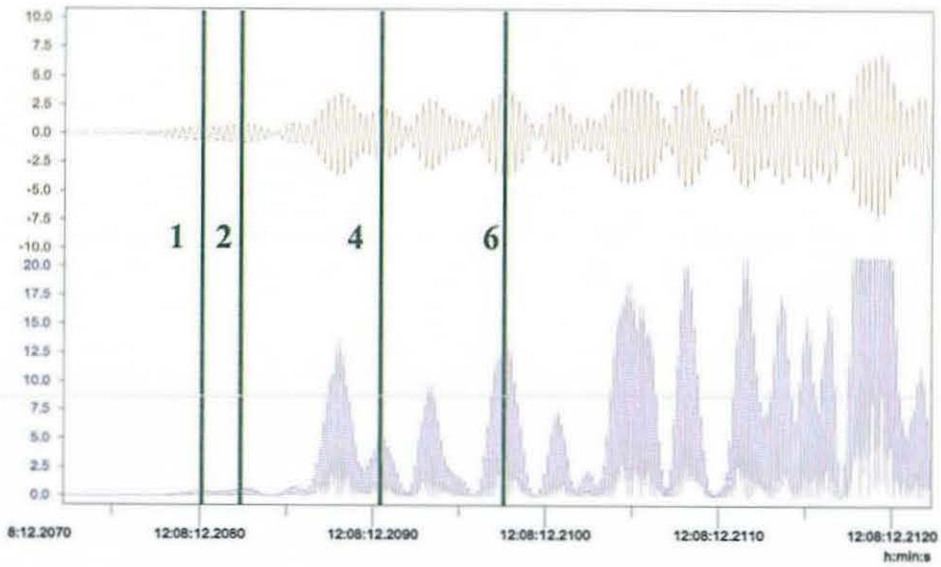

Figure 5.12 Amplitude verses time for pencil lead break generated AE at 8m
(units; x-axis = Time (h:min:s) Y-axis = Volts

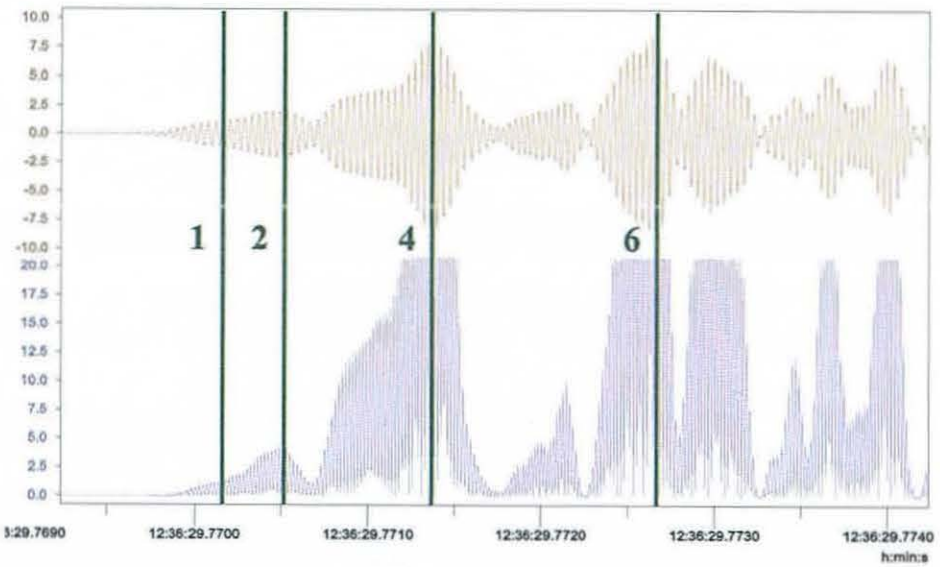

Figure 5.13 Amplitude verses time for pencil lead break generated AE at 12m
(units; x-axis = Time (h:min:s) Y-axis = Volts

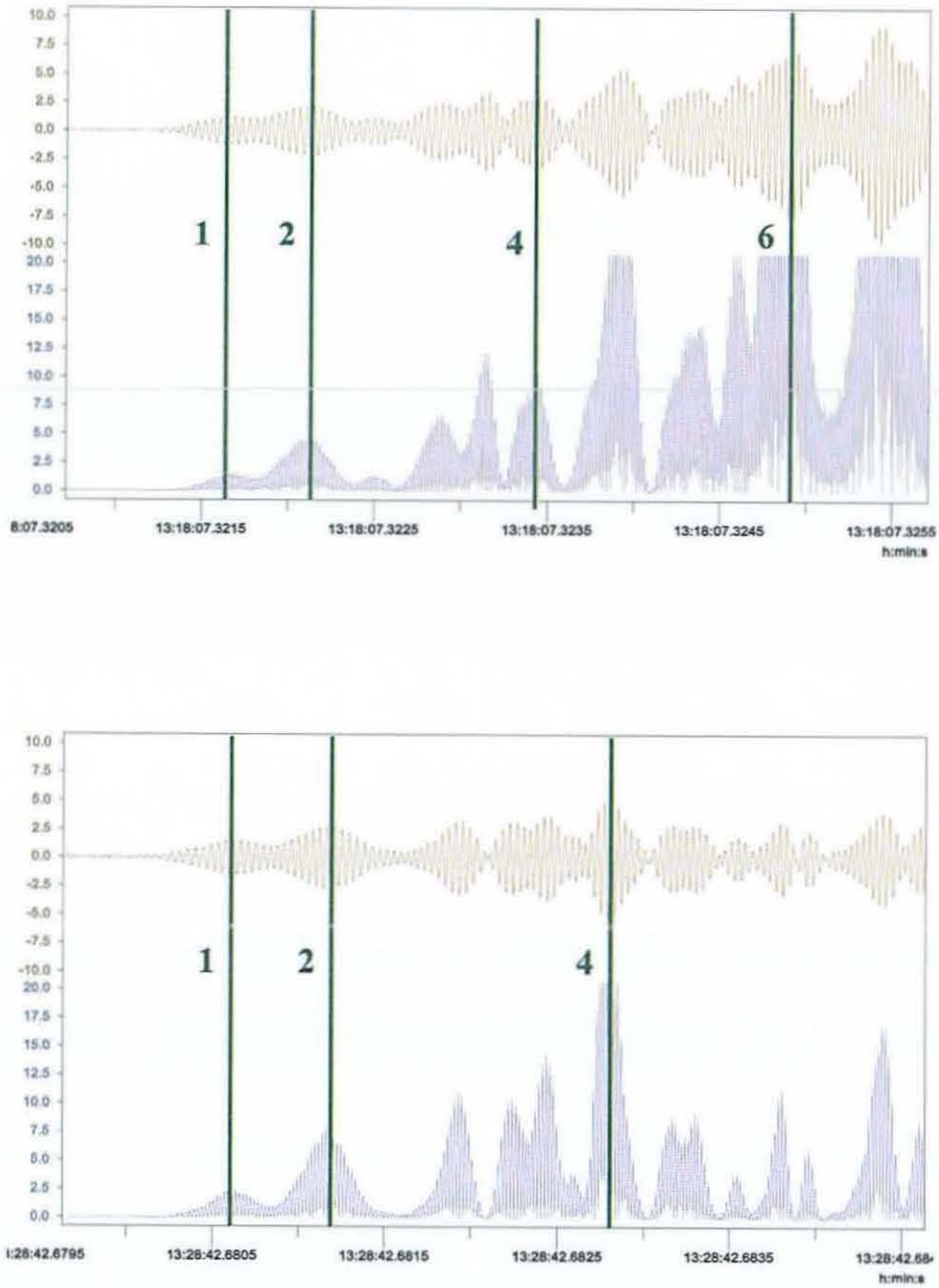

Figure 5.15 Amplitude verses time for pencil lead break generated AE at 20m (units; x-axis = Time (h:min:s) Y-axis = Volts

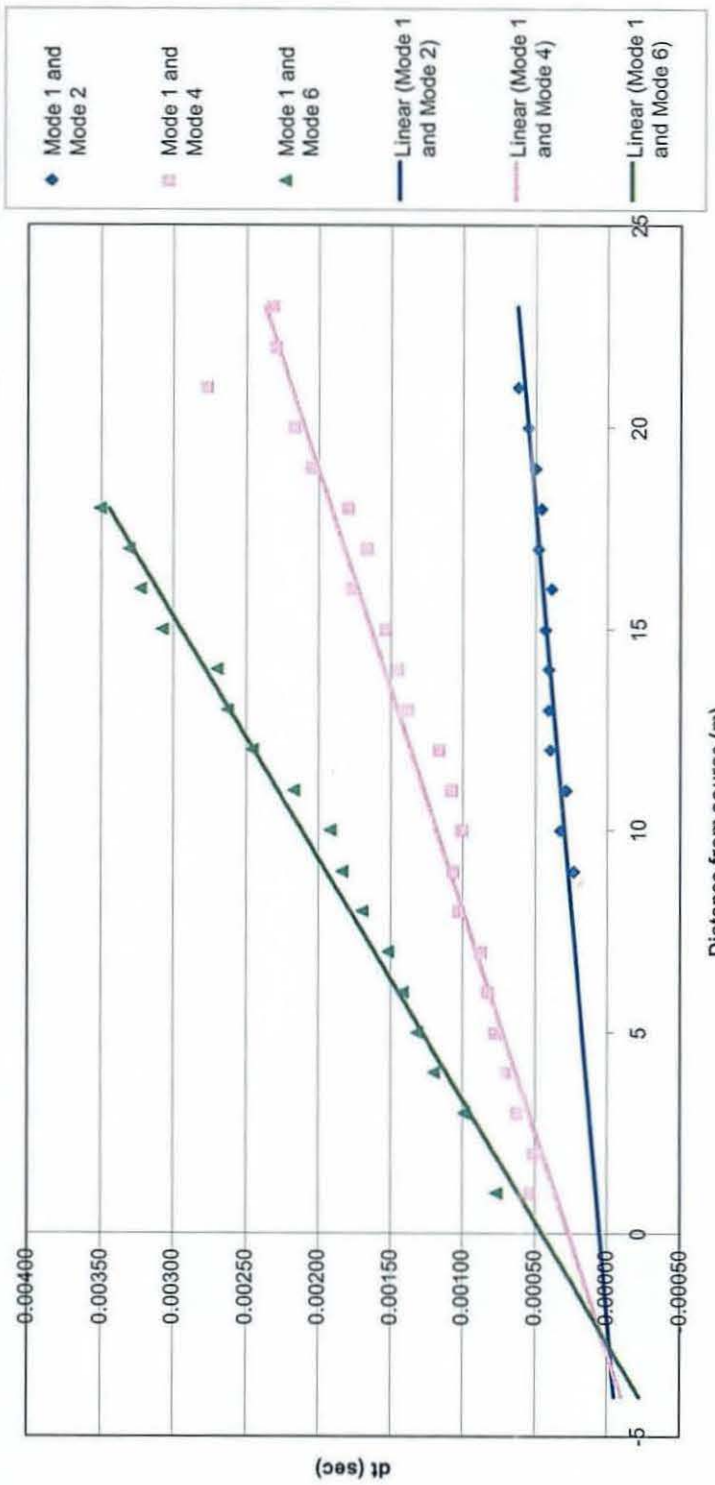

Figure 5.16 Relationship between dt and distance from source for exp105

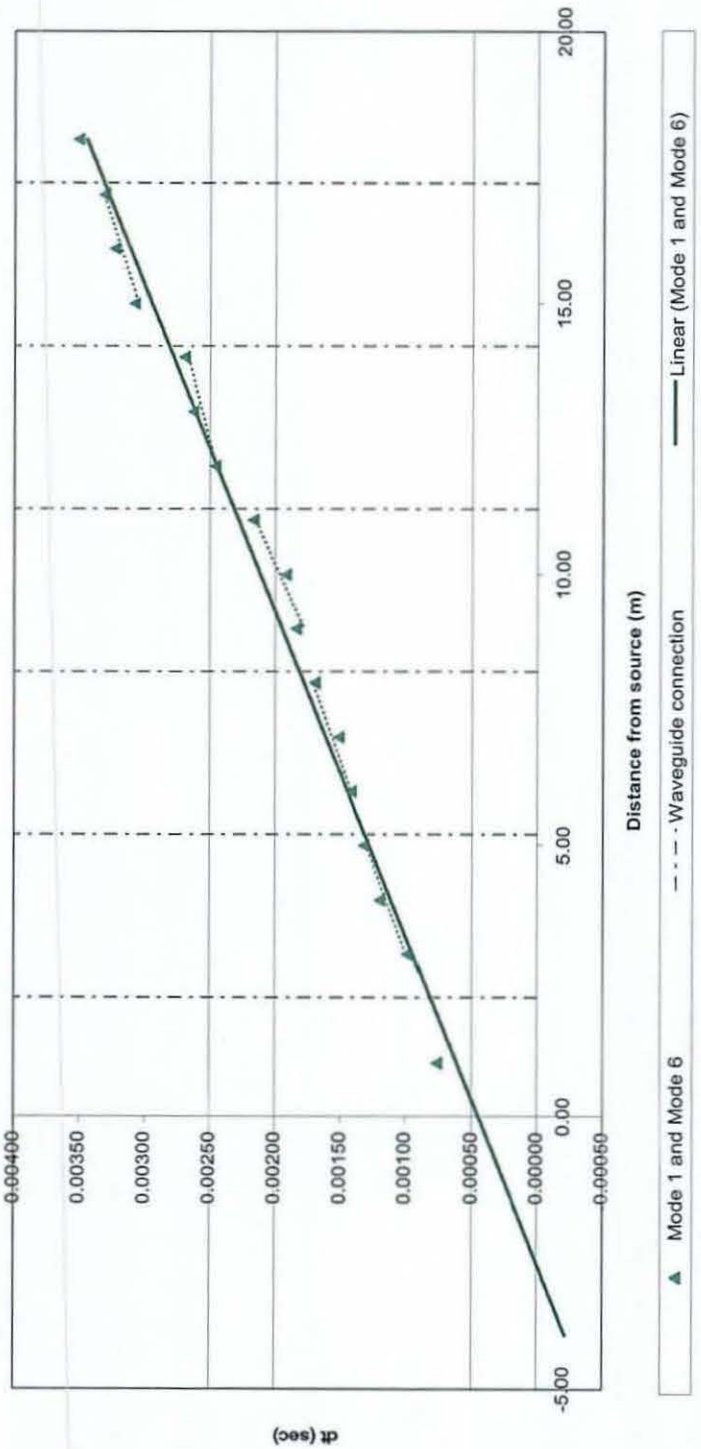

Figure 5.17 Modified graph showing localised effect of waveguide sections on Lamb wave mode velocities from exp105

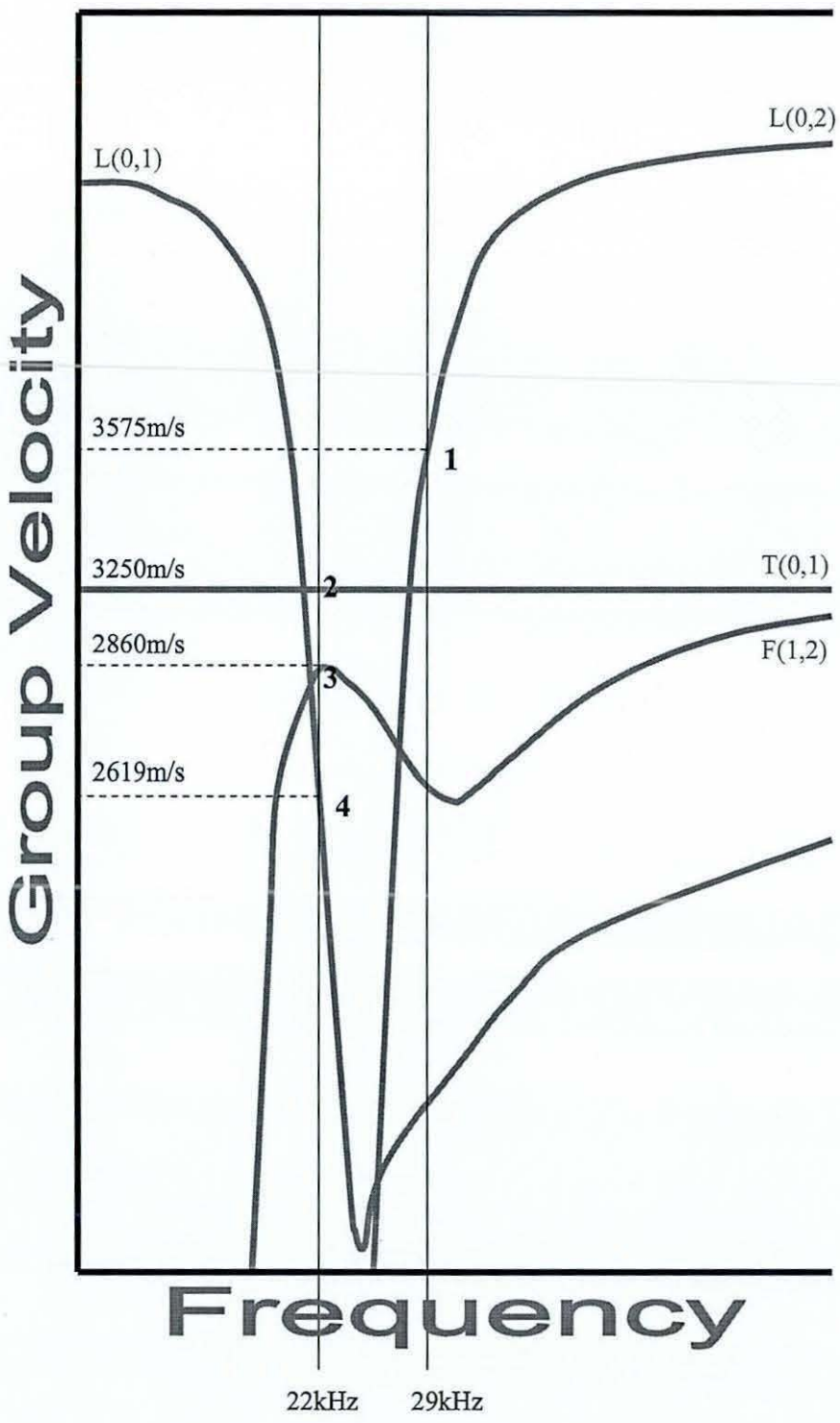

Figure 5.18 Group velocity graph for Lamb wave modes for a steel waveguide with pipe wall thickness of 3mm (after Alleyne and Crawley 1997)

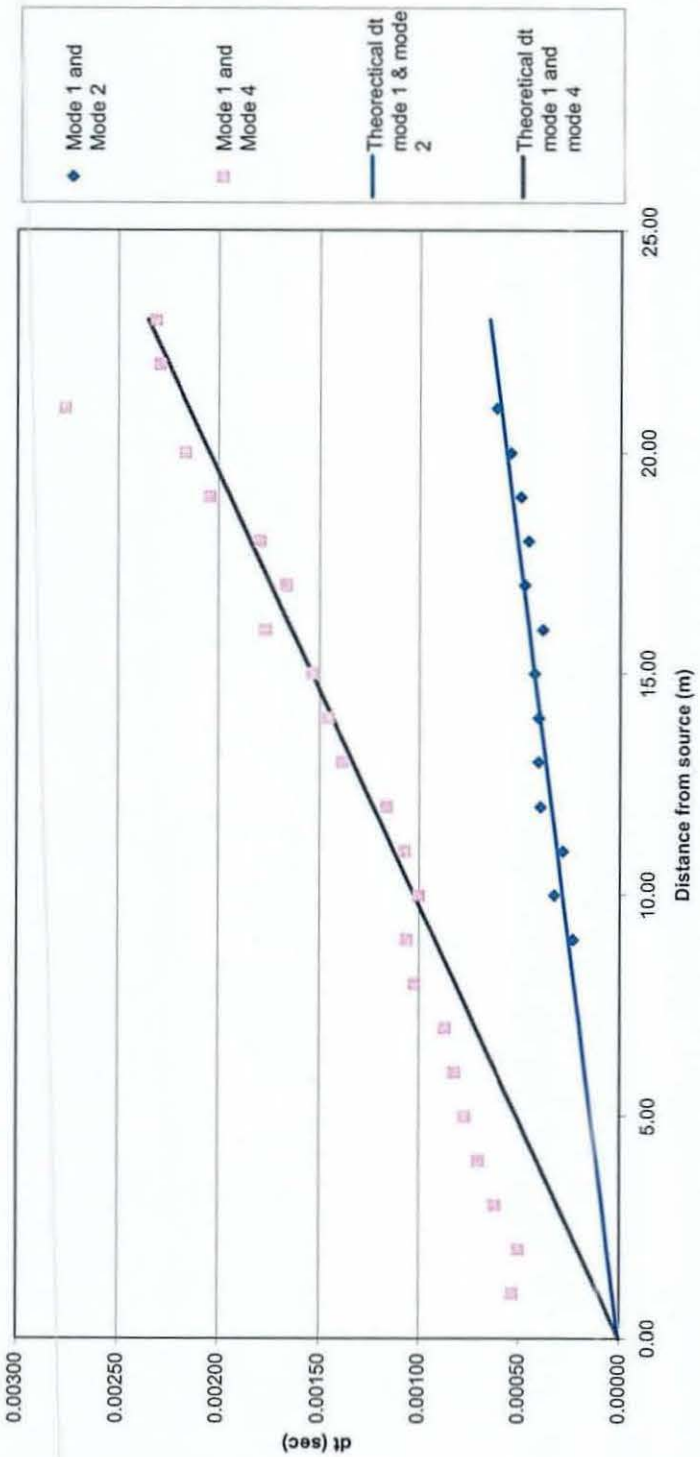

Figure 5.19 Theoretical relationships (calculated using equation 5.1) between dt and distance to source based on group velocity curves of Lamb wave modes.

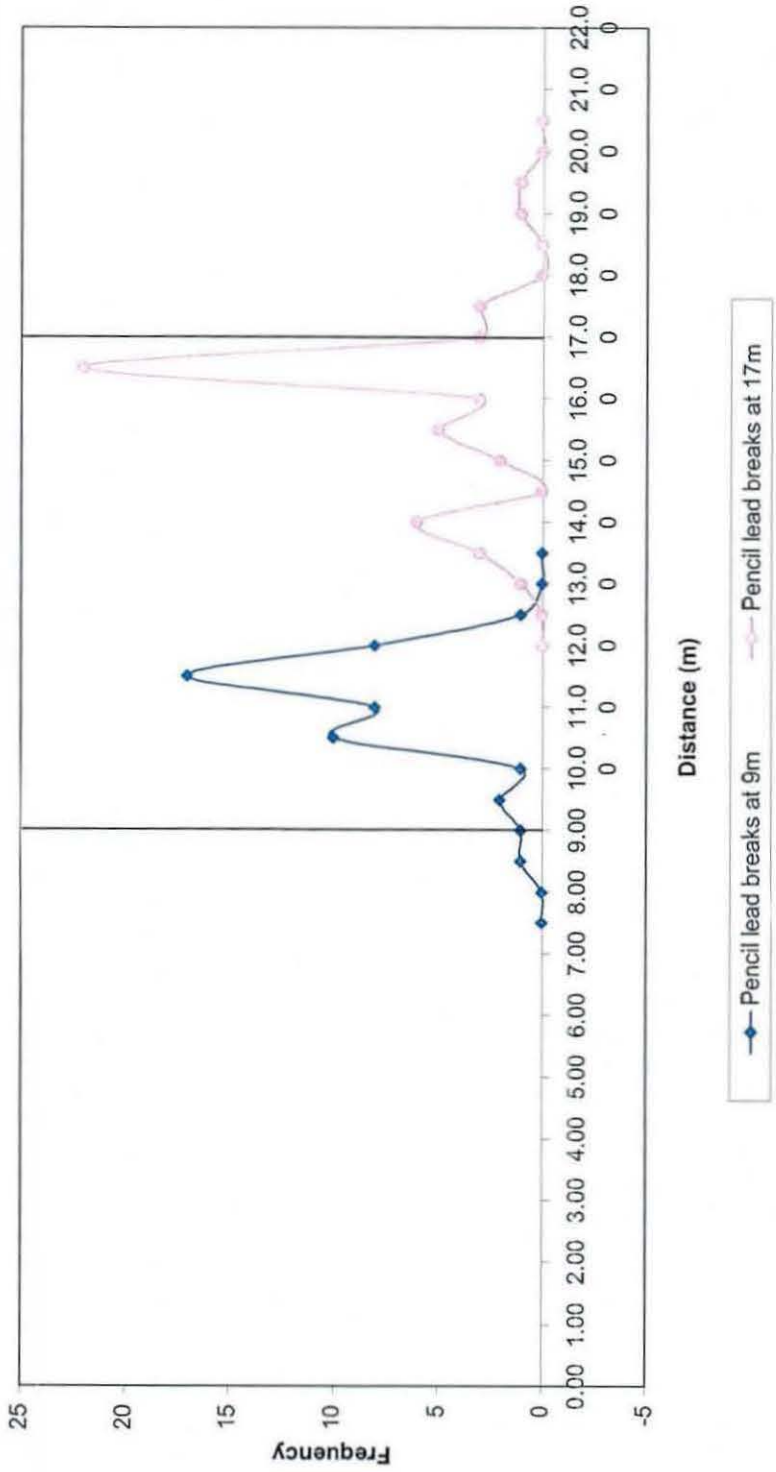

Figure 5.20 Histogram of exp 107 showing results from 9m and 17m

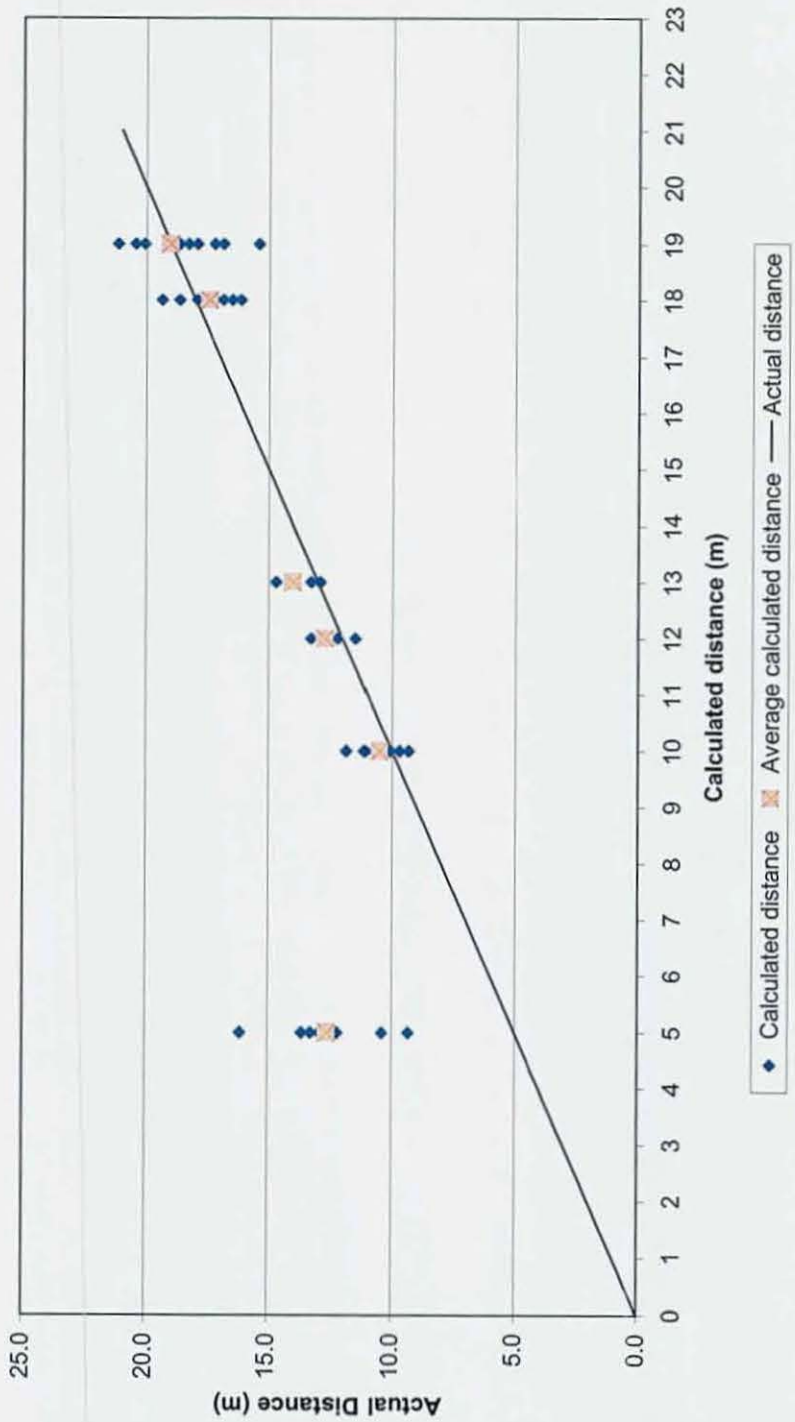

Figure 5.21 Comparison of calculated distance against actual distance to source from blind test

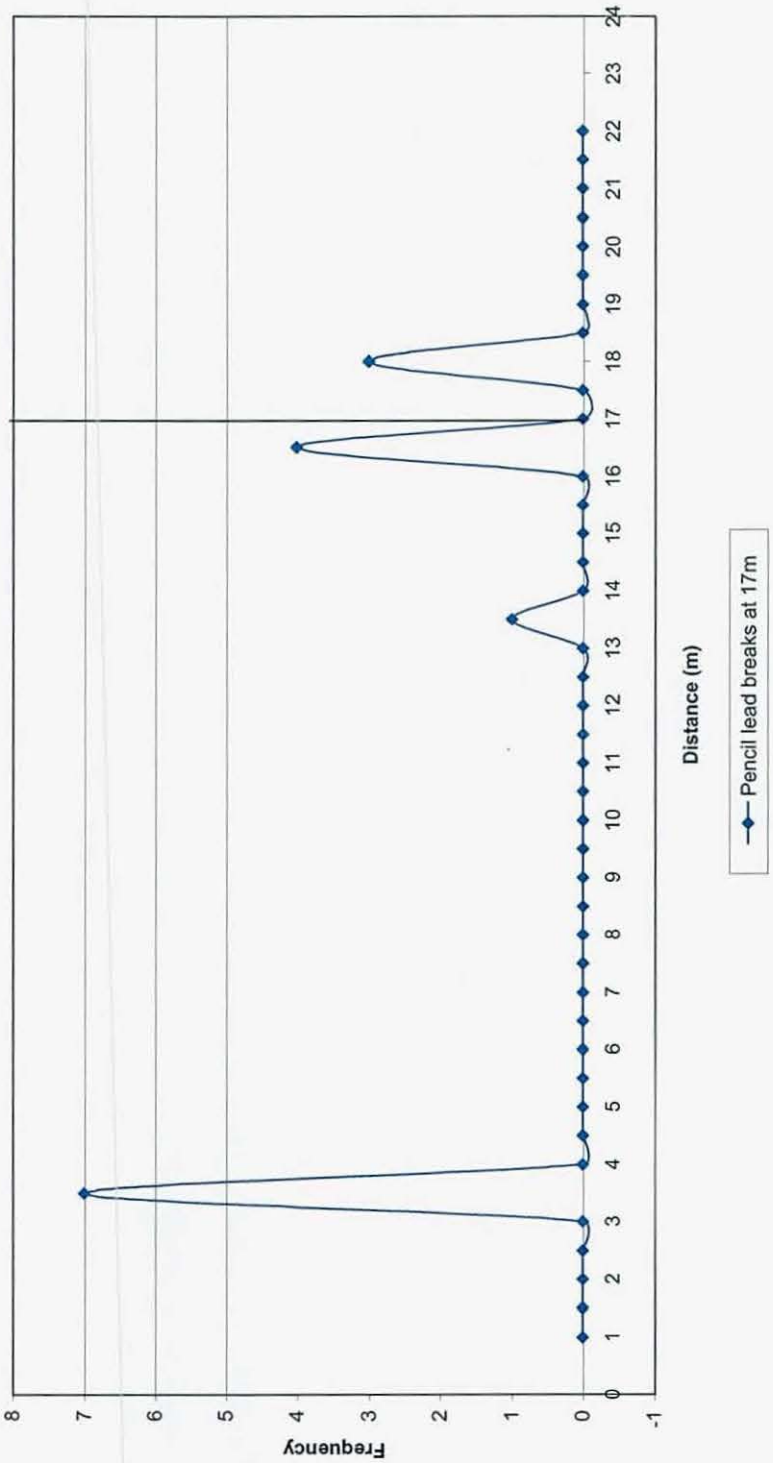

Figure 5.22 Histogram of exp 108 showing results from 17m

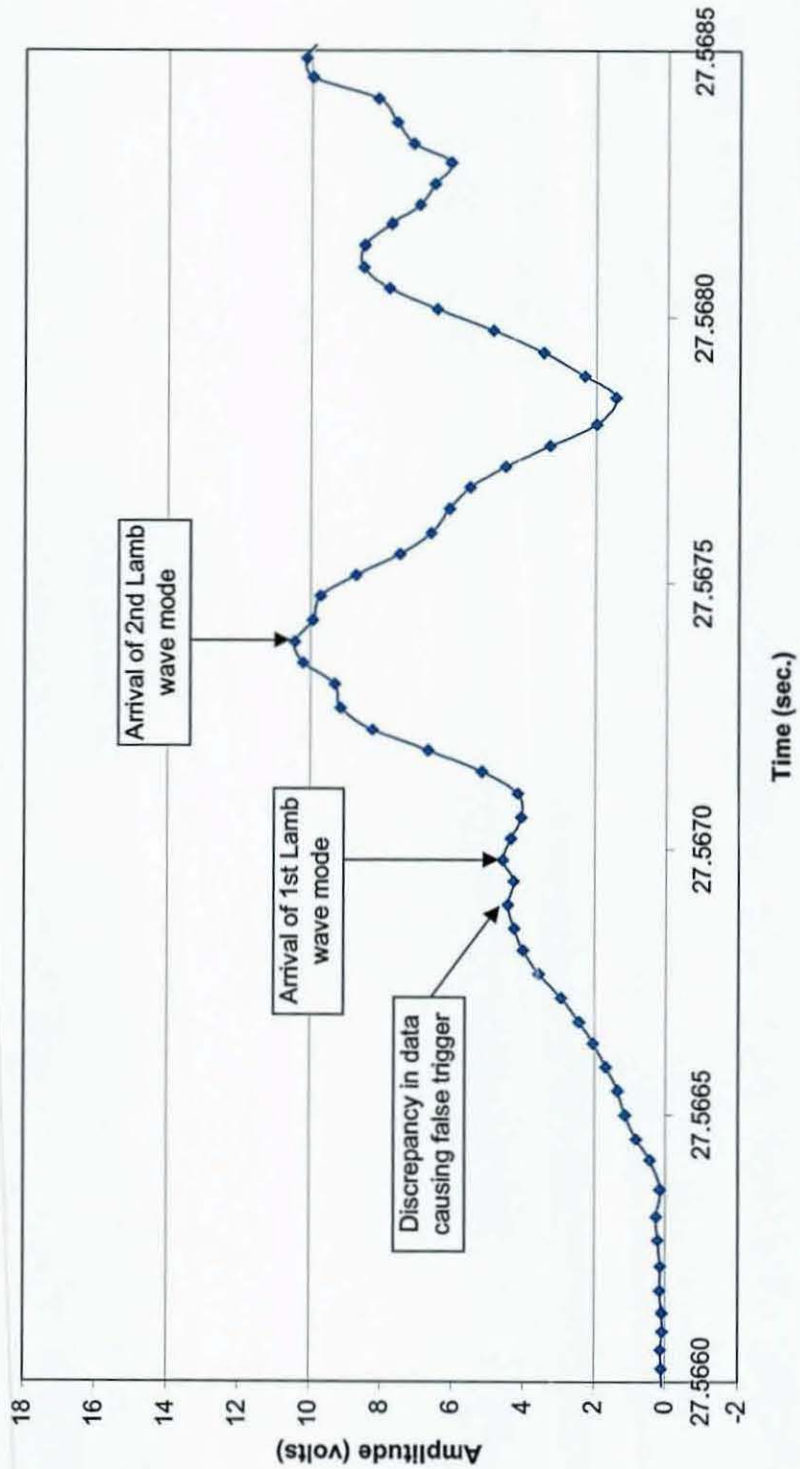

Figure 5.23 Example of automatic source location triggering on discrepancies within the AE waveform

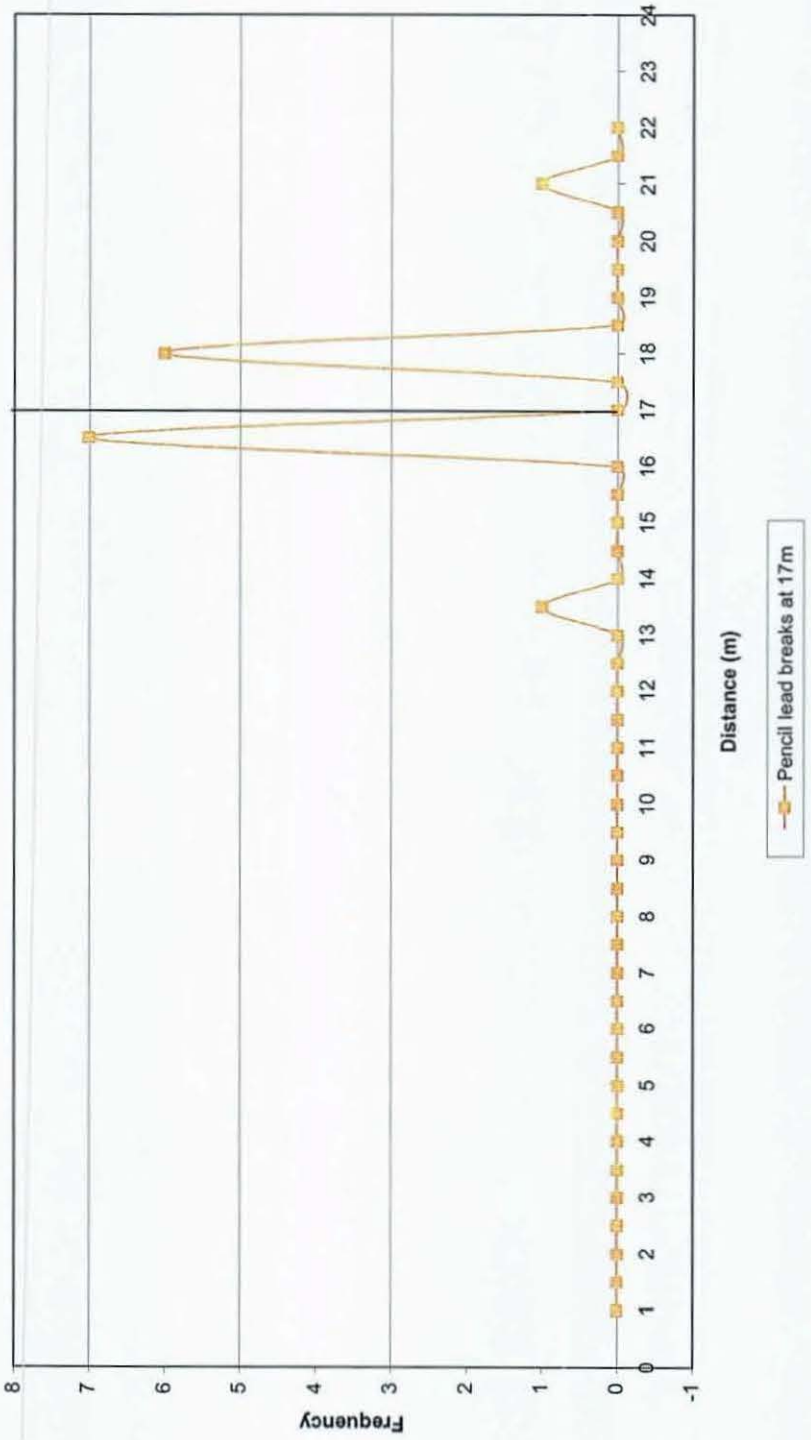

Figure 5.24 Histogram of exp 108 showing modified results from 17m

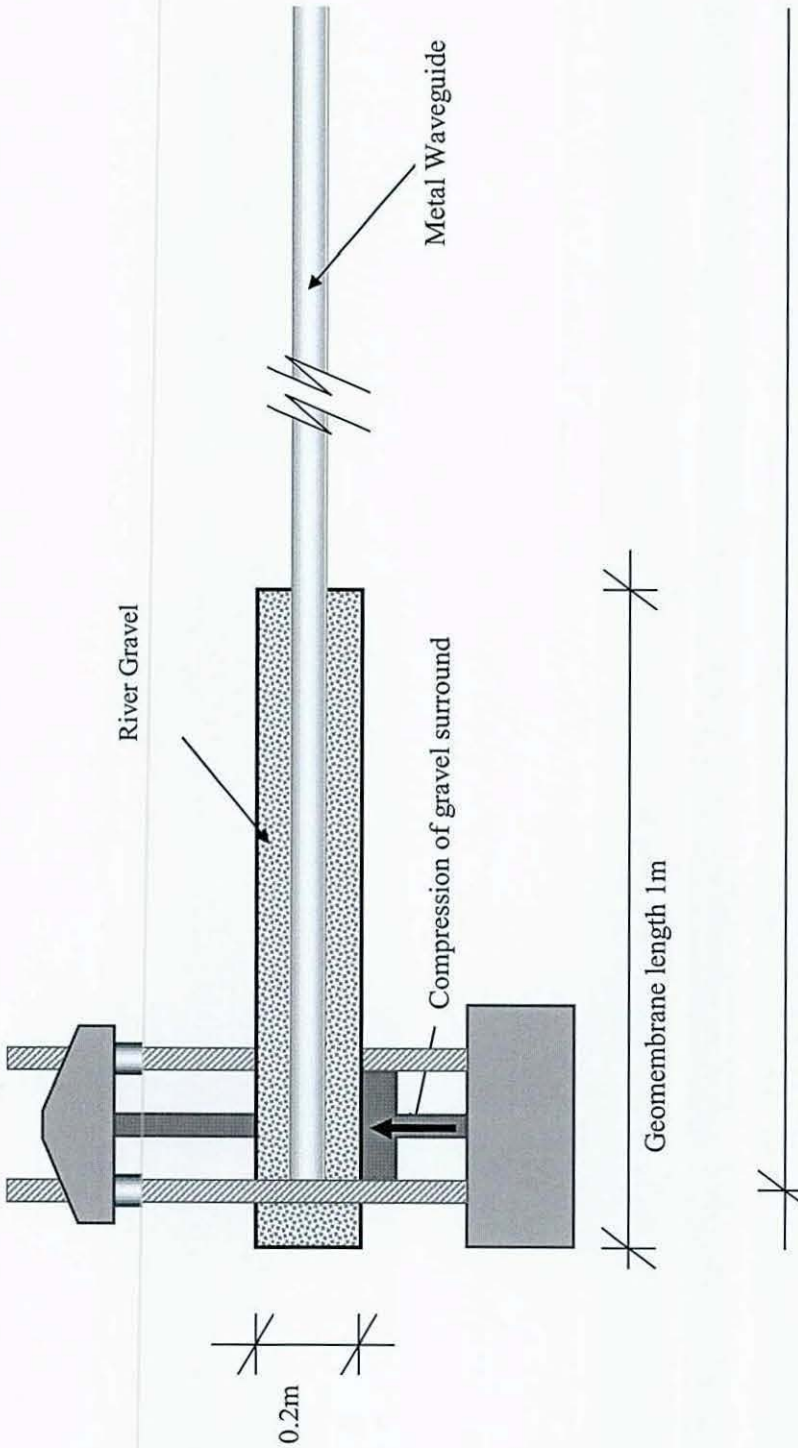

Figure 5.25 Experimental set up of the compression test used to generate AE for source location analysis.

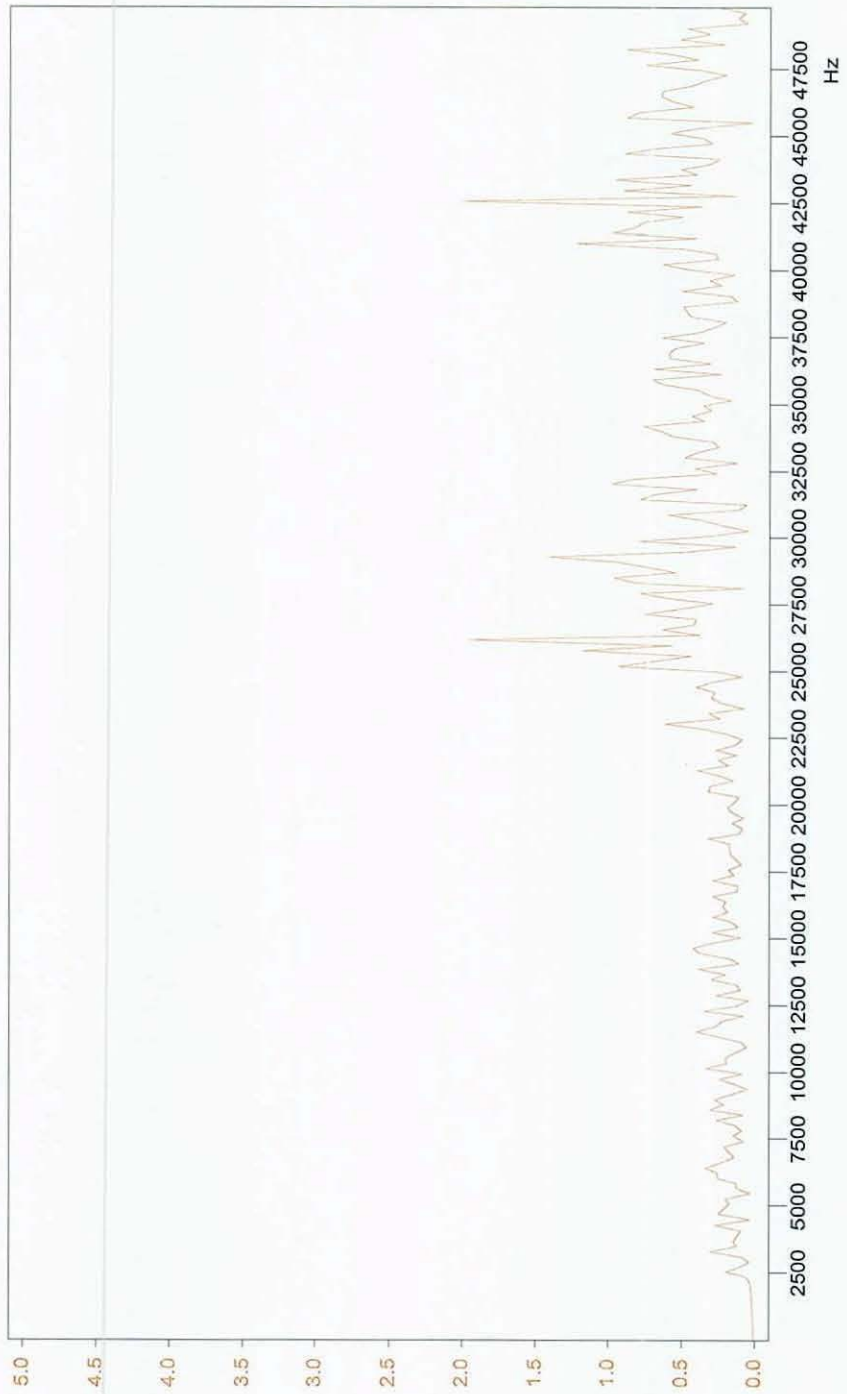

Figure 5.26 Frequency spectrum of backfill generated AE
(units: x-axis = frequency (Hz) y-axis = Volts)

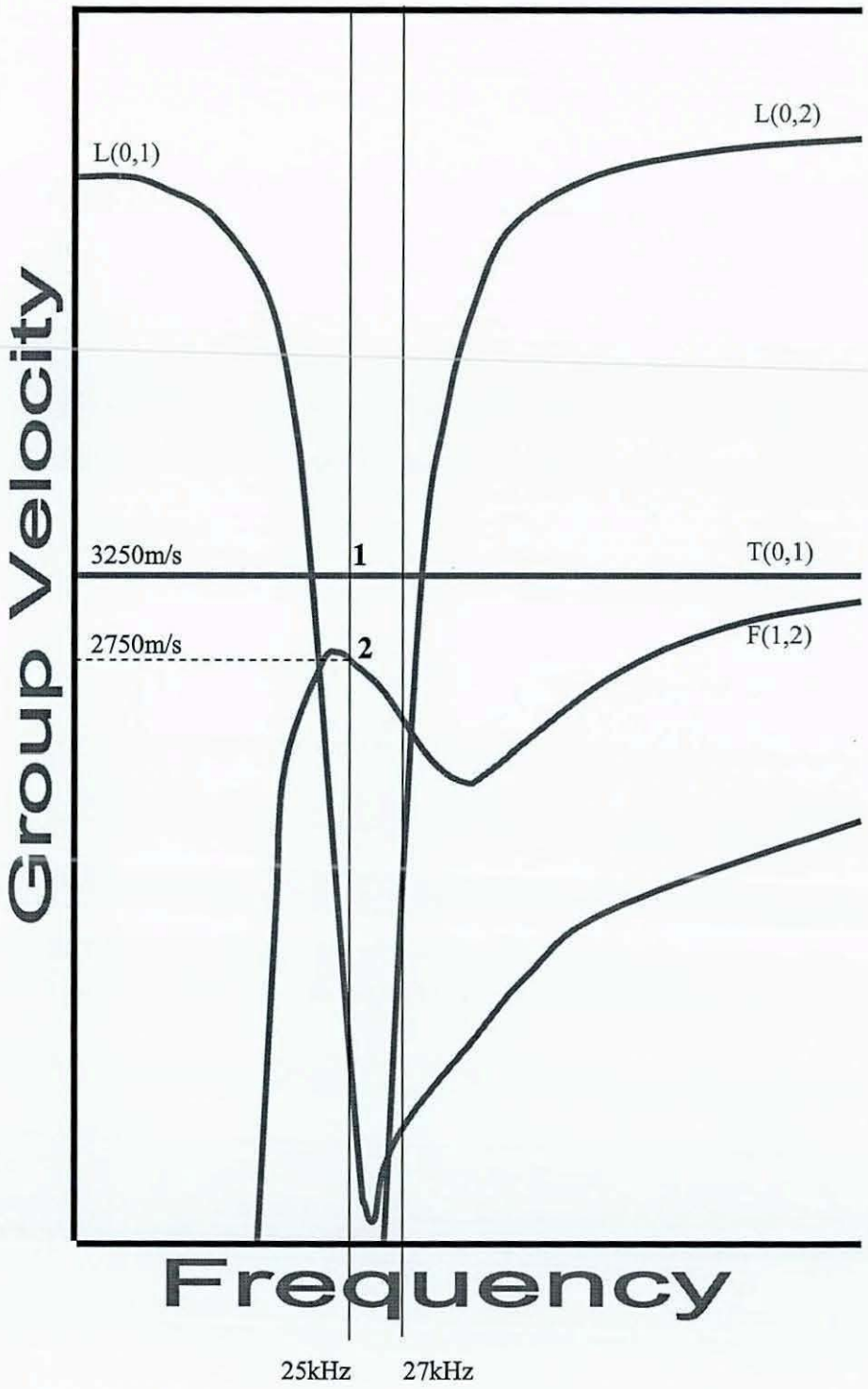

Figure 5.27 Group velocity graph for Lamb wave modes for a steel waveguide with pipe wall thickness of 3mm (after Alleyne and Crawley 1997)

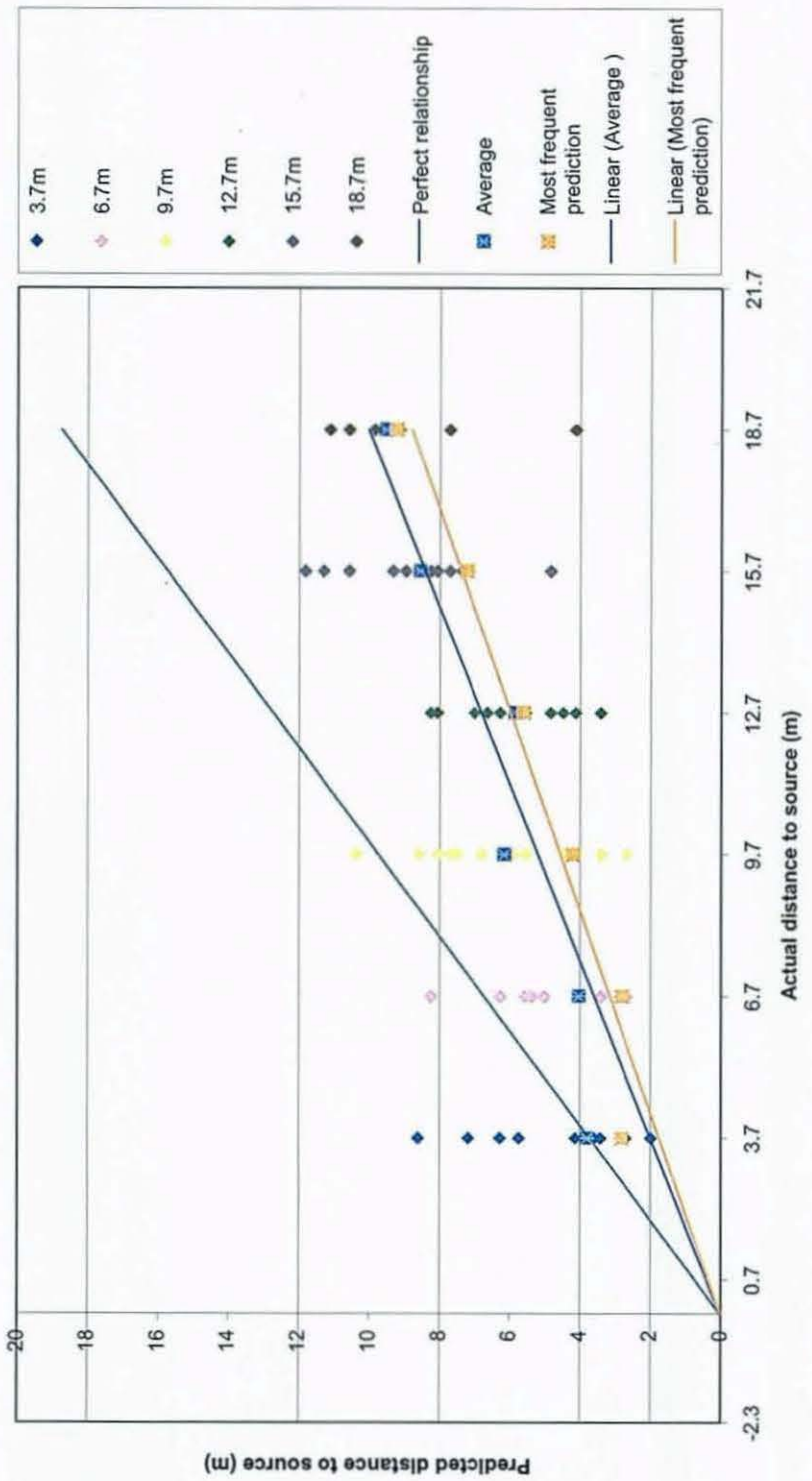

Figure 5.28 Relationships between the predicted distance to source, and the actual distance to source for manual source location on backfill generated AE

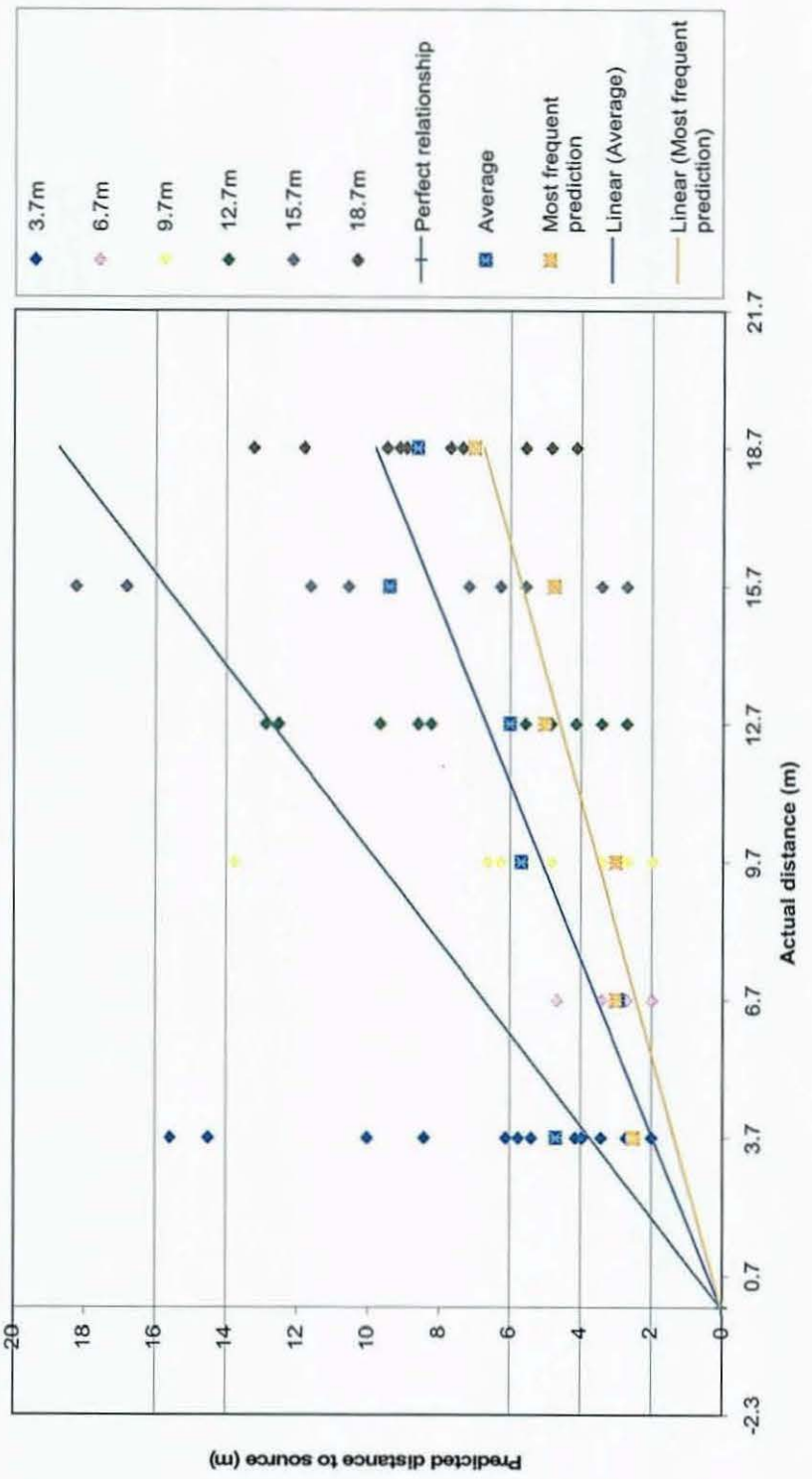

Figure 5.29 Relationships between the predicted distance to source, and the actual distance to source for automatic source location on backfill generated AE

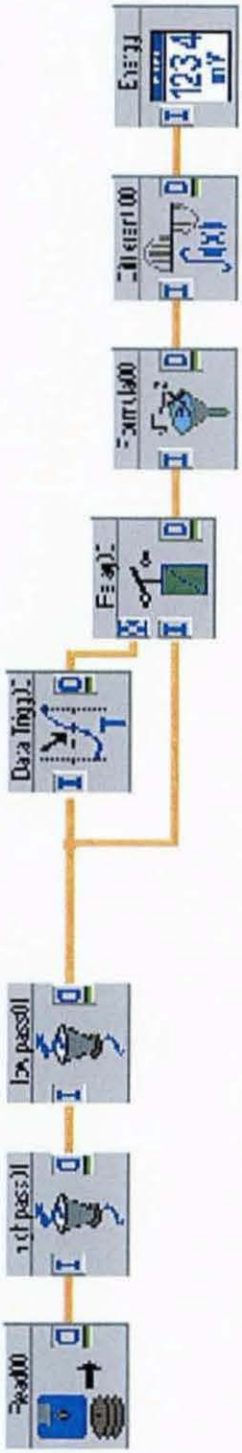

Figure 5.30 DASYLab worksheet for measuring attenuation along a waveguide

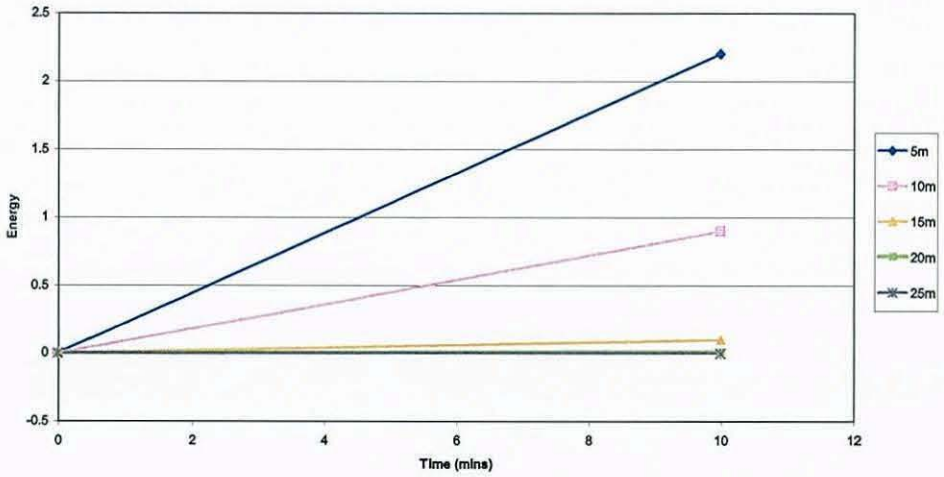

Figure 5.31 Energy (units = volt seconds) verses time

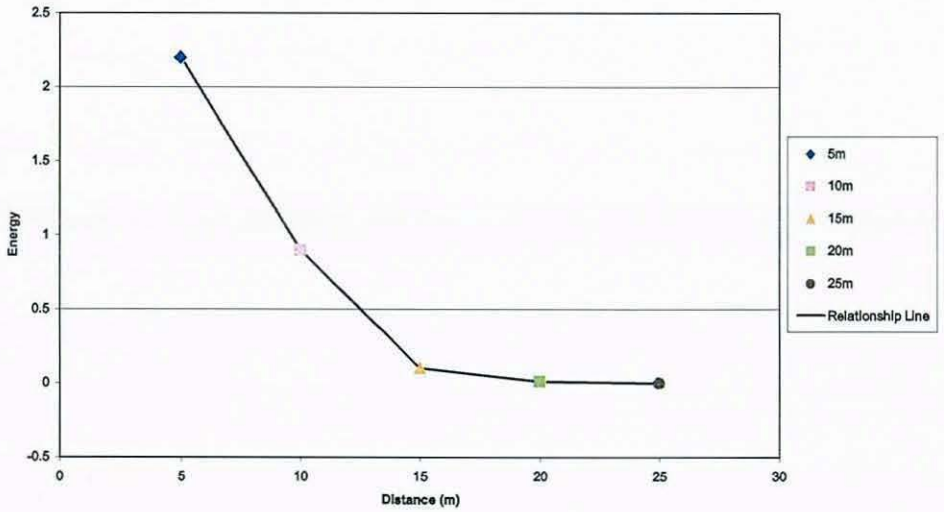

Figure 5.32 Energy (units = volt seconds) verses distance demonstrating attenuation

Chapter 6

Producing an Early Warning System

6.1 Introduction

Chapter 6 brings together the two strands of research within this thesis, namely the quantification of acoustic emission (AE) (chapter 4) and the identification of the zone of deformation (chapter 5), in an effort to consider its collective capacity as an early warning system for use within landslide hazard areas Section 6.2 summarises the conclusions put forth in chapters 4 and 5. Section 6 3 outlines a further test undertaken to demonstrate the systems ability to identify changes in the rate of displacement by an order of magnitude. A calibrated waveguide from chapter 4 was tested in section 6.4 to demonstrate the use of an automatic source location tool when analysing hundreds of AE events. The requirements of an early warning system are outlined within section 6.5, with consideration given to the hardware required (section 6.5.1) and the monitoring/analysis of the data (section 6.5.2). Conclusions as to whether or not an early warning system can be produced are given in section 6 6.

6.2 The story so far...

The production of an early warning system based on AE has been the goal of this investigation. Two areas of research were identified as vital to achieving that goal; the quantification of AE (chapter 4) and the identification of the zone of deformation (chapter 5).

Chapter 4 outlined the current standard of landslide classification, which distinguished displacement rates by orders of magnitude (see section 4.2.1). The chapter stressed the need to produce a quantified AE approach to landslide

classification using AE, in terms of rate of displacement. This output could then successfully monitor and potentially be used to predict the onset of slope failure.

The following conclusions were produced;

- Recorded AE could be quantified by monitoring the event rate
- Quantified AE could be grouped in to orders of magnitude of displacement rate.

Chapter 5 detailed the need to know the location of the deformation zone within an active waveguide. There were two reasons why this was necessary; firstly so that the correct level of amplification could be applied to the monitoring system, and secondly, to aid the effective design of mitigation and remediation strategies. Chapter 5 concluded that;

- The use of Lamb wave theory enabled source location to be performed from a single sensor.
- An automatic approach was developed to identify the location of the deformation zone in the backfill material to within +/-0.61m (tested on distances less than 17m).
- The attenuation suffered by Lamb waves travelling within the stated waveguide (see section 5 6) resulted in a decrease in order of magnitude of the energy (measured by the area under the waveform envelope) for every 5m of propagation (tested over a distance of 25m).

The two strands of this investigation were inextricably linked. The quantification of AE would always be compromised if the attenuation suffered by generated AE events was too great, resulting in true events below the amplitude threshold being undetected. In addition, knowledge of the depth of a deformation zone would only have limited use if no assessment of a slope's progressing instability could be given in terms of displacement rates. Together they would be able to utilise the advantage given by using AE (generated within the active waveguide); that being to detect movement at very low strains at very low strain rates.

6.3 Translating acoustic emission events into displacement rates

The strength of an early warning system lies in its ability to provide both a reliable quantifiable output, and to be sensitive to small changes within displacement rates Both of these aspects are considered below in the analysis of a 'blind' experiment. An experiment was carried out in which the displacement rates were not known prior to analysing the data.

6 3.1 Monitoring changes in displacement rates

In order to test the sensitivity of the monitoring system to changes within the rate of displacement, a blind test (named exp178) was conducted in which the rates of displacement were changed within an experiment The experiment was set up and then left to be conducted by a third person. It was down to the discretion of the operator to select different rates of displacement, and to carry out the experiment from start to finish. The chosen displacement rates remained unknown to the Author whilst analysis was performed on the data.

The aim was to determine the systems' ability to a) detect changes within the displacement rate and b) to estimate the rate of displacement at each stage of the experiment (see section 6.3.2). The experiment was carried out using the compression test apparatus employed in the quantification of AE experiments (shown in Figure 6.1). Crushed river gravel was placed around a 3m length of a steel waveguide (3mm wall thickness) as outlined in section 4.4 1. An AE sensor was placed 2m from the compression zone, and the following data acquisition parameters were set:

Filters	25 – 28 kHz
Amplification	98dB
Sampling rate	0.0556MHz

The data was recorded within DASYLab, and then post-analysis was conducted on the data using the DASYLab worksheet shown in Figure 6.2. Although this worksheet produced data on the ring down count, the event count and the energy of the recorded AE, only the event count was needed. The experiment was set running and then the Author left the room. The rate of the displacement was altered at various stages of deformation by the third person. The rates of displacement used were different to those used in section 4.4, but did represent different orders of magnitude of displacement. Each rate was labelled as classified by the Transport Research Board (1978). These are:

Classification:	Rate:
Rapid rate	**1.1025 mm/min (approx. 1mm/min)**
Moderate rate	**0.2205 mm/min (approx. 0.1mm/min)**
Slow rate	**0.0441 mm/min (approx. 0.01mm/min)**
Very slow rate	**0.001764 mm/min (approx. 0.001mm/min)**

The calculated event rate with time results are shown in Figure 6.3. A total of 9 separate rates were identified by visually examining the graph for distinct changes in the gradient of the event versus time relationship slope. This visual examination was done using Microsoft Excel which enabled areas of the graph to be magnified in order to obtain accurate timings of a change in the displacement rate. Black lines on the graph indicate at what time a change in displacement rate actually took place. It can be seen that the changes estimated from observing the gradient of the event count against time were identical to the actual changes which took place. The largest error that existed was no greater than 1.2 minutes, which is an acceptable error over an experiment which lasted 6 hours.

It was concluded that the AE monitoring system was able to detect changes in displacement rate of an order of magnitude. The ability of the system to respond to a change in displacement rate within one minute of that change taking place could be vital, especially in situations where landslides are suddenly triggered or displacement starts to accelerate e.g. in response to an intense rainfall event.

6.3.2 Deriving the displacement rate

The above experiment showed the sensitivity of the system to identify a change in rate of displacement; however, not knowing what that change in displacement rate is, greatly limits the use of the data. Chapter 4 considered the quantification of AE into orders of magnitude, this section sought to convert the event rate into a displacement rate. In section 4.5.1 a series of compression tests were carried out on the backfill/waveguide system. Four different rates of displacement were chosen to represent four different orders of magnitude of movement. The results of these tests are shown again in Figure 6 4 on a graph of log event rate versus log time. The test apparatus was shown to be a reliable representation of deformation mechanisms within an active waveguide, i.e. through comparison of the results with those from large scale tests (see section 4 5 2). The gradients of the each set of displacement rate results, plotted in Figure 6.4, were calculated and presented on a graph against the actual rate of displacement used during the experiment A best fit trend line was drawn through the average of each gradient to produce a linear relationship between the gradient of the event rate and the rate of displacement; this is shown in Figure 6.5. Figure 6.5 could then be used to convert recorded AE, in terms of events, to a quantified rate of displacement

In order to assess the use of the relationship shown in Figure 6.5, the results from the blind test (exp178) were analysed to check if the estimated rate of displacement measured was comparable to the actual rate of displacement used within the experiment (see section 6.3.1). A total of nine separate displacement rates were identified within the blind test shown in Figure 6.3. Each rate was plotted on a graph of event rate versus time (similar to Figure 6.4) and the gradient of each line was calculated. Using Figure 6.5, these gradients were then converted into a displacement rate, and the associated displacement for each section of Figure 6.3 was calculated.

The results are shown in Table 6.1. The estimated rate of displacement and the actual rate of displacement have been colour coded within the Table, each colour refers to the classification given to each rate by the Transport Research Board

(1978) and are separated by an order of magnitude: **rapid rate**, moderate rate, **slow rate** and .

From Table 6.1 it can be seen that all the rates (except rates 5 and 9 which were overestimated) were correctly classified into their order of magnitude. Rates 4 and 8 produced a negative gradient of event rate. That is to say, that over time the rate of events decreased. However Figure 6.4 shows that the event rate always seemed to increase over time as the backfill material was compressed. A reduction in event rate, whilst under a constant rate of displacement, must signify that either the displacement had stopped, or the load applied had been retracted.

Kavanagh (1997) demonstrated that the generation of AE only occurred within soil when the soil had been stressed beyond that which it had experienced in the past (called the Kaiser effect). If the stress upon a soil sample remains constant or is reduced, the AE in turn will cease to be generated. In exp 178, rates 4 and 8 actually had a displacement rate of 0 mm/min, during which the stress upon the backfill material remained constant. As the displacement rate was halted, events continued to occur due to a stress release caused by the reorganisation of particles. Over time, fewer and fewer events occurred as the particles reached an equilibrium. Load measurements were not taken during this experiment, but it is expected that the load dropped over this time period. The result was a trend that resembled a decrease in event rate over time as seen for rates 4 and 8.

Rates 5 and 9 were the only rates that were incorrectly estimated. Both of these rates were over estimated by one order of magnitude, and both followed a period of zero displacement. It is not known why this occurred, and further experiments would be required to test if this was a regular occurrence.

Figure 6 6 shows a displacement/time graph of the estimated and the actual results. Again it can be seen that the changes in displacement rates were accurate to 1 minute. Although rate 1 was correctly identified to within one order of magnitude, the actual rate was one third of the estimated rate, and this was primarily responsible for the separation of the two curves within Figure 6.6. The

technique wasn't able to provide magnitudes of displacement which of a greater accuracy than an order of magnitude.

The test outlined within section 6.3 demonstrated that the monitoring technique developed in chapter 4 was able to convert the event rate to a displacement rate. This was shown to be accurate to within an order of magnitude, and demonstrated a high degree of sensitivity when identifying changes within the rate of displacement. Particular attention should be given to the sensitivity of the technique when identifying periods of zero displacement rates, and hence the ability to detect signs of increasing stability within a slope. A decrease in event rate would indicate a reduction in stress in the backfill, and thus clearly show when a slope becomes more stable. This would enable the technique to be applied to the monitoring and assessment of remediation works.

6.4 Calibrating a waveguide for source location

In section 5.5 3 a waveguide was calibrated so that source location calculations could be performed. Although the actual Lamb wave modes used by the automatic approach were unknown, two distinct modes were repeatedly detected along the length of the waveguide. A linear relationship was produced between the actual distance from the sensor to the source and the distance calculated by the automatic source location tool. That relationship is shown in Figure 6.7. An experiment was set up to test the relationship shown in Figure 6.7 on a different sample of river gravel surrounding a waveguide. The waveguide arrangement used had the same properties as used in section 5.5.3. The backfill was compressed around the waveguide using the compression test apparatus (Figure 6.1), at a moderate rate of 0.2205 mm/min for approximately 7 minutes.

The sensor was placed 1.7m from the source on a 3m length of waveguide. Filters were set within DASYLab (Figure 6.8) to monitor between 25 & 27 kHz. The hardware and software set up was identical to that used in section 5.5.3. The DASYLab output was copied into Microsoft Excel to be analysed further using the macro detailed in section 5.3.2. The difference in arrival times was then

converted to a distance using equation 5.1, based on the velocities of the first two Lamb waves that were expected to be monitored. This distance was then converted using the relationship displayed within Figure 6.7 calibrated on a matching waveguide arrangement. Figure 6.9 displays the final results within a histogram, in which the intervals were set at 0.5m.

Figure 6.9 demonstrates the advantage of observing many events over time. A distance of 1.5m is clearly shown to be the most frequently calculated distance to source with 140 events out of a total 300 events analysed, registering a calculated distance of 1.5m. Although many events were identified within a range of 5m about the actual distance to source of 1.7m, the accuracy of the approach lies within the number of events analysed. The certainty of results would continue to improve over time as more events are analysed.

Although the Lamb wave modes could not be identified, this simple experiment demonstrated that automatic source location could be performed using a waveguide that had been calibrated within the laboratory. Further work would be required to demonstrate that Figure 6.9 could be repeated over longer lengths of the waveguide. However, provided the same active waveguide setup was used within the field, it is expected that automatic source location would provide a tool to identify the distance to a deformation zone within the backfill material, which in this case was accurate to within 0.5m.

In section 5.4.3 the use of equation 5.1 was discussed. The equation was used to demonstrate the use of Lamb wave theory when performing source location calculations. However, it was detailed that the use of equation 5.1 would lead to errors particularly at distances from source to sensor of less than 10m Having established the application of Lamb wave theory to monitoring waveguides, a simple calibration method could be used instead from laboratory experimentation. Figure 6.10 is an example of this and shows the linear relationship between the difference in the arrival times of Lamb wave modes against the actual distance to source for exp 137. This linear relationship is represented by a numerical equation (as displayed on the graph), which could be used directly to produce a histogram such as Figure 6.9.

6.5 The field monitoring system

The following is an outline of the necessary hardware and monitoring procedures required to produce a field system capable of providing quantified displacement rates and information as to the location/depth of deformation such that an early warning of slope instability could be provided. Where necessary the limitations of this system have been highlighted for further investigation. An early warning monitoring system should meet the following requirements:

- Provide sufficient warning to enable action to be taken (i.e. implementation of emergency plan).
- Minimise the number of false alarms as they undermine confidence.
- Enable the mode of failure to be identified as this is required to assess the significance of the event.
- Provide information on rates and magnitude of movement to help assess the significance of the event.

6 5.1 The hardware

The primary aim of this investigation was to devise a monitoring strategy capable of producing quantified outputs relating to the location and rate of displacement of an active waveguide within an unstable soil slope. Consideration has been given to the development of necessary hardware required to achieve this goal, but experimentation has not concentrated on this aspect. For example, 3m lengths of waveguide were used in laboratory experiments, but in the field, longer lengths could be used to reduce the AE attenuation experienced at a joint. Much thought still has to be given to the hardware used on site especially with respect to the ease of construction and installation of an active waveguide.

The installation of an active waveguide at a site of high landslide risk would require the construction of a borehole which would penetrate potential slip zones. A borehole log would be vital to obtain a geological profile of sub surface conditions. When movement occurs within an active waveguide and a displacement rate is obtained, it becomes very important to know what geological materials are deforming at that depth (and their in situ properties) to analyse and understand the failure. A number of waveguides across the slope would enable better monitoring of the slope as a whole, but also the ability to compare data ensures adequate coverage of redundancy within the system.

In order to ensure that an active waveguide intersects the potential zone of deformation, many tens of meters of waveguide may have to be installed. This presents a problem of quality control when placing the backfill and the waveguide at depths of 20, 30 or 40+ metres. Section 4.5.1 highlighted this concern. The backfill would need to be sufficiently compacted throughout its depth to achieve a sufficient density to prevent further settlement. This would also ensure that any displacement of the surrounding soil would immediately translate to a true deformation of the backfill, and subsequent generation of detectable AE. This has been achieved in documented field systems. Kavanagh (1997) installed 6m lengths of steel waveguide with a granular backfill surround to depths of 21m, and was able to detect first time deformation mechanisms within an unstable soil slope.

The active waveguide used within chapters 4 and 5 could certainly be used within a field trial. The backfill material, crushed river gravel, was identified as the most suitable backfill material for an active waveguide (section 3.3.2). But further changes to the waveguide alone i.e. length of section, type of connection and wall thickness, would require further calibration within the laboratory for source location analysis, and attenuation studies, but not for quantification measurements.

Consideration must also be given to selection of sensor and amplification hardware From chapters 4 and 5, it has been demonstrated that crushed river gravel exhibited strongest frequencies between 25 & 30 kHz. A resonant sensor with a greater sensitivity over that frequency range would perhaps provide

improved clarity and amplitude of the backfill generated AE. The total amplification provided in this investigation (using a preamplifier and an amplifier) was 101 dB. This was sufficient for a waveguide of 25m in length. For monitoring at greater lengths, more amplification would be required to detect backfill generated AE. The influence of a granular surround on the attenuation suffered by a propagating AE event has not be tested in this investigation, but previous work has demonstrated that a backfill surround does not create further attenuation on Lamb waves due to their nature of propagation (see section 2.3.3).

6.5.2 Monitoring procedures for an early warning system

The following is an outline of the necessary data handling procedures required when applying the monitoring system as outlined in chapters 4 and 5 to a field trial They have been summarised in a flow diagram shown in Figure 6.11.

After the installation of active waveguides at a site of potential landslide hazard, an initial assessment of slope stability would be performed to provide an approximate depth of failure. This would enable an approximate amplification to be set immediately, so that the event rate could be monitored to obtain a displacement rate very early on. A control waveguide would be installed close to the unstable slope, but away from any zones of potential deformation. This would provide information on the levels of background noise and enable an amplitude threshold to be set to prevent the monitoring of noise generated by sources other than those associated with the deformation of the waveguide backfill due to slope instability. A control waveguide was successfully used in field trials by Kavanagh (1997) who installed a control waveguide away from the unstable slope such that it wouldn't suffer any deformation, but would collect AE data from other existing sources.

Source location calculations (based on the difference in arrival times for the Lamb wave modes) would also begin to obtain the distance to source of the recorded AE. A histogram would be built up showing the calculated depths and the frequency of their occurrence. The calculated depth, or depths, which occurred

most frequently, would be taken as the location of deformation within the active waveguide. The amplification settings would then be revised based on this data. The histogram would be constantly updated as source location calculations provide more data over time, building up confidence within the calculated location, or highlighting possible changes in the location of source of AE, and hence information on the failure mechanism.

In section 5.5, a Table of amplification required at certain distances along the waveguide was produced (see Table 5.2) This Table was specific to the steel waveguide used in section 5 2, with a wall thickness of 3mm connected at 3m intervals. Alternative waveguides would require their own calibration prior to field installation.

Event rate data would be plotted onto an event rate versus time graph, and the gradient of that line would be calculated. Using Figure 6.5, a quantified output of AE in terms of a displacement rate would be obtained. Any changes within the displacement rate would indicate a decelerating or an accelerating of the landslide.

Knowledge of the soil slope's characteristics would be available from borehole logs created during installation of the active waveguides. By matching up the calculated depth of movement with the soil characteristics at that depth (across all installed waveguides) an assessment of the mechanism of failure could be made and potentially a time to failure predicted. Figure 6.11 demonstrates a potential output in terms of instructing an engineer what to do if certain rates of displacement are achieved. This of course would depend on the soil type and its in situ properties, but the setting of quantitative thresholds specific to the site conditions would enable certain levels of response to pre-determined.

In chapters 4 and 5 of this investigation, analysis was performed using two software packages, DASYLab (for acquiring and analysing AE data) and Microsoft Excel (source location analysis only). For both quantification and source location purposes, data was first recorded to the computer hard disk and then post analysed for the displacement rate and location of deformation zone. Within a field monitoring situation, time and money may not allow the luxury of a

person to constantly take a section of the data and perform post analysis. Such a process would also limit the early warning capability by not allowing real time monitoring to produce real time outputs. DASYLab is capable of acquiring and analysing data in real time, therefore further work would be required to enable the development of a worksheet within DASYLab, or other similar software, capable of performing the analysis outlined within chapters 4 and 5 in real time. Information relating to changes in the displacement rate and the depth of deformation could then be monitored in real time and from a remote location via an appropriate communications method.

6.6 Chapter summary

The question of whether or not the approach taken to quantify AE and locate the depth of a deformation zone (within an active waveguide) could lead to an early warning system has been the concern of this chapter. The blind test in section 6.3 proved the system's ability to handle unknown AE data and provide a calculated rate of displacement accurate to within an order of magnitude. It also demonstrated a high degree of sensitivity when identifying changes within the rate of displacement.

Section 6.4 demonstrated the use of the automatic approach to source location on a calibrated waveguide, enabling many hundreds of events to be analysed. By displaying the output within a histogram, not only was a distance between the source and the sensor calculated to within 0.5m of the actual distance, but a high degree of certainty could be placed on the data due to the large number of events analysed.

Section 6.5 discussed the limitations of using the present hardware (as used for laboratory tests in chapters 4 and 5) within the field, and proposed a flow diagram outlining an approach to handling data within a field monitoring context Further work was suggested to refine both the hardware (including the installation of an active waveguide) and the monitoring systems' capability to handle data in real time.

With these considerations in mind, it is the opinion of the author that it is possible to use the instrumentation and analysis approach as outlined in this investigation to provide the relevant information required to produce an early warning of slope instability.

Table 6.1 Comparison of estimated rate of displacement against actual rate of displacement

	Calculated Results				Actual Results		
Rate no.	From (hrs)	To (hrs)	Gradient of trend line (counts/hrs^2)	Rate of Displacement (mm/min)	Rate of Displacement (mm/min)	From (hrs)	To (hrs)
1	0.00	0.05	2000000	3.3333	1.1025	0.00	0.04
2	0.05	0.44	9846.9	0.0542	0.0441	0.04	0.43
3	0.44	3.46	126.87	0.0067	0.00176	0.43	3.43
4	3.46	4.47	-19.882	-	0	3.43	4.44
5	4.47	4.61	49557	0.1333	0.0441	4.44	4.61
6	4.61	4.78	184495	0.3333	0.2205	4.61	4.78
7	4.78	4.80	919606	1.0833	1.1025	4.78	4.79
8	4.80	5.13	-41.61	-	0	4.79	5.13
9	5.13	5.92	401.38	0.0125	0.00176	5.13	5.92

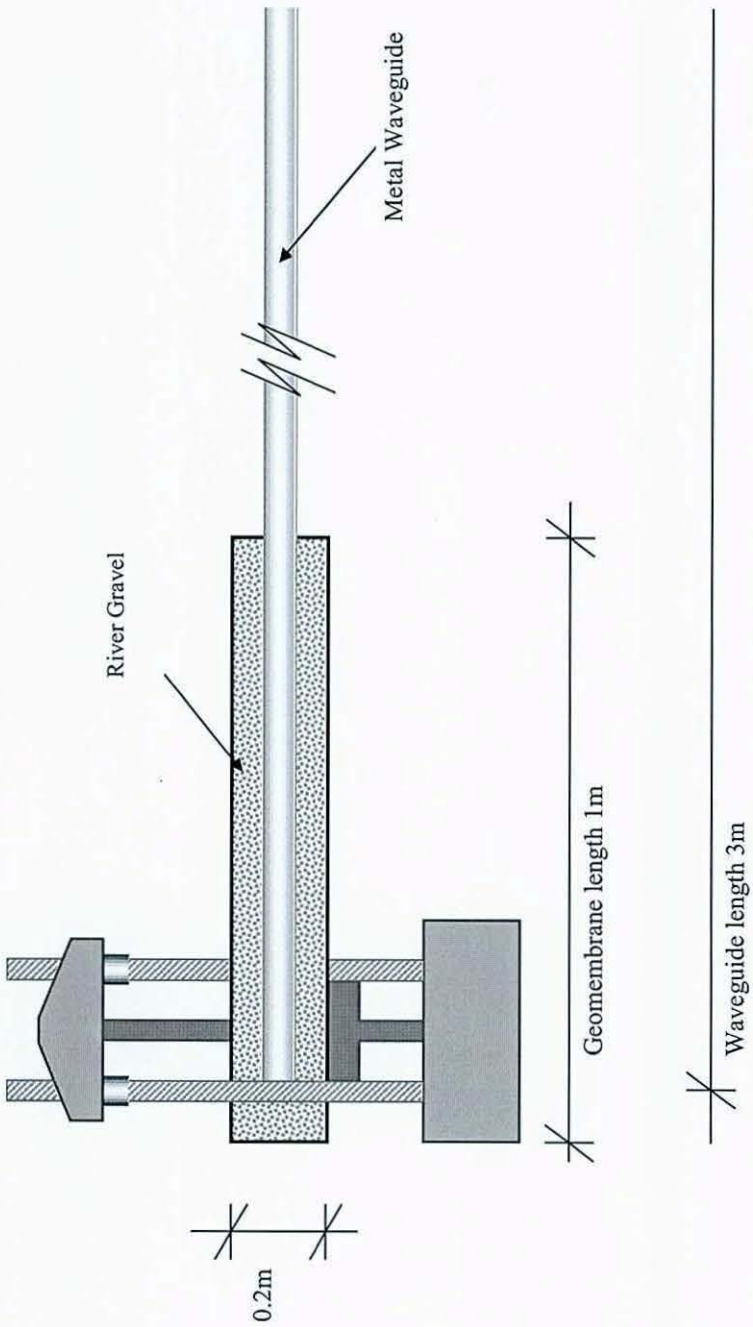

Figure 6.1 Compression test apparatus

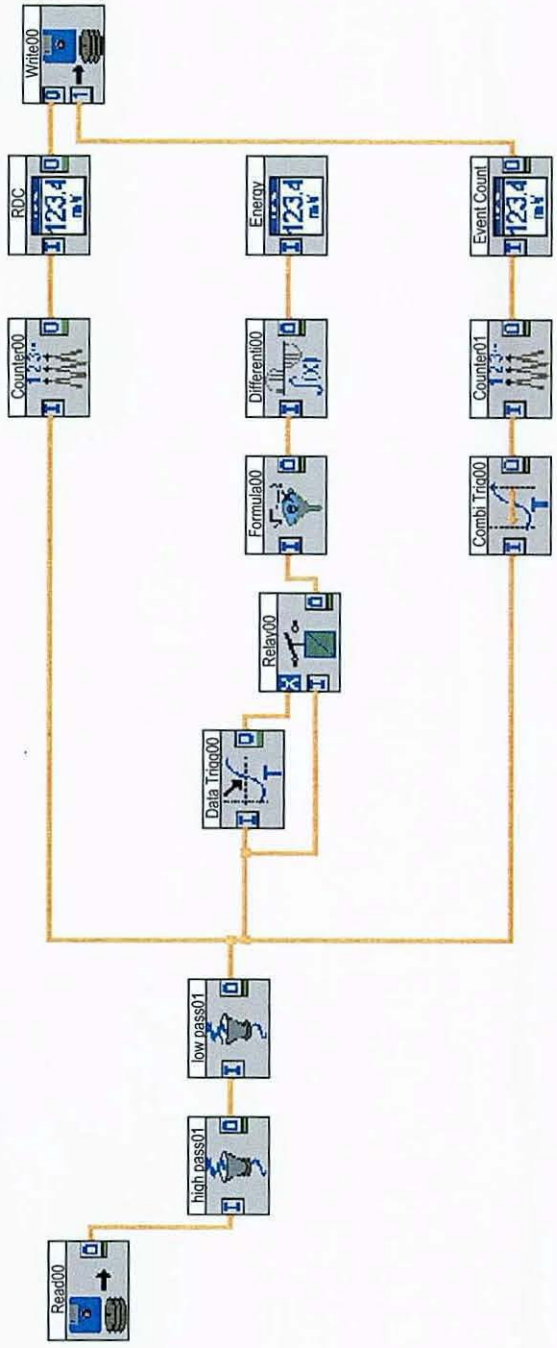

Figure 6.2 DASYLab worksheet for exp178

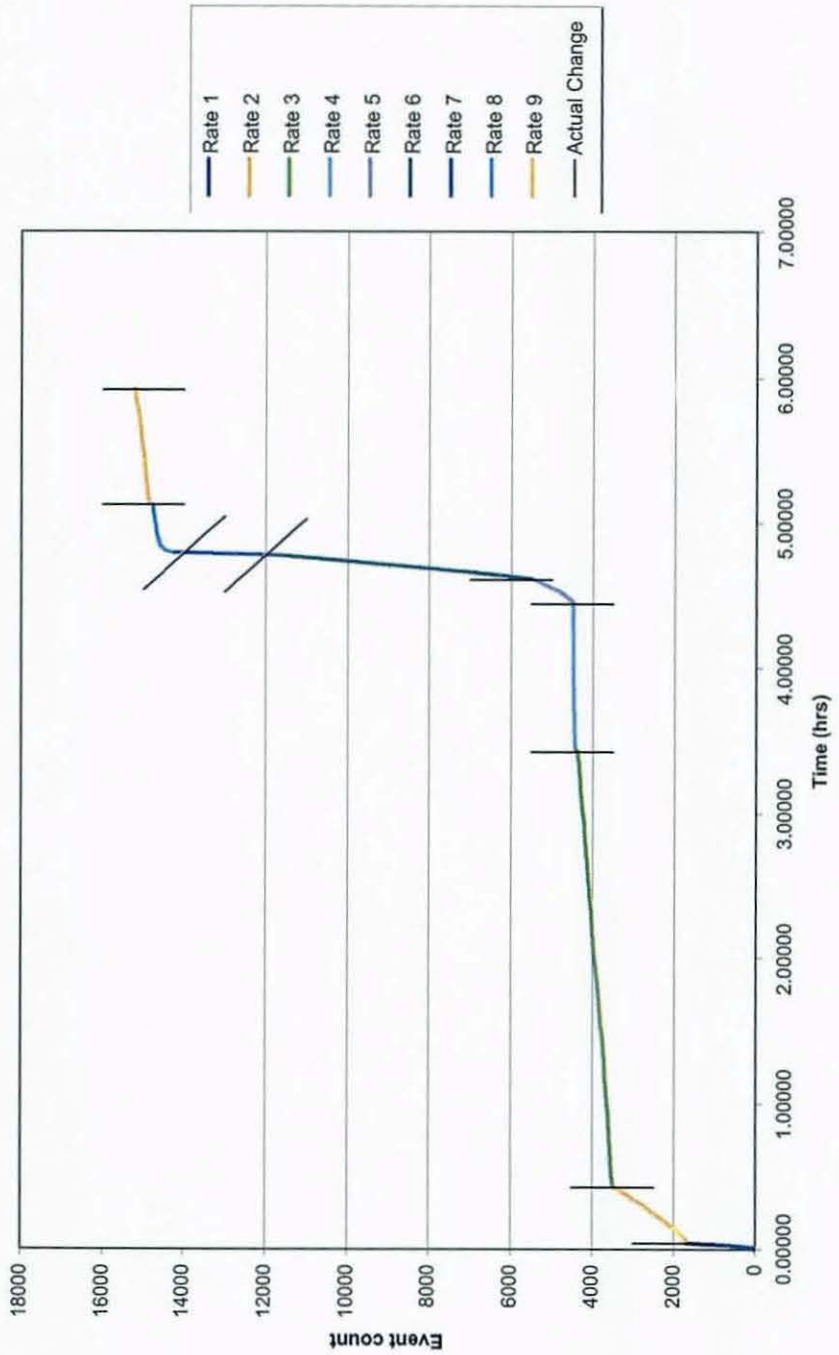

Figure 6.3 Event count versus time (exp178)

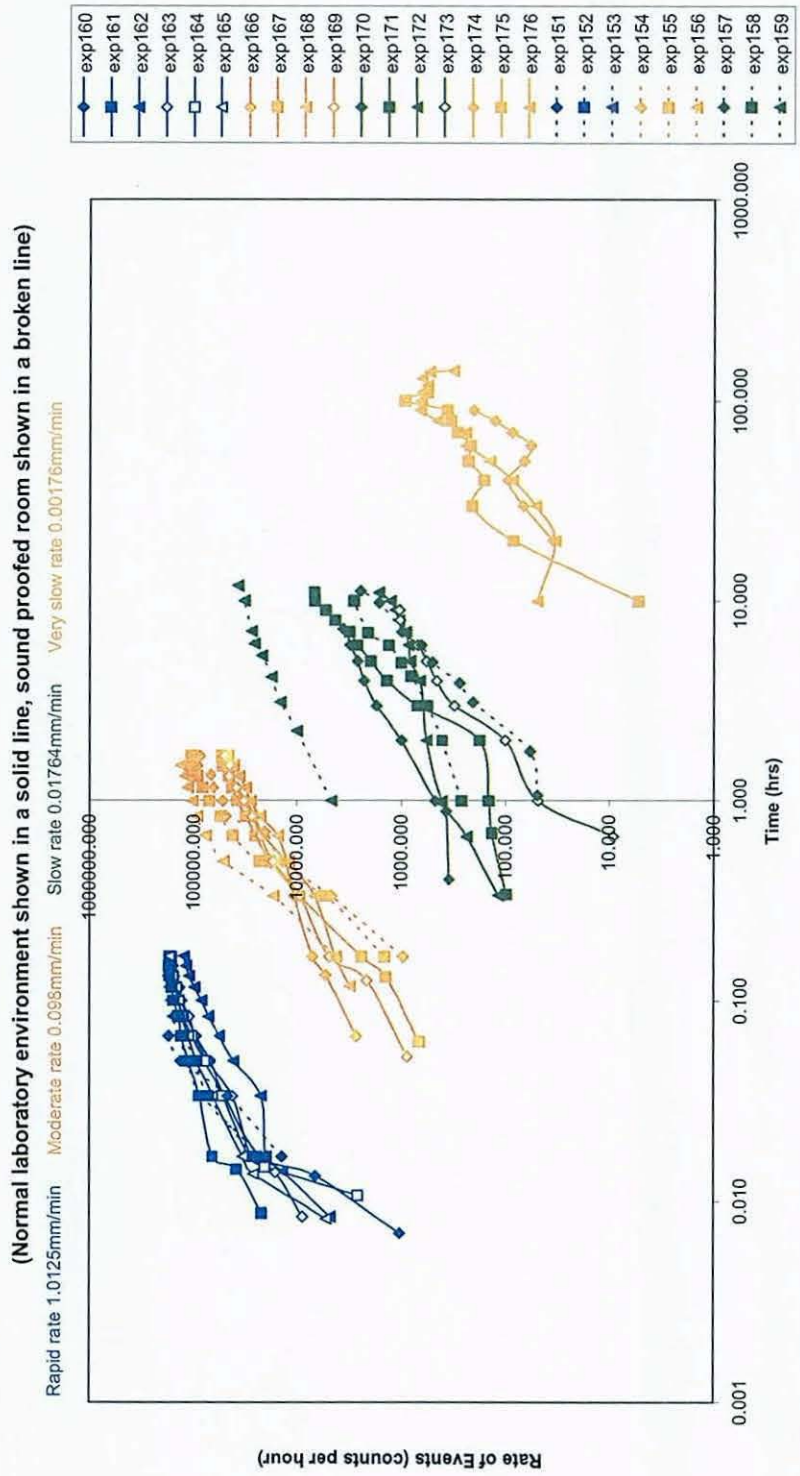

Figure 6.4 Rate of AE (events per hour) verses time for compression test

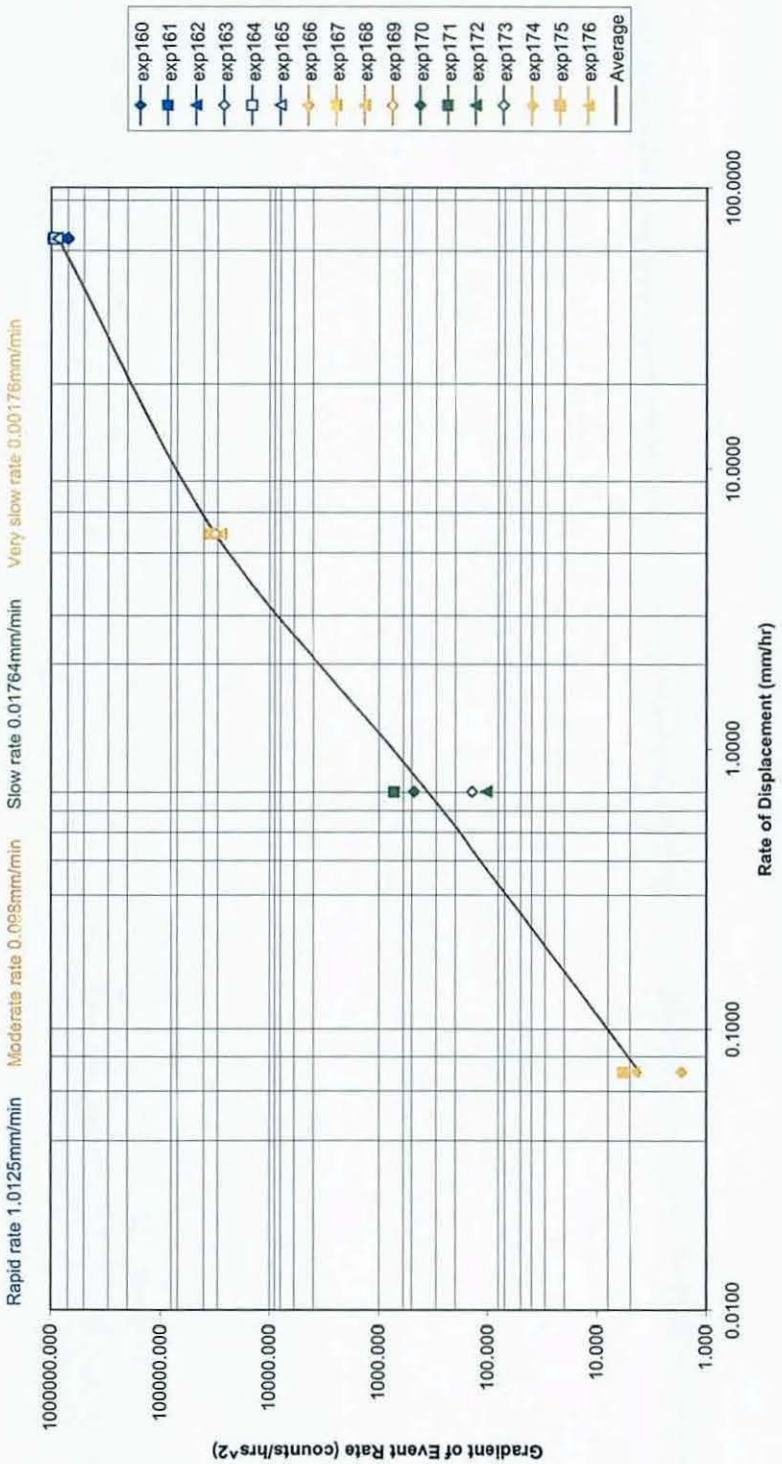

Figure 6.5 Relationship between gradient of event rate and rate of displacement for compression tests

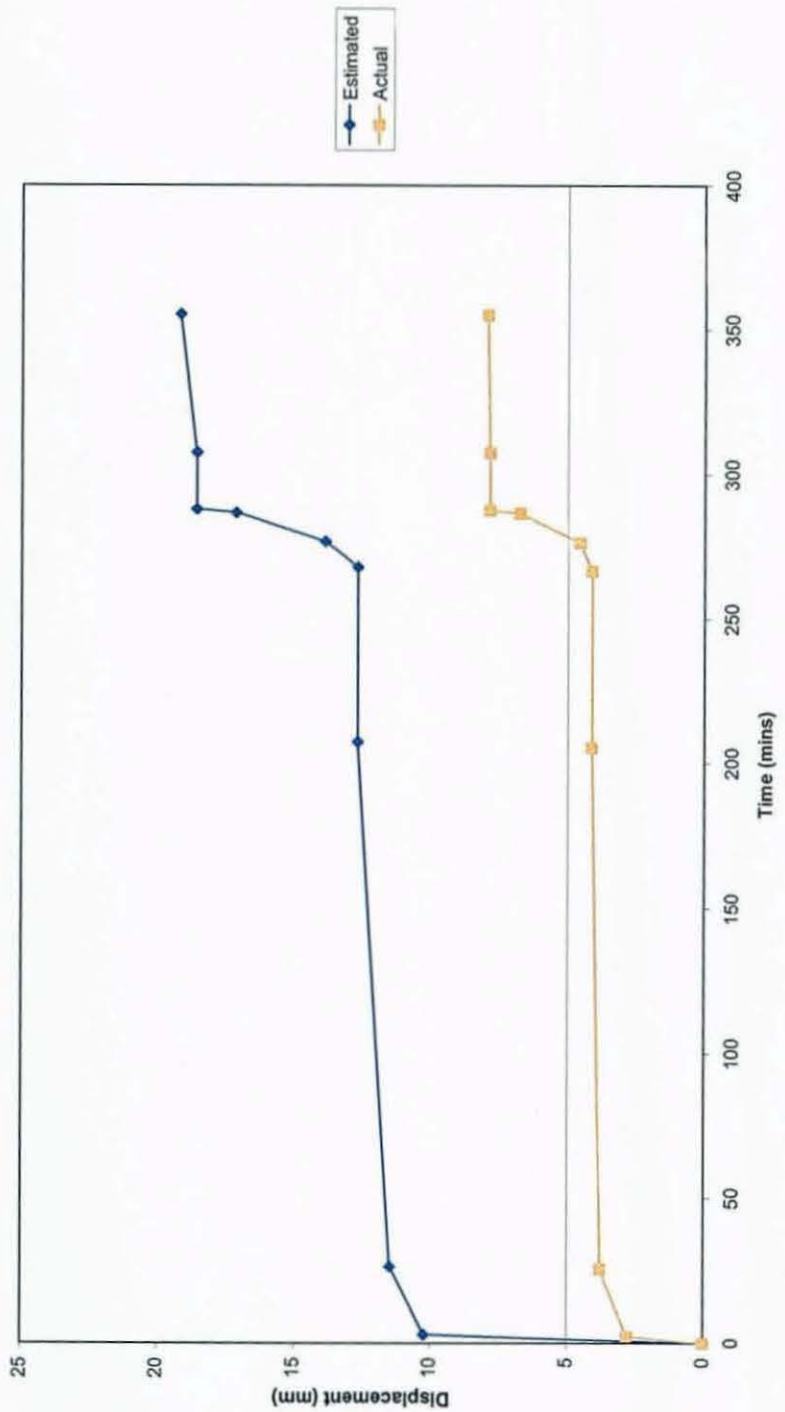

Figure 6.6 Displacement/time graph showing the estimated displacement and the actual displacement of the backfill.

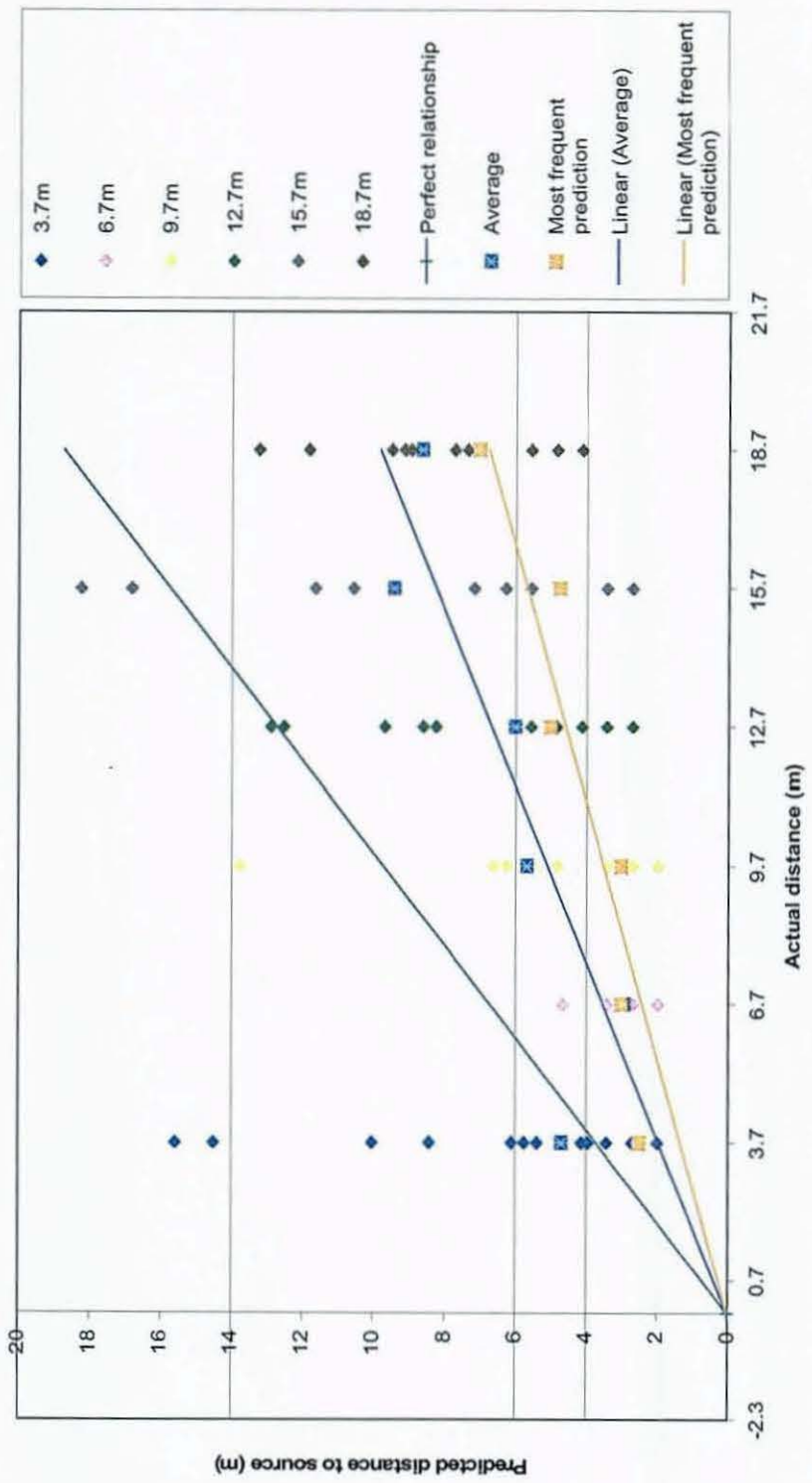

Figure 6.7 Relationship between the predicted distance to source, and the actual distance to source using automatic source location

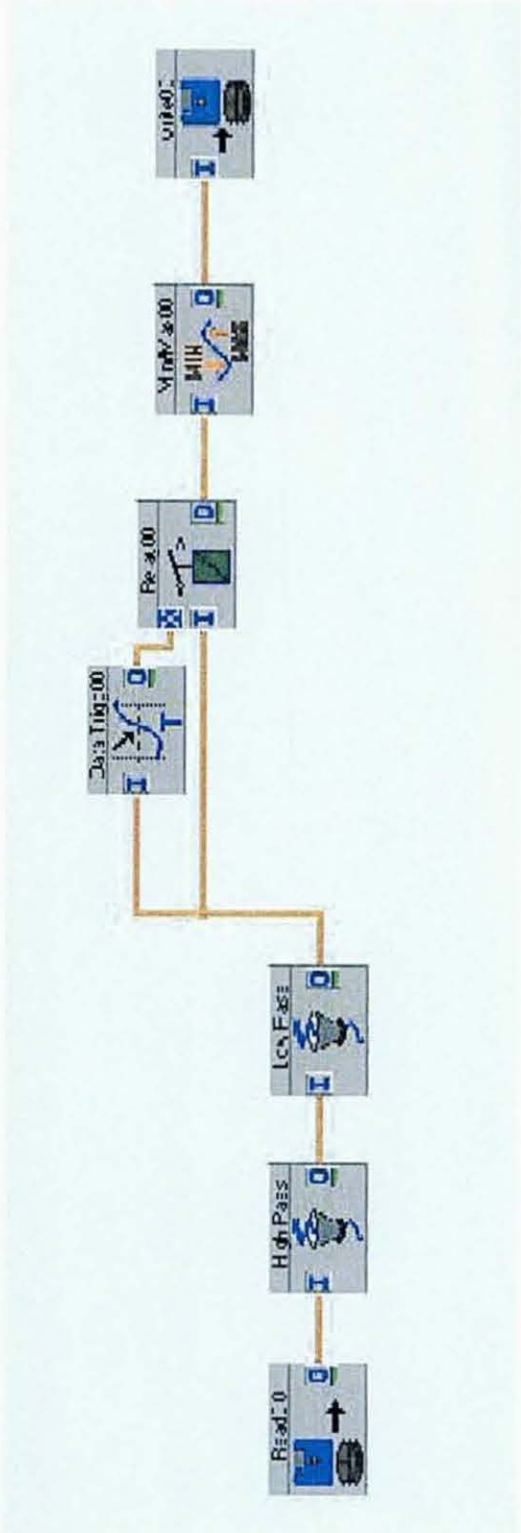

Figure 6.8 DASYLab worksheet for automatic source location calculations

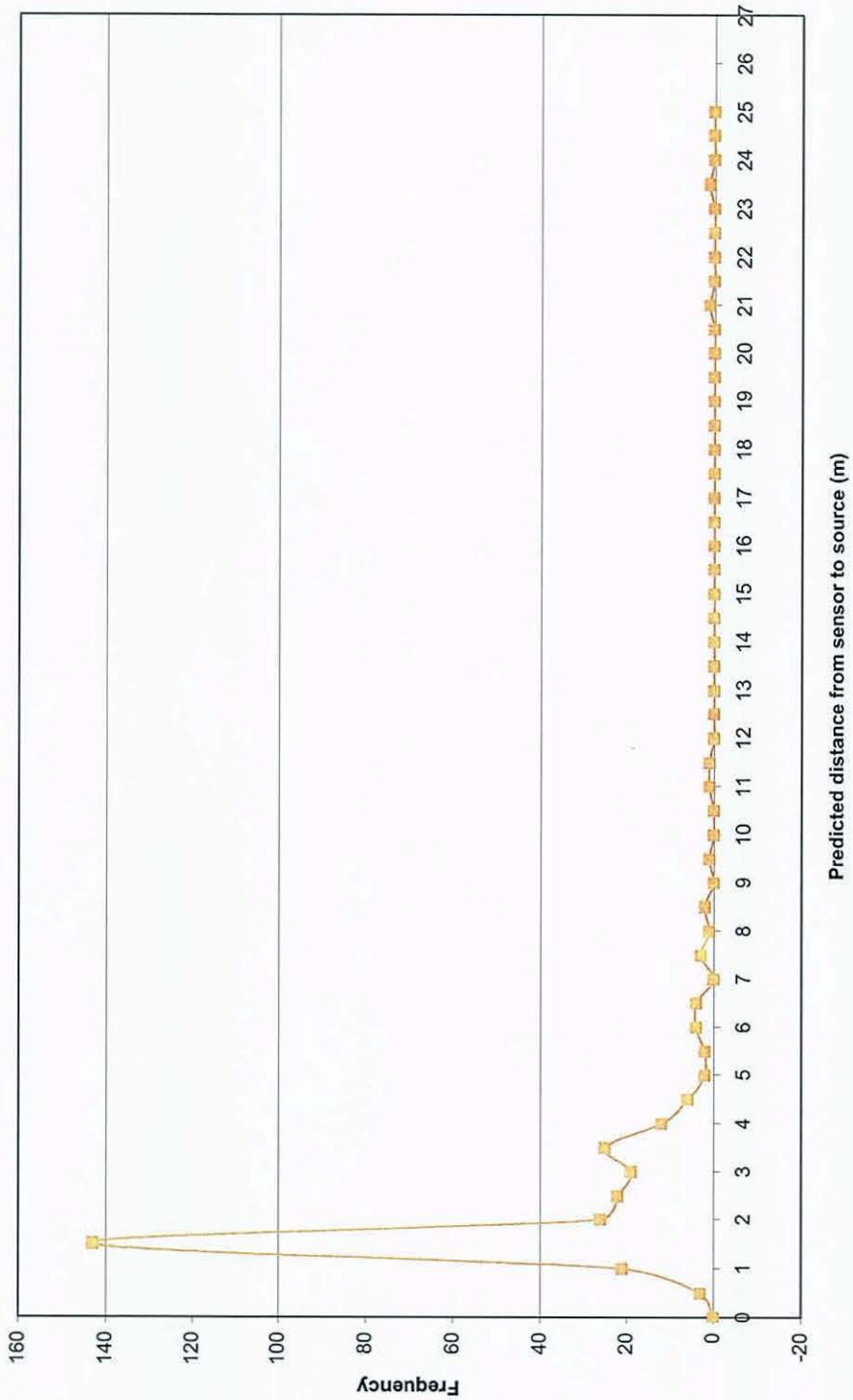

Figure 6.9 Histogram showing the frequency of estimated distance to source calculations using the automatic approach.

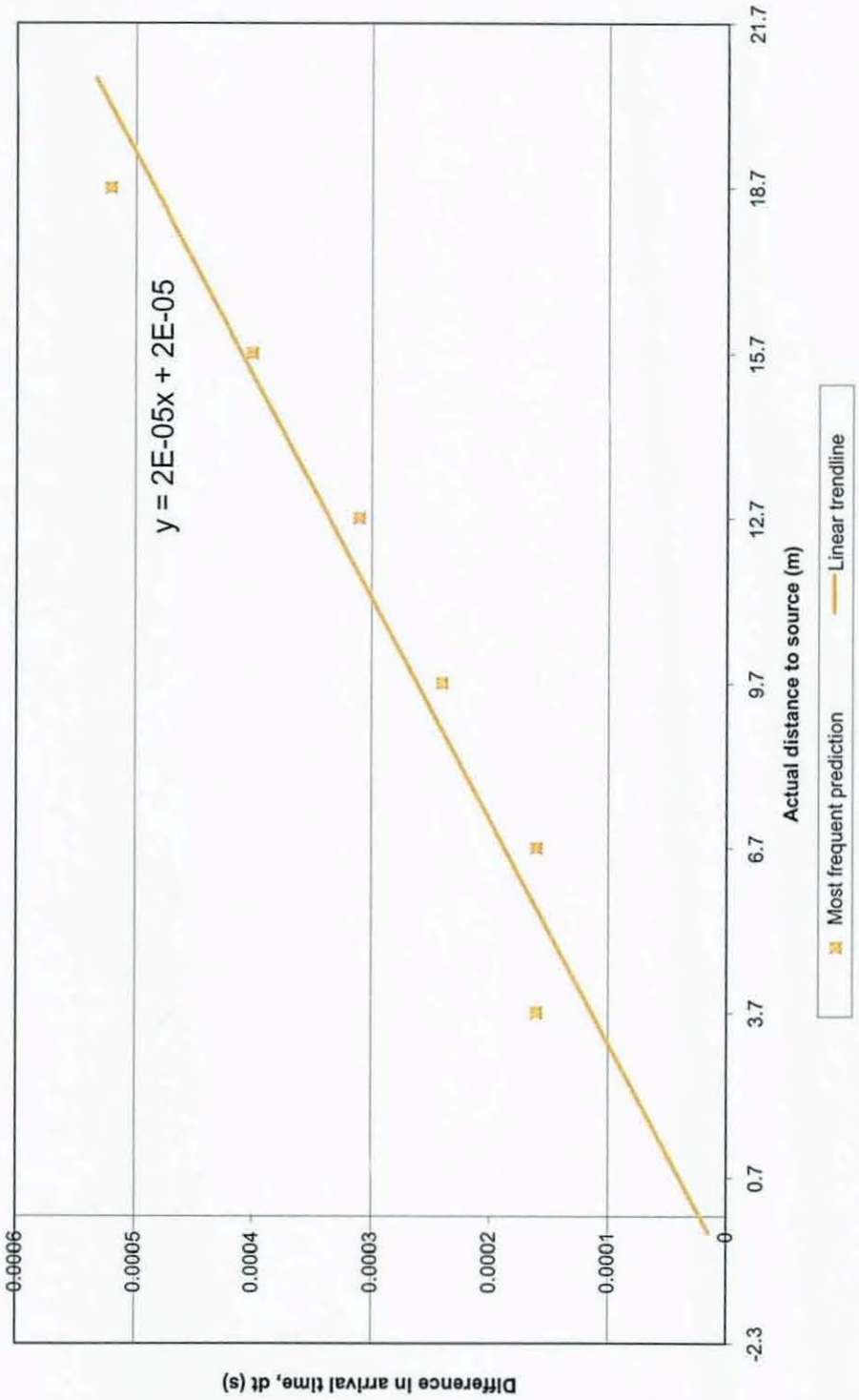

Figure 6.10 Linear relationships between the difference in arrival times of Lamb wave modes and the actual distance of AE propagation

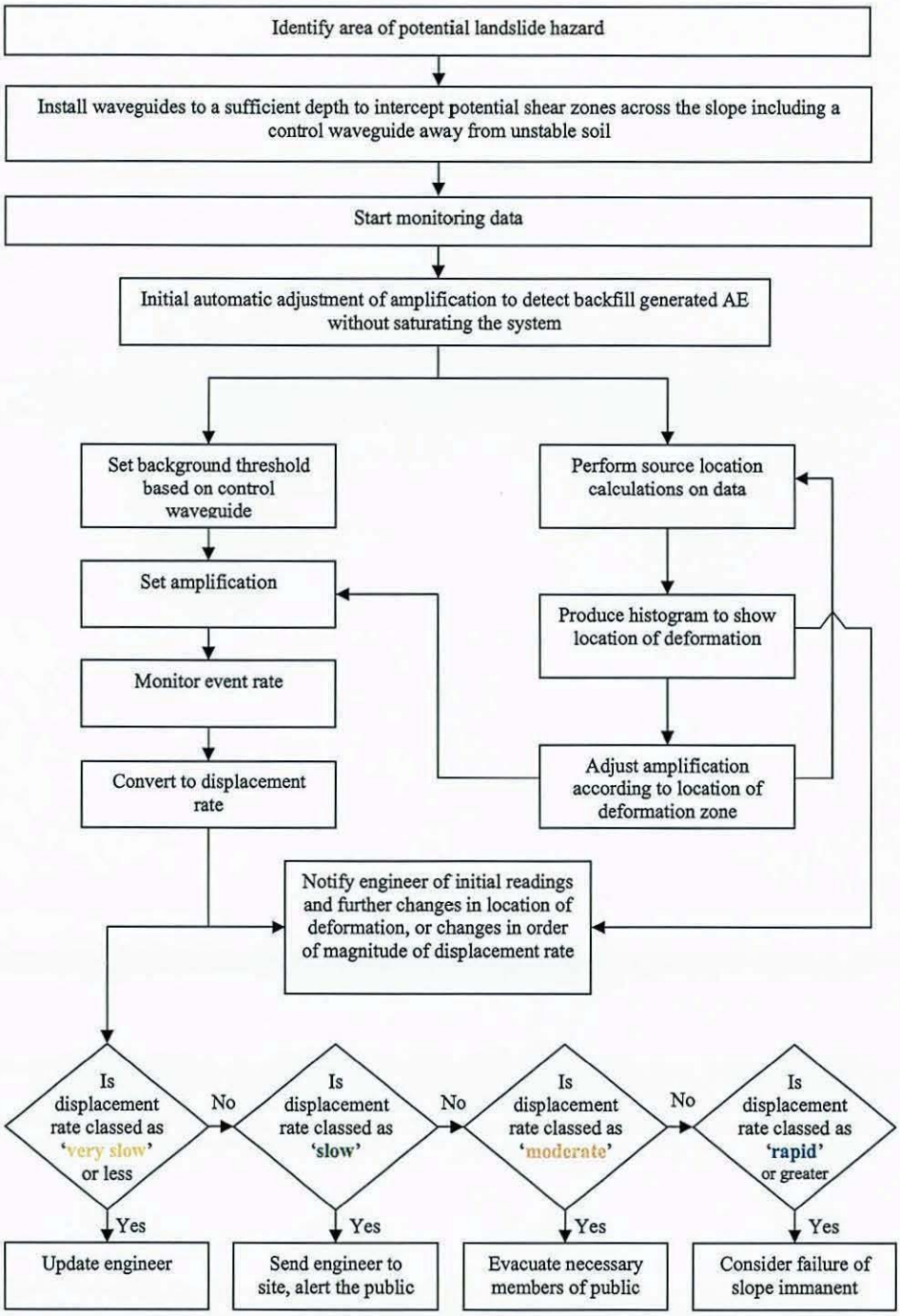

Figure 6.11 Flow chart of proposed field monitoring procedures

Chapter 7

Conclusions

7.1 Quantifying acoustic emission

The aim of this investigation was to quantify AE such that it could be used alongside existing standards of classifying landslide displacement rates within orders of magnitude. Compression tests on a steel waveguide with a river gravel surround have conclusively shown that it is possible to differentiate displacement rates by an order of magnitude when monitoring the incoming rate of AE events. The results obtained using relatively simple compression apparatus was validated by data from large scale tests that were designed to deform the waveguide backfill system in a more realistic testing environment.

A relationship between the gradient of the event rate against time and the displacement rate was produced. A blind test demonstrated that recorded backfill generated AE data in response to unknown displacement rates could be quantified, and a calculated displacement rate, based on the event rate, can be obtained with an accuracy of one order of magnitude.

By monitoring the event rate, the system was sensitive enough to correctly identify when changes within the rate of displacement took place, and were also able to correctly identify the new rate of displacement (as described above). A zero rate of displacement was recognised by a negative gradient of the event rate against time, thus indicating the systems capability to monitor the effectiveness of remediation works.

7.2 Locating the zone of deformation

Source location calculations were necessary in order to gain information as to the nature of the deformation mechanism, and to correctly set the levels of amplification to ensure that all backfill generated events were monitored. The application of Lamb wave theory was used, and the first two Lamb wave modes were used successfully on AE generated by pencil lead breaks over distances up to 23m The difference in the arrival times was measured, and along with the known velocities of each mode (for the specific waveguide in question), manual and automatic source location techniques were used to calculate the distance from source to sensor to within 1m of the actual distance.

Backfill generated AE was tested over distances of up to 19 metres. Lamb wave modes were again used to calculate the distance of propagation of AE. Although the actual modes were unknown due to the complexity of event waveforms, a linear relationship between the actual distance and the calculated distance to source was produced.

This relationship was specific to the waveguide used, but it demonstrated that individual waveguides could be easily calibrated for source location by plotting the difference in arrival time of the Lamb wave modes and the distance over which they had travelled. The resulting calibration can be represented by a linear equation.

The design of an automatic real time source location monitoring system was produced. This was shown to enable the analysis of hundreds of events Although many spurious events were analysed giving incorrectly calculated distances, the credibility of the technique increased with every added event analysed until a histogram of distance to source clearly identified a calculated distance to source. The technique was, however, never run in real time due to additional software being used to analyse the data. However, the capability of such a real time system exists.

7.3 Producing an early warning system

Consideration was given to a future field monitoring system based on the quantification of AE and the developed automatic source location technique. A proposed approach to field monitoring was explained. The end goal was the production of a monitoring system able to provide an early warning of slope instability, with the potential to predict slope failure.

In chapter 1 of this investigation, the current use of AE for slope monitoring was summarised within a qualitative guide produced by Koerner *et al.* (1981). That same guide can now, as a result of this investigation, be modified to produce a quantified method for assessing soil slope instability:

- Calculated displacement rate classified as '**Very Slow**' **(0.001mm/min)** or less than – Slope is probably not deforming and is therefore stable.
- Calculated displacement rate classified as **'Slow' (0.01mm/min)** – Deforming slightly but marginally stable, continued monitoring is necessary.
- Calculated displacement rate classified as '**Moderate**' **(0.1mm/min)** – Substantial deformations considered unstable, immediate remedial and public safety measures required.
- Calculated displacement rate classified as **'Rapid' (1mm/min)** or greater than – Slope is undergoing large deformations and is likely to be in a state of failure. Urgent need to implement public safety and remedial measures.

The development of a system to provide a quantified early warning of soil slope instability has been achieved. However, the fourth objective laid out in the introduction, 'To produce a quantitative approach for the prediction of slope instability' (section 1.2) has not been achieved. This investigation has not been able to provided a calculated time to failure based on the information provided by the active waveguide monitoring system (i.e. rate of deformation and location of deformation).

7.4 Recommendations for further work

The end goal of this research in soil slopes was the development of instrumentation that could provide a reliable warning of slope instability. This investigation has succeeded in making significant steps towards that goal within the confines of the laboratory. The conclusions herein provide a basis for recommending future work to achieve this aim within the field. The following areas have been highlighted for further work;

- Ongoing development of the automatic source location technique to produce a fully integrated self-reliant, real time monitoring system, integrating both the source location and the quantification of AE.
- To conduct field trials into the use of the procedures discussed within this report in unstable soil slopes. Including the development of installation and monitoring protocols.
- Research linking the displacement rate, magnitude and mechanism of movement provided by the measured AE, with in-situ soil properties to achieve a calculated time to slope failure based on the measured AE.
- The subsequent development of recommended emergency action to be taken when a pre-determined threshold of AE activity has been reached.

It is the opinion of the author that it is possible to use the instrumentation and analysis approach as outlined in this investigation to provide the relevant information required to produce an early warning of slope instability.

Reference List

ASTM (2001) Standard guide for determining the reproducibility of acoustic emission sensor response. *American National Standard*, Designation: E 976 – 00. P 409 – 417.

ASTM (2002) Standard guide for mounting piezoelectric acoustic emission sensors. *American National Standard*, Designation: E 650 – 97. P 277 – 279.

Alleyne, D. N. & Cawley, P. (1995) The long range detection of corrosion in pipes using lamb waves. *Review of Progress in Quantitative Nondestructive Evaluation*, Vol. 14, P. 2073 – 2080.

Alleyne, D. N. & Cawley, P. (1997) Long range propagation of lamb waves in chemical plant pipework. *American Society of Nondestructive Testing, Materials Evaluation*, Vol. 55, P. 504 – 508.

Atkinson, J. (1998) Basic Mechanics of Soils [online]. Available from: http://fbe.uwe.ac.uk/public/geocal/SoilMech/basic/soilbasi.htm [Accessed on August 2004].

British Standards Institution (1990) *Methods of test for soils for civil engineering purposes*. BS 1377 Parts 2, 7 & 9.

Barla, G. (2003) Lessons learned related to risk mitigation. *ICFSM 2003, Fast slope movements prediction and prevention for risk mitigation*, Naples, Vol. 1.

Beard, F. D. (1961) *Predicting slides in cut slopes*, Western Construction, No. 72.

Chichibu, K. Jo, M. Nakamura, T. Goto and M. Kamata (1989) Acoustic emission characteristics of unstable slopes. *Journal of Acoustic Emission*, Vol. 8, No. 4, P.107-112

Dixon, N. Kavanagh, J. & Hill, R (Oct. 1996) Monitoring landslide activity and hazard by acoustic emission. *Journal of the Geological Society of China*, Vol 39, No. 4, P.437-464.

Dixon, N. Spriggs, M. Hill, R. and Kousteni, A. (2003) Acoustic emission monitoring to detect slope instability. *Proceedings of the 4th British-Sino-Italian Congress*, Padua, Italy, pp. 163-168.

Forrester, K. (1987) The Carisbrooke Avenue landslide. *Proceedings of an Extension Course on Soil Slope Stability and Stabilisation*, P.337-346.

Garga, V. K. & Chichibu, A. (1990) A study of AE parameters and shear strength of sand. *Progress in Acoustic Emission V*, The Japanese Society for NDI, P.129 – 136.

Hardy Jnr, H. R. (1989) A review of international research relative to the geotechnical field application of acoustic emission/microseismic techniques. *Journal of Acoustic Emission*, Vol. 8, No. 4, P65-91.

Hardy Jnr, H. R. (1992) Laboratory studies relative to the development of mechanical waveguides for AE monitoring of geologic structures. *Italian Journal of Non-destructive Testing and Diagnostics*, Vol. XIII, No. 2, P32-38.

Highfield, R. (2004) Britain can expect to suffer more landslides, say experts. *The Daily Telegraph*, Sunday 8th August 2004.

J. Kavanagh (1997) *The use of acoustic emission to monitor the deformation of a soil body*. PhD. Thesis, The Nottingham Trent University.

Koerner, R. M. Lord Jnr, A. E. & McCabe, W. M. (1975) Acoustic Emission Studies of Soils Masses in the Laboratory and Field. *Proc. of the 1st Conference on Acoustic Emission/Microseismic Activity in Geological Structures and Materials,* P.243-256.

Koerner, R. M. McCabe, W. M. & Lord, A. E. (1981) Acoustic emission behaviour and monitoring of soils. *Proceedings of the First Synopsis on Acoustic Emission in Soils,* P93-141.

Koerner, R. M. Lord Jnr, A. E. & Deutsch, W. L. (1984a) Determination of pre-stresses in granular soils using AE. *Journal of Geotechnical Engineering Division, Proc. of the ASCE*, Vol. 110, No. 3, P.346-358.

Koerner, R. M. Lord Jnr, A. E. & Deutsch, W. L. (1984b) Determination of pre-stresses in cohesive soils using AE. *Journal of Geotechnical Engineering Division, Proc. of the ASCE,* Vol. 110, No. 11, P.1537-1548.

Kousteni, A. (2002) *Investigation of Acoustic Emission Waveguide Systems for Detecting Slope Instability.* PhD Thesis, The Nottingham Trent University.

Labuz, J. F. Dai, S. T. & Shah, K. R. (1996) Identifying failure through locations of acoustic emission. *Transport Research Record*, No. 1526, P.104-111.

Lord jnr, A. E. & Koerner, R. M. (1974) Acoustic emission response to dry soils. *Journal of Testing and Evaluation*, Vol. 2, No. 3, P.159-162.

Lord Jnr, A. E. Koerner, R. M. & Curran, J. W. (1977) Fundamental studies of acoustic emission in soils. *Proceedings of the 1st Conference on Acoustic Emission/Microseismic Activity in Geological Structures and Materials*, P.135-148.

Lord, E. Fisk, C. L. & Koerner, R. M. (1982) Utilisation of steel rods as AE waveguides. *Journal of the Geotechnical Engineering Division, Proceedings of the ASCE*, Vol. 108 No. GT2 P.300-305.

Maji, A. K. Satpathi, D. & Kratochvil, T. (1997) Acoustic emission source location using lamb wave modes. *Journal of Engineering Mechanics*, Vol. 123, No. 2, P.154-161.

McCauley, M. L. (1975) Monitoring slope stability with acoustic emission. *Proceedings of the 1st Conference of Acoustic Emission/Microseismic Activity in Geologic Structures and Materials*, P.257-269.

Mitchell, R. J. & Romeril, P. M. (1983) Acoustic emission distress in sensitive clay. *Canadian Geotechnical Journal*, Vol. 21, P.176-180.

Morgenstern, N. (2003) Risk Mitigation against fast slope movements. *ICFSM 2003, Fast Slope Movements Prediction and Prevention for Risk Mitigation*, Naples, Vol. 1.

Mouroux, P. (2003) Risk assessment and prevention for landslides and rockfalls at La Clapière slopes. *ICFSM 2003, Fast Slope Movements Prediction and Prevention for Risk Mitigation*, Naples, Vol. 1.

Naemura, S. Tanaka, M. Nishikawa, S. Nakamura, M. Jo, K. & Kishishita, T. (1990a) Acoustic emission of large-scale embankment experiment to evaluate collapse location. *Progress in Acoustic Emission V, the Japanese society for NDI*, P145 – 152.

Naemura, S. Tanaka, M. Nishikawa, S. Nakamura, M. Jo, K. & Kishishita, T. (1990b) Acoustic emission of penetration experiments to judge soil condition. *The International Joint Meeting, 1st Workshop on Acoustic Emission in Civil Engineering and 2nd Workshop on Acoustic Emission and Rock Fracture Mechanics*, Kumamoto, Japan, October, S55-S58.

Nakajima, M. Negishi, M. Ujihira & Tanabe, T. (1991) Application of the acoustic emission monitoring rod to landslide measurement. *Fifth Conference on Acoustic Emission/Microseismic Activity in Geologic Structures and Materials*, P1-15.

Pollock, A. (1989) Acoustic Emission Inspection. *Metals Handbook*, Ninth edition, Volume 17, pp 278-294, ASM International.

Public Works Research Institute, Japan (July 1998) Field experimentation on the Shirasu slope collapse. *PWRI Newsletter,* No. 73.

Public Works Research Institute, Japan (July 2000) Joint study on AE monitoring system for slope failure. *PWRI Newsletter,* No. 81.

Rouse, C. Styles, P. & Wilson, S. A. (1991) Acoustic emission from two landslip areas in south Wales. *Z. Geomorph. N. F. Suppl.* Bd. 83, P135 –154.

Shiotani, T. & Ohtsu, M. (1999) Prediction of slope failure based on AE activity. *Acoustic Emission Standards and Technology update,* P157-172

Styles, P. Rouse, C. & Wilson, S. A. (1998) Microseismic monitoring of landslip movement in south Wales. *Welsh Office Research Contract Report*: WEP/100/154/2, 120 pages.

Tanimoto, K. & Noda, T. (1977) A study of acoustic emission from sandy soils. *Proceedings of 9th International Conference on Soil Mechanics and Foundation Engineering*, Vol. 1, 315 – 318.

Tanimoto, K. Nishi, M. & Noda, T. (1978) A study of shear deformation process of sandy soils by the observation of acoustic emission response. *Proceedings of 2nd Conference on Microzonation*, Vol 2, P971 – 982.

Transport Research Board (1978) *Landslides, Analysis and Control.* National Academy of Sciences.

Versace, P. (2003) Flow slide mitigation in the Sarno area after the catastrophic events of May, 1998. *ICFSM 2003, Fast Slope Movements Prediction and Prevention for Risk Mitigation*, Naples, Vol. 1.

Wood, B. R. A. Flynn, T. G. Harris, R. W. & Noyes, L. M. (1990) Comparison between various waveguides in three long term acoustic emission monitoring projects. *Progress in Acoustic Emission*, Vol. 5, P501 – 506.

Yuda, S. Hashimoto, Y. Takahashi, K. & Kumagai, M. et al. (1984) Prediction of slope failure by acoustic emission technique. *Proceedings of 7th International Acoustic Emission Symposium*, P660 – 667.

Publications

Dixon, N., Spriggs, M., Hill, R. and Kousteni, A., "Acoustic Emissions Techniques for Assessing Landslides Hazard" , *International Conference on Fast Slope Movements - Prediction and Prevention for Risk Mitigation* , Sorrento, Italy, 2003, pp. 163-168 .

Dixon, N., Spriggs, M.P., Hill, R. and Kousteni, A., "Acoustic Emission Monitoring to Detect Slope Instability" , *Proceedings of the 4th British-Sino-Italian Congress* , Padua, Italy, June 2003, pp. 163-168 .

APPENDIX A

BS 1377 : Part 2 : 1990

Liquid limit and plastic limit (Cone penetrometer method) — Form 2.C

Location: TEST FOR MATT SPRIGGS.					Job ref.	MS1
					Borehole / Pit no.	NA
Soil description: RED BRICK CLAY					Sample no.	BAG1
					Depth	NA
					Date	
Test method	BS 1377 : Part 2 : 1990 : 4.3/4.4					
PLASTIC LIMIT	Test no.	1	2	3	4	Average
Container no.		1A	2A			
Mass of wet soil + container	g	11.91	12.19			
Mass of dry soil + container	g	10.91	11.12			
Mass of container	g	5.54	5.46			
Mass of moisture	g	1.00	1.07			
Mass of dry soil	g	5.37	5.66			
Moisture content	%	18.6%	18.9%			18.8%

LIQUID LIMIT	Test no.	1	2	3	4
Initial dial gauge reading	mm	0.00	0.00	0.00	0.00
Final dial gauge reading	mm	14.80	16.02	20.51	23.14
Penetration	mm	14.80	16.02	20.51	23.14
Container no.		1B	2B	3B	4B
Mass of wet soil + container	g	60.46	52.42	49.99	46.42
Mass of dry soil + container	g	48.65	42.19	39.52	36.63
Mass of container	g	5.05	5.07	4.68	5.79
Mass of moisture	g	11.81	10.23	10.47	9.79
Mass of dry soil	g	43.60	37.12	34.84	30.84
Moisture content	%	27.1%	27.6%	30.1%	31.7%

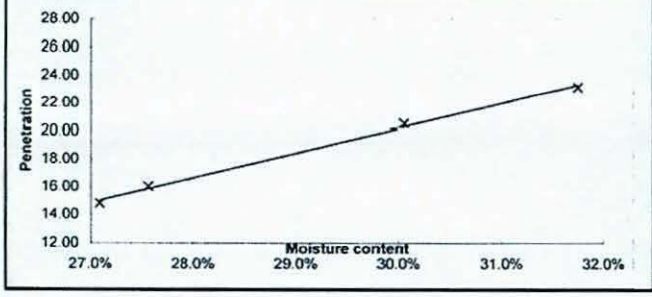

Sample preparation	
~~as received~~	
~~washed on 425µm sieve~~	
~~air dried at~~	
oven dried at	105 C
~~not known~~	
Proportion retained on 425µm sieve	
Liquid limit	29.9%
Plastic limit	18.8%
Plasticity index	11.1%

Operator	Checked	Approved

Table A4.3 Plasticity index and classification reports for Mercia Mudstone

BS 1377 : Part 2 : 1990

Particle Size Distribution (Sieving) — Form 2.M

Location				Job ref.	ms
Matt Spriggs Brick Clay				Borehole Pit no.	
Soil description				Sample No.	
Red Clay				Depth	
				Date	########
Test method	BS 1377:Part2:1990:9.2/9.3/9.4*				
Intial dry mass	m1		200 g		
BS test sieve	Mass Retained g		Percentage retained (m/m1)100	Cumlative percentage passing	
	Actual	Corrected m			
75mm	0	0	0.00	0.00	
63mm	0	0	0.00	0.00	
50mm	0	0	0.00	0.00	
37.5mm	0	0	0.00	0.00	
28mm	0	0	0.00	0.00	
20mm	0	0	0.00	0.00	
Passing 20 mm m2	200.00				
total (check with m1)	200.00				
riffled m3	200.00				
riffled and washed m4	200.00				
Correction factor (m2/m3)	1				
14mm	0	0	0.00	0.00	
10mm	0	0	0.00	0.00	
6.3mm	0	0	0.00	0.00	
Passing 6.3mm m5	200.00				
total (check with m4)	200.00				
riffled m6	200.00				
Correction factor (m2/m3)*(m5/m6)	1				
5mm	0.22	0.22	0.11	0.11	
3.35mm	0	0	0.00	0.11	
2mm	0	0	0.00	0.11	
1.18mm	0	0	0.00	0.11	
600um	0	0	0.00	0.11	
425um	0.1	0.1	0.05	0.16	
300um	0.11	0.11	0.06	0.22	
212um	0.03	0.03	0.02	0.23	
150um	5.59	5.59	2.80	3.03	
63um	8.04	8.04	4.02	7.05	
Passing 63um mf or me	185.91	185.91	92.96	100.00	
Total (check with m6)	200				
* Delete as appropriate					
			Operator	Checked	Approved

Table A4.3 Plasticity index and classification reports for Mercia Mudstone cont…

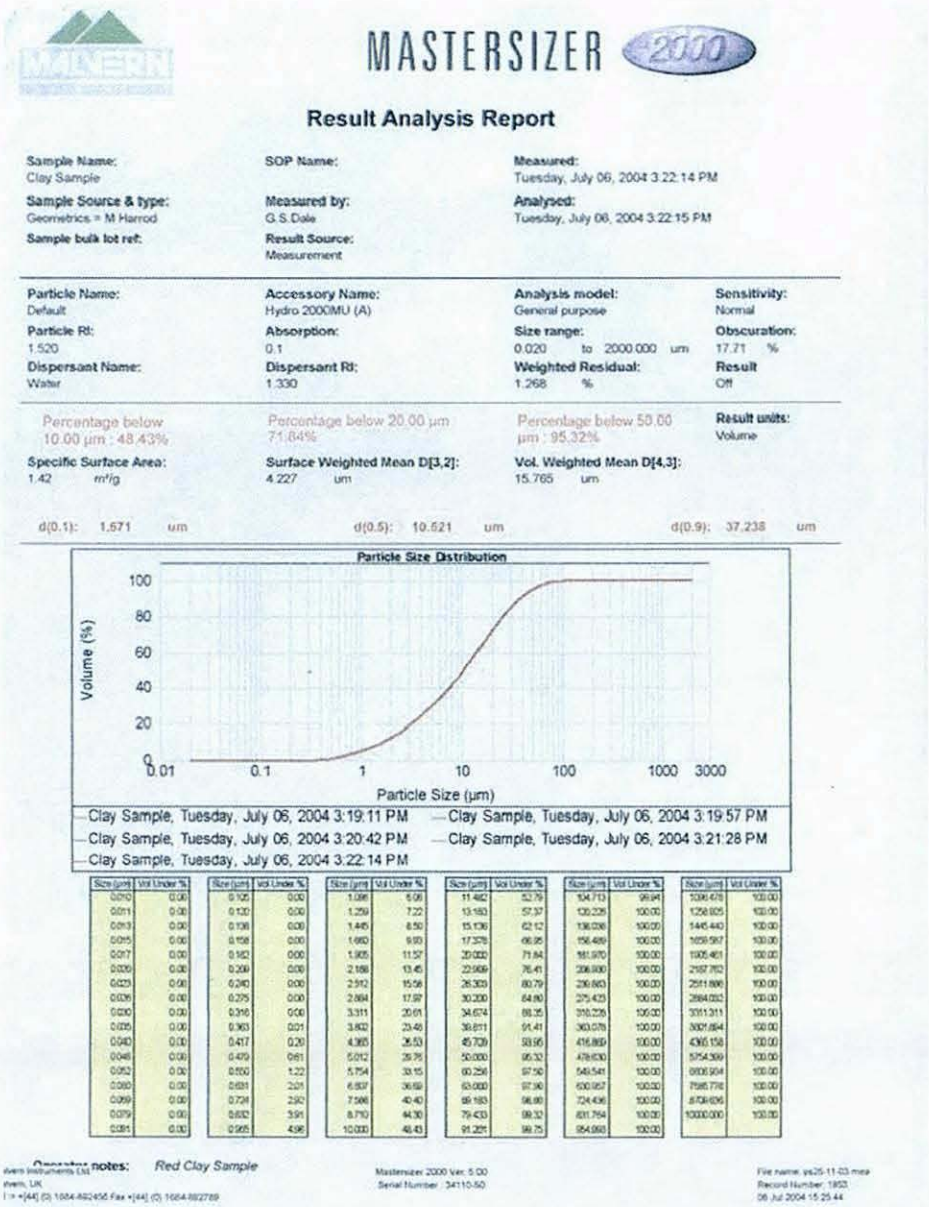

MASTERSIZER 2000

Result Analysis Report

Sample Name: Clay Sample	**SOP Name:**	**Measured:** Tuesday, July 06, 2004 3:22:14 PM	
Sample Source & type: Geometrics = M Harrod	**Measured by:** G.S.Dale	**Analysed:** Tuesday, July 06, 2004 3:22:15 PM	
Sample bulk lot ref:	**Result Source:** Measurement		
Particle Name: Default	**Accessory Name:** Hydro 2000MU (A)	**Analysis model:** General purpose	**Sensitivity:** Normal
Particle RI: 1.520	**Absorption:** 0.1	**Size range:** 0.020 to 2000.000 um	**Obscuration:** 17.71 %
Dispersant Name: Water	**Dispersant RI:** 1.330	**Weighted Residual:** 1.268 %	**Result** Off
Percentage below 10.00 µm : 48.43%	Percentage below 20.00 µm 71.84%	Percentage below 50.00 µm : 95.32%	**Result units:** Volume
Specific Surface Area: 1.42 m²/g	**Surface Weighted Mean D[3,2]:** 4.227 um	**Vol. Weighted Mean D[4,3]:** 15.765 um	

d(0.1): 1.571 um d(0.5): 10.521 um d(0.9): 37.238 um

Operator notes: *Red Clay Sample*

Table A4.3 Plasticity index and classification reports for Mercia Mudstone cont…

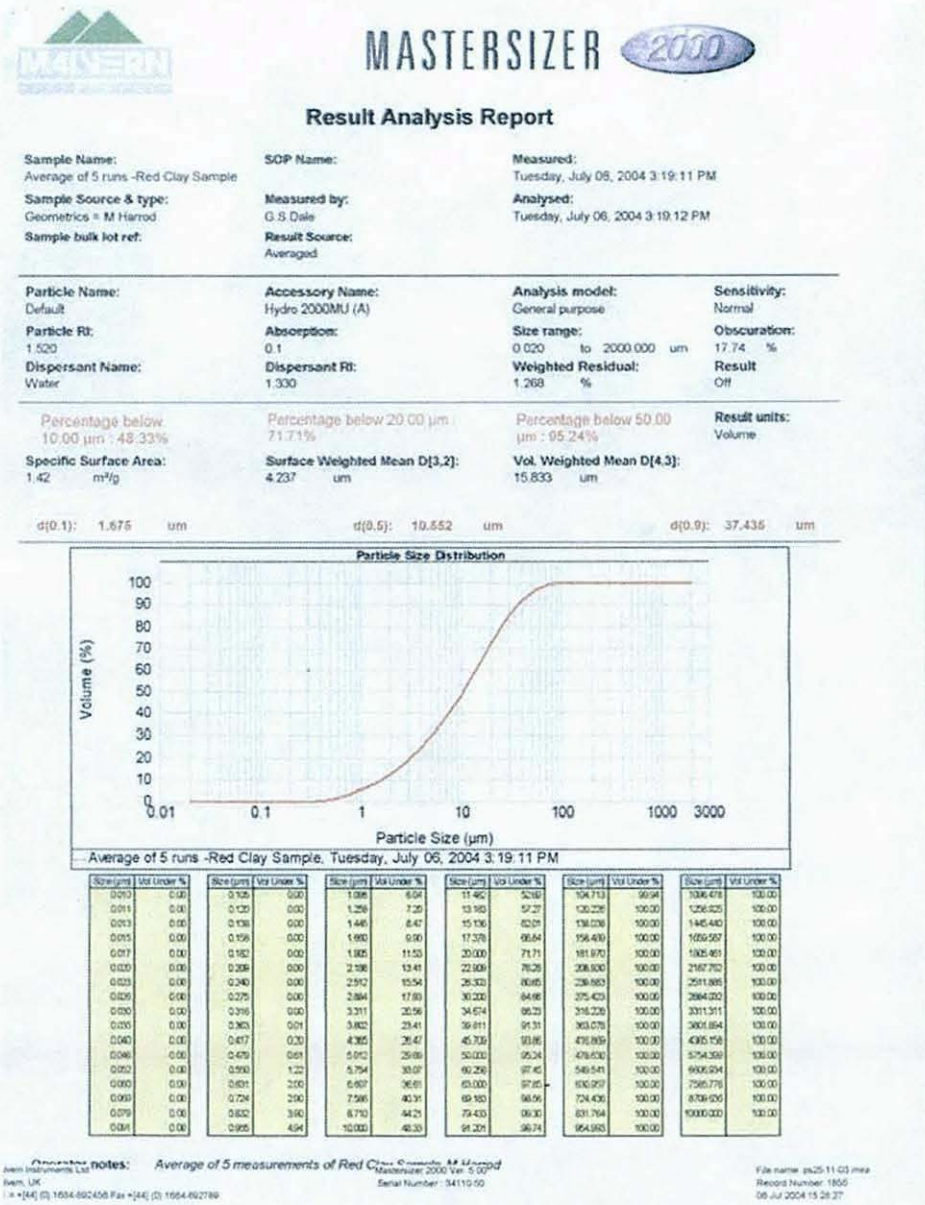

Table A4.3 Plasticity index and classification reports for Mercia Mudstone cont…

River gravel		Rapid 1 1025mm/min		River gravel		Rapid 1 1025mm/min		River gravel		Rapid 1 1025mm/min	
exp151				exp152				exp153			
Time (hrs)	Displacement (mm)	Load (kN)	Energy	Time (hrs)	Displacement (mm)	Load (kN)	Energy	Time (hrs)	Displacement (mm)	Load (kN)	Energy
0 000	0.000	0.000	0.000	0 000	0.000	0 000	0 000	0 000	0 000	0 000	0 000
0 017	1 103	0.045	2.130	0 017	1 103	0 117	9 930	0 017	1 103	0 107	10.400
0 033	2.205	0 100	6 760	0 033	2.205	0 283	53 000	0 033	2.205	0.255	65.270
0 050	3.308	0.242	19 780	0.050	3.308	0 436	114 000	0 050	3.308	0.404	163 000
0 067	4.410	0.390	36.550	0 067	4.410	0 648	218.000	0 067	4.410	0 583	314 000
0.079	5.200	0.518	43.250	0 083	5.513	0 890	353.000	0 083	5.513	0.811	518 000
				0 100	6.615	1 163	529 000	0 100	6 615	1 025	746 000
				0 117	7 718	1.484	740.000	0 117	7 718	1.297	1005.000
				0 133	8.820	1.832	975.000	0 133	8.820	1.594	1283.000
				0 150	9.923	2.174	1252.000				
exp151				exp152				exp153			
Time (hrs)	Displacement (mm)	RDC	Event	Time (hrs)	Displacement (mm)	RDC	Event	Time (hrs)	Displacement (mm)	RDC	Event
0 000	0 000	0	0	0 000	0 000	0	0	0 000	0.000	0	0
0 017	1 103	9134	226	0 017	1 103	9728	416	0.017	1 103	8950	347
0 033	2.205	45842	972	0 033	2.205	44880	1568	0.033	2.205	56120	1691
0 050	3.308	277561	3130	0 050	3.308	97998	3131	0.050	3.308	138285	3514
0 067	4.410	866459	5956	0 067	4.410	187538	5160	0.067	4.410	272714	5784
				0.083	5.513	304062	7390	0 083	5.513	466222	8338
				0 100	6 615	472712	9890	0 100	6 615	692177	11016
				0 117	7 718	674983	12520	0 117	7 718	955700	13763
				0 133	8.820	918133	15280	0 133	8.820	1269747	16609
				0 150	9 923	1212256	18083				
exp151				exp152				exp153			
Time (hrs)	Displacement (mm)	RDC Rate RDC per hr	Event Rate Event per hr	Time (hrs)	Displacement (mm)	RDC Rate RDC per hr	Event Rate Event per hr	Time (hrs)	Displacement (mm)	RDC Rate RDC per hr	Event Rate Event per hr
0 000	0.000	0	0 00	0 000	0 000	0.00	0 00	0 000	0 000	0	0 00
0 017	1 103	548040 00	13680.00	0 017	1 103	583680 00	24960 00	0.017	1 103	537000.00	20820.00
0 033	2.205	2202480 00	44640 00	0 033	2.205	2109120 00	70320 00	0.033	2.205	2630200 00	80640 00
0 050	3.308	13903140 00	129480 00	0 050	3.308	3187080 00	92580 00	0 050	3.308	4929900 00	109380 00
0 067	4.410	35333880 00	169560 00	0 067	4.410	5372400.00	121740.00	0.067	4.410	8065740 00	136200 00
				0.083	5.513	6991440.00	133800.00	0.083	5.513	11730480.00	153240.00
				0 100	6 615	10119000 00	150540.00	0 100	6 615	13437300.00	160680.00
				0 117	7 718	12136260 00	157260.00	0 117	7 718	15811380.00	164820.00
				0 133	8.820	14569000 00	165600.00	0.133	8.820	18842820 00	170760.00
				0 150	9 923	17647320 00	166180.00				

Table A4.4 Results from compression testing in sound proofed room

River gravel		Moderate 0.098mm/min		River gravel		Moderate 0 098mm/min		River gravel		Moderate 0 098mm/min	
exp154				exp155				exp156			
Time (hrs)	Displacement (mm)	Load (kN)	Energy	Time (hrs)	Displacement (mm)	Load (kN)	Energy	Time (hrs)	Displacement (mm)	Load (kN)	Energy
0.000	0 000	0.000	0.000	0 000	0 000	0.000	0.000	0 000	0.000	0 000	0 000
0 167	0 980	0.036	0.240	0 167	0 980	0.031	0.240	0 167	0 980	0 035	0 990
0.333	1 960	0 114	1 180	0 333	1 960	0 104	1.240	0 333	1.960	0 124	5 100
0.500	2.940	0.224	4.040	0.500	2.940	0.221	8.320	0 500	2.940	0.255	19.300
0 700	4.116	0.366	12.330	0.667	3.920	0.352	17.630	0 667	3.920	0.431	51 640
0.833	4 900	0.528	20.450	0.833	4 900	0.500	32.700	0 833	4.900	0.583	80 000
1.000	5.880	0.714	37 010	1 000	5.880	0.680	54 140	1 000	5.880	0 759	122.000
1 167	6.860	0 928	57 190	1 167	6.860	0.863	85 170	1 167	6.860	0 952	173.000
1.350	7 938	1 183	85.970	1.333	7.840	1 094	122.000	1 333	7.840	1.245	236.000
1.500	8.820	1 426	113.000	1 500	8.820	1.342	167 000	1 500	8.820	1.449	302.000
1 667	9 800	1 756	150 000	1 667	9.800	1 615	222.000				
exp154				exp155				exp156			
Time (hrs)	Displacement (mm)	RDC	Event	Time (hrs)	Displacement (mm)	RDC	Event	Time (hrs)	Displacement (mm)	RDC	Event
0.000	0.000	0 000	0.000	0 000	0 000	0.000	0 000	0 000	0.000	0 000	0 000
0 167	0.980	7287	160	0 167	0 980	7694	236	0 167	0 980	33394	696
0.333	1 960	36671	926	0.333	1.960	42171	1117	0.333	1.960	169354	3478
0.500	2.940	134932	3224	0 500	2.940	214834	4668	0.500	2.940	541586	11854
0 700	4.116	336749	7286	0 667	3 920	574083	11738	0 667	3.920	1494013	24481
0.833	4 900	668780	13704	0 833	4 900	1082288	20619	0 833	4.900	2823500	39783
1.000	5.880	1181895	22239	1 000	5.880	1839436	32507	1 000	5.880	3992424	56782
1 167	6.860	1859537	32878	1 167	6.860	2830110	46080	1 167	6.860	5666576	75557
1.350	7 938	2716436	45311	1.333	7.840	4015694	61096	1.333	7.840	7500139	95299
1.500	8.820	3714694	59124	1 500	8.820	5485198	78088	1.500	8.820	9846555	116967
1.667	9.800	4852243	73535	1 667	9.800	7134822	95482				
exp154				exp155				exp156			
Time (hrs)	Displacement (mm)	RDC Rate RDC per hr	Event Rate Event per hr	Time (hrs)	Displacement (mm)	RDC Rate RDC per hr	Event Rate Event per hr	Time (hrs)	Displacement (mm)	RDC Rate RDC per hr	Event Rate Event per hr
0.000	0.000	0	0	0.000	0 000	0	0	0 000	0.000	0	0
0 167	0.980	43722.02	960 00	0 167	0 980	46164.02	1416.00	0 167	0 980	200364.08	4176.00
0.333	1 960	176304 07	4608.00	0 333	1 960	206862.06	5256.00	0.333	1 960	815780.33	16692.01
0.500	2.940	589566.24	13776.01	0 500	2.940	1035978.41	22626.01	0 500	2 940	2833993.13	50256.02
0 700	4 116	1009083.99	20309 98	0 667	3 920	2155494.86	41100.02	0 667	3 920	5113964 05	75642.03
0.833	4.900	2490238.73	48135.12	0 833	4 900	3049231.22	54486.02	0 833	4.900	6776924 71	91812.04
1.000	5.880	3078691.23	51210.02	1 000	5.880	4542889.82	70128.03	1 000	5.880	8213547.29	102114 04
1 167	6.860	4065853.93	63834.03	1 167	6.860	5944046.36	81318.03	1 167	6.860	10044918.02	112650.05
1.350	7 938	4873982.55	67816.19	1 333	7.840	7113508.85	90216.04	1 333	7.840	11001382.49	118452.06
1.500	8.820	6655079 95	92087.04	1 500	8.820	8817027.53	101632.04	1 500	8.820	14078501 63	129408.06
1.667	9.800	8625296.73	86466.03	1 667	9.800	9697747 98	104484.04				

Table A4.4 Results from compression testing in sound proofed room (continued...)

River gravel		Slow 0.01176mm/min		River gravel		Slow 0.01176mm/min		River gravel		Slow 0.01176mm/min	
exp157				exp158				exp159			
Time (hrs)	Displacement (mm)	Load (kN)	Energy	Time (hrs)	Displacement (mm)	Load (kN)	Energy	Time (hrs)	Displacement (mm)	Load (kN)	Energy
0.000	0.000	0.000	0.000	0.000	0.000	0.000	0.000	0.000	0.000	0.000	0.000
1.067	0.753	0.024	1.100	1.000	0.706	0.069	4.990	1.000	0.706	0.110	8.760
1.767	1.247	0.052	1.810	2.000	1.411	0.152	13.810	2.233	1.576	0.269	22.860
3.117	2.199	0.131	6.860	3.000	2.117	0.242	25.360	3.117	2.199	0.393	39.200
3.900	2.752	0.190	10.700	4.217	2.975	0.369	47.750	4.167	2.940	0.580	55.840
4.933	3.481	0.266		4.917	3.469	0.455	65.390	5.300	3.740	0.762	96.370
6.000	4.234	0.373	39.690	6.000	4.234	0.614	98.300	6.100	4.304	0.914	126.000
7.033	4.963	0.478	62.250	6.933	4.892	0.742	150.000	7.067	4.986	1.094	164.000
9.833	6.938	0.869	173.000					11.883	8.385	2.064	412.000
11.183	7.891	1.060	260.000								

exp157				exp158				exp159			
Time (hrs)	Displacement (mm)	RDC	Event	Time (hrs)	Displacement (mm)	RDC	Event	Time (hrs)	Displacement (mm)	RDC	Event
0.000	0.000	0.000	0.000	0.000	0.000	0.000	0.000	0.000	0.000	0.000	0.000
1.067	0.753	1110	52	1.000	0.706	4299	259	1.000	0.706	191485	4570
1.767	1.247	1708	92	2.000	1.411	12416	655	2.233	1.576	743734	16505
3.117	2.199	5695	365	3.000	2.117	22629	1211	3.117	2.199	1291840	29157
3.900	2.752	9368	576	4.217	2.975	41178	2170	4.167	2.940	2103371	47296
4.933	3.481	22317	1069	4.917	3.469	54419	2855	5.300	3.740	3222028	71449
6.000	4.234	34630	1766	6.000	4.234	83356	4349	6.100	4.304	4190325	91689
7.033	4.963	53069	2744	6.933	4.892	123722	6146	7.067	4.986	5425992	117864
9.833	6.938	146909	7188	10.000	7.056	301659	14677	10.000	7.056	10040739	210026
11.183	7.891	216207	10446	15.000	10.584	740489	35607	11.883	8.385	13450522	276324

exp157		RDC Rate	Event Rate	exp158		RDC Rate	Event Rate	exp159		RDC Rate	Event Rate
Time (hrs)	Displacement (mm)	RDC per hr	Event per hr	Time (hrs)	Displacement (mm)	RDC per hr	Event per hr	Time (hrs)	Displacement (mm)	RDC per hr	Event per hr
0.000	0.000	0	0	0.000	0.000	0	0	0.000	0.000	0	0
1.067	0.753	1040.62	48.75	1.000	0.706	4299.00	259.00	1.000	0.706	191485.00	4570.00
1.767	1.247	854.29	87.14	2.000	1.411	8117.00	396.00	2.233	1.576	447770.67	9758.13
3.117	2.199	3101.48	202.22	3.000	2.117	10213.00	656.00	3.117	2.199	620495.02	14243.72
3.900	2.752	4433.62	269.36	4.217	2.975	15245.75	788.22	4.167	2.940	772886.67	17246.67
4.933	3.481	12531.28	496.45	4.917	3.469	18915.71	978.57	5.300	3.740	987060.29	21311.47
6.000	4.234	11543.44	634.89	6.000	4.234	25711.06	1286.77	6.100	4.304	1210371.25	25275.00
7.033	4.963	17844.18	946.48	6.933	4.892	43249.29	2032.50	7.067	4.986	1278276.20	26891.38
9.833	6.938	33514.29	1587.50	10.000	7.056	58022.93	2761.85	10.000	7.056	1573209.21	31487.05
11.183	7.891	51331.85	2411.86					11.883	8.385	1810504.25	36264.42

Table A4.4 Results from compression testing in sound proofed room (continued...)

River gravel		Rapid 1 1025mm/min		River gravel		Rapid 1 1025mm/min	
exp160				exp161			
Time (hrs)	Displacement (mm)	Load (kN)	Energy	Time (hrs)	Displacement (mm)	Load (kN)	Energy
0 000	0 000	0 000	0 000	0 000	0 000	0 000	0 000
0 017	1 103	0 104	3 050	0 017	1 103	0 162	15 310
0 033	2 205	0 245	32 300	0 033	2 205	0 324	79 000
0 050	3 308	0 380	78 000	0 050	3 308	0 478	173 000
0 067	4 410	0 559	148 000	0 067	4 410	0 666	310 000
0 083	5 513	0 759	247 000	0 083	5 513	0 849	474 000
0 100	6 615	0 945	378 000	0 100	6 615	1 063	685 000
0 117	7 718	1 168	528 000	0 117	7 718	1 287	906 000
0 133	8 820	1 415	716 000	0 133	8 820	1 546	1168 000
0 150	9 923	1 687	931 000	0 150	9 923	1 846	1460 000
0 167	11 025	2 004	1161 000	0 167	11 025	2 118	1726 000
exp160				exp161			
Time (hrs)	Displacement (mm)	RDC	Event	Time (hrs)	Displacement (mm)	RDC	Event
0 000	0 000	0 000	0 000	0 000	0 000	0 000	0 000
0 007	0 458	101 000	7 000	0 001	0 072	2 000	1 000
0 013	0 879	1081 000	48 000	0 009	0 578	3421 000	163 000
0 017	1 103	2695 000	121 000	0 014	0 951	8206 000	372 000
0 033	2 205	27406 000	925 000	0 017	1 103	12999 000	518 000
0 050	3 308	62151 000	2041 000	0 033	2.205	61550 000	1954 000
0 067	4 410	116724 000	3586 000	0 050	3 308	138170 000	3783 000
0 083	5 513	191176 000	5448 000	0 067	4 410	253532 000	5902 000
0 100	6 615	296660 000	7565 000	0 083	5 513	391075 000	8180 000
0 117	7 718	414355 000	9793 000	0 100	6 615	583053 000	10722 000
0 133	8 820	583101 000	12276 000	0 117	7 718	789372 000	13316 000
0 150	9 923	758600 000	14824 000	0 133	8 820	1059208 000	16061 000
0 167	11 025	966206 000	17481 000	0 150	9 923	1344749 000	18819 000
				0 167	11 025	1630381 000	21589 000
exp160		RDC Rate	Event Rate	exp161		RDC Rate	Event Rate
Time (hrs)	Displacement (mm)	RDC per hr	Event per hr	Time (hrs)	Displacement (mm)	RDC per hr	Event per hr
0 000	0 000	0 000	0 000	0 000	0 000	0 000	0 000
0 007	0 458	14600 252	1011 899	0 001	0 072	1831 055	915 527
0 013	0 879	153808 594	6434 849	0 009	0 578	447169 713	21187 919
0 017	1 103	477879 250	21614 117	0 014	0 951	847896 453	37034 558
0 033	2.205	1482660 000	48240 000	0 017	1 103	2097450 210	63890 618
0 050	3 308	2084700 000	66960 000	0 033	2.205	2913060 000	86160 000
0 067	4 410	3274380 000	92700 000	0 050	3 308	4597200 000	109740 000
0 083	5 513	4467120 000	111720 000	0 067	4 410	6921720 000	127140 000
0 100	6 615	6329040 000	127020 000	0 083	5 513	8252580 000	136680 000
0 117	7 718	7061700 000	133680 000	0 100	6 615	11518680 000	152520 000
0 133	8 820	10124760 000	148980 000	0 117	7 718	12379140 000	155640 000
0 150	9 923	10529940 000	152880 000	0 133	8 820	16190160 000	164700 000
0 167	11 025	12456360 000	159420 000	0 150	9 923	17132460 000	165480 000
				0 167	11 025	17137920 000	166200 000

Table A4.5 Results from compression testing in normal laboratory environment

River gravel		Rapid 1 1025mm/min		River gravel		Moderate 1 1025mm/min	
exp162				**exp163**			
Time (hrs)	Displacement (mm)	Load (kN)	Energy	Time (hrs)	Displacement (mm)	Load (kN)	Energy
0 000	0 000	0 000	0 000	0 000	0 000	0 000	0 000
0 017	1 103	0 131	1 940	0 017	1 103	0 100	4 470
0 033	2 205	0 300	9 470	0 033	2 205	0 252	24 000
0 050	3 308	0 497	25 000	0 050	3 308	0 428	69 000
0 067	4 410	0 762	50 000	0 067	4 410	0 590	133 000
0 083	5 513	1 066	90 000	0 083	5 513	0 790	222 000
0 100	6 615	1 408	140 000	0 100	6 615	1 011	340 000
0 117	7 718	1 787	201 000	0 117	7 718	1 242	480 000
0 133	8 820	2 177	280 000	0 133	8 820	1 508	652 000
0 150	9 923	2 619	369 000	0 150	9 923	1 808	862 000
0 167	11 025	3 036	471 000	0 167	11 025	2 073	1080 000
exp162				**exp163**			
Time (hrs)	Displacement (mm)	RDC	Event	Time (hrs)	Displacement (mm)	RDC	Event
0 000	0 000	0 000	0 000	0 000	0 000	0 000	0 000
0 008	0 554	348 000	39 000	0 001	0 072	0 000	0 000
0 014	0 927	1233 000	115 000	0 008	0 554	950 000	63 000
0 017	1 103	1953 000	166 000	0 014	0 915	2734 000	149 000
0 033	2 205	8342 000	527 000	0 017	1 103	4826 000	224 000
0 050	3 308	21273 000	1184 000	0 033	1 960	19960 000	899 000
0 067	4 410	39256 000	2088 000	0 050	2 940	58693 000	2087 000
0 083	5 513	69049 000	3258 000	0 067	4 116	109709 000	3668 000
0 100	6 615	107334 000	4629 000	0 083	4 900	182303 000	5469 000
0 117	7 718	157870 000	6216 000	0 100	5 880	282108 000	7595 000
0 133	8 820	224523 000	8013 000	0 117	6 860	402763 000	9940 000
0 150	9 923	293615 000	9929 000	0 133	7 938	561896 000	12456 000
0 167	11 025	374186 000	11945 000	0 150	8 820	759368 000	15054 000
				0 167	9 800	976321 000	17745 000
exp162		RDC Rate	Event Rate	**exp163**		RDC Rate	Event Rate
Time (hrs)	Displacement (mm)	RDC per hr	Event per hr	Time (hrs)	Displacement (mm)	RDC per hr	Event per hr
0 000	0 000	0 000	0 000	0 000	0 000	0 000	0 000
0 008	0 554	41556 980	4657 248	0 001	0 072	0 000	0 000
0 014	0 927	156820 974	13467 112	0 008	0 554	130462 646	8651 733
0 017	1 103	271775 601	19250 772	0 014	0 915	326660 156	15747 070
0 033	2 205	383340 000	21660 000	0 017	0 980	738886 098	26489 702
0 050	3 308	775860 000	39420 000	0 033	1 960	908040 000	40500 000
0 067	4 410	1078980 000	54240 000	0 050	2 940	2323980 000	71280 000
0 083	5 513	1787580 000	70200 000	0 067	4 116	3060960 000	94860 000
0 100	6 615	2297100 000	82260 000	0 083	4 900	4355640 000	108060 000
0 117	7 718	3032160 000	95220 000	0 100	5 880	5988300 000	127560 000
0 133	8 820	3999180 000	107820 000	0 117	6 860	7239300 000	140700 000
0 150	9 923	4145520 000	114960 000	0 133	7 938	9547980 000	150960 000
0 167	11 025	4834260 000	120960 000	0 150	8 820	11848320 000	155880 000
				0 167	9 800	13017180 000	161460 000

Table A4.5 Results from compression testing in normal laboratory environment (continued...)

River gravel		Moderate 1 1025mm/min		River gravel		Moderate 1 1025mm/min	
exp164				exp165			
Time (hrs)	Displacement (mm)	Load (kN)	Energy	Time (hrs)	Displacement (mm)	Load (kN)	Energy
0 000	0 000	0 000	0 000	0 000	0 000	0 000	0 000
0 017	1 103	0 214	3 240	0 017	1 103	0 193	7 270
0 033	2 205	0 431	33 750	0 033	2 205	0 362	47 000
0 050	3 308	0 645	86 000	0 050	3 308	0 528	114 000
0 067	4 410	0 869	174 000	0 067	4 410	0 714	210 000
0 083	5 513	1 114	293 000	0 083	5 513	0 918	342 000
0 100	6 615	1 390	450 000	0 100	6 615	1 128	487 000
0 117	7 718	1 684	621 000	0 117	7 718	1 328	661 000
0 133	8 820	1 987	826 000	0 133	8 820	1 587	879 000
0 150	9 923	2 258	1054 000	0 150	9 923	1 887	1079 000
0 167	11 025	2 667	1285 000	0 167	11 025	2 201	1382 000
exp164				exp165			
Time (hrs)	Displacement (mm)	RDC	Event	Time (hrs)	Displacement (mm)	RDC	Event
0 000	0 000	0 000	0 000	0 000	0 000	0 000	0 000
0 001	0 076	0 000	0 000	0 001	0 076	4 000	1 000
0 011	0 704	300 000	24 000	0 008	0 542	814 000	37 000
0 015	0 975	1435 000	105 000	0 014	0 900	4716 000	175 000
0 017	1 103	2808 000	159 000	0 017	1 103	6935 000	274 000
0 033	1 960	27989 000	998 000	0 033	2.205	39882 000	1322 000
0 050	2 940	72522 000	2269 000	0 050	3 308	102669 000	2848 000
0 067	3 920	150355 000	3954 000	0 067	4 410	188315 000	4676 000
0 083	4 900	264440 000	5992 000	0 083	5 513	301796 000	6795 000
0 100	5 880	405896 000	8292 000	0 100	6 615	437207 000	9049 000
0 117	6 860	562809 000	10686 000	0 117	7 718	605265 000	11429 000
0 133	7 840	771304 000	13216 000	0 133	8 820	835399 000	14035 000
0 150	8 820	1009064 000	15882 000	0 150	9 923	1085204 000	16719 000
0 167	9 800	1235460 000	18536 000	0 167	11 025	1385111 000	19523 000
exp164		RDC Rate	Event Rate	exp165		RDC Rate	Event Rate
Time (hrs)	Displacement (mm)	RDC per hr	Event per hr	Time (hrs)	Displacement (mm)	RDC per hr	Event per hr
0 000	0 000	0 000	0 000	0 000	0 000	0 000	0 000
0 001	0 076	0 000	0 000	0 001	0 076	3487 723	871 931
0 011	0 704	31569 908	2525 593	0 008	0 542	114973.201	5109 920
0 015	0 975	277099 609	19775 391	0 014	0 900	721694 484	25523 793
0 017	0 980	714707 107	28109 384	0 017	1 103	723285 064	32269 140
0 033	1 960	1510860 000	50340 000	0 033	2.205	1976820 000	62880 000
0 050	2 940	2671980 000	76260 000	0 050	3 308	3767220 000	91560 000
0 067	3 920	4669980 000	101100 000	0 067	4 410	5138760 000	109680 000
0 083	4 900	6845100 000	122280 000	0 083	5 513	6808860 000	127140 000
0 100	5 880	8487360 000	138000 000	0 100	6 615	8124660 000	135240 000
0 117	6 860	9414780 000	143640 000	0 117	7 718	10083480 000	142800 000
0 133	7 840	12509700 000	151800 000	0 133	8 820	13808040 000	156360 000
0 150	8 820	14265600 000	159960 000	0 150	9 923	14988300 000	161040 000
0 167	9 800	13583760 000	159240 000	0 167	11 025	17994420 000	168240 000

Table A4.5 Results from compression testing in normal laboratory environment (continued...)

River gravel		Slow 0 098mm/min		River gravel		Slow 0 098mm/min	
exp166				exp167			
Time (hrs)	Displacement (mm)	Load (kN)	Energy	Time (hrs)	Displacement (mm)	Load (kN)	Energy
0 000	0 000	0 000	0 000	0 000	0 000	0 000	0 000
0 167	0 980	0 138	19 620	0 167	0 980	0 069	5 300
0 333	1 960	0 276	67 000	0 333	1 960	0 231	47 000
0 500	2 940	0 411	130 000	0 500	2 940	0 359	139 000
0 667	3 920	0 552	236 000	0 667	3 920	0 490	271 000
0 833	4 900	0 724	369 000	0 833	4 900	0 642	460 000
1 000	5 880	0 894	527 000	1 000	5 880	0 790	657 000
1 167	6 860	1 090	731 000	1 167	6 860	0 952	906 000
1 333	7 840	1 270	993 000	1 333	7 840	1 166	1171 000
1 500	8 820	1 525	1259 000	1 500	8 820	1 359	1488 000
1 667	9 800	1 770	1548 000	1 667	9 800	1 584	1805 000
exp166				exp167			
Time (hrs)	Displacement (mm)	RDC	Event	Time (hrs)	Displacement (mm)	RDC	Event
0 000	0 000	0 000	0 000	0 000	0 000	0 000	0 000
0 001	0 007	11 000	3 000	0 001	0 007	7 000	3 000
0 010	0 060	197 000	14 000	0 010	0 060	323 000	23 000
0 067	0 392	3856 000	164 000	0 063	0 368	1345 000	58 000
0 135	0 794	13131 000	521 000	0 132	0 776	4020 000	154 000
0 167	0 980	19375 000	743 000	0 167	0 980	5936 000	236 000
0 333	1 960	62933 000	2506 000	0 333	1 960	50319 000	1774 000
0 500	2 940	119710 000	4687 000	0 500	2 940	150682 000	4743 000
0 667	3 920	221068 000	8156 000	0 667	3 920	287553 000	8895 000
0 833	4 900	346667 000	12408 000	0 833	4 900	467388 000	13984 000
1 000	5 880	495761 000	17484 000	1 000	5 880	698982 000	20195 000
1 167	6 860	694719 000	23698 000	1 167	6 860	977017 000	27058 000
1 333	7 840	956453 000	31004 000	1 333	7 840	1261299 000	34433 000
1 500	8 820	1223320 000	38692 000	1 500	8 820	1601199 000	42929 000
1 667	9 800	1507952 000	46845 000	1 667	9 800	1930833 000	51619 000
exp166		RDC Rate	Event Rate	exp167		RDC Rate	Event Rate
Time (hrs)	Displacement (mm)	RDC per hr	Event per hr	Time (hrs)	Displacement (mm)	RDC per hr	Event per hr
0 000	0 000	0 000	0 000	0 000	0 000	0 000	0 000
0 001	0 007	9591 239	2615 792	0 001	0 007	6103 516	2615 792
0 010	0 060	20640 980	1220 703	0 010	0 060	35067 472	2219 460
0 067	0 392	64732 648	2653 702	0 063	0 368	19493 103	667 572
0 135	0 794	135755 653	5225 312	0 132	0 776	38506 850	1381 928
0 167	0 980	197204 854	7011 447	0 167	0 980	55357 121	2369 146
0 333	1 960	261348 000	10578 000	0 333	1 960	266298 000	9228 000
0 500	2 940	340662 000	13086 000	0 500	2 940	602178 000	17814 000
0 667	3 920	608148 000	20814 000	0 667	3 920	821226 000	24912 000
0 833	4 900	753594 000	25512 000	0 833	4 900	1079010 000	30534 000
1 000	5 880	894564 000	30456 000	1 000	5 880	1389564 000	37266 000
1 167	6 860	1193748 000	37284 000	1 167	6 860	1668210 000	41178 000
1 333	7 840	1570404 000	43836 000	1 333	7 840	1705692 000	44250 000
1 500	8 820	1601202 000	46128 000	1 500	8 820	2039400 000	50976 000
1 667	9 800	1707792 000	48918 000	1 667	9 800	1977804 000	52140 000

Table A4.5 Results from compression testing in normal laboratory environment (continued. .)

River gravel		Slow 0 098mm/min		River gravel		Very Slow 0 098mm/min	
exp168				exp169			
Time (hrs)	Displacement (mm)	Load (kN)	Energy	Time (hrs)	Displacement (mm)	Load (kN)	Energy
0 000	0 000	0 000	0 000	0 000	0 000	0 000	0 000
0 200	1 176	0 152	10 670	0 167	0 980	0 124	6 900
0 467	2 744	0 279	30 600	0 333	1 960	0 259	36 940
0 500	2 940	0 428	78 900	0 500	2 940	0 393	106 000
0 717	4 214	0 676	163 390	0 667	3 920	0 549	198 000
0 833	4 900	0 804	245 000	0 833	4 900	0 711	312 000
0 933	5 488	0 945	318 000	1 000	5 880	0 890	458 000
1 683	9 898	1 760	904 530	1 217	7 154	1 111	709 000
1 917	11 270	3 947	3260 000	1 333	7 840	1 263	860 000
				1 517	8 918	1 428	1094 000
				1 667	9 800	1 625	1335 000
exp168				exp169			
Time (hrs)	Displacement (mm)	RDC	Event	Time (hrs)	Displacement (mm)	RDC	Event
0 000	0 000	0 000	0 000	0 000	0 000	0 000	0 000
0 001	0 007	0 000	0 000	0 001	0 007	6 000	1 000
0 010	0 060	108 000	5 000	0 010	0 060	179 000	8 000
0 065	0 382	2564 000	104 000	0 053	0 310	838 000	45 000
0 118	0 695	6213 000	267 000	0 127	0 746	3822 000	201 000
0 167	0 980	9726 000	471 000	0 167	0 980	8009 000	393 000
0 333	1 960	35520 000	1581 000	0 333	1 960	41616 000	1932 000
0 500	2 940	88542 000	3570 000	0 500	2 940	115660 000	4770 000
0 667	3 920	151938 000	6090 000	0 667	3 920	210665 000	8449 000
0 833	4 900	260382 000	9798 000	0 833	4 900	324559 000	12910 000
1 000	5 880	391938 000	14380 000	1 000	5 880	470783 000	18275 000
1 167	6 860	536627 000	19491 000	1 167	6 860	665667 000	24591 000
1 333	7 840	707232 000	25392 000	1 333	7 840	897219 000	32071 000
1 500	8 820	900771 000	32108 000	1 500	8 820	1114318 000	39429 000
1 667	9 800	1151544 000	39716 000	1 667	9 800	1371633 000	47658 000
exp168		RDC Rate	Event Rate	exp169		RDC Rate	Event Rate
Time (hrs)	Displacement (mm)	RDC per hr	Event per hr	Time (hrs)	Displacement (mm)	RDC per hr	Event per hr
0 000	0 000	0 000	0 000	0 000	0 000	0 000	0 000
0 001	0 007	0 000	0 000	0 001	0 007	5231 585	871 931
0 010	0 060	11985 085	554 865	0 010	0 060	19198 331	776 811
0 065	0 382	44746 968	1803 726	0 053	0 310	15470 065	868 577
0 118	0 695	68739 903	3070 596	0 127	0 746	40294 006	2106 523
0 167	0 980	72376 243	4202 890	0 167	0 980	105057 128	4817 523
0 333	1 960	154764 000	6660 000	0 333	1 960	201642 000	9234 000
0 500	2 940	318132 000	11934 000	0 500	2 940	444264 000	17028 000
0 667	3 920	380376 000	15120 000	0 667	3 920	570030 000	22074 000
0 833	4 900	650664 000	22248 000	0 833	4 900	683364 000	26766 000
1 000	5 880	789336 000	27492 000	1 000	5 880	877344 000	32190 000
1 167	6 860	868134 000	30666 000	1 167	6 860	1169304 000	37896 000
1 333	7 840	1023630 000	35406 000	1 333	7 840	1389312 000	44880 000
1 500	8 820	1161234 000	40296 000	1 500	8 820	1302594 000	44148 000
1 667	9 800	1504638 000	45648 000	1 667	9 800	1543890 000	49374 000

Table A4.5 Results from compression testing in normal laboratory environment (continued...)

River gravel		Very Slow 0 01176mm/min		River gravel		Very Slow 0 01176mm/min	
exp170				exp171			
Time (hrs)	Displacement (mm)	Load (kN)	Energy	Time (hrs)	Displacement (mm)	Load (kN)	Energy
0 000	0 000	0 000	0 000	0 000	0 000	0 000	0 000
1 000	0 706	0 035	0 012	1 050	0 741	0 070	0 024
2 000	1 411	0 124	0 043	1 990	1.404	0 260	0 090
3 667	2 587	0 645	0.223	4 190	2 956	1 130	0 390
4 000	2 822	0 676	0.233	5 000	3 528	1 360	0 469
4 833	3 410	0 411	0 142	11 090	7 825	3 950	1 363
6 333	4 469	1 021	0 352				
exp170				exp171			
Time (hrs)	Displacement (mm)	RDC	Event	Time (hrs)	Displacement (mm)	RDC	Event
0 000	0 000	0 000	0 000	0 000	0 000	0 000	0 000
0 001	0 001	63 000	3 000	0 001	0 001	237 000	3 000
0 010	0 007	86 000	9 000	0 010	0 007	319 000	7 000
0 100	0 071	765 000	61 000	0 100	0 071	657 000	25 000
0 406	0 286	3287 000	165 000	0 340	0 240	1148 000	48 000
0 886	0 625	6991 000	340 000	0 689	0 486	2609 000	94 000
1 000	0 706	8315 000	393 000	1 000	0 706	3904 000	138 000
2 000	1 411	28030 000	1376 000	2 000	1 411	8309 000	312 000
3 000	2 117	67062 000	3073 000	3 000	2 117	24753 000	996 000
4 000	2 822	115536 000	5301 000	4 000	2 822	57525 000	2345 000
5 000	3 528	172515 000	7873 000	5 000	3 528	106517 000	4271 000
6 000	4 234	247283 000	10916 000	6 000	4 234	174814 000	6858 000
7 000	4 939	325279 000	14135 000	7 000	4 939	256376 000	9926 000
7 250	5 116	347029 000	15012 000	8 000	5 645	369616 000	14124 000
				9 000	6 350	513458 000	19315 000
				10 000	7 056	699446 000	25888 000
				11 000	7 762	874307 000	32513 000
exp170		RDC Rate	Event Rate	exp171		RDC Rate	Event Rate
Time (hrs)	Displacement (mm)	RDC per hr	Event per hr	Time (hrs)	Displacement (mm)	RDC per hr	Event per hr
0 000	0 000	0 000	0 000	0 000	0 000	0 000	0 000
0 001	0 001	54931 641	2615 792	0 001	0 001	206647 600	2615 792
0 010	0 007	2552 379	665 838	0 010	0 007	9099 787	443 892
0 100	0 071	7548 793	578 111	0 100	0 071	3757 720	200 115
0 406	0 286	8253 655	340 357	0 340	0 240	2047 012	95 889
0 886	0 625	7713 211	364 420	0 689	0 486	4186 496	131 813
1 000	0 706	11602 115	464 435	1 000	0 706	4163 280	141 455
2 000	1 411	19715 000	983 000	2 000	1 411	4405 000	174 000
3 000	2 117	39032 000	1697 000	3 000	2 117	16444 000	684 000
4 000	2 822	48474 000	2228 000	4 000	2 822	32772 000	1349 000
5 000	3 528	56979 000	2572 000	5 000	3 528	48992 000	1926 000
6 000	4 234	74768 000	3043 000	6 000	4 234	68297 000	2587 000
7 000	4 939	77996 000	3219 000	7 000	4 939	81562 000	3068 000
7 250	5 116	87000 000	3508 000	8 000	5 645	113240 000	4198 000
				9 000	6 350	143842 000	5191 000
				10 000	7 056	185988 000	6573 000
				11 000	7 762	174861 000	6625 000

Table A4.5 Results from compression testing in normal laboratory environment (continued...)

River gravel		Very Slow 0 01176mm/min		River gravel		Very Slow 0 01176mm/min	
exp172				exp173			
Time (hrs)	Displacement (mm)	Load (kN)	Energy	Time (hrs)	Displacement (mm)	Load (kN)	Energy
0 000	0 000	0 000	0 000	0 000	0 000	0 000	0 000
1 333	0 941	0 131	5 720	1 333	0 941	0 104	0 330
2 167	1 529	0 221	12 810	2 383	1 682	0 252	1 790
4 167	2 940	0 428	29 440	3 483	2 458	0 380	5 210
6 550	4 622	0 704	57 710	4 700	3 316	0 528	10 760
12 117	8 550	1 397	139 000	5 767	4 069	0 643	16 450
				9 333	6 586	1 139	48 960

exp172 Time (hrs)	Displacement (mm)	RDC	Event	exp173 Time (hrs)	Displacement (mm)	RDC	Event
0 000	0 000	0 000	0 000	0 000	0 000	0 000	0 000
0 001	0 001	9 000	1 000	0 001	0 001	0 000	0 000
0 010	0 007	13 000	4 000	0 010	0 007	1 000	1 000
0 100	0 071	327 000	17 000	0 100	0 071	62 000	5 000
0 335	0 237	762 000	44 000	0 338	0 238	71 000	9 000
0 662	0 467	1739 000	119 000	0 667	0 471	106 000	12 000
1 000	0 706	3376 000	254 000	1 000	0 706	399 000	28 000
2 000	1.411	10887 000	818 000	2 000	1 411	1425 000	127 000
3 000	2 117	18310 000	1421 000	3 000	2 117	5749 000	430 000
4 000	2 822	24868 000	2076 000	4 000	2 822	11474 000	879 000
5 000	3 528	33305 000	2888 000	5 000	3 528	18666 000	1443 000
6 000	4 234	43738 000	3724 000	6 000	4 234	27384 000	2129 000
7 000	4 939	54890 000	4617 000	7 000	4 939	41173 000	3103 000
8 000	5 645	68106 000	5651 000	8 000	5 645	57307 000	4116 000
9 000	6 350	82785 000	6774 000	9 000	6 350	73180 000	5147 000
10 000	7 056	100012 000	8021 000				
11 000	7 762	121101 000	9626 000				

exp172 Time (hrs)	Displacement (mm)	RDC Rate RDC per hr	Event Rate Event per hr	exp173 Time (hrs)	Displacement (mm)	RDC Rate RDC per hr	Event Rate Event per hr
0 000	0 000	0 000	0 000	0 000	0 000	0 000	0 000
0 001	0 001	7847 377	871 931	0 001	0 001	0 000	0 000
0 010	0 007	443 892	332 919	0 010	0 007	110 973	110 973
0 100	0 071	3490 900	144 528	0 100	0 071	678 168	44 470
0 335	0.237	1848 906	114 760	0 338	0 238	37 884	16 837
0 662	0 467	2989 040	229 455	0 667	0 471	106 333	9 114
1 000	0 706	4846 655	399 694	1 000	0 706	879 428	48 023
2 000	1 411	7511 000	564 000	2 000	1 411	1026 000	99 000
3 000	2 117	7423 000	603 000	3 000	2 117	4324 000	303 000
4 000	2 822	6558 000	655 000	4 000	2 822	5725 000	449 000
5 000	3 528	8437 000	812 000	5 000	3 528	7192 000	564 000
6 000	4 234	10433 000	836 000	6 000	4.234	8718 000	686 000
7 000	4 939	11152 000	893 000	7 000	4 939	13789 000	974 000
8 000	5 645	13216 000	1034 000	8 000	5 645	16134 000	1013 000
9 000	6 350	14679 000	1123 000	9 000	6 350	15873 000	1031 000
10 000	7 056	17227 000	1247 000				
11 000	7 762	21089 000	1605 000				

Table A4 5 Results from compression testing in normal laboratory environment (continued...)

River gravel	Very Slow 0 001176mm/min			River gravel	Very Slow 0 001176mm/min		
exp174				exp175			
Time (hrs)	Displacement (mm)	Load (kN)	Energy	Time (hrs)	Displacement (mm)	Load (kN)	Energy
0 000	0 000	0 000	0 000	0 000	0 000	0 000	0 000
14.250	1 005	0 148	2 490	16 617	1 172	0 107	3 520
25 410	1 793	0 290	8 360	24 367	1 719	0 214	15 040
44 830	3 163	0 500	26 760	89.250	6.297	0 966	307 000
61 130	4 313	0 707	41 760	95 500	6 738	0 997	509 000
69 830	4 927	0 776	57 070	111 666	7 879	1 194	650 000
86 560	6 108	0 990	84 740	119 717	8 447	1 250	752 000
92 160	6 503	1 032	96 950	135 983	9 595	1 500	925 000
				138 217	9 753	1 520	957 000
exp174				exp175			
Time (hrs)	Displacement (mm)	RDC	Event	Time (hrs)	Displacement (mm)	RDC	Event
0 000	0 000	0 000	0 000	0 000	0 000	0 000	0 000
0 001	0 000	0 000	0 000	0 001	0 000	7 000	2 000
0 010	0 001	1 000	1 000	0 010	0 001	256 000	9 000
0 100	0 007	31 000	9 000	0 100	0 007	725 000	31 000
1 000	0 071	371 000	35 000	1 000	0 071	2185 000	92 000
3 551	0.251	879 000	74 000	3 545	0 250	3165 000	117 000
6.259	0 442	1294 000	113 000	6 738	0 475	3461 000	147 000
10 000	0 706	2074 000	182 000	10 000	0 706	3823 000	164 000
20 000	1 411	6210 000	530 000	20 000	1 411	16367 000	1001 000
30 000	2 117	15585 000	1199 000	30 000	2 117	48114 000	3078 000
40 000	2 822	28772 000	2139 000	40 000	2 822	72832 000	4667 000
50 000	3 528	37696 000	2801 000	50 000	3 528	111755 000	6908 000
60 000	4.234	45388 000	3367 000	60 000	4.234	146981 000	9048 000
70 000	4 939	57959 000	4229 000	70 000	4 939	196285 000	11884 000
80 000	5 645	75265 000	5480 000	80 000	5 645	255949 000	15198 000
90 000	6 350	106940 000	7483 000	90 000	6 350	320378 000	18764 000
				100 000	7 056	476840 000	27886 000
				110 000	7 762	577242 000	33402 000
exp174		RDC Rate	Event Rate	exp175		RDC Rate	Event Rate
Time (hrs)	Displacement (mm)	RDC per hr	Event per hr	Time (hrs)	Displacement (mm)	RDC per hr	Event per hr
0 000	0 000	0 000	0 000	0 000	0 000	0 000	0 000
0 001	0 000	0 000	0 000	0 001	0 000	6103 516	1743 862
0 010	0 001	110 973	110 973	0 010	0 001	27632 280	776 811
0 100	0 007	333 525	88 940	0 100	0 007	5214 114	244 585
1 000	0 071	377 789	28 890	1 000	0 071	1622.271	67 780
3 551	0.251	199 113	15.286	3 545	0.250	385 080	9 823
6.259	0.442	153 253	14 402	6 738	0 475	92 691	9 394
10 000	0 706	208 520	18 446	10 000	0 706	110 989	5.212
20 000	1 411	413 600	34 800	20 000	1 411	1254 400	83 700
30 000	2 117	937 500	66 900	30 000	2 117	3174 700	207 700
40 000	2 822	1318 700	94 000	40 000	2 822	2471 800	158 900
50 000	3 528	892 400	66 200	50 000	3 528	3892 300	224 100
60 000	4.234	769.200	56 600	60 000	4.234	3522 600	214 000
70 000	4 939	1257 100	88.200	70 000	4 939	4930 400	283 600
80 000	5 645	1730 600	125 100	80 000	5 645	5966 400	331 400
90 000	6 350	3167 500	200 300	90 000	6 350	6442 900	356 600
				100 000	7 056	15646 200	912 200
				110 000	7 762	10040 200	551 600

Table A4.5 Results from compression testing in normal laboratory environment (continued...)

River gravel		Very Slow 0 001176mm/min	
exp176			
Time (hrs)	Displacement (mm)	Load (kN)	Energy
0 000	0 000	0 000	0 000
5 067	0 358	0 003	5 040
21 917	1 546	0 124	14 300
30 667	2 164	0 193	22 770
78 167	5 515	0 742	168 000
92 833	6 550	0 949	277 000
101 166	7 138	1 080	343 000
118 166	8 338	1 394	486 000
129 416	9 132	1 521	599 000
142 667	10 067	1 818	727 000
exp176			
Time (hrs)	Displacement (mm)	RDC	Event
0 000	0 000	0 000	0 000
0 001	0 000	0 000	0 000
0 010	0 001	124 000	1 000
0 100	0 007	315 000	11 000
1 000	0 071	1716 000	79 000
3 335	0 235	5071 000	252 000
6 765	0 477	9311 000	465 000
10 000	0 706	12630 000	625 000
20 000	1 411	19259 000	958 000
30 000	2 117	28718 000	1467 000
40 000	2 822	44233 000	2316 000
50 000	3 528	72461 000	3717 000
60 000	4 234	120159 000	6066 000
70 000	4 939	168446 000	8452 000
80 000	5 645	262514 000	12877 000
90 000	6 350	394057 000	19401 000
100 000	7 056	546908 000	25721 000
110 000	7 762	676630 000	31893 000
exp176		RDC Rate	Event Rate
Time (hrs)	Displacement (mm)	RDC per hr	Event per hr
0 000	0 000	0 000	0 000
0 001	0 000	0 000	0 000
0 010	0 001	13760 653	110 973
0 100	0 007	2123 445	111 175
1 000	0 071	1556 713	75 558
3 335	0 235	1436 701	74 083
6 765	0 477	1236 332	62 108
10 000	0 706	1025 899	49 456
20 000	1 411	662 900	33 300
30 000	2 117	945 900	50 900
40 000	2 822	1551 500	84 900
50 000	3 528	2822 800	140 100
60 000	4 234	4769 800	234 900
70 000	4 939	4828 700	238 600
80 000	5 645	9406 800	442 500
90 000	6 350	13154 300	652 400
100 000	7 056	15285 100	632 000
110 000	7 762	12972 200	617 200

Table A4.5 Results from compression testing in normal laboratory environment (continued...)

Exp	Gradient	R^2
151	0 1009	0 9463
152	0 2198	0 9726
153	0 1798	0 9785
154	0 1785	0 9518
155	0 166	0 9577
156	0.169	0 9675
157	0.1385	0 9481
158	0 1517	0 9837
159	0 2492	0 988
160	0 18	0 9795
161	0 1897	0 9867
162	0 2802	0 9731
163	0 1898	0 9827
164	0 2372	0 992
165	0 1935	0 9886
166	0.177	0 988
167	0.1611	0 9882
168	0 1834	0 9867
169	0 1666	0 9954
170	0 2245	0 8404
171	0 5249	0 9827
172	0 1639	0 9979
173	0 1746	0 9956
174	0 162	0 9991
175	0.1571	0 9973
176	0 117	0 9816

Statistics of Gradient	
MAX	0 5249
MIN	0 1009
MEDIAN	0 17775
AVE	0 1936885
STDEV	0 0776875
VAR	0 0060354

Statistics of R^2	
MAX	0 9991
MIN	0 8404
MEDIAN	0 9832
AVE	0 9749885
STDEV	0 0313311
VAR	0 0009816

Table A4.6 Statistics relating to figure 4.16 load verses displacement graph for compression tests

Exp 197 - Strain rate approximated from Graph = 0 2186 mm/min						
Time (hours)	Displacement (mm)	Load (kN)	RDC	Events	Energy	Event rate (Events per hr)
0	0	0	0	0	0	0
0 1	0	0	0	0	0	0
0 2	0	0	0	0	0	0
0 3	0	1 56	0	0	0	0
0 4	1 2728	7 15	959	75	1 3	750
0 5	2 5844	10 2	5040	307	6 3	2320
0 6	3 896	12.13	10856	728	14 97	4210
0 7	5 2076	13 89	28202	1638	35 78	9100
0 8	6 5192	15 46	51502	2855	64 07	12170
0 9	7 8308	16 61	79021	4284	98 13	14290
1	9 1424	17 61	112422	5910	137 8	16260
1 091667	10 3447	18 55	141955	7382	173	16058

Exp 198 - Strain rate approximated from Graph = 0 24324mm/min						
Time (hours)	Displacement (mm)	Load (kN)	RDC	Events	Energy	Event rate (Events per hr)
0	0	unknown	0	0	0	0
0.1	1.4604	unknown	169	4	0 0171	40
0 2	2 9208	unknown	698	29	0 74	250
0 3	4 3812	unknown	1609	110	2 55	810
0 4	5 8416	unknown	3822	297	6 56	1870
0 5	7 302	unknown	9134	625	13 51	3280
0 6	8 7624	unknown	13314	928	20 78	3030
0 7	10 2228	unknown	19550	1353	30 68	4250
0 8	11 6832	unknown	26502	1829	41 364	4760
0 9	13 1436	unknown	32300	2292	51 8345	4630
1	14 604	unknown	38298	2758	62 3893	4660
1 1	16 0644	unknown	44302	3306	74 827	5480
1 2	17 5248	unknown	51360	3958	88 5193	6520

Exp 199 - Strain rate approximated 0 0221mm/min						
Time (hours)	Displacement (mm)	Load (kN)	RDC	Events	Energy	Event rate (Events per hr)
0 000	0	0	0	0	0	0
1 667	2 21	6 37	3097	186	3 94	111 6
3 333	4 42	9 52	12009	698	18 2	307 2
5 000	6 63	11 83	23331	1438	43 3	444
6 667	8 84	13 83	47991	2871	74 1	859 8
8 333	11 05	15 54	72402	4257	109 05	831 6
10 000	13 26	17 04	100800	5676	148 36	851 4
11 667	15 47	18 45	136764	7417	196 86	1044 6

Table A4.7 Results from large scale testing

APPENDIX B

Microsoft Macro used within Chapter 5 for automatic source location analysis.

```
Sub Landslide1()
'
' Landslide1 Macro
' Macro recorded 18/03/2003 by Harshal
'

   Dim StartNum, EndNum, TimeLetter, AmplLetter, HrsLetter, MinLetter,
SecLetter, countin
   Dim csl, cel, numpeaks, maxwaves, Condition, ampcond, wave, temp1, temp2,
temp3, wave1
   Dim TimePeak(), temp4

   StartNum = InputBox("Enter the Time Starting Row Number : ", , 2)
   EndNum = InputBox("Enter the Time Ending Row Number : ", , 250)
   HrsLetter = InputBox("Enter the Hours Column Letter : ", , "A")
   MinLetter = InputBox("Enter the Minutes Column Letter : ", , "B")
   SecLetter = InputBox("Enter the Seconds Column Letter : ", , "C")
   AmplLetter = InputBox("Enter the Amplitude Column Letter : ", , "D")
   numpeaks = InputBox("Enter the Number of Peaks to determine : ", , 2)
   Condition = InputBox("Enter the Time difference Condition to determine New
Wave Starts : ", , 0.01)
   ampcond = InputBox("Enter the threshold value of Amplitude : ", , 1)

   Columns("" & AmplLetter & ":" & AmplLetter & "") Select
   Selection.Insert Shift:=xlToRight
   Range("" & AmplLetter & "1").Select
   ActiveCell.FormulaR1C1 = "Time"
   Range("" & AmplLetter & StartNum & "") Select
   ActiveCell.FormulaR1C1 = "=RC[-3]*3600+RC[-2]*60+RC[-1]"
   Range("" & AmplLetter & StartNum & "").Select
   Selection AutoFill Destination:=Range("" & AmplLetter & StartNum & "." &
AmplLetter & EndNum & ""), Type =xlFillDefault
   Range("" & AmplLetter & StartNum & "").Select

   TimeLetter = AmplLetter
   AmplLetter = Chr(Asc(UCase(AmplLetter)) + 1)

   If Len(UCase(TimeLetter)) > 1 Then
      csl = (Asc(UCase(Left(TimeLetter, 1))) - 65 + 1)
      csl = csl * 26 + Asc(UCase(Right(TimeLetter, 1))) - 65
   Else
      csl = Asc(UCase(TimeLetter)) - 65
   End If
```

```
    If Len(UCase(AmplLetter)) > 1 Then
       cel = (Asc(UCase(Left(AmplLetter, 1))) - 65 + 1) + 1
       cel = cel * 26 + Asc(UCase(Right(AmplLetter, 1))) - 65 + 1
    Else
       cel = Asc(UCase(AmplLetter)) - 65 + 1
    End If

    Sheets("Data Process") Select
    Cells.Select
    Selection ClearContents

    Sheets("Data Input").Select
    Range("" & TimeLetter & StartNum & "." & AmplLetter & EndNum &
"") Select
    Selection.Copy

    Sheets("Data Process") Select
    Range("A1") Select
    ActiveCell.FormulaR1C1 = "Time"
    Range("B1").Select
    ActiveCell.FormulaR1C1 = "Amplitude"
    Range("C1").Select
    ActiveCell.FormulaR1C1 = "Wave start"
    Range("D1").Select
    ActiveCell.FormulaR1C1 = "Wave Numbers"
    Range("E1").Select
    ActiveCell.FormulaR1C1 = "Max Time"
    Range("F1").Select
    ActiveCell.FormulaR1C1 = "No. of Peaks"
    Cells.Select
    Cells.EntireColumn.AutoFit
    Range("B2").Select
    ActiveWindow.FreezePanes = True

    Range("A2").Select
    Selection.PasteSpecial Paste:=xlValues, Operation:=xlNone, SkipBlanks:= _
       False, Transpose:=False
    Columns("A:A") EntireColumn AutoFit

'Determining Wave
    wave = 0
    wave1 = 0
    If (Range("B2").Value >= ampcond) Then
       wave = 1
    End If
    Range("G2").Select
    ActiveCell FormulaR1C1 = "=if(RC[-5] >= " & ampcond & ",1,0)"
    Range("G2").Select
    Selection.AutoFill Destination.=Range("G2.G" & (EndNum - (StartNum - 2))
& ""), Type.=xlFillDefault
```

```
   Range("G2:G" & (EndNum - (StartNum - 2)) & "").Select
   Range("H2").Select
   ActiveCell.FormulaR1C1 = "0"
   Range("H3").Select
   ActiveCell.FormulaR1C1 = "=if((RC[-7] - R[-1]C[-7]) > " & Condition &
",1,0)"
   Range("H3") Select
   Selection AutoFill Destination:=Range("H3.H" & (EndNum - (StartNum - 2))
& ""), Type.=xlFillDefault
   Range("H3:H" & (EndNum - (StartNum - 2)) & "").Select
   Range("C2").Select
   ActiveCell.FormulaR1C1 = "" & wave
   countin = 0
   For i = 3 To (EndNum - (StartNum - 2))
      Range("C" & i & "").Select
      temp1 = Range("B" & i & "").Value
      temp1 = temp1 - ampcond
      If wave = 0 Then
         If temp1 < 0 Then
            wave = 0
         Else
            wave = 1
         End If
      End If
      If wave = 1 Then
         temp2 = Range("A" & i & "").Value
         temp3 = Range("A" & (i - 1) & "").Value
         If ((temp2 - temp3) > Condition) Then
            temp4 = Range("H" & i & "").Value
         Else
            temp4 = Range("H" & i & "").Value
         End If
         'MsgBox "T1 = " & temp2 & ", T2 = " & temp3 & " Time Diff : " & temp4
         If (temp4 = 0) Then
            wave = 1
            countin = countin + 1
            If countin = 1 Then
               wave1 = 1
            Else
               wave1 = 0
            End If
         Else
            countin = 0
            wave1 = 0
            If temp1 < 0 Then
               wave = 0
            Else
               wave = 1
               countin = countin + 1
               wave1 = 1
```

```
            End If
          End If
        End If
        ActiveCell.FormulaR1C1 = "" & wave1
    Next i
    Range("D2") Select
    ActiveCell.FormulaR1C1 = "0"
    Range("D3").Select
    ActiveCell.FormulaR1C1 = "=IF(RC[-1]=1,R[-1]C+1,R[-1]C)"
    Range("D3") Select
    Selection.AutoFill Destination:=Range("D3 D" & (EndNum - (StartNum - 2))
& ""), Type:=xlFillDefault
    Range("D3:D" & (EndNum - (StartNum - 2)) & "").Select
    maxwaves = Range("D" & (EndNum - (StartNum - 2)) & "").Value

'Determining Peak Times in each Wave
    Range("E2") Select
    ActiveCell.FormulaR1C1 = "0"
    Range("E3") Select
    ActiveCell.FormulaR1C1 = "=IF(RC[-1]=0,0,IF(RC[-1]>R[-1]C[-
1],0,IF(AND(R[1]C[-3]<RC[-3],R[-1]C[-3]< RC[-3]), RC[-4],0)))"
    Range("E3").Select
    Selection.AutoFill Destination =Range("E3:E" & (EndNum - (StartNum - 2)) &
""), Type:=xlFillDefault
    Range("E3:E" & (EndNum - (StartNum - 2)) & "") Select

'Determining Number of Peaks in each wave
    Range("F2").Select
    ActiveCell.FormulaR1C1 = "0"
    Range("F3").Select
    ActiveCell.FormulaR1C1 = "=IF(RC[-2]=R[-1]C[-2],IF(RC[-1]>0,R[-
1]C+1,R[-1]C+0),0)"
    Range("F3") Select
    Selection.AutoFill Destination:=Range("F3:F" & (EndNum - (StartNum - 2)) &
""), Type:=xlFillDefault
    Range("F3:F" & (EndNum - (StartNum - 2)) & "").Select
    Range("F" & EndNum + 1 & "").Select
    ActiveCell.FormulaR1C1 = "=MAX(R[-" & (EndNum - (StartNum - 2) - 1) &
"]C:R[-1]C)"
    Range("F" & EndNum + 1 & "").Select
    maxpeak = Range("F" & EndNum + 1 & "").Value

'Determining times
    ReDim TimePeak(1 To maxwaves, 1 To maxpeak)
    For i = 1 To maxwaves
      For j = 1 To numpeaks
        TimePeak(i, j) = 0
      Next j
    Next i
    For i = 2 To (EndNum - (StartNum - 2))
```